

Expression profile of components of the acetylcholine-system in rat testicular tissue and function in non-germ cell populations

INAUGURALDISSERTATION

zur Erlangung des Grades
Doktor rerum naturalium
des Fachbereichs Biologie der
Justus-Liebig-Universität Gießen

vorgelegt von

Sylvia Schirmer
aus Kleineutersdorf, Thüringen

Gießen 2011

Diese Arbeit wurde am
Institut für Anatomie und Zellbiologie
der Justus-Liebig-Universität Gießen
in der
Arbeitsgruppe Reproduktionsbiologie
angefertigt.

Erstgutachter: Prof. Dr. R. Lakes-Harlan
Institut für Tierphysiologie
Fachbereichs Biologie
Justus-Liebig-Universität Gießen

Zweitgutachter: Prof. Dr. A. Meinhardt
Institut für Anatomie und Zellbiologie
Fachbereichs Medizin
Justus-Liebig-Universität Gießen

Tag der Disputation:
30.05.2011

I. List of contents

I. List of contents	I
II. List of Tables	VII
III. List of Figures	VIII
IV. Abbreviations	XII
Introduction	1
<i>1. Structure, function and impairment of the rat testis</i>	<i>1</i>
1.1. The testis: spermatogenesis and steroidogenesis	1
1.2. Anatomy of the rat testis and adjacent structures	2
1.3. The testicular parenchyma	2
1.3.1. The tubular compartment	3
1.3.2. The interstitial compartment	4
1.4. Immunology of the testis	5
1.4.1. Immune privilege of the testis	5
1.4.2. Male infertility	6
1.4.3. Cytokines and chemokines in the testis	6
1.5. Experimental autoimmune orchitis: a model of inflammatory infertility in rodents	7
<i>2. Innervation of the testis</i>	<i>7</i>
2.1. The nervous system and sensory neurons	7
2.2. Sensory neurons are divided in subpopulations	8
2.3. Neuronal markers	9
2.4. Innervation of the testis	10
<i>3. The cholinergic system</i>	<i>11</i>
3.1. Acetylcholine	11
3.2. Non-neuronal cholinergic system	12
3.3. Synthesis, release, degradation and recycling of acetylcholine in neuronal and non-neuronal tissue	13
3.3.1. Synthesis of acetylcholine	13
3.3.2. Storage and release of acetylcholine	13
3.3.3. Degradation and recycling of acetylcholine	14
	I

3.4. Acetylcholine receptors	15
3.4.1. Structure and functionality of nicotinic acetylcholine receptors	16
3.4.2. Structure and functionality of muscarinic acetylcholine receptors	19
3.5. Cholinergic system within the testis	20
4. <i>Aim of this study</i>	21
Materials and Methods	22
5. <i>Animals and tissues</i>	22
5.1. Animals	22
5.2. Tissue culture	22
5.2.1. Isolation of testicular macrophages	22
5.2.2. Isolation of peritubular cells and Sertoli cells	23
6. <i>Molecular biology</i>	24
6.1. RNA isolation	24
6.2. Examination of RNA quality	25
6.3. Reverse transcription	26
6.4. Polymerase chain reaction	26
6.4.1. Primer design	26
6.4.2. Standard PCR	30
6.4.3. Quantitative real-time PCR	31
6.5. <i>In situ</i> hybridisation	33
6.5.1. Preparation of the probe	34
6.5.2. <i>In situ</i> hybridisation on frozen tissue sections	36
7. <i>Immunohistochemistry</i>	39
7.1. Tissue immersion fixation and xylene-processing for whole mounts and sections	40
7.2. Single and multiple labelling immunohistochemistry	41
7.4. Whole mount	43
8. <i>In vitro and in vivo experiments</i>	44
8.1. Measurement of intracellular calcium concentrations	44
8.2. Retrograde tracing with Cholera toxin-B	46
8.3. Induction of experimental autoimmune orchitis	48

Results	49
<i>9. The cholinergic system of rat testicular parenchyma and testicular capsul under non-inflammatory conditions</i>	49
9.1. Relative mRNA expression analysis of nicotinic AChR-subunits	49
9.2. Relative mRNA expression analysis of muscarinic AChR-subtypes	51
9.3. Relative mRNA expression analysis of ChAT, ChT1, OCT2 and VACHT in rat testicular parenchyma	52
9.4. Relative mRNA expression of mAChR, ChAT, ChT1, VACHT and OCT2 in mouse testicular parenchyma and -capsule	54
9.5. Immunohistochemical detection of ChAT, ChT1 and VACHT in rat testis	56
9.6. <i>In situ</i> hybridisation for the $\alpha 7$ nAChR-subunit and ChAT in rat testis	60
9.6.1. Optimisation of <i>in situ</i> hybridisation probes using spinal cord as control tissue	60
9.6.2. Localisation of mRNA expression for the $\alpha 7$ nAChR-subunit and ChAT in rat testis	61
<i>10. Testicular somatic cells: peritubular cells, Sertoli cells and testicular macrophages</i>	63
10.1. Immunohistochemical characterisation of isolated and cultured testicular somatic cells	63
10.2. The cholinergic system in testicular somatic cells	64
10.3. Cell specific functional analysis of ACh receptors using calcium-imaging experiments	67
10.3.1. Peritubular cells showed muscarine-induced increase in $[Ca^{2+}]_i$	67
10.3.2. Blockade of muscarine-induced receptor activation in PTC	72
10.3.3. Testicular macrophages showed no direct response to AChR stimulation	74
10.3.4. Sertoli cells showed no direct response to AChR stimulation	77
10.3.5. AChR blockade modulates the ATP-induced calcium response in Sertoli cells	80
<i>11. The cholinergic system in an inflammatory model (EAO)</i>	82
11.2. Relative mRNA expression analysis of nicotinic AChR-subunits in orchitis	84
11.3. Relative mRNA expression analysis of muscarinic AChR subtypes in orchitis	86
11.4. Relative mRNA expression analysis of ChAT, ChT1, OCT2 and VACHT in orchitis	87

<i>12. Sensory innervation of the rat testis</i>	89
12.1. Morphological observations of the rat testis	89
12.2. Neurochemical characterisation of testicular nerve fibres	90
12.2.1. Sensory nerve fibres (Nf200 & peripherin)	92
12.2.2. Sensory nociceptive nerve fibres (Nf200 & CGRP)	92
12.2.3. Nerve fibres in meso-structures are positive for IB4, TRPV1 and VGluT1	97
12.3. Tracing from the mesodeferens I and II to the dorsal root ganglia	99
Discussion	103
<i>13. The non-neuronal cholinergic system in rat testis</i>	103
13.1. ACh synthesizing enzyme and transporters are present in testicular parenchyma and capsule	103
13.2. Presence of nAChRs in testicular cells	107
13.2.1. Presence of nAChRs in testicular parenchyma and -capsule	107
13.2.2. Presence of nAChRs in PTC, SC and TM	110
13.3. MRs are present within the testis	112
13.3.1. Presence of MRs in testicular parenchyma and -capsule	112
13.3.2. Presence of MRs in PTC, SC and TM	114
13.4. Similarities of the cholinergic system in mouse and rat testes	115
13.5. The function of the cholinergic system in EAO	116
13.6. Functional evidence for ACh receptors in testicular cells	119
13.6.1. PTCs express neuronal-like muscarinic receptors	120
13.6.2. ATP-induced Ca ²⁺ -influx is influenced by ACh or -agonists	122
13.6.3. Nicotinic antagonists modulate the ATP-induced Ca ²⁺ -influx in SC	124
<i>14. Sensory innervation of testicular adjacent structures</i>	126
14.1. Meso-structures show dense innervation of nociceptive nerve fibres	127
14.2. Neurons of DRG L1 projecting to mesodeferens	128
<i>15. Summary</i>	131
<i>16. Zusammenfassung</i>	133
<i>17. References</i>	135
<i>18. Appendix</i>	158
18.1. Curriculum vitae	158
18.2 Acknowledgements	160
18.3. Declaration	162

II. List of Tables

Tab. 1: α -Bgt-sensitive receptors.	16
Tab. 2: α -Bgt non-sensitive receptors.	17
Tab. 3: Rat primer sequences for MR.	27
Tab. 4: Rat primer sequences for pro-inflammatory molecules.	27
Tab. 5: Rat primer sequences for nAChR.	28
Tab. 6: Rat primer sequences for ChAT, transporter and HKG.	29
Tab. 7: Mouse primer sequences for mAChR, ChAT and transporters.	30
Tab. 8: Rat primer sequences for in situ hybridisation.	35
Tab. 9: Primary and secondary antibody or antisera.	42
Tab. 10: Comparison of relative mRNA expression levels of nAChR subunits in TP and TC	50
Tab. 11: Expression of MR subtypes in TP and TC.	51
Tab. 12: Expression of ChAT, ChT1, OCT2 and VACHT in TP and TC.	53
Tab. 13: Expression of MR subtypes and ACh-related molecules in mouse TP and TC.	54
Tab. 14: Standard PCR for nAChR-subunits in PTC, SC and TM	65
Tab. 15: Standard PCR for MR subtypes in PTC, SC and TM.	66
Tab. 16: Standard PCR for ChAT, ChT1, VACHT and OCT2 in TM.	66
Tab. 17: Statistical analysis for calcium-imaging experiments on TM.	77
Tab. 18: P-value for experiments with nicotinic inhibitors on SC.	82
Tab. 19: Statistical analysis for MCP-1, TNF- α and IL-6.	83
Tab. 20: Statistical analysis for nAChR-subunits α and β .	84
Tab. 21: Statistical analysis of MR-subtype expression.	86
Tab. 22: Statistical analysis for ChAT, ChT1, OCT2 and VACHT.	88
Tab. 23: Tissue samples used for whole mount multiple labelling IHC.	90

Tab. 24: Neurochemical characteristics of nerve fibres running alongside with blood vessels or in non-vascular tissue.	93
Tab. 25: IB4, TRPV1 and VGluT1 positive nerve fibres within meso-structures.	97
Tab. 26: Data of the first tracing experiment.	99
Tab. 27: Data of the second tracing experiment.	101

III. List of Figures

Fig. 1: Spermatogenesis	3
Fig. 2: Blood-testis barrier	4
Fig. 3: Localisation of sensory neurons and segmentation of the vertebrate.	9
Fig. 4: Recycling pathway of acetylcholine (ACh) synthesis, release, action and breakdown at a cholinergic nerve terminal.	14
Fig. 5: Nicotine and muscarine.	15
Fig. 6: Muscarinic and nicotinic ACh receptors	18
Fig. 7: Real-time PCR flow chart	32
Fig. 8: Melt curves of real-time PCR products.	33
Fig. 9: <i>In situ</i> hybridisation probe design and binding within tissue.	35
Fig. 10: Immunohistochemistry (direct and indirect method)	39
Fig. 11: Flow chart for calcium-imaging experiments.	45
Fig. 12: Fluorescence intensity after excitation with $\lambda = 380$ nm.	46
Fig. 13: mRNA expression level of nAChR subunits in TP and TC.	50
Fig. 14: mRNA expression level of MR subtypes in rat TP and TC.	52
Fig. 15: mRNA expression level of OCT2, VACHT, ChAT and ChT1 in rat TP and TC.	53
Fig. 16: mRNA expression level of MR subtypes in mouse TP and TC.	55
Fig. 17: mRNA expression level of OCT2, VACHT, ChAT and ChT1 in mouse TP and TC.	55
Fig. 18: Multiple labelling immunohistochemistry for ChAT.	57
Fig. 19: Validation of ChAT antiserum.	58
Fig. 20: Multiple labelling immunohistochemistry for ChT1.	58
Fig. 21: VACHT multiple labelling immunohistochemistry.	59
Fig. 22: Validation of the VACHT antiserum.	59
Fig. 23: Control PCR with ISH primer pairs.	60

Fig. 24: ChAT mRNA detection in rat spinal cord via ISH.	61
Fig. 25: ChAT mRNA detection at rat testis via ISH.	62
Fig. 26: $\alpha 7$ mRNA detection at rat testis via ISH.	62
Fig. 27: Cell-type specific labelling of PTC, SC and TM.	63
Fig. 28: PTCs show an oscillatory effect.	67
Fig. 29: ACh induces a $[Ca^{2+}]_i$ in PTC.	68
Fig. 30: Muscarine induces a $[Ca^{2+}]_i$ in PTC.	69
Fig. 31: Distribution of muscarine, ACh and ATP responsiveness of PTC.	70
Fig. 32: Nicotine has no influence on the $[Ca^{2+}]_i$ in PTC.	71
Fig. 33: <i>P</i> -values after agonist application in PTC-populations.	71
Fig. 34: Flow chart for inhibition experiment with PTC.	72
Fig. 35: ACh or muscarine induced calcium-influx can be blocked by atropine.	73
Fig. 36: Muscarine and ACh induced calcium-influx can be blocked by atropine.	74
Fig. 37: ACh or -agonists have no direct effect on TM.	76
Fig. 38: SC treatment with nicotine, muscarine or ACh.	78
Fig. 39: <i>P</i> -values after ATP application between SC-populations.	79
Fig. 40: Flow chart for inhibition experiment on SC.	80
Fig. 41: nAChR-inhibitor influence ATP reaction in SCs.	81
Fig. 42: The mRNA expression level of MCP-1, TNF- α and IL-6 in orchitis induced animals.	83
Fig. 43: mRNA expression level of nAChR α - and β -subunits in orchitis induced testis.	85
Fig. 44: mRNA expression level of MR subtypes in orchitis induced animals.	87
Fig. 45: mRNA expression level of ChAT, ChT1, OCT2 and VACHT in orchitis induced animals.	88
Fig. 46: Mesos of the rat testis.	89
Fig. 47: Immunohistochemistry of nerve fibres in structures adjacent to the testicular parenchyma.	91

Fig. 48: PGP9.5 IHC on testicular parenchyma.	92
Fig. 49: Nerve endings labelled positive for PGP9.5.	94
Fig. 50: Myelinated and unmyelinated nociceptive nerve fibres.	96
Fig. 51: IB4, VGluT1 and TRPV1 positive nerve fibres in meso-structures.	98
Fig. 52: Retrograde tracing of cells projecting to mesoepididymis I and II.	102
Fig. 53: Distribution of nerve fibres within the testicular capsule.	127

IV. Abbreviations

α -Bgt	α -Bungarotoxin
ACh	acetylcholine
AChR	acetylcholine receptor
nAChR	nicotinic acetylcholine receptor
AM	alveolar macrophages
BSA	bovine serum albumin
$[Ca^{2+}]_i$	intracellular Ca^{2+} concentration
cAMP	cyclic adenosine monophosphate
CarAT	carnitine acetyltransferase
CGRP	calcitonin-gene-related-peptide
ChAT	choline acetyltransferase
Ctx	Cholera toxin
Cy3	Indocarbocyanid
Cy5	Indodicarbocyanin
DAG	diacylglycerol
DAPI	4', 6'-diamidino-2-phenylindole, dihydrochloride
DMEM:F12	Dulbecco's Modified Eagle Medium: Nutrient Mixture F-12
DRG	dorsal root ganglia
EAO	experimental autoimmune orchitis
EDTA	ethylendinitrilo-N, N, N', N', -tetra-acetic acid disodium salt
ER	endoplasmic reticulum
FCS	Fetal calf serum
FITC	fluorescein isothiocyanate
Fura-2	fura 2 acetoxymethyl (AM) ester
GPCR	G-protein-coupled receptors
HEPES	(2-Hydroxyethyl)-1-piperazineethanesulphonic acid
HPRT1	hypoxanthine guanine phosphoribosyl transferase 1
HRP	horse radish peroxidase
IB4	isolectin B4
IFN	interferon
IL	interleukin

IP3	inositol-1,4,5-trisphosphate
LPS	lipopolisacharyde
MCP-1	monocyte chemoattractant protein-1
MR	muscarinic acetylcholine receptor
Nf200	neurofilament 200
PBS	Dublecco's phosphate buffered saline
PCR	polymerase chain reaction
PGP9.5	protein-gene-product-9.5
PI3K	phosphoinositide 3-kinase
PKC	protein kinase C
PLC	phospholipase C
PM	peritoneal macrophages
qRT-PCR	quantitative real-time PCR
rpm	revolutions per minute
RPMI	Roswell Park Memorial Institute medium
RT	reverse transcription
SD	standard deviation
sma	smooth muscle actin
TAE	Tris-acetate-EDTA buffer
TC	testicular capsule
TE	Tris-EDTA
TNF	tumor necrosis factor
TP	testicular parenchyma
TRPV1	transient receptor potential vanilloid receptor subtype 1
U	units
VACht	vesicular acetylcholine transporter
VGluT1	vesicular glutamate transporter 1

Introduction

1. Structure, function and impairment of the rat testis

1.1. The testis: spermatogenesis and steroidogenesis

The testis has two main functions the production of germ cells (spermatogenesis) and the synthesis of sex hormones (steroidogenesis).

Mammalian **spermatogenesis** is a complex process initiated by mitotic proliferation of spermatogonia that are located on the basal lamina. Defined spermatogonial daughter cells then enter the first meiotic division resulting as primary spermatocytes that become secondary spermatocytes after completion of the first meiotic division. Haploid round spermatids result after secondary spermatocytes, which divide in the second meiotic division. Round spermatids are transformed into elongated spermatids [1-3]. During spermatogenesis the maturing cells move from the periphery of the tubule to the luminal part. After reaching the luminal part the elongated spermatids are finally released from the Sertoli cells (SC) and are termed spermatozoa. These cells are transported to and leave the testis via the rete testis (Fig. 1).

Endocrine regulation of spermatogenesis and **steroidogenesis** occur by the hypothalamus and the anterior pituitary gland under the control of the central nervous system. Gonadotropin releasing hormone (GnRH), secreted by the hypothalamus, stimulates the release of luteinizing hormone (LH) and follicle-stimulating hormone (FSH) from the anterior pituitary gland [4, 5]. They are distributed by the vascular system (blood vessels). LH stimulates cell development, secretion of testosterone in Leydig cells and can influence cell morphology [6-8]. Due to the absence of testosterone receptors on germ cells, spermatogenesis is not direct influenced by androgens. Indirectly, spermatogenesis is regulated by binding of testosterone and FSH to SC [9]. As part of a negative feedback loop to the hypothalamus testosterone and inhibin, which is secreted by SC, regulate the production of GnRH, LH and FSH [4, 6, 7]. Additionally, testosterone directly regulates proliferation and differentiation of peritubular cells via nuclear androgen receptors [10, 11].

1.2. Anatomy of the rat testis and adjacent structures

Mammalian testes are located outside of the peritoneal cavity within the scrotum. The scrotum covers the fascia underneath, which consists of 3 almost indistinguishable parts: (1) external spermatic fascia, (2) cremaster muscle (external circular and internal longitudinal) and (3) internal spermatic fascia. The fascia is connected to the abdominal wall. In contrast to humans, in rats the connection between scrotal sac and peritoneum is still wide enough to withdraw the testis into the peritoneal cavity in situations of danger. Longitudinally the testis is connected to the epididymis. The head and tail of the epididymis are linked to the anterior and caudal pole of the testis by the inferior and superior ligament (IL, SL). The testicular artery and pampiniform plexus reach the testis via the spermatic cord on the same side as the epididymis. The vas deferens originates from the tail of the epididymis and joins the spermatic cord.

The testicular parenchyma is surrounded by two layers, tunica albuginea and tunica vaginalis. These layers are grown together as one and is called testicular capsule. Testis, epididymis and vas deferens are connected to each other by thin layers of connective meso-structures. According to Zhu et al. [12] they are termed mesoepididymis, which is situated between the testis and the epididymis, and mesodeferens, which is situated between the epididymis and the vas deferens. The testis and the epididymis are kept in position within the scrotum by another meso, which connects the vas deferens to the fascia.

1.3. The testicular parenchyma

In rodent species (rats and mice) the testicular parenchyma can be subdivided into seminiferous tubules and the interstitial space, the latter containing blood vessels and free intertubular connective tissue. In rodents the seminiferous tubules are, in contrast to humans, not separated by septa [13, 14]. As described above the testis has two main functions spermatogenesis, which takes place within the seminiferous tubules and steroidogenesis, which occurs by the Leydig cells in the interstitial space [15].

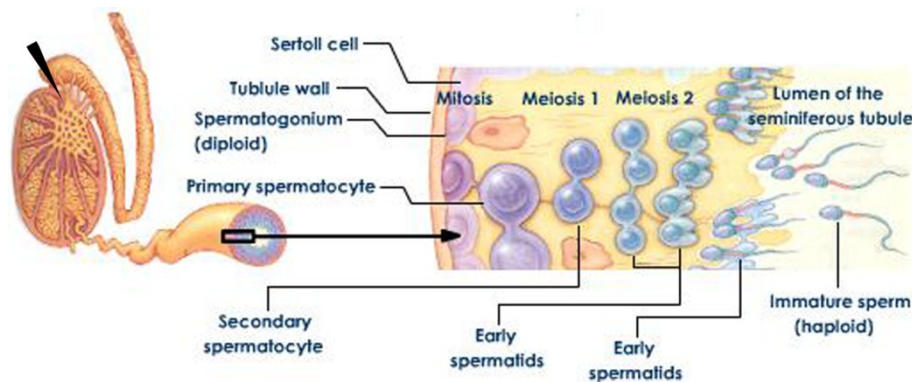


Fig. 1: Spermatogenesis

Maturing germ cells move from the basal lamina towards the lumen of the seminiferous tubule. During this journey germ cells undergo mitosis and two steps of meiosis. Haploid immature sperms leave the testis via the rete testis and are transported to the epididymis. From tutorvista.com.

1.3.1. The tubular compartment

The main cell types within seminiferous tubules are germ cells and Sertoli cells. Germ cells start to proliferate and mature with the beginning of the puberty. Different germ cell stages, embedded between the adjacent SC, are present within individual tubules (Fig. 2). SCs support the germ cells with essential nutrients, growth factors and are responsible for physical support and structure of the germ cells [17]. Each tubule is surrounded by peritubular cells (PTC) that morphologically separate germ cells and SCs from the interstitial space.

Sertoli cells provide the structural framework of the seminiferous epithelium. They are attached to the basal lamina and extend towards the tubular lumen. SCs have a columnar shape with several multiform processes [18]. In the juvenile testis they proliferate but lose this ability when the first meiotic germ cells appear. Germ cells and SC are connected to each other via adherence junctions, desmosomes and gap junctions [15, 19-21] (Fig. 2). Neighbouring SCs are forming highly specialized tight junctions (zonula occludens) near the basal lamina (Fig.2), which are capable of restricting the passage of hydrophilic molecules [22, 23]. This so called **blood-testis barrier** [23] separates the tubule in two compartments: the basal region and the adluminal region. In this way, spermatogonia and early meiotic cells in the basal region are separated from spermatocytes and spermatids in the adluminal region. Therefore, a large majority of the developing germ cells are

effectively isolated from the immune system. To make sure that the developing germ cells can move through the junctional complex the barrier is opened and closed in a coordinated fashion [24].

Peritubular cells originate from mesenchymal tissue and have a polygonal shape [25]. At least one layer of these cells as seen in rodents [26] is surrounding the seminiferous tubules (Fig. 1 & 2), but there are species specific variations. In humans five to seven layers were found [27]. Both, rat and human PTC express marker proteins such as F-actin and myosin, which are typical for smooth muscle cells [26, 28, 29]. PTCs contain contractile elements and mediate the transport of the still non-motile spermatozoa within the tubules [29, 30].

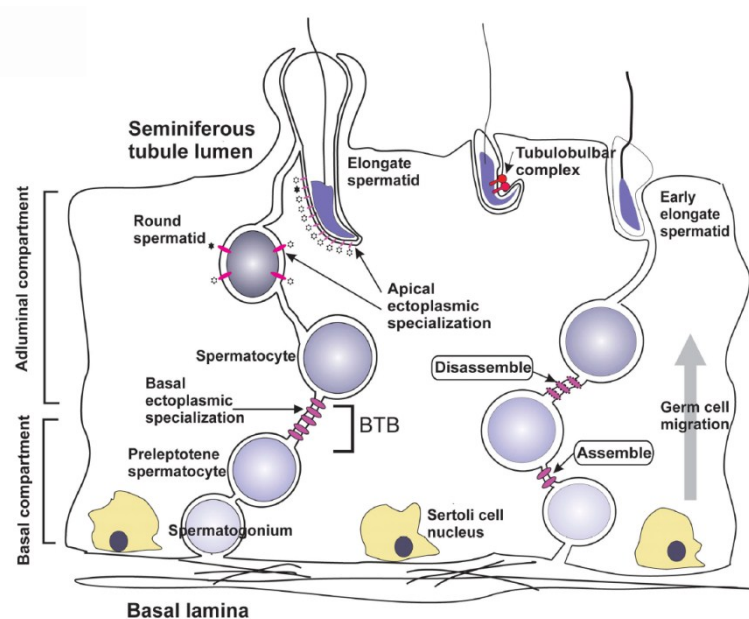


Fig. 2: Blood-testis barrier

Germ cells are embedded between the adjacent SC, which are attached to the basal lamina and extend towards the tubular lumen. Germ cells and SC are connected to each other via adherence junctions, desmosomes and gap junctions. Neighbouring SCs are forming highly specialized tight junctions (zonula occludens) near the basal lamina: the blood-testis-barrier. From [16].

1.3.2. The interstitial compartment

The interstitial space surrounds the seminiferous tubules and contains blood vessels (arterioles, capillaries and lymphatic vessels), Leydig cells, fibroblasts and immune cells (monocytes, lymphocytes, macrophages, dendritic cells, mast cells). Excluding blood vessels, 80% of the cells within the interstitial space are testosterone-producing Leydig

cells. The human interstitial compartment also contains nerve fibres which are absent in rat testicular parenchyma [12]. The arterioles, capillaries and venules of the testis completely permeate the interstitial tissue.

A variety of immune cells are found within the interstitial space in rat testis with macrophages as the largest cohort. **Testicular macrophages (TM)** are recruited into the testis by chemokines. They originate from CD68 positive monocytes [31]. Reaching their target tissue the monocytes transform into resident macrophages. During this process the cells lose the CD68 marker and start to express CD163, albeit for a certain time both markers are co-expressed. In rats these markers can be detected by specific antibodies named ED1 (CD68) and ED2 (CD163) [31-34]. The majority of the testicular macrophages express CD163. About 50% of these CD163 positive cells are either CD68 positive or negative. Around 15-20% of the total number of TM expresses only CD68. This indicates the existence of several macrophage subpopulations in different developmental stages within the rat testis [31]. TMs play an important role in inflammatory processes by secreting different cytokines. A comparable lower secretion of IL-1 and TNF- α differentiates TM from macrophages within other tissues [3, 31, 35].

1.4. Immunology of the testis

1.4.1. Immune privilege of the testis

A key element of immune privileged organs such as eye, brain or placenta [36], is the tolerance to xenografts placed within these organs. This tolerance was also demonstrated for the testis by Head et al. in 1983 [37]. The need for immune privilege within the testis results from the embryonic development of a male mammalian. To prevent immune responses against auto-antigens, the immune system has to distinguish between self- and foreign-antigens. Progenitor cells and spermatogonia are ignored by the immune system, because they existed during establishment of self-tolerance in the perinatal period. Cells appearing with and after the first meiotic division carry neo-antigens, which would spark an attack of the immune system. For a long time the protection of developing germ cells was supposed to be based only on the blood-testis-barrier, but since a few years the involvement of TM seem to be relevant too [31]. In the testis, resident macrophages, mast cells and lymphocytes show a suppressed immune response on inflammatory stimuli such as a

reduced secretion of pro-inflammatory cytokines by resident testicular macrophages. It seemed that these cells have an immune-regulatory and anti-inflammatory character, whereas fresh immigrated cells have pro-inflammatory character [31, 38].

1.4.2. Male infertility

Infertility affects one in ten couples, in nearly 50% of the cases the cause can be attributed to a factor in the male. In men, infertility can be caused for example by physical trauma, infections disease (bacteria, virus) cancer or genetic disorders. In men about 12-13%, in some studies even more, of all diagnosed infertility is related to an immunological reason [39-42].

Symptomatic and non-symptomatic inflammation of the testis (orchitis) as a result to reproductive tract infections, systemic infection and autoimmune disease such as anti-sperm antibodies lead to the disruption of testicular androgen production and spermatogenesis [38, 43, 44]. Autoimmune orchitis is characterised by auto-antibodies and immune cells targeting germ cells including spermatozoa and sperm [31, 38, 45]. Acute or chronic animal models are used for investigations of orchitis. These models mimic the immunological factors which result in male infertility. However, despite the significant progress that has been made in the identification of local, genetic, and immunological factors, the pathology of experimental autoimmune orchitis (EAO) is still not understood [46, 47].

1.4.3. Cytokines and chemokines in the testis

Pro- and anti-inflammatory mediators and the cells secreting them play a crucial role in inflammatory processes. These mediators are produced mainly by immune cells. In contrast to other organs, “inflammatory” mediators are constitutively expressed in the testis also during non-inflammatory conditions. Pro-inflammatory cytokines (TNF- α , IL-1, IL-6) effect spermatogenic cell differentiation and steroidogenesis, whereas anti-inflammatory cytokines (activin) influence the testicular development. Activin stimulates spermatogonial development *in vitro* and regulates the differentiation of the primary spermatocytes [38, 48]. Beside immune cells Leydig cells, SC and PTC also express cytokines such as IL-1 IL-6 and TGF- β .

The influence of the nervous system on inflammatory processes was shown in several studies [49, 50]. Cytokines such as TNF- α , HMGB1 or IL-1 β play an important role within this interaction [51-54]. In addition to cytokines the nervous system communicates with the immune system by ACh, the main neurotransmitter of the vagus nerve [55]. Vagus nerve stimulation and ACh are known to activate the $\alpha 7$ nAChR. This activation inhibits the expression and release of TNF- α or HMGB1 in immune cells such as macrophages [56, 57].

1.5. Experimental autoimmune orchitis: a model of inflammatory infertility in rodents

Most EAO studies are performed in rodents (mouse [58, 59] and rat [60-62]) and have been induced by active immunisation with spermatic antigens, adoptive T-cell transfer or neonatal thymectomy [46]. In this study, EAO was induced by active immunisation with testicular homogenates. Inducing of EAO in a test animal results in an acute and later on chronic inflammation provoked by the activation of immune cells, which are release pro- or anti-inflammatory cytokines [63]. With the progression of the disease histopathological alterations in the testis occur such as infiltration of lymphocytes and macrophages into the interstitium, autoantibody production, different degrees of germ cells degeneration, granuloma formation, necrosis [64], and the complete absence of spermatogenesis [60, 61, 65]. The numbers of Leydig cells are considerably lower in EAO testis [65, 66], which results in decreased serum androgen levels. Furthermore, an increased number of CD68 and CD163 positive macrophages were reported at early and late time points in orchitis [61].

2. Innervation of the testis

2.1. The nervous system and sensory neurons

The mammalian nervous system consists of two parts: the central nervous system (CNS) and peripheral nervous system (PNS). The CNS includes the brain and spinal cord, whereas all neuronal structures outside the CNS belong to the PNS. According to the innervating structures the PNS is subdivided into the somatic and visceral nervous system. The visceral nervous system is also called autonomic nervous system (ANS) and has two interacting partners the sympathetic and parasympathetic pathways.

The vertebral column is made of a species-specific amount of vertebrae, which are subdivided into four parts: cervical, thoracic, lumbar and sacral. Both rat and human have 12 thoracic vertebrae but differ in the number of the lumbar vertebrae (rats have six but human only five). The same segmentation is used for further characterisations of both spinal cord and dorsal root ganglia (DRGs) (Fig. 3A).

The cell-bodies of motoneurons are located in the spinal cord and information is transmitted from the CNS into the PNS. Sensory neurons collect information in the periphery and transmit these to the CNS. The cell-bodies are located in the DRGs (Fig. 3B).

2.2. Sensory neurons are divided in subpopulations

Sensory neurons are pseudo-unipolar neurons, which have a bifurcated axon with a peripheral and central branch (Fig. 3B). The peripheral branch terminates in specific receptors in skin, muscles or other tissues, whereas the central process enters the spinal cord and results either in the activation of local reflex circuits or in the uptake of information into the brain. Sensory neurons identify changes in the environment, which could be harmful for the organism. Their receptors, which are ubiquitous found, recognise pain, touch or temperature differences.

Four types of axons can be distinguished for sensory neurons: $A\alpha$, $A\beta$, $A\delta$ and C. Nerve fibres consisting type-A-axons are myelinated in a decreasing intensity from $A\alpha$ to $A\delta$, whereas type-C-nerve fibres (short: C-fibres) are not myelinated. The increasing myelinisation of the nerve fibres results in increasing speed of the transported signals. Nociceptive neurons, one subpopulation of sensory neurons, mediate pain. These neurons have thin myelinated ($A\delta$) or unmyelinated (C) axons (Fig. 3B).

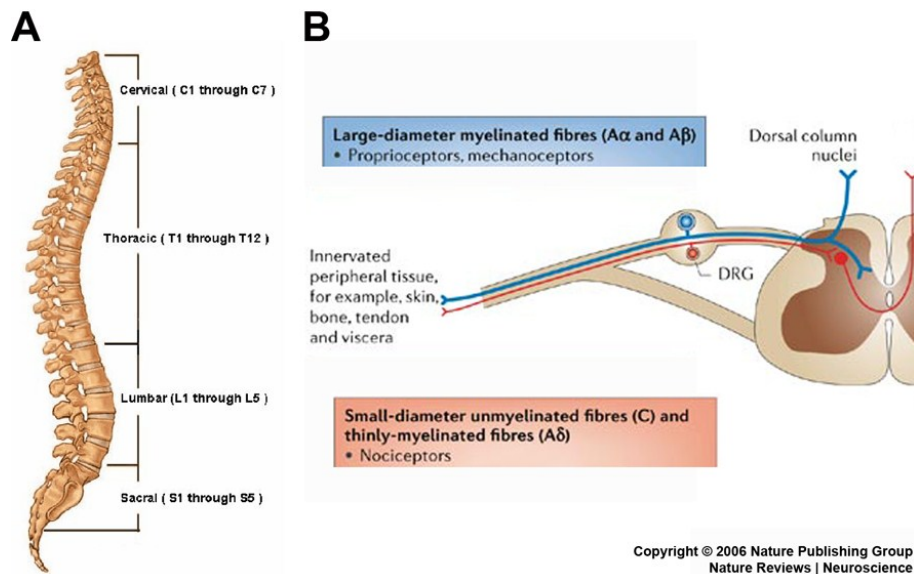


Fig. 3: Localisation of sensory neurons and segmentation of the vertebrate.

The segmentation of the human vertebrate and consequently of spinal cord and DRGs is shown in (A). The four sections (cervical, thoracic, lumbar and sacral) are inscribed within the drawing. Location and characterisation of sensory neurons is shown in (B). Primary afferent neurons have their cell bodies in DRG and transmit sensory information from the peripheral tissues to the spinal cord. Myelinated A α and A β sensory fibres are involved in detecting non-noxious sensations, including light, touch, vibration and proprioceptive stimuli. In contrast, unmyelinated C and thinly-myelinated A δ fibres are known as nociceptors and detect noxious chemicals, thermal and mechanical stimuli.

2.3. Neuronal markers

Different populations of neurons can be distinguished by several marker-molecules. Markers used in this study are described briefly below.

The **protein-gene-product-9.5** (PGP-9.5) is a pan-neuronal marker for afferent and efferent nerve fibres [67-70], but also labels cells of neuro-endocrine origin and non-neuronal cells such as porcine spermatogonia [68, 71].

The **calcitonin-gene-related-peptide** (CGRP) is a neuropeptide widely expressed in the CNS and also in the PNS. It is used as a marker for nociceptive neurons.

The **neurofilament 200** (Nf200) belongs to one of five classes of a family called intermediate filaments (IF) which have all a diameter of 8-10 nm. Neurofilaments are found predominantly in neuronal myelinated cells and nerve fibres and are distinguished by their molecular weight (68, 160 and 200 kDa) [72].

Peripherin another intermediate filament protein, was found initially in sensory neurons of the PNS, but subsequently observed in some sensory and other neurons of the CNS, neuroendocrine tumours and in insulin-producing cells of the pancreas. Peripherin labels thin myelinated and un-myelinated nerve fibres.

Vesicular glutamate transporter 1 (VGluT1) is one of three transporters expressed from sensory neurons, which is essential for the uptake of the neurotransmitter glutamate into small synaptic vesicles prior to its exocytotic release into the synapse. Beside VGluT2, VGluT1 is currently one of the best markers for glutamatergic nerve terminals and glutamatergic synapses.

Isolectin B₄ (IB4) or lectins in general are sugar-binding proteins, which occur ubiquitously in nature and have the ability to agglutinate animal cells and/or precipitate complex carbohydrates. IB4 also binds to a subpopulation of primary sensory afferent neurons in rat DRGs, which were identified as unmyelinated neurons of small diameter. The majority of these neurons supply nociception.

The **transient receptor potential vanilloid receptor subtype 1 (TRPV1, VR1)** is belonging to the transient receptor potential (TRP) superfamily, whose members are sensors for temperature. TRPV1 projects to sensory nociceptive neurons, which are sensitive to capsaicin [73]. The heat sensor TRPV1 was found to be activated at > 43°C. Beside heat and capsaicin TRPV1 can be activated by protons.

2.4. Innervation of the testis

The rat genitofemoral nerve (GF_n), arising from lumbar spinal nerves 1 and 2 [74-77], divides into a genital and femoral branch [77, 78]. Both branches split again in several ramifications. Cremaster muscle [77] and scrotal skin [74, 77, 79-81] are innervated from both femoral and genital branch whereas the spermatic cord and tunica vaginalis [82, 83] are innervated just by the genital branch of the GF_n. Dissection of GF_n results in temperature dependent decrease of testicular weight and degenerative changes of the seminiferous tubules in rats kept at 4°C [84]. A major consequence of spinal cord injury in human male patients is infertility caused by poor semen quality [85, 86]. Defective temperature regulation and impaired ejaculation were postulated to be the underlying reason by Brindley and Mallidis [87, 88]. Defective temperature regulation is supported by the finding of temperature receptors TRPV1 and TRPM8 in human and rat testis [89].

Testicular innervation in rats occurs by the superior and inferior spermatic nerve (SSN and ISN). The SSN runs alongside the testicular artery and reaches the capsule via SL, whereas the ISN accompanies the vas deferens, penetrates the epididymis and reaches the capsule via IL [12]. PGP9.5 and CPON (C-flanking peptide of neuropeptide Y) positive nerve fibres were found in the mesorchial ligaments (IL and SL), which are the source of a nerve-network innervating the capsule and the mesoepididymis [12]. Furthermore, AChE, CGRP and NPY-containing fibres have been found in the rat capsule [90, 91]. In some mammalian species, autonomic nerves are associated with testicular parenchyma and capsule [27, 92]. No nerve fibres are detectable in rat testicular parenchyma [91], whereas the human testicular parenchyma is innervated [92]. Sensory afferent terminals are generally described as “free nerve endings”. Their possible function was studied in a variety of tissues such as rodent testis [93, 94] and rat testicular capsule by Silverman and Kruger [93].

CGRP, VIP and SP positive nerve fibres innervating the human and guinea-pig vas deferens have been described without information of their neuronal supply [95, 96]. Kolbeck & Steers demonstrated by tracing-experiments the vas deferens-innervation in rats originating from ipsi-lateral DRG L1, L2, L6 and S1 [97]. Nerve fibres labelled positive for Nf200 were observed in the vas deferens of bull [98] and in the testis of bull, donkey and camel [99-101].

3. The cholinergic system

3.1. Acetylcholine

Acetylcholine (ACh), a well-known chemical neurotransmitter in both ANS and CNS, was first described by Loewi in 1921 [102]. In evolution ACh was present long time before the design of the nervous system. Uni- and multicellular organism such as bacteria, protozoa, fungi and plants produce ACh [103, 104]. In organism with a nervous system, ACh is not limited to it, but also present in non-neuronal tissue. For functional action ACh has to bind to specific receptors: the nicotinic acetylcholine receptor (nAChR) and the muscarinic acetylcholine receptor (MR).

3.2. Non-neuronal cholinergic system

The presence of a cholinergic system in mammalian non-neuronal tissue was first described for human placenta by Morris in 1966 [105]. Since then, ACh and AChRs were found in many other tissues as well as in single cells of different species (see also chap. 3.4.). Until now the complete functionality of the non-neuronal cholinergic system is not fully discovered, although some functions could be illustrated. Non-neuronal cells use ACh for inter-cell communications and regulate cellular functions by ACh-binding in an autocrine and paracrine manner [106, 107]. ACh is known to alter the morphology of cells [108], to stimulate the proliferation of lymphocytes [109, 110] and to control the cytoskeleton and cell-cell contacts [111, 112].

Beside these functions the cholinergic system seems to be involved in cancer and inflammatory processes, too. Increased cell proliferation after stimulation of nAChRs was demonstrated in cancer and non-cancer tissue such as mesothelioma [113] and human colon adenocarcinoma cell line (HT29) [114]. The up- ($\alpha 5$, $\alpha 7$, $\alpha 9$, $\beta 2$, $\beta 4$, ChAT) and down- ($\alpha 4$, AChE, M_2R) regulation of ACh-related molecules was shown in non-small-cell lung cancer (NSCLC) [115, 116]. Subsequently ACh-related molecules were analysed in NSCLC-patients, who were smokers or non-smoker. In smokers increased mRNA expression level of $\alpha 6$ and $\beta 3$ were observed [115]. The following alterations were shown in tissues and cell lines: (1) nicotine stimulation of SCLC results in cell proliferation, which can be blocked by α -Bungarotoxin (α -Bgt, *Bungarus multicinctus*) [117]; (2) treatment with nicotine stimulates and pre-treatment with mecamylamine blocks the VEGF-mediated angiogenesis in endothelial cells [118]; (3) nicotine significantly suppresses apoptosis in NSCLC mediated by nAChR $\alpha 3$ and the PI3-K/AKT pathways [119] and (4) the pro-apoptotic molecule Bad gets phosphorylated and therefore inactivated after nicotine treatment on human lung cancer cells [120].

Cytokines are essential molecules released by immune cells, which regulate inflammatory processes by acting as pro- or anti-inflammatory mediators. Nicotine or ACh are able to modulate the production of cytokines by binding to AChR [56, 57, 121]. Additionally, it was shown that nicotine and ACh enhance the phagocytic potential of macrophages [122]. The finding that electrical vagus nerve stimulation results in ameliorated disease in animal models of inflammatory conditions such as colitis [123] or peritonitis [124, 125] suggests a strong connection between the immune system and cholinergic nervous system.

3.3. Synthesis, release, degradation and recycling of acetylcholine in neuronal and non-neuronal tissue

3.3.1. Synthesis of acetylcholine

ACh is synthesised by choline acetyltransferase (ChAT, EC 2.3.1.6) from acetyl-CoA and choline within the cell. Acetyl-CoA is generated in mitochondria. It is produced during carbohydrate, protein and lipid catabolism in aerobic organism [253]. In non-neuronal cells ACh can be synthesised in two different ways via ChAT or via carnitine acetyltransferase (CarAT, EC 2.3.1.7) (Fig. 4). CarAT is an important part of the lipid metabolism and is present in the mitochondria. Both enzymes are nearly ubiquitously expressed. However, in mice and human urothelium, CarAT, but no ChAT was detected [126], whereas in rat urothelial cells the mRNA for both enzymes, ChAT and CarAT, has been demonstrated [127]. Furthermore, ChAT mRNA and ChAT protein were detected in human epithelial cells [128, 129], human immune cells [130-132], human placenta [133] and mouse embryonic stem cells [134].

3.3.2. Storage and release of acetylcholine

After its generation, ACh is translocated into small synaptic vesicles via the vesicular acetylcholine transporter (VACHT) (Fig. 4). This transporter is a 12 transmembrane-domain protein, which is acting as an H^+ /ACh exchanger. The vesicles are stored in the cell until a trigger is activating them. In neurons this trigger is the depolarisation of the nerve terminal which leads to exocytotic release of ACh. The vesicle-fusion with the presynaptic membrane is a calcium-dependent process. The extracellular ACh moves through the synaptic cleft and binds to their receptor on the postsynaptic cell.

In non-neuronal tissue VACHT could be detected for example in pulmonary arterial endothelial cells [135, 136], in parts of the rat placenta [137] and in secretory cells of airway surface epithelium [138] but the expression of VACHT is not ubiquitous in non-neuronal tissue. This implies that ACh is not stored in vesicles in all cells but is released direct from the cytoplasm. There is evidence for alternative release mechanism via organic cation transporters (OCTs) (Fig. 4).

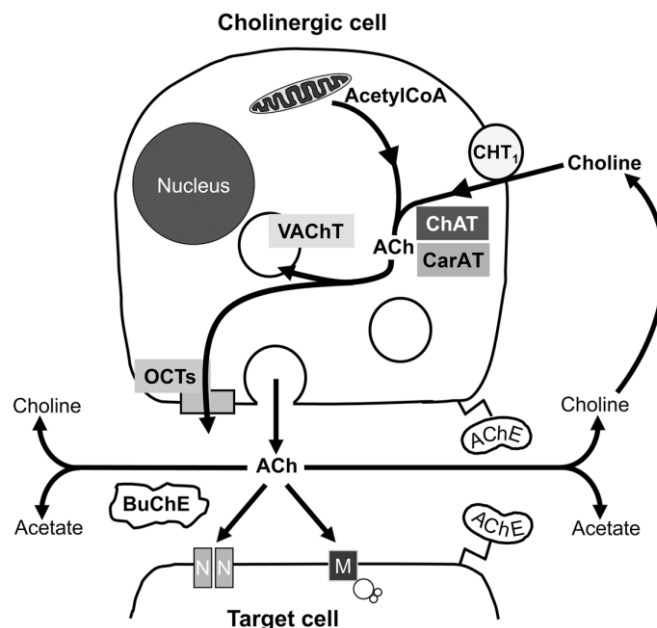


Fig. 4: Recycling pathway of acetylcholine (ACh) synthesis, release, action and breakdown at a cholinergic nerve terminal.

AChE = acetylcholinesterase, BChE = butyrylcholinesterase, ChT1 = high-affinity choline transporter-1, ChAT = choline acetyltransferase, M = muscarinic receptor, G-protein coupled, N = nicotinic receptor, ligand-gated ion channel, VAcHT = vesicular ACh transporter, OCTs = organic cation transporter. Modified after Kummer et al. [139].

OCTs are expressed on the surface of a wide range of cells. All OCTs transport small hydrophilic substances in a sodium-dependent manner. The three subtypes OCT1, 2 and 3 seem to be differentially expressed in cells or tissues. OCT subtypes could be detected in rat bronchial epithelium (OCT1/2) [140], in human placenta (OCT1/3) [141], in rat and mouse placenta (OCT3) [142, 143] and in rat kidney (OCT2) [144].

3.3.3. Degradation and recycling of acetylcholine

The action of ACh is terminated by butyrylcholinesterase (BChE) or ACh-esterase (AChE). These enzymes exist in a soluble form or bound to the membrane and are able to cleave ACh into choline and acetate (Fig. 4). Cholinergic neurons synthesise esterases by themselves to ensure equilibrium of released and degraded ACh. AChE is present in both neuronal and non-neuronal cells [145]. After degradation of ACh, choline is taken up from the extracellular space into the cell by a sodium-dependent high-affinity choline transporter (ChT1). The existence of ChT1 in non-neuronal tissue could be demonstrated for example

in rat and human epithelial and vascular smooth muscle cells [127, 146]. In addition to its role as a precursor for ACh choline is an essential molecule within plasma membrane lipids, e.g. in the form of phosphatidylcholine. For the ACh-synthesis, the uptake of choline via ChT1 is the rate limiting step (Fig. 4). Therefore choline uptake is crucial for every cell. Beside ChT1 and the OCTs the choline transporter-like (CTL) proteins of the CTL family are established choline transporters [147], which could be an alternative way of importing choline into the cell in the absence of ChT1.

3.4. Acetylcholine receptors

Acetylcholine receptors are two structurally diverse classes of membrane-bound proteins, the ionotropic nicotinic AChR and the metabotropic muscarinic AChR. The receptors are named after their selective agonists: (1) nicotine, which is an alkaloid of the tobacco plant and (2) muscarine, which is an alkaloid of fly agaric (*Amanita muscaria*) [148] (Fig. 5). Both receptor classes differ in structure, function and their underlying signalling system [149]. For one example, nAChR are fast acting receptors, whereas activation of MRs leads to latency in response.

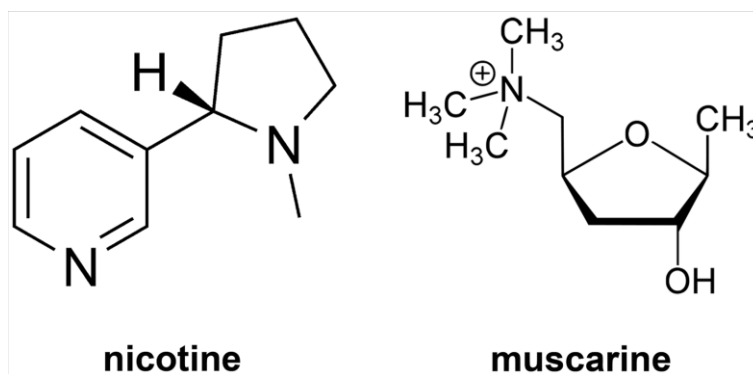


Fig. 5: Nicotine and muscarine.

Nicotine ($C_{10}H_{14}N_2$) is an alkaloid found in the nightshade family of plants (*Solanaceae*) such as tobacco. Muscarine ($C_9H_{20}NO_2^+$) is a natural product found in certain mushrooms and was first isolated from *Amanita muscaria* in 1869.

3.4.1. Structure and functionality of nicotinic acetylcholine receptors

AChR can be distinguished in muscle-type, which is situated at skeletal-muscle neuromuscular junctions, and neuronal-type, which is situated in the nervous system. The muscle-type nAChR exist as embryonal- and adult- heteropentameric isoform. The muscle-type contains 5 subunits: $\alpha 1$, $\beta 1$, γ , δ and ϵ with fixed compositions: (1) $[(\alpha 1)_2\beta 1\gamma\delta]$ in embryonic tissue and non-innervated muscles and (2) $[(\alpha 1)_2\beta 1\delta\epsilon]$ in adult muscles [152] (Fig. 6A).

The neuronal-type nAChR exist as homo- and heteropentamers. The neuronal-types, which are present in neuronal and non-neuronal tissues, consist of 12 subunits $\alpha 2$ - $\alpha 10$ and $\beta 2$ - $\beta 4$. With the exception of $\alpha 8$, all α -subunits and $\beta 2$ - $\beta 4$ have been described in mammals [153-155]. nAChR subunit $\alpha 8$ is only expressed in chicken/avian species [156]. Most of the nAChR subunits form heteropentamers. Only $\alpha 7$, $\alpha 8$ and $\alpha 9$ are able to homopentamer-formation (Fig. 6A). The subunits show a homology in the amino acid sequence with app. 30-40% identity of amino acid residues mainly in hydrophobic regions [150, 151]. nAChR α -subunits can be subdivided due to their sensitivity to snake α -toxins such as α -bungarotoxin. α -Bgt-sensitive subunits are $\alpha 7$ - $\alpha 10$ [154, 157-159] and the nAChR at the motoric endplate [160]. α -Bgt-non-sensitive subunits are $\alpha 2$ - $\alpha 6$ and $\beta 2$ - $\beta 4$ [153, 161-163]. Table 1 & 2 show the known possible combinations of nAChR oligomers subdivided in α -Bgt-sensitive and α -Bgt non-sensitive subunits.

Tab. 1: α -Bgt-sensitive receptors.

receptor composition	reference(s)
$\alpha 7$	[164, 165]
$\alpha 7\beta 2$	[166]
$\alpha 7\beta 3$	[167]
$\alpha 3\alpha 7\beta$	[168]
$\alpha 3\alpha 5\alpha 7\beta$	[168]
$\alpha 5\alpha 7\beta$	[169]
$\alpha 9$	[159, 170]
$\alpha 9\alpha 10$	[159, 170]

Receptor composition of nAChR-subunits $\alpha 7$, $\alpha 9$, $\alpha 10$ in vertebrate. Modified after Lips and Gotti [138, 171].

Tab. 2: α -Bgt non-sensitive receptors.

receptor composition	reference(s)		receptor composition	reference(s)
$\alpha 2\beta 2$	[172, 173]		$\alpha 3\alpha 5\beta 4$	[174]
$\alpha 2\beta 4$	[172, 173]		$\alpha 3\alpha 6\beta 2$	[185]
$\alpha 3\beta 2$	[173, 174]		$\alpha 3\alpha 6\beta 4$	[180, 185]
$\alpha 3\beta 3$	[175]		$\alpha 3\beta 3\beta 4$	[186]
$\alpha 3\beta 4$	[173, 174]		$\alpha 4\alpha 5\beta 2$	[176, 187]
$\alpha 4\beta 2$	[176-178]		$\alpha 4\beta 2\beta 3$	[188]
$\alpha 4\beta 4$	[173]		$\alpha 5\alpha 6\beta 2$	[185]
$\alpha 6\beta 2$	[179]		$\alpha 6\beta 2\beta 3$	[189]
$\alpha 6\beta 3$	[175]		$\alpha 6\beta 3\beta 4$	[185, 190]
$\alpha 6\beta 4$	[180]		$\alpha 3\alpha 5\beta 2\beta 4$	[191]
$\alpha 2\alpha 4\beta 2$	[181]		$\alpha 3\alpha 6\beta 3\beta 4$	[190]
$\alpha 2\alpha 5\beta 2$	[182]		$\alpha 4\alpha 5\alpha 6\beta 2$	[192]
$\alpha 2\alpha 6\beta 2$	[183]		$\alpha 4\beta 2\beta 3\beta 4$	[186]
$\alpha 3\alpha 4\beta 2$	[184]		$\alpha 4\alpha 6\beta 2\beta 3$	[183]
$\alpha 3\alpha 4\beta 4$	[184]			
$\alpha 3\alpha 5\beta 2$	[174]			

Receptor composition of nAChR-subunits $\alpha 2$ - $\alpha 6$, $\beta 2$ - $\beta 4$ in vertebrate. Modified after Lips and Gotti [138, 171].

nAChR are responsible for the cholinergic neurotransmission within the CNS. They mediate the excitatory postsynaptic potential on postsynaptic cells [193] and are able to regulate the release of neurotransmitter on presynaptic cells [194, 195].

The subunit composition of nAChR influences their functions such as (1) ligand- specificity and ligand-affinity, (2) permeability for cations and (3) and pharmacology [196, 197]. The binding of a ligand to a nAChR leads to conformational changes in the receptor structure. This process is reversible. Antagonists are able to block the permeability for ions by binding to the nAChR. The blocking of the nAChR can be reversible (methyllycaconitin, mecamylamine) or irreversible (α -Bgt). The permeability for cations (Ca^{2+} , Na^+ , K^+ and Mg^{2+}) is dependent on the subunit composition of the nAChR (Fig. 6A) [198, 199]. α -Bgt-sensitive nAChR show high permeability for Ca^{2+} and Mg^{2+} but lower permeability for Na^+ and K^+ ([156, 165]. Homopentamers and nAChR containing $\alpha 7$ -subunit show a distinct high permeability for Ca^{2+} [200]. α -Bgt non-sensitive nAChR show high permeability for Na^+ but lower permeability for Ca^{2+} [187].

The receptor activation leads to a Ca^{2+} -current, which changes the membrane potential and activates or mediates intracellular signalling pathways such as transmitter-release [194] and gene expression [201].

Na^+ -influx depolarises the cell membrane and activates voltage-dependent Ca^{2+} -channels with a following Ca^{2+} -influx [200, 202]. The release of Ca^{2+} from intracellular Ca^{2+} -depots is also possible. The consequence of this mechanisms is a prolonged intracellular Ca^{2+} -signalling [200, 203-205].

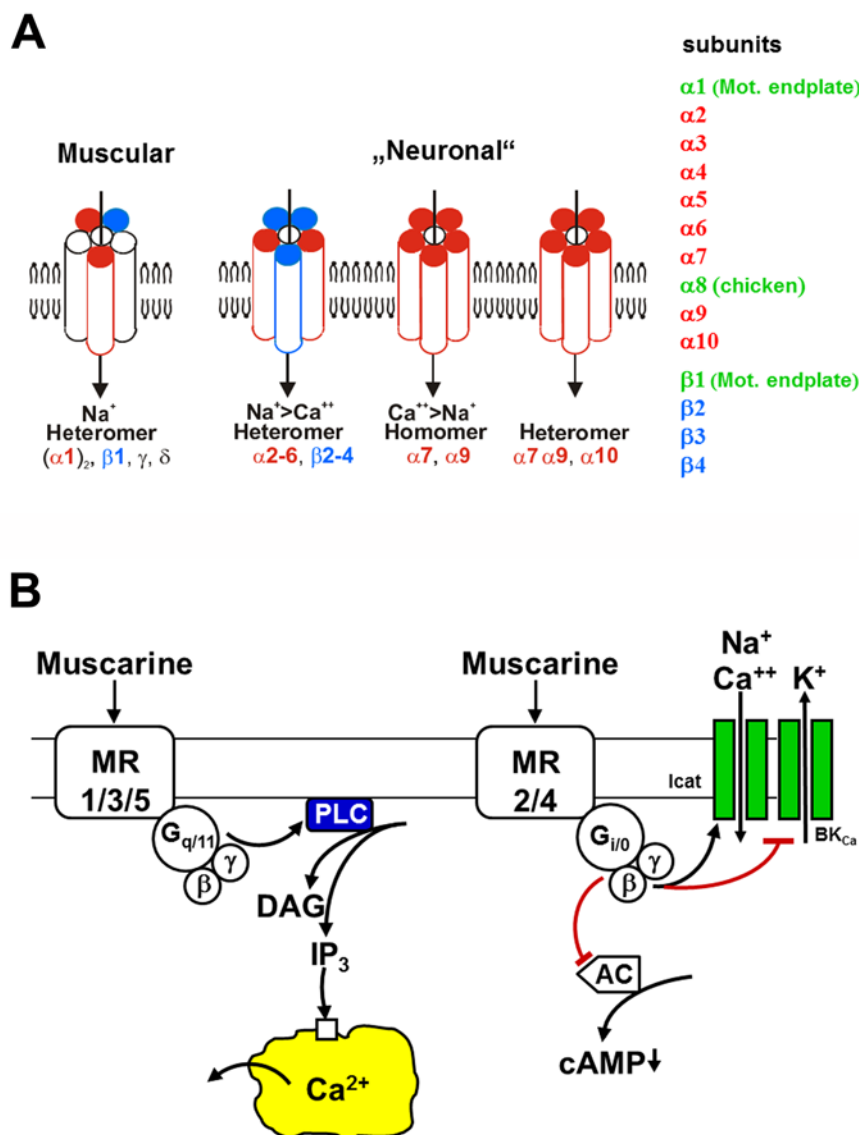


Fig. 6: Muscarinic and nicotinic ACh receptors

The vertebrate nAChR subunits, the pentameric structure of the subunits and resulting permeability for ion channels are shown in (A). The MR subtypes subdivided regarding their preference for specific GPCR α -subunits and their resulting intracellular signalling pathway are shown in (B).

3.4.2. Structure and functionality of muscarinic acetylcholine receptors

The first evidence for the existence of MR was reported in an investigation with respect to heart-function by Riker and Wesco in 1951 [206]. Today, five receptor subtypes, encoded by intron-less genes (m1-m5), are known from several species including human, mouse and rat [206-208]. The MR exhibit a high sequence homology across species and form heptahelical G-protein-coupled receptors (GPCR). More than 100 members are known belonging to the GPCRs [209]. All these receptors share a common structure with: (1) seven transmembrane-domains connected to each other by intra- and extracellular loops, (2) an extracellular ligand binding site, (3) an intracellular C- and extracellular N-terminus and (4) the ability to couple to a cytoplasmic heterotrimeric G-protein [206, 210].

MRs are widely expressed in neuronal and non-neuronal cells. Individual subtypes are predominantly expressed in specific tissues like M₂R in the myocardium [211] and, together with M₃R, in smooth muscle cells [212]. The presence of M₃R within the CNS is markedly lower than other MR subtypes [213-215]. M₄R and M₅R are predominantly expressed by dopaminergic neurons [213, 216, 217]. The presences of MR-subtypes could be demonstrated in non-neuronal tissue such as human macrophages [218] or mouse trachea [219, 220]. Receptor activation is known to mediate proliferation and differentiation in embryonic cells, DRGs and Schwann cells [221].

MRs are coupled to G-proteins which consist of three subunits α , β and γ (Fig. 6B). The 20 known α -subunits are subdivided into four families G α s, G α i/o, G α q/11, and G α 12/13 [222].

The G-protein, which is associated with the cell membrane, is not couple to the MR in the absence of an agonist. The binding of a ligand results in a conformational change of the receptor, which allows interaction with a G-protein. After the receptor and the G-protein are coupled to each other, GDP is replaced by GTP and the α -subunit leaves the $\alpha\beta\gamma$ -complex. The β and γ subunits stay together [223]. G-proteins regulate intracellular functions via effector molecules such as ion channel activity, transporters, gene transcription or secretion. These down-stream intracellular functions are defined by the α -subunit-family-member located within the G-protein-complex and its interaction with the receptor- and effector-molecule (Fig. 6B).

Muscarinic receptor subtypes M_2 and M_4 preferentially couple to $G_{ai/o}$ and subtypes M_1 , M_3 and M_5 to $G_{aq/11}$ [224]. For a long time, it seemed to be that the $\beta\gamma$ -complex is not active, but there is evidence for its activating function of phospholipase C (PLC) and the opening of ion channels [225].

G_{aq} activates the plasma-membrane-bound enzyme phospholipase C- β (PLC- β). This enzyme transforms phosphatidylinositol-4,5-bisphosphate [PI(4,5)P₂] into inositol-1,4,5-trisphosphate (IP₃) and diacylglycerol (DAG). IP₃, a soluble molecule, diffuses to the endoplasmic reticulum (ER) and binds to IP₃-gated Ca^{2+} -release channels. After opening these channels the Ca^{2+} stored in the ER is liberated into the cytosol. DAG activates protein kinase C (PKC), which translocate from the cytosol to the plasma membrane. PKC activates its targets in a cell dependent manner [223, 226]. The transmembrane protein adenylate cyclase (AC) is inhibited by binding to a G_{ai} -subunit and activated by binding to a G_{as} -subunit. The binding of ACh to M_2R or M_4R activates G_{ai} , which then competes with G_{as} for the α -subunit binding-site within the $\alpha\beta\gamma$ -complex. This results in a decreasing cAMP formation, which leads to a reduced activity of the cyclic-AMP-dependent protein kinase (PKA) [223, 224, 226]. Additionally, the binding of ACh to M_2R or M_4R mediates a prolonged opening of potassium channels or non-selective cation channels [224].

3.5. Cholinergic system within the testis

Up to now, the knowledge about the presence and function of the cholinergic system within the testis is far from complete. There is evidence of its presence but neither a cell specific localisation nor its function is established. Bacetti et al. found nAChR-like molecules in post-acrosomal and mid-piece region of rabbit, ram and human sperm [227]. nAChRs containing the $\alpha 7$ -subunit are involved in acrosome reaction in humans [228, 229], whereas the absence of subunit $\alpha 7$ results in impaired sperm motility in mice [230]. Additionally, nAChR subunits $\alpha 3$, $\alpha 5$, $\alpha 9$ and $\beta 4$ were found in human sperm [231] and treatment with ACh causes an increase of intracellular calcium in human sperm [232]. AChE-R, which is a stress-induced AChE-splice variant (AChE-R), is up-regulated in the testis of mice and humans and dependent on its binding partners. AChE-R can mediate apoptosis or elevates sperm motility within the testis [233].

Studies focusing more detailed in cell populations demonstrated a decreased testosterone secretion of Leydig cells after ACh and nicotine application [234], the presence of M_1R to

M₃R in SC [235], and predicted the activation of Sertoli cell proliferation by muscarinic AChR [236]. Muscarinic AChR subtypes found in rat epididymis [237] are influenced by the testosterone level [238]. Orchidectomy decreased the level of m2 transcript, but increased the level of m3 transcript in rats. These effects on m2 and m3 transcripts were prevented by testosterone replacement to castrated rats [238].

4. Aim of this study

Male infertility can be caused by physical trauma, infections disease, cancer or genetic disorders but can also be related to immunological reasons or smoking [39-42]. In the male, nicotine as major component of cigarette smoke showed impairment of spermatogenesis and steroidogenesis [239-241]. The disruption of testicular androgen production and spermatogenesis can also be caused by inflammation of the testis (orchitis) as a result of infection and autoimmune reactions to testicular and sperm antigens [38, 43, 63]. Interestingly, an involvement of nAChR in counterbalancing inflammatory effects was documented recently [49, 54, 55]. Recently, the presence of ACh was determined in testicular homogenates [414]. The absence of nerve fibres in the testicular parenchyma of rats [12], indicates a non-neuronal source for ACh.

The present study aimed to determine nAChR-subunits and MR-subtypes as putative targets for ACh in testicular parenchyma and -capsule. Subsequently, molecules related to the ACh-system should be investigated for isolated TM, PTC and SC. Changes in $[Ca^{2+}]_i$ after stimulation with agonists could determine a neuronal-like function of AChR. Moreover, changes in expression levels should be monitored in a model of experimental autoimmune orchitis to reveal a possible involvement of ACh in counterbalancing testicular inflammation.

Materials and Methods

5. Animals and tissues

5.1. Animals

Male Wistar Furth rats and male C57/BL6 mice, both 8-12 weeks old, were used for organ collections and subsequent *in vitro* experiments. Male Wistar Kyoto rats (10 weeks old) were used for the *in vivo* experiment. The animals were kept in a 12 h light, 12 h dark cycle at 22°C. They had free access to food pellets and water. For the experiments at Flinders University Adelaide, Australia, the rats and mice were purchased from the animal house of the Flinders Medical Centre (FMC), Adelaide. For the experiments, which were conducted at the Justus-Liebig-University Giessen, Germany, the rats were purchased from Harlan Winkelmann (Borchen, Germany, *in vitro* experiments) or Charles River Laboratories (Sulzfeld/Kisslegg, Germany, *in vivo* experiments). The animal experiments were approved by the local animal welfare committees (Giessen: Regierungspraesidium; Adelaide: project 645/07, Animal welfare committee 19.12.2007). For *in vitro* experiments both rats and mice were killed with an overdose of isoflurane (1-chloro-2,2,2-trifluoroethyl difluoromethyl) and tissue samples were collected.

5.2. Tissue culture

5.2.1. Isolation of testicular macrophages

Testicular macrophages (TM) were isolated from two testes without any enzymatic treatment. The testes were decapsulated in 10 ml pre-warmed endotoxin-free DMEM:F12 medium (PAA Laboratories, Coelbe, Germany). The seminiferous tubules were gently separated using straight Semken forceps and the volume was adjusted to 50 ml. After gently stirring for 3 to 4 times the tubule fragments were allowed to settle for 5 min before the supernatant was centrifuged at 300 g for 10 min at room temperature. The interstitial cell pellet was resuspended in 5 ml DMEM:F12. The cell suspension was plated as required in a 60 mm cell culture dish, a 6-well-multidish or on glass coverslips in a 24-well-multidish and incubated at 32°C and 5% CO₂. The differentiation between TM and the remaining interstitial cells

occurred by the fast adherence of the TM to plastic or glass surfaces. Contaminating cells were removed by washing. After the first 30 min cells, which were not attached to the surface, were removed by rotating the plate and changing the medium 2 to 3 times. 30 min later TMs were washed by gently pipetting directly on the surface of the dish until loosely attached cells detached.

5.2.2. Isolation of peritubular cells and Sertoli cells

Peritubular- and Sertoli cells were isolated from 18-19 days old male Wistar rats (Charles River). Testes were removed, disinfected in 1% iodine-ethanol once and rinsed three times in PBS-G (without Ca^{2+} and Mg^{2+} , with 1000 U/ml penicillin and 1000 U/ml streptomycin all from PAA and 750 mg D-glucose [Merck, Darmstadt, Germany]). After decapsulation, the tissue was minced in PBS-G and the testes fragments were trypsinised (2.5 mg/ml trypsin [Boehringer, Mannheim, Germany] and 20 $\mu\text{g}/\text{ml}$ DNase I [Boehringer] in PBS-G) for 10-15 min at 32°C and 140 rpm. The enzymatic reaction was stopped with 5 mg/ml trypsin-inhibitor (Boehringer) in PBS-G and tubule fragments were allowed to settle for 10 min. The pellet was resuspended in 10 ml of 2.5 mg/ml trypsin-inhibitor in PBS-G, and incubated for 5 min. Afterwards the tubules were washed eight to ten times with 25 ml PBS-G with intermittent settling for 8 min. Subsequently, the fragmented tubules were incubated with 1 mg/ml collagenase (Boehringer), 1 mg/ml hyaluronidase (Boehringer) and 20 $\mu\text{g}/\text{ml}$ DNase I in PBS-G for 10-15 min at 32°C in a shaking water bath (120 rpm). After adding 20 ml of PBS-G the tubule fragments were allowed to settle for about 10 min.

The supernatant containing the PTC, was removed carefully, supplemented with 20 ml RPMI-A (with 12.5 ml L-glutamine, 1000 U/ml penicillin, 10% FCS and 100 $\mu\text{g}/\text{ml}$ streptomycin; all PAA) and centrifuged at 300 g for 10 min at room temperature. The PTC pellet was resuspended within 30 ml RPMI-A, the cells were seeded in 75 cm^2 -culture flasks (5 ml/flask) and incubated at 37°C with 5% CO_2 . After three passages (day 3, 5 and 7 after isolation) by briefly trypsinising (0.05% trypsin and 0.02% EDTA [Merck] for 3 min) and splitting (1:2) the cells were seeded on glass coverslips in a 24-well multidishes or in a 6-well-multidishes with a density of

5×10^5 /well during the last splitting. Before experimental usage at day 9 PTC were incubated 24 h with RPMI without FCS.

For the isolation of SC, the remaining seminiferous tubule fragments were washed five to six times in PBS-G before incubating in 20 ml of 1 mg/ml hyaluronidase and 10 mg/ml DNase I in PBS-G for 10-15 min at 32°C and 120 rpm. After the tubules were digested in small fragments they were rinsed five times in PBS-G, resuspended in RPMI-B (without FCS) and passed through an 18G needle for better separation. SC were cultured in RPMI-B at a density of about 4×10^6 /well in 6-well multi-dish and 5×10^5 /well on glass coverslips in a 24-well multidish. After 3 days, the contaminating germ cells were lysed by hypotonic shock treatment in 20 mM Tris-HCl (pH 7.4) for 15-30 s and washed away using PBS-G. Sertoli cells were allowed to recover 3 more days before experimental setup.

6. Molecular biology

6.1. RNA isolation

Rat and mouse testes were taken and vas deferens, blood vessels and the epididymis were removed. The testis was decapsulated and 30 mg of the rat testicular parenchyma and the whole testicular capsule was shock frozen in liquid nitrogen. Due to the limited amount of material per mouse, the complete parenchyma of one testis and one or both testicular capsules were used for the isolation of total RNA. In addition, control samples (liver, heart, spinal cord, dorsal root ganglia) were collected. The tissues were stored at -80°C until further use. Primary isolated cells were washed twice with PBS, lysed in RLT lysis buffer (Qiagen; Doncaster, Australia and Hilden, Germany) and frozen at -80°C.

Total RNA was isolated with the RNeasy Mini or Micro Kit (Qiagen) depending on the amount of tissue or cells. 350 to 600 µl lysis buffer (RLT, including 1% β-mercaptoethanol) were added to the frozen tissue and then homogenized with a tissue lyser (Qiagen) using RNA-free 2 mm iron balls for 3 to 6 min at 30 Hz. Afterwards the homogenate was centrifuged for 5 min at 13 000 g and the supernatant was collected. The cell culture samples were homogenized passing the cell lysate 5 times through a 26G or 27G needle. The lysate was not centrifuged. The following

precipitation of the nucleic acids, loading on the column and the wash steps with RW1 and RPE buffer occurred according to the manufacture's manual.

For on column DNA removal 10 µl DNase A (27.27 U) and 70 µl RDD DNA digest-buffer (Qiagen) were mixed and added to the column for 15-25 min at room temperature. The RNA was eluted with 15 to 50 µl of RNase-free water depending on the expected amount of RNA. The concentration of the total RNA was measured using a spectrophotometer (Nanodrop, peqlab, Erlangen, Germany) and RNA was stored at -80°C.

6.2. Examination of RNA quality

The quality of total RNA especially contaminations with genomic DNA were analysed by standard PCR or performance of positive and negative RT-PCR.

For samples with a high amount of RNA such as TP, TC or PTC, reverse transcription (RT) was performed as a positive and negative RT (-RT in absence of RT-transcriptase). The +RT (cDNA) and the -RT samples were checked using standard PCR and primer for a reference or housekeeping gene (HKG) such as β -actin. The PCR was performed with 25 cycles for +RT and with 50 cycles for -RT. For samples with a low amount of RNA, such as primary cell culture of TM, RNA was examined using standard PCR with 50 cycles and primer for a HKG to detect possible DNA contaminations. Samples with no DNA contamination were transcribed into cDNA and the relative quality was checked using standard PCR with primer for a HKG and 25 cycles.

The PCR products were mixed with 1x DNA-sample buffer and separated by electrophoresis using the Wide Mini-Sub®Cell-System and the PowerPac 200 power-supply (Bio-Rad: Munich, Germany; Gladesvill, Australia) with a 1.8% agarose gel (Invitrogen, Eugene, USA). The agarose was dissolved in TAE containing ethidiumbromid (0,00001%). 10 µl TriDye 100 bp DNA ladder (New England Bio Labs, Genesearch PTY. LTD, Arundel, AUS) or 100 bp DNA leader (Promega, Heidelberg, Germany) were used as a marker. The GeneGenius Bio Imaging System (Syngene, In Vitro Technologies, Noble Park, Australia) and Intas (Goettingen, Germany) were used to visualise the DNA.

TAE (Tris acetate EDTA buffer)

	50x	1x	
Tris base	242 g	4.84 g	adjust to 1000 ml and pH 8.0
0.5 M EDTA	100 ml	2 ml	
glacial acetic acid	57.1 ml	1.142 ml	

10x DNA-sample buffer

100% glycerol	30% (v/v)
xylene-cyanol FF	0.25% (w/v)
orange G	0.25% (w/v)

6.3. Reverse transcription

Reverse transcription is a process which enables some RNA-viruses to integrate their RNA-genome into the host DNA-genome by transcription of RNA into DNA. The iScript cDNA synthesis Kit (Bio-Rad) uses the RNase H⁺ reverse transcriptase from Moloney Murine Leukemia Virus (M-MLV). 1 µg RNA was mixed with 4 µl RT-reaction buffer containing premixed RNase-inhibitor to prevent indiscriminate degradation of RNA template, oligo (dT), random primer to ensure complete and unbiased RNA sequence representation and 1 µl reverse transcriptase. The 20 µl reaction was incubated for 5 min at 25°C and 30 min at 42°C. The transcriptase was then heat inactivated for 5 min at 85°C. The cDNA was stored at -20°C.

6.4. Polymerase chain reaction**6.4.1. Primer design**

For analysing the mRNA expression level within the target tissue primer directed against rat or mouse specific mRNA sequences were designed. Information regarding the mRNA sequences for the genes has been obtained from Pubmed (<http://www.ncbi.nlm.nih.gov/pubmed/>). Each sequence was aligned with the rat or mouse genome to determine intron-spanning sites within the mRNA of interest.

Tab. 3: Rat primer sequences for MR.

target		sequence (5' → 3')	length (bp) localisation	accession number
rM1_204	fw	AGCAGCAGCTCAGAGAGGTC	204	NM_080773
	rev	GGGCATCTTGATCACCACCTT	(712-915)	
rM1_110	fw	TCCCTGTCACGGTCATGTGTA	110	NM_080773
	rev	ACCACCTTTGCCTGGTGTCT	(595-705)	
rM2_193	fw	CGAGTCTGGTGCAAGGAAGA	193	AB017655
	rev	CTCATATTGGAGGCCACAGC	(698-890)	
rM2_192	fw	TGCCTCCGTTATGAATCTCC	192	AB017655
	rev	TCCACAGTCCTCACCCCTAC	(324-515)	
rM3_140	fw	TACGGTCGCTGTCACTTCTG	140	NM_012527
	rev	TCATCGGAGGAAGCAGAGTT	(959-1098)	
rM3_287	fw	AGGTTTGCTCTCAAGACCAG	287	NM_012527
	rev	CACAAGAGGAGCGTCTTGAA	(1433-1719)	
rM4_163	fw	GACGGTGCCTGATAACCAGT	163	XM_345403
	rev	CTCAGGTCGATGCTTGTGAA	(1005-1167)	
rM4_166	fw	TCGATCGTTACTTCTGCGTCA	166	XM_345403
	rev	TTATCAGGCACCGTCCTCTTG	(854-1019)	
rM5_118	fw	CCACCACTGACCCTGTCTTT	118	NM_017362
	rev	CTGTTTTTCAGTCCGGGTGTT	(1914-2031)	
rM5_180	fw	GACAGAGAAGCGAACCAAGGA	180	NM_017362
	rev	GAGGTGCTTCTACGGGAGGAT	(1626-1806)	

Sequences for forward (fw.) and reverse (rev.) primers are given in 5' → 3' order. First column: r = rat, M1-5 = MR-subtype, number = length of expected PCR-product.

Tab. 4: Rat primer sequences for pro-inflammatory molecules.

target		sequence (5' → 3')	length (bp)	accession number
MCP-1 (CCL2)		Qiagen: QT00183253	117	NM_031530
IL-6		Qiagen: QT00182896	128	NM_012589
TNF-α	fw	GCCTCTTCTCATTCTGCTC	101	AJ002278
	rev	CCCATTGGAACCTTCTCCT		

Sequences for forward (fw.) and reverse (rev.) primers are given in 5' → 3' order.

Tab. 5: Rat primer sequences for nAChR.

target		sequence (5' → 3')	length (bp) localisation	accession number
$\alpha 1_{285}$	fw	AACTTCATGGAGAGCGGAGA	285	NM_
	rev	CAGCTCCACAATGACGAGAA	(626-910)	024485
$\alpha 2_{216}$	fw	GGAGCAGATGGAGAGGACAG	216	NM_
	rev	AGCACAGTGAGGCAGGAGAT	(874-1089)	133420
$\alpha 3_{208}$	fw	GCCAACCTCACAAGAAGCTC	208	NM_
	rev	CCAGGATGAAAACCCAGAGA	(1231-1438)	052805
$\alpha 4_{137}$	fw	GGACCTGGTGACTACGAGA	137	NM_
	rev	CATAGAACAGGTGGGCCTTG	(315-452)	024354
$\alpha 5_{112}$	fw	CACGTCGTGAAAGAGAACGA	112	NM_
	rev	TCCCAATGATTGACACCAGA	(1270-1381)	017078
$\alpha 6_{286}$	fw	ACAGCTCTTCCACACGCTCT	286	NM_
	rev	GAAGTCACCGACGGCATTAT	(283-568)	057184
$\alpha 6_{139}$	fw	GCTCTTCGCCCCACTACAACC	139	NM_
	rev	CAGCCACAGATTGGTCTCCA	(298-436)	057184
$\alpha 7_{286}$	fw	GGCTCTGCTGGTATTCTTGC	286	NM_
	rev	AAACCATGCACACCAGTTCA	(741-1026)	012832
$\alpha 9_{142}$	fw	CGTGGGATCGAGACCAGTAT	142	AY 574257
	rev	TCATATCGCAGCACACATT	(278-419)	
$\alpha 9_{242}$	fw	CGTGGGATCGAGACCAGTAT	242	NM_
	rev	AAAGGTCAGGTTGCACTGCT	(365-606)	022930
$\alpha 10_{317}$	fw	CTGCTGACTCTGGGGAGAAG	317	NM_
	rev	GGCTGACTCTAGTGGCTTGG	(845-1161)	022639
$\alpha 10_{107}$	fw	GTGCCACTCATCGGAAAGTA	107	NM_
	rev	TGTGCATTAGGGCCACAGTA	(946-1052)	022639
$\alpha 10_{168}$	fw	TCTGACCTCACAACCCACAA	168	NM_
	rev	TCCTGTCTCAGCCTCCATGT	(1561-1728)	022639
$\beta 1_{206}$	fw	CATCGAGTCTCTCCGTGTCA	206	NM_
	rev	TGCAATTCTGCCAGTCAAAG	(361-566)	012528
$\beta 2_{142}$	fw	AAGCCTGAGGACTTCGACAA	142	NM_
	rev	TGCCATCATAGGAGACCACA	(468-609)	019297
$\beta 3_{196}$	fw	CACTCTGCGCTTGAAAGGAA	196	NM_
	rev	GCGGACCCATTCTGGTAAC	(135-330)	133597
$\beta 4_{371}$	fw	CTCCTGAACAAAACCCGGTA	371	NM_
	rev	ACCTCAATCTTGCAGGCACT	(97-467)	052806

Sequences for forward (fw.) and reverse (rev.) primers are given in 5' → 3' order. All primer sequences except $\alpha 2_{216}$ and $\alpha 10_{168}$ are intron-spanning. First column: α and β = nAChR subunits, number = length of expected PCR-product.

Subsequently, primers were automatically designed using the Pubmed primer- Basic Local Alignment Search Tool (BLAST) programme ([http://www.ncbi.nlm.nih.gov/tools/primer-blast/index.cgi? LINK_LOC= BlastHome Ad](http://www.ncbi.nlm.nih.gov/tools/primer-blast/index.cgi?LINK_LOC=BlastHome_Ad)) with the following parameters: melting temperature 60°C, primer length 20 bp and PCR product length

100-300 bp (Tab. 3, 5-7). If possible, intron-spanning primers were constructed to prevent false positive amplification results from DNA contamination within the RNA. DNA-contaminations would result in a bigger amplification product compared to the expected amplicon. Primers were ordered by Sigma (Sigma-Aldrich, Castle Hill, Australia) and Eurofins (MWG Operon, Ebersberg, Germany). In some cases, several alternative primer-pairs were used for the same target such as rM1_204 and rM1_110 (Tab. 3). The length of the expected PCR-product is part of the primer-name. Different primer-variants can be distinguished by the number (primer-length) within the primer-name.

Tab. 6: Rat primer sequences for ChAT, transporter and HKG.

target		sequence (5' → 3')	length (bp) localisation	accession number
rChAT_272	fw	TGAACGCCTGCCTCCATTCGGC CTGCTGA	272 (1017-1289)	XM- 224626
	rev	GTGCCATCTCGGCCACCACG AACTGCA		
rVACHT_149	fw	GCCACATCGTTCACTCTCTTG	149 (1319-1467)	X80395
	rev	CGGTTCATCAAGCAACACATC		
rOCT2_226	fw	GCCTCCTGATCCTGGCTG	226 (780-1005)	X98334
	rev	GGTGTCAGGTTCTGAAGAGAG		
rOCT2_162	fw	ATCACGCCTTTCCTCGTCTA	162 (1475-1636)	X98334
	rev	CTGCATATTCTCGGCATCCT		
rCHT_189	fw	ATGGCTCTACCAGCCATTTG	189 (1073-1261)	AB030947
	rev	GGACATGACAGCAGCAGAAA		
rCHT_150	fw	CAAGACCAAGGAGGAAGCAG	150 (1152-1302)	AB030947
	rev	GCAAACATGGAACCTTGTCGA		
RPL19	fw	CATGGAGCACATCCACAAAC	216 (442-657)	NM- 031103
	rev	CCATAGCCTGGCCACTATGT		
18S	fw	CCGCAGCTAGGAATAATGGA	245 (735-981)	M11188
	rev	AGTCGGCATCGTTTATGGTC		
β-actin	fw	ATGGTGGGTATGGGTCAGAA	232 (210-442)	NM- 031144
	rev	GGGTCATCTTTTCACGGTTG		

Sequences for forward (fw.) and reverse (rev.) primers are given in 5' → 3' order. All primer sequences except VACHT are intron-spanning. First column: r = rat, number = length of expected PCR-product.

Tab. 7: Mouse primer sequences for mAChR, ChAT and transporters.

target		sequence (5' → 3')	length (bp) localisation	accession number
msHPRT	fw	GCCCCAAAATGGTTAAGGTT	208	NM_013556.2
	rev	TTGCGCTCATCTTAGGCTTT	(607-814)	
msM1	fw	GCGTTTAGGCAGGAAGTCAG	227	NM_007698.2
	rev	AGGGCCTACCTGGATGAGTT	(1842-2069)	
msM2	fw	CGGCTTTCTATCTGCCTGTC	169	NM_203491.1
	rev	GGCATGTTGTTGTTGTTTGG	(578-747)	
msM3	fw	ACAGTCGCTGTCTCCGAAC	181	NM_033269.2
	rev	TCCACAGTCCACTGAGCAAG	(415-595)	
msM4	fw	TCCTCACCTGGACACCCTAC	154	NM_007699.1
	rev	TTGAAAGTGGCATTGCAGAG	(1229-1382)	
msM5	fw	TCAGCCATCAAATGACCAAA	180	NM_205783.1
	rev	AGTAACCCAAGTGCCACAGG	(1264-1444)	
msCHT	fw	TTTCAGCTGCTGTCATGTCC	247	NM_021815.2
	rev	AGCAGCTGTGGGAAGATGAT	(1045-1292)	
msChAT	fw	AGGGCAGCCTCTCTGTATGA	181	NM_009891.1
	rev	GAGACGGCGGAAATTAATGA	(801-983)	
msVACHT	fw	TTGATCGCATGAGCTACGAC	246	NM_021712.2
	rev	CCACTAGGCTTCCAAAGCTG	(437-683)	
msOCT2	fw	AAATGGTCTGCCTGGTCAAC	172	NM_013667.1
	rev	AGGCCAACCACAGCAAATAC	(1435-1606)	


Sequences for forward (fw.) and reverse (rev.) primers are given in 5' → 3' order. Sequences for MR subtypes and VACHT are intron-less. First column: ms = mouse, M1-5 = MR-subtype, number = length of expected PCR-product.

6.4.2. Standard PCR

With the PCR technique it is possible to amplify small amounts of DNA until its visualisation. The PCR is an endpoint analysis, which means the product is measured during the plateau phase. At this point differences in mRNA levels are not proportional and cannot be compared between samples.

For the PCR reaction a 25 µl volume was used with 1 µl cDNA, 1x reaction buffer, 1.5 mM MgCl₂, 0.2 mM dNTP, 0.2 µM primer (each: forward and reverse) and Taq-DNA polymerase (Adelaide: 0,625 units HotStar Taq^R plus DNA-polymerase; Giessen: 0,625 units GoTaq DNA-polymerase) For the experiments in Adelaide the reagents were purchase from Qiagen and in Giessen from Promega. The iCycler (Adelaide, Bio-Rad) and the PTC-200 (Giessen, Peqlab) were used with the cycling

steps described below. The PCR-products were separated via gel electrophoresis in a 1.8% agarose gel.

step	time	temperature	
initial denaturation	5 min	94°C	
denaturation	30 s	94°C	
annealing	30 s	60°C	
elongation	30 s	72°C	
final elongation	7 min	72°C	
cooling	∞	4°C	

6.4.3. Quantitative real-time PCR

Real-time PCR is a technique to collect data throughout the PCR amplification process. Therefore, it is possible to combine the amplification and detection of the PCR product in a single step. After each cycle the amount of DNA is measured and will be displayed as an amplification curve.

In theory the amount of product should double in each cycle of PCR, which results in an exponential increase during the amplification process. In reality the first few cycles remain at background level and an increase of fluorescence is not detectable (linear ground phase). Then, the amplification curve is entering the early exponential phase and afterwards the log-linear or exponential phase (Fig.7). The last phase is called non-exponential or plateau phase and occur due to limitation of reaction components.

An important point within the real-time PCR is the threshold cycle or C_T . Here the fluorescence is rising over the background level. If template is available in a high amount it needs only few cycles and generates an early or low C_T number. Low concentrations of template result in a late or high C_T number. Quantitative real-time PCR allows accurate and precise quantification of product during the exponential phase. In this phase the amplification rate is similar between samples regardless of the amount of target cDNA. The visualisation is possible with fluorescence dyes. Here, SYBR Green I was used, which is a DNA binding dye. An increasing amount of double stranded PCR product results in an increase of fluorescence. After the last cycle the PCR reaction gets heated up, which results in the dissociation of all double-

stranded PCR products. The decreasing fluorescence intensity can be displayed as a melting curve with melt peaks at a specific temperature. This can be used to clarify the purification of the real-time PCR product.

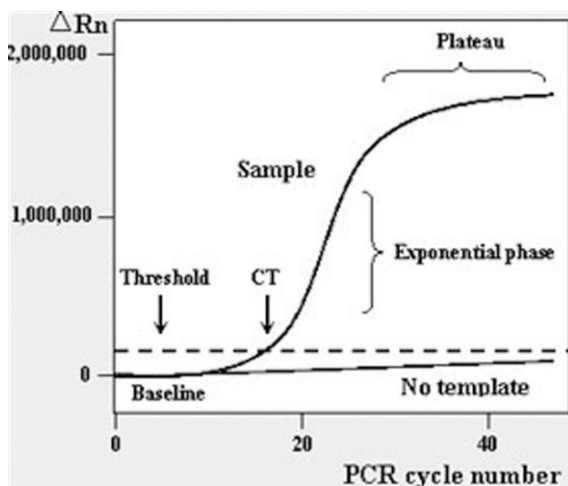


Fig. 7: Real-time PCR flow chart.

The PCR amplification curve charts the accumulation of fluorescent emission at each reaction cycle. The curve can be divided into different phases: the ground phase below the threshold, the exponential phase and the plateau phase. Threshold cycle (C_T) and amplification efficiency can be calculated from the data gathered from these phases. Rn is the intensity of fluorescent emission of the reporter dye divided by the intensity of fluorescent emission of the passive dye (a reference dye

incorporated into the PCR master mix to control for differences in master mix volume). ΔRn is calculated as the difference in Rn values of a sample and either no template control or background, and thus represents the magnitude of signal generated during PCR. Taken from www.ionchannels.org.

The volume per PCR reaction was 25 μ l containing 1 μ l cDNA, 0.2 μ M primer (mix of fw and rev), 9 μ l water and 14 μ l iQ SYBR Green Supermix (Bio-Rad). Each sample was prepared at least in duplicates and analysed with the real-time rotary analyser Rotor-Gene 3000 (Corbett Life Science, Mortlake, Australia) or iQTM5 Cyclor (Giessen, Bio-Rad) with the parameter described underneath. The data were analysed with the Rotor-Gene 6 software (Corbett Life Science) or iCycler Software (Bio-Rad).

step	time	temperature	
initial denaturation	8.5 min	95°C	
denaturation	20 s	95°C	
annealing	20 s	60°C	
elongation	20 s	72°C	
final elongation	10 min	72°C	
melting*			
cooling	∞	4°C	

*After the final elongation the PCR products were melted. The first step was 72°C for 45 sec. Then the temperature was increased about 1°C and each temperature was kept for 5 s until reaching 95°C

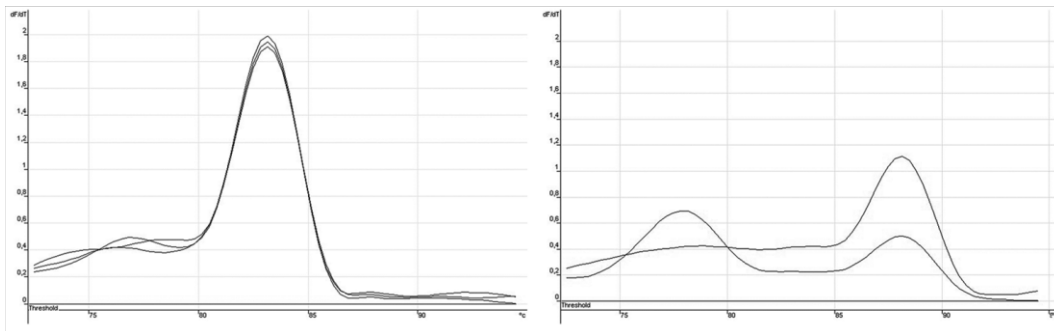


Fig. 8: Melt curves of real-time PCR products.

The PCR product produced by real-time RT-PCR is heated up to dissociate the double-stranded DNA. The melt curve informs about the specificity of the product. In the left panel all triplicates have the same melt temperature, whereas in right panel one of two duplicates showed an additional peak at the incorrect melting. Images were taken from an own experiment.

Primer optimisation and verifying the real-time PCR results

For reproducible results the real-time PCR primer needed to work with a comparable PCR efficiency (optimum $100\% \pm 20\%$). Therefore every primer was optimised using a positive control in different dilutions (neat, 1:10 and 1:100). The primers were added always in the same concentration.

To avoid false positive data real-time PCR result for every target and every sample were checked. Samples which showed a melting curve with more than one peak or a peak at an incorrect position have been excluded (Fig. 8). In addition all PCR products were separated via electrophoresis in a 1.8% agarose gel and samples which revealed a band at an incorrect size or a double band were excluded. The other samples were used for further analysis.

6.5. *In situ* hybridisation

In situ hybridisation is used for localising and detecting specific nucleic acid sequences (DNA or RNA) in morphologically preserved chromosomes, cells or tissue sections by hybridising a labelled complementary-nucleotide-strand (probe) to the sequence of interest. The detection of nucleic acid sequences within cells and tissue instead of proteins is the major difference between immunohistochemistry and *in situ* hybridisation (ISH).

The technique was originally developed independently by Pardue et al. [242] and John et al. [243] using radioisotope-labelled probes and autoradiography for detection. Although, radioactive-labelled probes are more sensitive than non-radioactive-labelled probes most users prefer non-radioactive ISH originally described by Langer et al. [244]. There are two types of non-radioactive hybridisation methods: direct (fluorochromes) and indirect (digoxigenin, biotin). In this study digoxigenin (DIG), a steroid isolated from digitalis plants (*Digitalis purpurea* and *Digitalis lanata*), was used for probe-labelling (Fig. 9).

6.5.1. Preparation of the probe

In situ hybridisation probes were prepared with the DIG RNA-Labelling Kit (SP6/T7) from Roche (Dee Why, Australia). The supplied NTP-mix contains the nucleotide uridintriphosphat (UTPs), which are coupled to DIG. These DIG-UTPs are incorporated into nucleic acid probes with a defined density by DNA and/or RNA polymerases. The necessary primers have been designed as described in 6.4.1 (Tab. 5 & 6). Furthermore, sequences were added to the mRNA-specific primer, which enables the binding of either the T7 or the SP6 RNA-polymerase (Tab. 8). These sequences are important for the generation of sense and antisense specific probes. The T7 labelled probes are binding to the mRNA, therefore it represents the antisense-probe. Sp6 labelled probes are the sense-probes which is the control and important for the specificity of T7 (Fig. 9).

Firstly, 75 µl PCR product was amplified using the specific *in situ* primer. 10 µl of the PCR product were analysed via gel electrophoresis to confirm a successful amplification. The remaining 65 µl were purified using the GFXTM PCR DNA and Gel Band Purification Kit (GE Healthcare, Buckinghamshire, UK) according to the manufacture's instructions. The eluted purified PCR product (50 µl) was precipitated with 1/10 volume sodium acetate (3 mM) and 1 volume 100% ethanol. The solution was incubated at -20°C for 30 min, centrifuged (13 000 g, 20 min and 4°C), washed with 70% ethanol and air dried in an RNase-free environment. The resulting pellet was resuspended in 11 µl RNase-free water and used for preparation of DIG-labelled RNA probes.

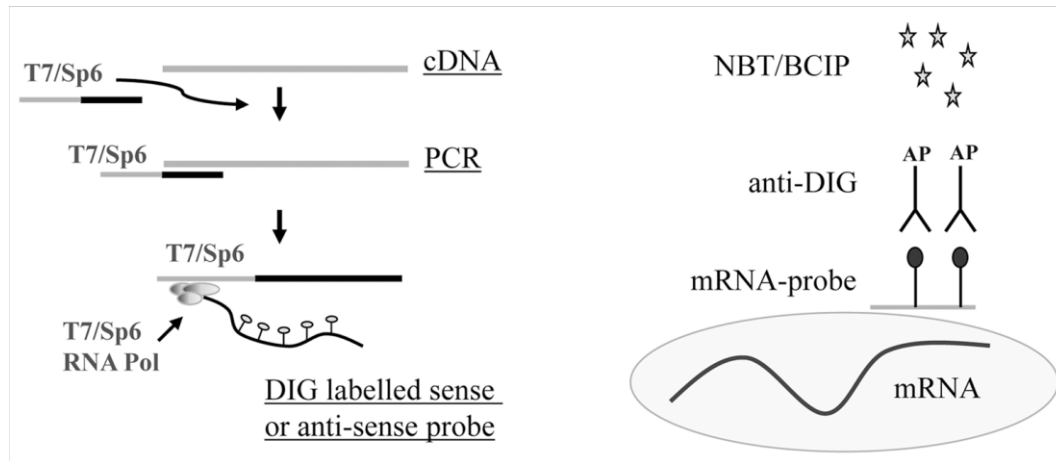


Fig. 9: *In situ* hybridisation probe design and binding within tissue.

Left panel: ISH probes were amplified using T7 and Sp6 RNA polymerase and DIG-labelled UTPs. Right panel: the DIG-labelled ISH-probes were detected with AP-labelled anti-DIG antibody and visualised with colorimetric AP substrates (NBT and BCIP). AP = alkaline phosphatase.

Tab. 8: Rat primer sequences for *in situ* hybridisation.

T7 binding site	TAATACGACTCACTATAGGG
SP6 binding site	ATTTAGGTGACACTATAGAA
situ_ChAT (312 bp)	
fw:	TAATACGACTCACTATAGGG TGAACGCCTGCCTCCATTTCGGCCTGCTGA
rev:	ATTTAGGTGACACTATAGAA GTGCCATCTCGGCCACACGAAC TGCA
situ_alpha7 (326 bp)	
fw:	TAATACGACTCACTATAGGGGG GCTCTGCTGGTATTCTTGC
rev:	ATTTAGGTGACACTATAGAAA AACCATGCACACCAGTTCA

Sequences for forward (fw.) and reverse (rev.) primers are given in 5'→3' order. The T7 and SP6 binding sites are in bold.

5.5 µl of the PCR-product was mixed with 2 µl 10x DIG RNA labelling-mix, 8.5 µl RNase-free water, 2 µl 10x reaction buffer and either 100 U T7 or 40 U Sp6 RNA-polymerase (2 µl). The reaction was incubated 2 h at 37°C. By adding 2 µl EDTA (0.2 M, pH 8.0) the reaction was stopped. The probe was then precipitated adding 2.5 µl LiCl (4 M) and 75 µl pre-chilled 100% ethanol. After 30 min incubation at -80°C the mix was centrifuged (13 000 g, 20 min, 4°C), washed with 70% ethanol and air dried in an RNase-free environment. The pellet was resuspended in 50 µl RNase-free water. Aliquots of the probes were stored at -80°C.

The reactivity of the amplified probes was compared to a DIG-labelled control RNA sample (100 ng/µl, Roche) supplied by the company using a dot blot system. RNA sample and probes were diluted in DEPC water 1:10, 1:100 and 1:1000 at room temperature. 1 µl of the dilutions and a neat sample were added to a nitrocellulose membrane and cross-linked with UV light for 10 min. The membrane was washed in 1x washing buffer (Roche) for 2 min and blocked with 1x blocking buffer (Roche) dissolved in maleic acid buffer (0.1 M Maleic acid, 0.15 M NaCl, with NaOH to pH 7.5) for 30 min with gentle shaking. The high-affinity anti-DIG antibody (Fab-fragments) diluted 1:5000 in 1x blocking buffer was added to the membrane for 30 min, followed by an incubation with 1x washing buffer for 2 x 15 min and with 1x detection buffer (Roche) for 2 min. The anti-DIG antibody is conjugated to alkaline phosphatase (AP), which can be visualised with colorimetric AP substrates (NBT and BCIP). The detection occurred with NBT/BCIP solution (1:200, Roche) diluted in 1x detection buffer in darkness without shaking for not more than 1h. The reaction was stopped by incubating the membrane in DEPC water for 5 min and the dot intensity of the probes was compared to the DIG-labelled control RNA samples.

6.5.2. *In situ* hybridisation on frozen tissue sections

In isopentane cryo-protected and shock frozen rat DRG and testis were cut in 12 to 14 µm sections and transferred to polyethyleneimine (PEI)-coated slides (0.1%). The sections were incubated as described below. All steps were performed at room temperature. The probes were diluted in preheated hybridisation buffer and again preheated to 80°C. After the probes were cooled down for 5 min they were applied to

the sections. The sections were incubated overnight at 65°C in a humid chamber containing 5x saline-sodium citrate (SSC) buffer.

step	time	components of the solutions
fixation with PFA	10 min	4% paraformaldehyde in sterile 1x PBS
wash with 1x PBS	3x 3 min	
proteinase K digestion	7 min	2 µg/ml proteinase K in 50 mM Tris, 5 mM EDTA
fixation with 4% PFA	5 min	
wash with 1x PBS	3x 3 min	
acetylation	10 min	29.6 ml water, 0.4 ml triethanolamine, 53.4 µl concentrated HCl, 76.3 µl acetic anhydride
wash with 1x PBS	3x 3 min	
pre-hybridisation with hybridisation buffer, preheated to 72°C	2 h in a humid chamber containing 5x SSC	4x SSC, 50% deionised formamide, 1x Denhardt's reagents, 10% dextran sulphate, 100 µg/ml yeast tRNA, 250 µg/ml Hering sperm DNA, 100 µg/ml yeast total RNA (stored at -20°C)
hybridisation with sense, anti-sense or buffer at 65°C	overnight in a humid chamber containing 5x SSC	preheated (80°C) hybridisation buffer

Note: Reagents for acetylation-buffer must be mixed in order of appearance with continuously stirring in the fume hood.

To avoid mixing the probes on the sections they were removed using preheated 72°C 5x SSC buffer. The wash conditions have been optimised for the probes which were used for this protocol. These can be different for every probe.

step	time	components of the solutions
wash with 5x SSC	20-30 min, RT gently shaking	
wash with 1x or 0.2x SSC	1 h at 65°C	
wash with 1x or 0.2x SSC	5 min, RT	
wash with levamisole buffer	5 min, RT	100 mM Tris pH 7.5, 150 mM NaCl, 1 mM levamisole
blocking buffer	1 h, RT	5 ml 10x blocking solution, 5 ml 10x maleic acid, 40 ml DEPC water
detection	overnight, RT, darkness	anti-DIG AP-Fab-fragments (1:5000) in blocking-buffer

To remove the unused antibody, the sections were washed with wash buffer (100 mM Tris pH 7.5, 150 mM NaCl) 3x for 5 min each. Afterwards they were incubated with 1x detection buffer (100 mM Tris-HCl, 100 mM NaCl pH 9.5) for 10 min. The anti-DIG antibody was detected with NBT/BCIP diluted 1:500 in detection buffer. The sections were placed in the dark and checked after 1, 2, 4 h and overnight. The reaction was stopped by incubating the sections in DEPC water for 10 min. Finally, the slides were covered with buffered glycerol, cover-slipped and sealed with nail polish. Visualisation occurred with Olympus bright field microscope (Olympus, Hamburg, Germany) and the manufacture's software.

PBS (phosphate buffered saline)

NaCl	8.5 g	adjust to 1000 ml and pH ~7.1
Na ₂ HPO ₄	1.07 g	
NaH ₂ PO ₄ 1x H ₂ O	0.39 g	

Buffered glycerol pH 8.6

1.5 M Na₂CO₃ and 1.5 M NaHCO₃ are mixed until the solution has pH 8.6. One volume carbonate buffer is mixed with one volume 100% glycerol.

7. Immunohistochemistry

Immunohistochemistry (IHC) is used for identifying cellular or tissue antigens by antigen-antibody-interactions. Epitopes are mostly peptides, but could also be carbohydrate moieties. The antibody-binding is highly specific, which enables even the differentiation of labelled compartments within the cells. The detection of antigens is possible via a direct- or indirect-labelling method. Direct-conjugated primary antibodies (for exp. fluorophore) can be used for a fast detection with less unspecific binding but have a reduced intensity and therefore weaker signals (Fig. 10A). To increase the signal the indirect-labelling method was established. A non-conjugated primary antibody binds to its epitope. One or more labelled secondary antibodies can bind to the primary antibody and therefore amplify the signal (Fig. 10B). Both, primary and secondary antibodies can be bound to a fluorophore, biotin or an enzyme (Fig. 10). Immunoreactivity (IR) can be visualised by light (enzyme, biotin) or fluorescence (biotin, fluorophore) microscopy.

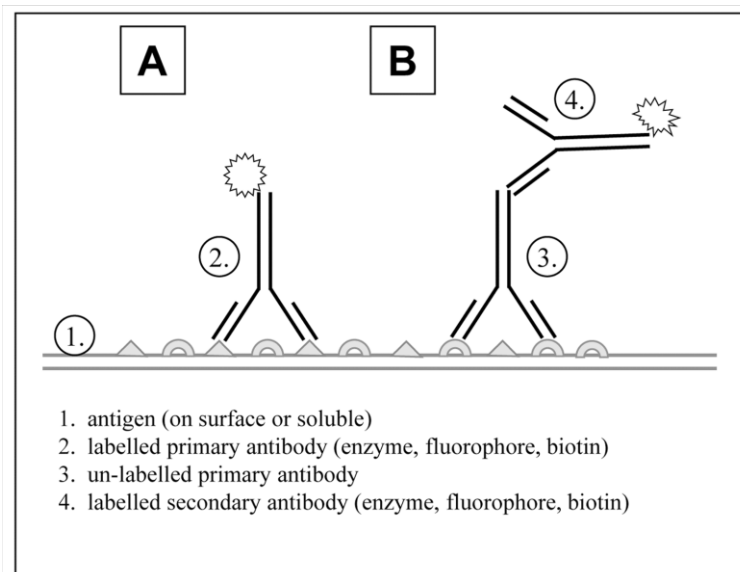


Fig. 10: Immunohistochemistry (direct and indirect method)

Primary antibodies bind to specific antigens (1), which are either direct-conjugated (2.) or non-conjugated (3.). Conjugated secondary antibodies (4.) bind to non-conjugated primary antibodies (3.). Antibodies can be conjugated to enzymes (AP, HRP), fluorophores (FITC, Cy3) or biotin. Biotin binds specific to avidin or streptavidin, which are conjugated either to an enzyme or a fluorophore.

7.1. Tissue immersion fixation and xylene-processing for whole mounts and sections

For IHC experiments the male reproductive organs and DRG were either fixed with Zamboni's fixative [245] (390 ml 0.2 M Na_2HPO_4 , 110 ml 0.2 M NaH_2PO_4 , 25 ml 16% paraformaldehyde, 15 ml saturated picric acid, 10 ml distilled Water) or cryo-protected with isopentane and shock frozen in liquid nitrogen. Dependent on the size, the tissue was incubated in Zamboni's fixative at 4°C for one to three days. To remove the fixative from the tissue it was incubated at room temperature (RT) in 10x tissue-volume with the solutions described below:

wash-step	time
80% ethanol	3x 20 min, RT
90% ethanol	30 min, RT
100% ethanol	2x 30 min, RT
xylene	2x 30 min, RT
100% ethanol	2x 30 min, RT
80% ethanol	30 min, RT
50% ethanol	30 min, RT
distilled water	30 min, RT
1x PBS	30 min, RT

The tissue was stored in PBS/azide (0.1%) at 4°C. For whole mount experiments the tissue could be used without further blocking of unspecific binding sites. For cryo-sectioning the tissue was cryo-protected in 18% sucrose at 4°C for one or two days. Before freezing the tissue was embedded in tissue Tek®OCT compound (Sakura Finetek Europe B.V., Zoeterwoude, The Netherlands) and stored at -20 or -80°C until further use.

7.2. Single and multiple labelling immunohistochemistry

Frozen tissue samples were used for cryo-sectioning. The cryostat had a temperature of -18 to -22°C and the knife had an angle of five degree. 12 to 16 µm thick sections were mounted on 0.1% PEI-coated glass slides (Adelaide) or superfrost glass slides (Giessen). The sections were dried for 30 min to 1 h at room temperature and either used immediately or stored at -20°C. Sections of pre-fixed tissue could be used directly. Sections of unfixed tissue had to be fixed before further use. Unfixed sections were incubated immediately after defrosting with ice cold methanol, acetone or isopropanol for 10 to 15 min at -20°C and air dried until all fixative was evaporated. Afterwards the slides could be processed like explained further down. Sections of fixed tissue were air dried for 10 min after thawing and washed with 1x PBS for 10 min. For both fixation methods the slides were incubated with 0.05% Tween®20 for 20 min, which increases the permeability of the tissues for a better antibody penetration. This step and all following were performed at room temperature. The slides were washed 3x with 1x PBS for 10 min each. To block unspecific binding sites the sections were incubated with 0.1% BSA (Roth, Karlsruhe, Germany) and 10% normal donkey serum (NDS, Dako, Hamburg, Germany) or 10% normal horse serum (NHS, PAA) diluted in 1x PBS/azide for 1 h. The primary antibodies were applied to the slides without further wash steps in 1x PBS/azide with double NaCl concentration and incubated overnight in a humid chamber (Tab. 9). To remove the primary antibodies the slides were washed 3 times with 1x PBS for 10 min each and secondary antibodies diluted in 1x PBS/azide were added to the slides (Tab. 9). After 2 h incubation in a humid chamber the slides were washed 3x with 1x PBS for 10 min each. For visualising the DNA the sections were incubated with Hoechst or DAPI diluted in 1x PBS after the first wash step, followed by 3 wash steps with 1x PBS for 10 min each. To exclude a cross-reaction between the specimens and the secondary antibodies they were tested by omission of primary antibodies on control sections. Finally the slides were covered with buffered glycerol, a cover slip and sealed with nail polish. Visualisation occurred with Olympus BX50, Olympus AX70, Confocal Laser Scanning Microscope, TCS SP2 (Leica) or Leica LSM (Wetzlar, Germany) and the manufacture's software.

Tab. 9: Primary and secondary antibody or antisera.

primary antibody	host	supplier	dilution section	dilution w/m
CGRP	goat	Arnel	1:1000	1:500
CGRP	rabbit	Peninsula	1:2000	
ChAT	sheep	Chemicon	1:2000	
ChT1	rabbit	Chemicon	1:100	
ED1 (CD68)	mouse	Serotec	1:100	
ED2 (CD163)	mouse	Serotec	1:100	
IB4-Alexa ₄₈₈		Mol. Probes	1:400	1:200
IB4-biotin		Sigma	1:100	
NF200	mouse	Sigma	1:2000	1:1000
Peripherin	mouse	Chemicon	1:500	1:50
PGP9.5	rabbit	Neuromics	1:500	1:500
α SMA-FITC		Sigma	1:800	1:500
TRPV1	guinea pig	Neuromics	1:1000	1:500
VACHT	goat	Chemicon	1:800	
VGluT1	rabbit	Syn. Systems	1:4000	1:1000

secondary antibody & reagents	host	conjugate	supplier	dilution
anti-rabbit-Ig	dky	FITC	Jackson	1:100
anti-rabbit-Ig	dky	FITC	Chemicon	1:100
anti-mouse-Ig	dky	FITC	Jackson	1:50
anti-rabbit-Ig	dky	cy3	Jackson	1:100
anti-rabbit-Ig	dky	cy3	Chemicon	1:2000
anti-sheep/goat-Ig	dky	cy3	Jackson	1:100
anti-mouse-Ig	dky	cy3	Jackson	1:100
anti-mouse-Ig	gt	cy3	Dianova	1:1000
anti-guinea pig-Ig	dky	cy3	Jackson	1:100
anti-sheep/goat-Ig	dky	cy5	Jackson	1:50
anti-mouse-Ig	dky	cy5	Jackson	1:50
anti-mouse-Ig	gt	cy5	Dianova	1:400
Streptavidin		AMCA	Vectorlabs	1:100
Hoechst			Mol. Probes	1:2000
DAPI			Sigma	1:1000

Supplier: Arnel Products (N.Y., USA), Peninsula Lab. (San Carlos, USA), Chemicon (Millipore, Schwalbach/Ts Germany), Serotec (Düsseldorf, Germany), Mol. Probes (Molecular Probes, Invitrogen) Neuromics (Edina, USA), Syn. Systems (Synaptic Systems, Göttingen), Jackson (Jackson ImmunoResearch Lab, West Grove, USA), Dianova (Hamburg, Germany), Sigma (Sigma-Aldrich, Munich, Germany). Vectorlabs (Peterborough, UK) Abbreviations: dky = donkey, gt = goat.

7.3. Pre-absorption of antisera

The specificity of ChAT and VACHT antisera were analysed by pre-absorption experiments. For this purpose the antisera were mixed with their complementary peptides. The antibodies within the sera bound to the peptide, therefore no free antibodies were left for binding to the analysing tissue. 100 ng/μl of the specific ChAT-peptide were pre-incubated with the ChAT antiserum for 6 h at room temperature and the mixture was applied to a cryo-section afterwards. VACHT antiserum (1:1600) was mixed with 80 ng/μl VACHT-peptide and incubated overnight at room temperature. The following procedure was done as described for IHC in the chapter 7.2.

7.4. Whole mount

Tissue samples, which have been stored in 1x PBS/azide, were used for whole mount experiments. The tissue was cut in small pieces (2-3 mm²) and if necessary multiple layers were separated as far as possible without tissue damage using forceps. The samples were placed in agglutination tiles (Southern Biological, Nunawading, Australia) for further incubation steps and covered with 1x PBS until all samples were ready for the first antibodies. Without any blocking step the samples were covered with 10 to 15 μl primary-antibody-mix diluted in 1x PBS/azide and incubated for 48 h in a humid chamber. To remove excess primary antibodies the tissue was washed 3x with 1x PBS for 10 min each and the secondary-antibody-mix diluted in 1x PBS/azide was applied to the samples. After 24 h incubation in a humid chamber the tissue was washed 3x with 1x PBS for 15 min each. For better penetration 50 μl buffered glycerol was applied to the samples and incubated 6 to 12 h in a humid chamber. In the end the tissue (or separated tissue layers) was prepared on uncoated slides with fresh buffered glycerol, covered with a cover slip and sealed with nail

polish. Visualisation occurred with Olympus BX50 or Olympus AX70 and the manufacture's software.

8. *In vitro* and *in vivo* experiments

8.1. Measurement of intracellular calcium concentrations

The intracellular calcium concentration can be measured by different fluorescent dyes such as Fura-2 or Fluo-3. Here Fura-2AM (fura 2 acetoxymethyl ester, Mol. Probes) was used, which gets modified after entering the cell and is therefore unable to leave the cell again. Fura-2 binds to free intracellular Ca^{2+} and forms a chelate-complex. The fluorescence intensity of Fura-2 is depending on the amount of free calcium. This emission maximum of 510 nm can be reached by stimulation with light of 340 nm, if the calcium is bound, or with light of 380 nm, if the calcium is free. The amount of free intracellular calcium can be analysed by calculating the ratio 340/380 nm.

Peritubular cells and SC have been cultured as described in chapter 5.2.2 and were ready to use after the incubation time mentioned before. Testicular macrophages needed to be incubated after the final washing step for another 2-3 h. All cells were seeded on glass coverslips. In advance, the coverslips were washed with acetone, rinsed twice with 100% ethanol, air dried and sterilised. After settlement, the cells were washed 2x with HEPES-buffer, loaded with 3.3 μM Fura-2 AM for 30 min to 1 h at 32°C or 37°C and washed again 3x 10 min in HEPES-buffer to remove unused Fura-2. The coverslips with the dye-loaded cells were placed in a measuring chamber (culture dish, Delta T-system, Biotech Inc., Butler, USA) with 1 ml HEPES-buffer at a constant temperature of 32°C (TM, SC) or 37°C (PTC). All used solutions were pre-warmed. Nicotine and ACh have been prepared fresh as a stock solution (10 mM) for each experiment. ATP (100 mM) and muscarine (10 mM) could be stored as aliquots at -20°C. During the experiments nicotine and ATP were used with 100 μM and muscarine and ACh with 10 μM . The dilutions were made in HEPES.

The basic experiment continued 400 s (Fig. 11). Three applications were made at $t = 40$ s (HEPES), $t = 160$ s (HEPES, ACh, nicotine or muscarine) and at $t = 280$ s (ATP). Following this general set-up modified experiments including an inhibitor were conducted. For one set up the buffer was changed continuously using a Gilson-minipuls 2-pump (Gilson, Limburg-Offheim, Germany).

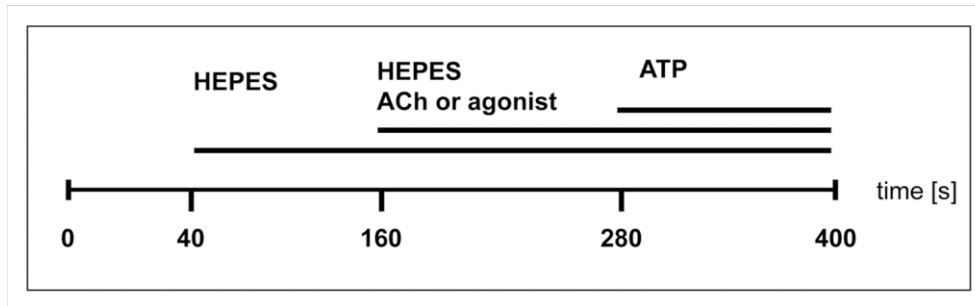


Fig. 11: Flow chart for calcium-imaging experiments.

In the course of the experiment the cells got stimulated at three time points: with HEPES at $t = 40$ s, with HEPES, ACh, nicotine or muscarine at $t = 160$ s and with ATP at $t = 280$ s.

Every two seconds fluorescence images were taken with a slow-scan charged-coupled device camera system with a fast monochromator (camera IMGO, TiLL Photonics, Gräfeling, Germany). The monochromator was coupled to an inverted microscope (Olympus BX50WI) with a 20x water immersion objective. The cells were excited with 340 nm and 380 nm wavelengths (λ) and fluorescence emission intensities were collected with $\lambda > 420$ nm (Fig. 12). The images (200 images in 400 s) were analysed with the TiLLVision software (TiLL Photonics). Each cell was labelled individually and the fluorescence intensity ratio of 340nm/380nm was calculated. The threshold was set to $< 5\%$ change in $[\text{Ca}^{2+}]_i$. Viability of the cells was observed by trypan blue and dead cells were excluded from the analysis.

Signal intensity of $t = 0$ s was set as 100%, so the baseline was usually at 100%. The course of the experiment was plotted into a diagram (mean, SEM) using Microsoft office Excel 2003.

HEPES-buffer	5.6 mM KCl, 136.4 mM NaCl, 1 mM MgCl_2 , 2.2 mM CaCl_2 , 11 mM D-glucose and 10 mM Hepes
ATP	adenosine 5'-triphosphate di(tris) salt dihydrate Sigma
nicotine	nicotine hydrogen tartrate, Sigma
muscarine	muscarine
ACh	acetylcholine chloride, Sigma
atropine	atropine sulfate, Sigma

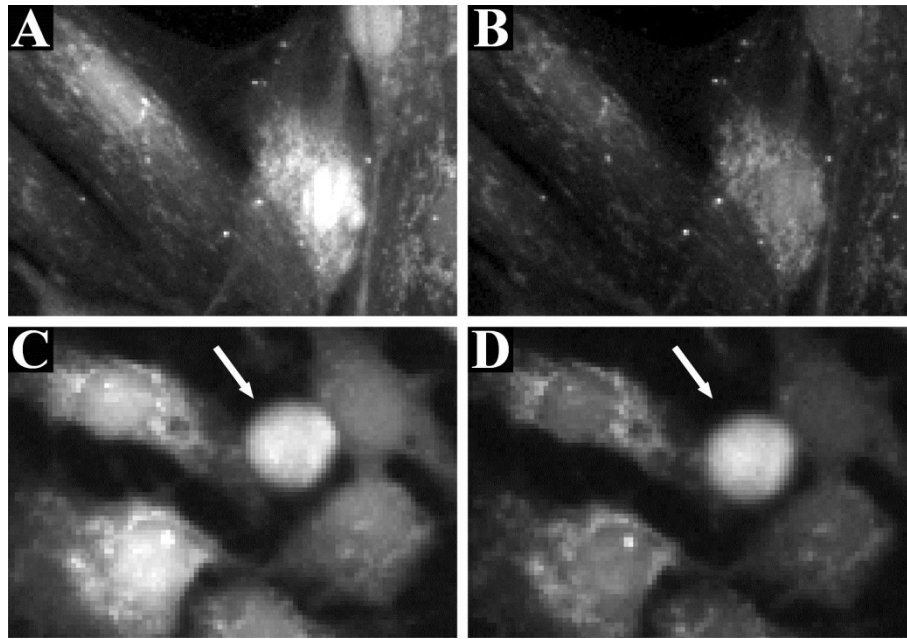


Fig. 12: Fluorescence intensity after excitation with $\lambda = 380$ nm.

PTC (A & B) and SC (C & D) were exposed to ATP. Excitation with monochrome light at $\lambda = 380$ nm is shown before (A & C) and after (B & D) ATP application. Fluorescence intensity of the cells decreases for all PTC and SC. The arrow labels a germ cell within the SC, which does not respond to ATP.

8.2. Retrograde tracing with Cholera toxin-B

Neuronal tracing means the application of a tracer to either peripheral endings of nerve fibres for retrograde transport to the cell body situated in a ganglion or into the ganglion or brain for anterograde transport to peripheral endings. The identification of the projecting neurons from the CNS to the peripheral tissue is the aim in both cases. Possible tracers are horseradish peroxidase (HRP), DiI or Cholera toxin-B (Ctx-B). In contrast to DiI or HRP, which are passively taken up by neurons, Ctx is actively taken up and transported by the neuron. Cholera toxin is secreted by the bacterium *Vibrio cholerae* and is composed of two subunits: A and B. The five non-toxic B subunits form a pentamere and are required for the binding to the cell. The A subunit is the enzymatic active subunit that must eventually dissociate to fulfil its function. The binding of the B subunits results in the internalisation of the entire Ctx-A₁B₅ complex. This characteristic is used for Ctx-tracer. The tracer used in this study is Alexa₅₅₅ conjugated Ctx-B, which is prepared from recombinant Ctx subunit B (Mol Probes).

Male Wistar Furth (FMC) rats 180 g of weight were used in the experiments. The surgery was performed unilateral at the left testis of each rat. The rats were anaesthetised i.p. with a combination of 12 mg/kg xylazine hydrochloride, 80 mg/kg ketamine hydrochloride and 50 µg/kg atropine. In addition they received 50 µg/kg buprenorphine i.m. against post-surgery pain. After they were under deep anaesthesia the scrotum was shaved with an electric shaver and disinfected with 70% ethanol. A 2 cm cut through scrotum, fascia externa and fascia interna was made using a scissor and the skin was fixed with a haemostat. Each rat was traced with two dyes.

In the first experiment 70 nl Ctx-B-Alexa₅₅₅ (0.5 µg/µl) were applied on the meso between the epididymis and the vas deferens using a Hamilton syringe. 50 nl of the second tracer, Ctx-B-biotin (0.5 µg/µl), were injected in the following tissues: (1) into the testis parenchyma, (2) between the vas deferens and the surrounding adventitia and (3) into the epididymis. In the second experiment 50 nl Ctx-B-biotin (0.5 µg/µl) were injected into the testis parenchyma and 20 µl Ctx-B-Alexa₅₅₅ (0.5 µg/µl) were again applied on the meso between the epididymis and the vas deferens. Here three rats were treated with the same conditions. After the surgery the wound was sutured with 5.0 black silk and cleaned with iodine solution. The animals were placed in individual cages and illuminated with a heating lamp until they woke up.

After 6 days the animals were deeply anesthetized with isoflurane and perfused with Zamboni's fixative. At first the blood was removed by injecting 200 ml pre-heated medium into the heart. Then the medium was replaced by 200 ml Zamboni's fixative and the animal was incubated 20 min at room temperature. All DRGs from thoracic 12 to sacral 1 from both sides, contra- and ipsi-lateral, were isolated and incubated in fixative for another 24 h. The samples were washed three to four times with PBS until the yellow colour disappeared. After incubation in 18% sucrose for 24 h the samples were embedded in tissue tec© and slowly frozen in -20°C. The samples were cut, whereas every section was collected, and used for multi-labelling IHC.

8.3. Induction of experimental autoimmune orchitis

Male inbred Wistar Kyoto rats (Charles River) were actively immunised with syngeneic testicular homogenate (TH) as previously described by Doncel et al. (1989) [60].

Briefly, 10 rats (180–220 g body weight) were anesthetized by i.p. administration of 100 mg/kg ketamine (Ketavet; Pharmacia, Erlangen, Germany) and 10 mg/kg Xylazine (Rompun; Bayer Vital, Leverkusen, Germany). The rats were immunised with a mixture of 0.4 ml syngeneic TH and 0.4 ml complete Freund's adjuvant (Sigma) which was injected subcutaneously into the hind paws and at various sites at the back. Injection sites at the footpads were sealed using Histoacryl^R tissue glue (Braun, Tuttlingen, Germany). These injections were repeated twice at 14 d intervals. In addition an injection of inactivated *Bordetella pertussis* (Bp) bacteria (DSMZ, Braunschweig, Germany) was applied to the rats. The first two immunisations were followed by an intravenous injection (in the tail vein) of 10^{10} Bp bacteria dispersed in 0.5 ml isotonic saline. The third immunisation with TH was followed by intraperitoneal injection of 5×10^9 bacteria applied in 0.5 ml isotonic saline. Control animals ($n = 7$) received complete Freund's adjuvant and Bp, but no testis homogenate, following the same scheme.

Fifty days after the first immunisation, the three animal groups; EAO, adjuvant control and untreated control ($n = 5-9$); were killed by a lethal dose of isoflurane. Testes were removed, weighed and decapsulated. 30 mg of TP from each rat were snap-frozen in liquid nitrogen and stored until needed at -80°C .

Experimental procedures were approved by the local authority (Regierungspraesidium Giessen) and conformed to the Code of Practice for the Care and Use of Animals for Experimental Purposes.

Results

9. The cholinergic system of rat testicular parenchyma and testicular capsule under non-inflammatory conditions

The testicular parenchyma shows no innervation although there is evidence for the presence of ACh within the testis (Prof. Klein, Frankfurt, Germany, unpublished). To prove if the rat testis is a source for ACh or if testicular cells express ACh-receptors themselves mRNA isolated from the testis was analysed using real-time PCR.

Testicular parenchyma and testicular capsule were separated and used for RNA extraction. The mRNA was reverse transcribed into cDNA. In a first approach, three samples from each tissue were analysed via real-time PCR for nAChR subunits $\alpha 1$ - $\alpha 7$, $\alpha 9$, $\alpha 10$, $\beta 1$ - $\beta 4$, ChAT, OCT2 and VAcHT. Dependent on the presence of the targets at least two more samples were analysed for complete statistical analysis. In case of similar results in TC and TP the number of analysed experiments was three.

9.1. Relative mRNA expression analysis of nicotinic AChR-subunits

In contrast to the parenchyma, which contained the mRNAs for 11 out of 13 nAChR subunits including mRNAs for so-called “muscle specific” $\alpha 1$ and $\beta 1$ subunits (Tab. 10), the capsule expressed all α - and β - nAChR subunits (Tab. 10). In TP, mRNA for nAChR subunit $\beta 4$ could not be detected. The $\alpha 6$ subunit was not detectable in 3/5 samples and in two samples the expression was very low. Both receptor subunits, $\alpha 6$ and $\beta 4$, were present in TC (Tab. 10, Fig. 13). In parenchyma, the rank order of the mRNA expression levels was nAChR α -subunits $\alpha 4 > \alpha 7 > \alpha 5 > \alpha 9$, whereas in the capsule the order was $\alpha 4 > \alpha 7 > \alpha 5 > \alpha 2$ (Fig. 13A & B).

For the subunits $\alpha 2$, $\alpha 3$, $\alpha 4$, $\alpha 6$ and $\alpha 9$ a significant difference in the expression level could be observed between the parenchyma and the capsule. The relative expression of $\alpha 2$ and $\alpha 6$ was significantly ($P = 0.008$, Tab. 10) higher in the capsule compared to the parenchyma whereas the subunits $\alpha 3$, $\alpha 4$ and $\alpha 9$ were significantly lower expressed (Tab. 10). The relative expression levels for nAChR subunits $\beta 1$ - $\beta 3$ were similar in parenchyma and capsule. In the capsule, the $\beta 4$ subunit showed a lower expression level than $\beta 1$ - $\beta 3$ and as mentioned before $\beta 4$ was absent within the parenchyma (Fig. 13C & D).

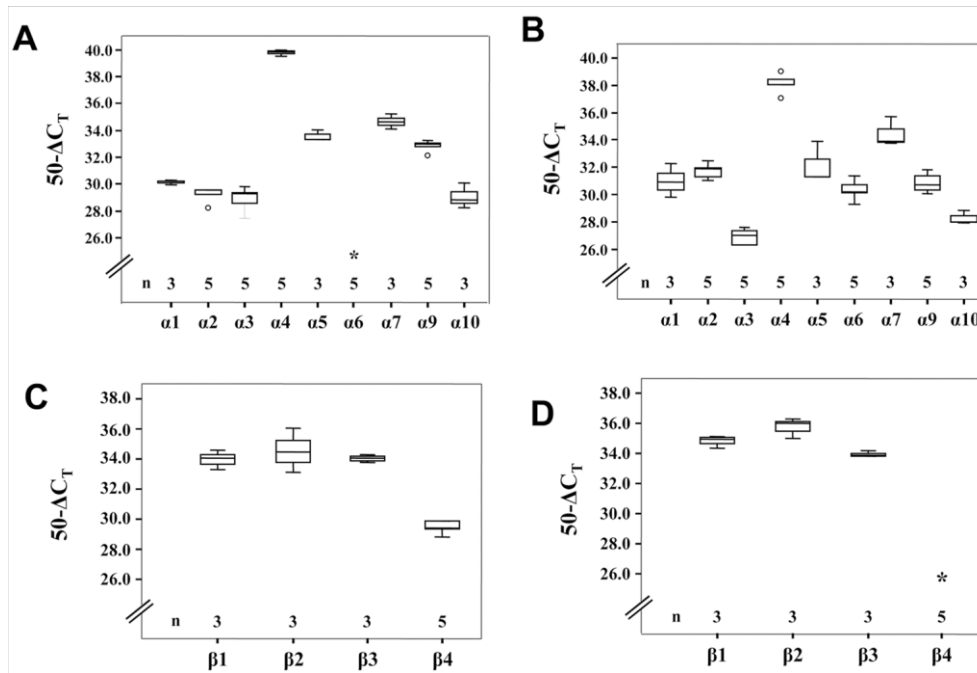


Fig. 13: mRNA expression level of nAChR subunits in TP and TC.

Three to five animals (n) were analysed for mRNA expression of nAChR. Exact values are shown in Tab. 10. Data are plotted as Box plots with nAChR α - subunits shown for TC (A) and TP (B); and β -subunits shown for TC (C) and TP (D). For primer with more than one primer-set the following variants were used: $\alpha2$ _216, $\alpha6$ _286, $\alpha9$ _242, $\alpha10$ _317 (Tab. 5). The asterisk at $\alpha6$ (B) indicates the absence of mRNA in 3/5 replicates whilst the other 2 replicates revealed very low expression levels. The asterisk in D indicates the absence of detectable mRNA for $\beta4$. The circles represent outlier. The ΔC_T values were subtracted from 50 showing higher values with higher expression.

Tab. 10: Comparison of relative mRNA expression levels of nAChR subunits in TP and TC

target	samples n	TP mean \pm SD	TC mean \pm SD	<i>P</i> -values TP vs. TC
$\alpha1$	3	30.1 ± 0.17	31.0 ± 1.23	n.s.
$\alpha2$	5	29.2 ± 0.54	31.7 ± 0.55	0.008
$\alpha3$	5	28.9 ± 0.92	27.2 ± 0.58	0.016
$\alpha4$	5	39.8 ± 0.19	38.1 ± 0.70	0.008
$\alpha5$	3	33.5 ± 0.42	32.2 ± 1.50	n.s.
$\alpha6$	5	8.7 ± 11.94	30.3 ± 0.78	0.008
$\alpha7$	3	34.6 ± 0.55	34.5 ± 1.10	n.s.
$\alpha9$	5	32.9 ± 0.39	30.9 ± 0.73	0.008
$\alpha10$	3	29.0 ± 0.94	28.3 ± 0.52	n.s.

target	samples n	TP mean \pm SD	TC mean \pm SD	<i>P</i> -values TP vs. TC
$\beta 1$	3	34.8 \pm 0.40	34.0 \pm 0.64	n.s.
$\beta 2$	3	35.8 \pm 0.68	34.6 \pm 1.50	n.s.
$\beta 3$	3	33.9 \pm 0.19	34.0 \pm 0.28	n.s.
$\beta 4$	5	0.0 \pm 0.00	29.4 \pm 0.44	0.008

Relative mRNA expression level of three to five samples collected from individual animals (n) were analysed using qRT-PCR. Data expressed as $50-\Delta C_T$ values (columns three and four) were evaluated using Mann-Whitney-test. Column 5 shows the *P*-values for individual targets. TP = testicular parenchyma, TC = testicular capsule, n.s. = not significant.

9.2. Relative mRNA expression analysis of muscarinic AChR-subtypes

To determine the existence of MR-subtypes within the testis, relative mRNA expression levels were analysed in TP and TC. All five MR-subtypes, M_1R to M_5R were expressed in TP and TC (Fig. 14, Tab. 11). The expression pattern differed between TP and TC. Whereas in parenchyma M_4R and M_3R showed the highest expression levels, mRNAs for M_2R and M_4R were the most abundant in the capsule. M_1R - M_3R were significantly lower expressed in TP compared to TC whereas M_4R was significantly higher expressed (Fig. 14). The M_5R was expressed similar in TP and TC. Exact numbers and *P*-values are shown in Tab. 11.

Tab. 11: Expression of MR subtypes in TP and TC.

target	samples n	TP mean \pm SD	TC mean \pm SD	<i>P</i> -values TP vs. TC
M_1R	5	30.48 \pm 0.87	32.56 \pm 0.38	0.008
M_2R	5	29.31 \pm 0.76	40.49 \pm 0.46	0.008
M_3R	5	33.42 \pm 0.29	34.00 \pm 0.40	0.016
M_4R	5	38.52 \pm 0.22	37.01 \pm 0.36	0.008
M_5R	5	32.45 \pm 0.33	31.69 \pm 0.56	n.s.

The relative mRNA expression levels of five samples collected from individual animals (n) were investigated via qRT-PCR. The resulting data (columns three and four) expressed as $50-\Delta C_T$ were analysed via Mann-Whitney-test (see *P*-values in column 5). TP = testicular parenchyma, TC = testicular capsule, n.s. = not significant.

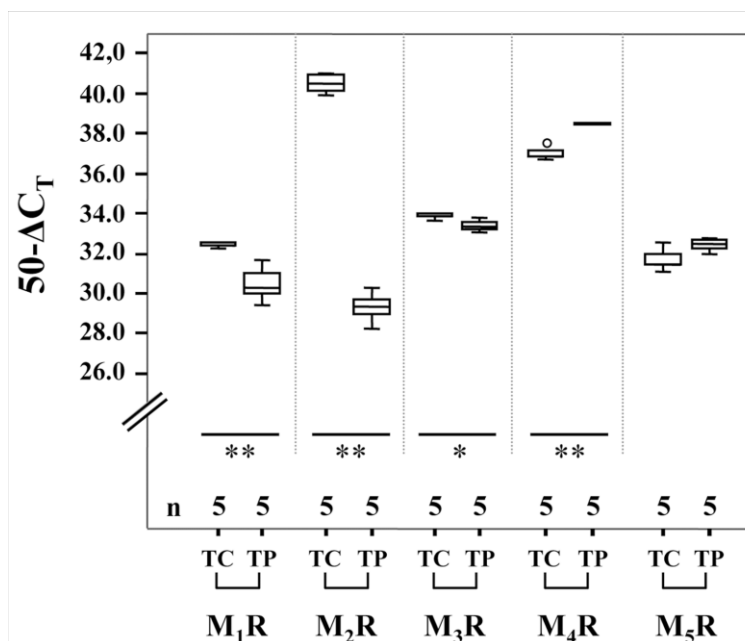


Fig. 14: mRNA expression level of MR subtypes in rat TP and TC.

Data are plotted as Box plot with $n = 5$. For primer with more than one primer-set the following variants were used: M1_204, M2_193, M3_140, M4_163, M5_118 (Tab. 3). The circle represents outlier. The ΔC_T values were subtracted from 50 showing higher values with higher expression. Significances were analysed by Mann-Whitney-test and are shown in Tab. 11.

9.3. Relative mRNA expression analysis of ChAT, ChT1, OCT2 and VACHT in rat testicular parenchyma

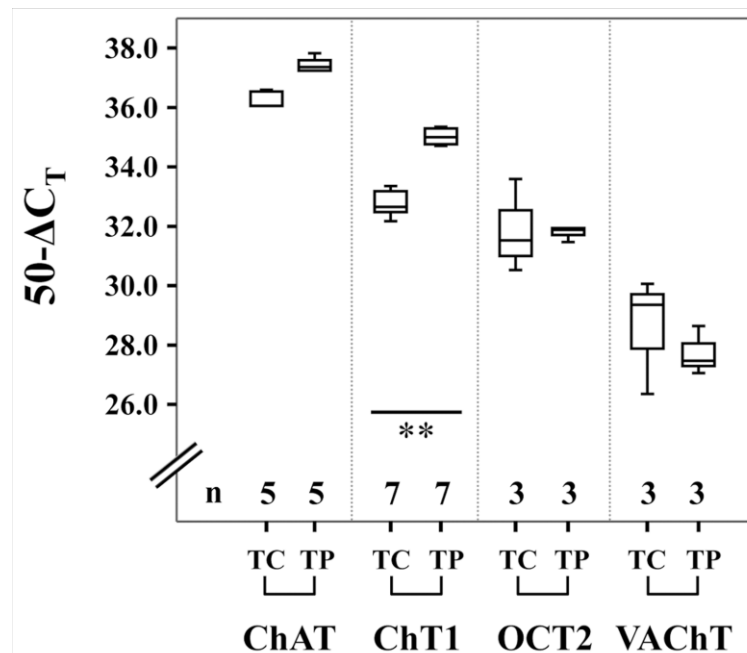
All four molecules were expressed in TP and TC and the rank order of the relative mRNA expression levels was ChAT > ChT1 > OCT2 > VACHT for both tissues.

Comparison of relative expression levels of TP and TC showed significantly higher ChT1 mRNA expression in TP (Tab. 12, Fig. 15).

Tab. 12: Expression of ChAT, ChT1, OCT2 and VACHT in TP and TC.

target	samples n	TP mean \pm SD	TC mean \pm SD	<i>P</i> -values TP vs. TC
ChAT	5	37.17 \pm 0.81	35.97 \pm 0.86	n.s.
ChT1	7	35.03 \pm 0.30	32.79 \pm 0.46	0.001
OCT2	3	31.77 \pm 0.28	31.89 \pm 1.56	n.s.
VACHT	3	27.72 \pm 0.81	28.59 \pm 1.98	n.s.

Relative mRNA expression levels of three to seven samples collected from individual animals (n) were investigated via qRT-PCR. The resulting data expressed as $50-\Delta C_T$ (columns three and four) were analysed via Mann-Whitney-test. Column 5 shows *P*-values for individual targets. TP = testicular parenchyma, TC = testicular capsule. n.s. = not significant.

**Fig. 15: mRNA expression level of OCT2, VACHT, ChAT and ChT1 in rat TP and TC.**

Data for choline acetyltransferase (ChAT), high-affinity choline transporter (ChT1), vesicular ACh transporter (VACHT) and organic cation transporter 2 (OCT2) are shown as $50-\Delta C_T$ as Box plot. For primer with more than one primer-set the following variants were used: ChT1_189, OCT2_226 (Tab. 6.). Data were analysed by Mann-Whitney-test and *P*-values are shown as asterisk within the plot.

9.4. Relative mRNA expression of mAChR, ChAT, ChT1, VACHT and OCT2 in mouse testicular parenchyma and -capsule

Additionally to rat samples, mouse samples were analysed for mRNA expression level of muscarinic ACh-receptors, the synthesizing enzyme and the transporters. All five MR-subtypes, M₁R-M₅R, are expressed in TC and TP of mice (Fig. 16). In the parenchyma, the M₄R-subtype showed the highest and M₃R-subtype the lowest expression level whereas within the capsule a similar mRNA expression level was observed for M₄R and M₃R subtypes. M₁R, M₂R and M₅R were expressed similarly in parenchyma and capsule. A significant difference in the expression level could be observed for M₁R, M₃R and M₅R between the TC and TP (Tab. 13).

The relative mRNA expression profiles for ChAT, ChT1, VACHT and OCT2 were also determined in murine tissue. All four molecules were expressed in TP and TC. The relative mRNA expression levels of ChAT and OCT2 were similarly in TP and TC. In contrast to the rats VACHT showed the highest mRNA expression level of these four molecules and ChT1 was absent in three out of five analysed TC-samples (Fig. 17, Tab. 13).

Tab. 13: Expression of MR subtypes and ACh-related molecules in mouse TP and TC.

target	samples n	TP mean \pm SD	TC mean \pm SD	<i>P</i> -values TP vs. TC
M ₁ R	5	42.40 \pm 0.80	40.94 \pm 0.90	0.032
M ₂ R	5	41.56 \pm 0.63	40.91 \pm 0.58	n.s.
M ₃ R	5	38.35 \pm 1.17	43.70 \pm 0.43	0.008
M ₄ R	5	45.59 \pm 1.07	44.46 \pm 1.17	n.s.
M ₅ R	5	42.68 \pm 0.98	41.13 \pm 0.82	0.032
ChAT	6 & 7	38.02 \pm 0.81	37.41 \pm 1.17	n.s.
ChT1	2 & 5	36.25 \pm 0.81	34.97 \pm 0.06	n.s.
OCT2	5	38.74 \pm 1.11	38.09 \pm 1.10	n.s.
VACHT	5	45.21 \pm 1.11	43.13 \pm 1.03	0.032

The relative mRNA expression level of two to seven samples (n) collected from individual animals was investigated via qRT-PCR. The resulting data expressed as 50- ΔC_T (columns three and four) were analysed via Mann-Whitney-test. Column 5 shows the *P*-values for individual targets. TP = testicular parenchyma, TC = testicular capsule, n.s. = not significant.

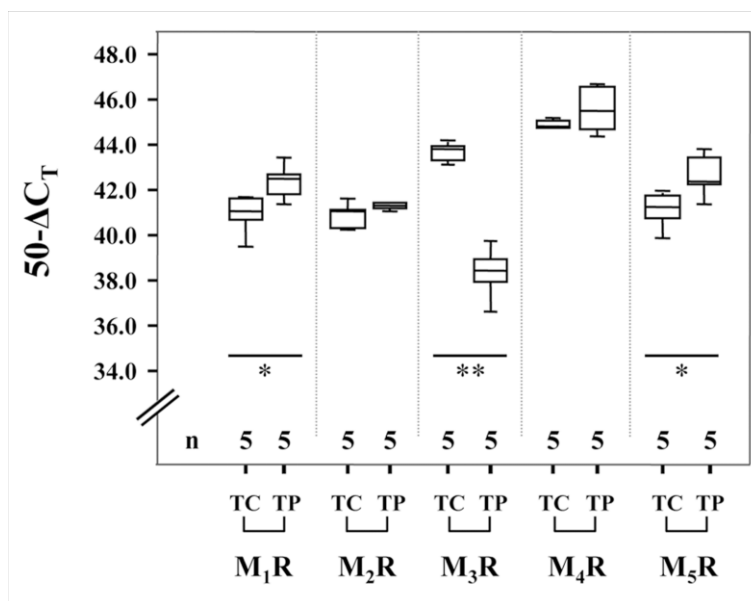


Fig. 16: mRNA expression level of MR subtypes in mouse TP and TC.

Data are plotted as Box plot with $n = 5$. Used primers are described in Tab. 7. The ΔC_T values were subtracted from 50 showing higher values with higher expression. Significances were analysed by Mann-Whitney-test and are indicated by asterisk (Tab. 13).

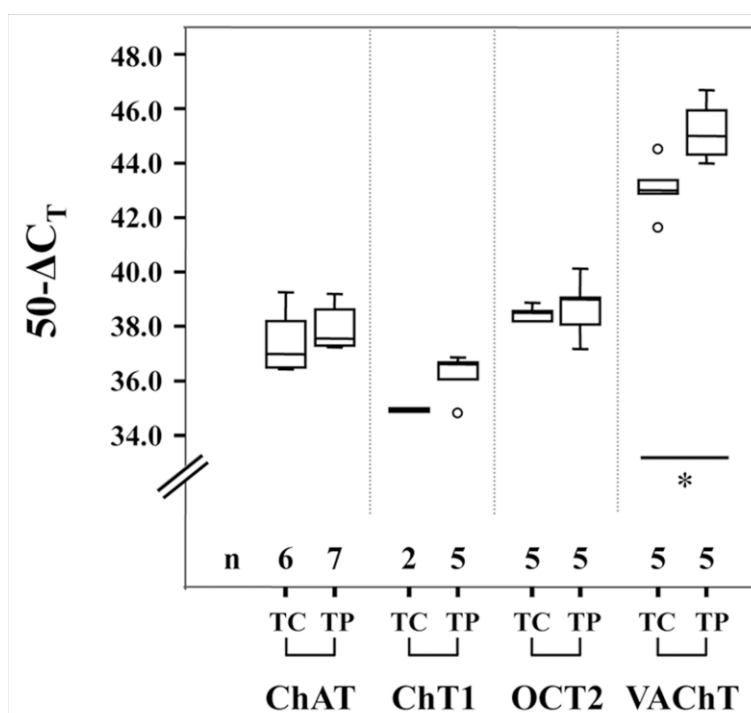


Fig. 17: mRNA expression level of OCT2, VACHT, ChAT and ChT1 in mouse TP and TC.

Data for choline acetyltransferase (ChAT), high-affinity choline transporter (ChT1), vesicular ACh transporter (VACHT) and organic cation transporter 2 (OCT2) are plotted as Box plot $50-\Delta C_T$ (n = number of experiments). The circles represent outlier. Significances were analysed by Mann-Whitney-test and are indicated by asterisk (Tab. 13)

9.5. Immunohistochemical detection of ChAT, ChT1 and VACHT in rat testis

Immunoreactivity for ChAT-, ChT1- and VACHT-proteins were detected in testicular parenchyma. The labelling was present mainly within the seminiferous tubules.

9.5.1. Immunoreactivity for ChAT in testicular parenchyma

ChAT-IR could be found in primary and secondary spermatocytes as well in spermatids (Fig. 18A, B & D). In addition, ChAT-IR was present in blood vessels (Fig. 18D arrow) and individual cells at the base of the tubules which might represent spermatogonia (Fig. 18 C arrow). The specificity of the antibody was verified by pre-absorption, which abolished immunolabelling in spermatocytes (Fig. 19B & D arrows) and reduced it in spermatids (Fig. 19B & D arrowheads).

9.5.2. Immunoreactivity for ChT1 in testicular parenchyma

In addition to ChAT, ChT1-IR was present in spermatocytes of seminiferous tubules (Fig. 18B, 20E & F). Furthermore it could be observed that the localisation of ChT1-IR varied in tubules in a stage dependent manner (Fig. 20D & E). In tubules of a later stage with more mature spermatids, the ChT1-IR was weaker and more diffuse than in tubules in an earlier stage of spermatogenesis (Fig. 20A & B). In addition, individual cells at the base of the seminiferous epithelium that likely represent spermatogonia were labelled positive for ChT1 (Fig. 20C arrow).

9.5.3. Immunoreactivity for VACHT in testicular parenchyma

Immunoreactivity for the VACHT protein could be detected in cells within the basal layer of the seminiferous epithelium as seen for ChT1 and ChAT. In comparison to ChT1 and ChAT the VACHT-IR was more intense and visualised the presence of branches passing the surrounding layer of PTC (Fig. 21D, arrow). The morphology of the VACHT-immunoreactive cells was similar indicating spermatogonia or a spermatogonial subpopulation as their numbers were low (Fig. 21), but could not be observed in every tubule within one section of the rat testis. VACHT-IR was present

in blood vessels too (Fig. 21A arrow). Except the obvious labelling of these cells, the VACHT labelling was weak within the tubules; therefore no specific cell type could be identified. Specificity of VACHT-antiserum was determined by a pre-absorption experiment with VACHT peptide on rat heart sections. No nerve fibres positive for VACHT were observed after incubation with a mixture of VACHT-antiserum and VACHT-peptide, whereas VACHT-positive fibres were visible in the sections incubated with VACHT-antiserum alone (Fig. 22B & D, arrows).

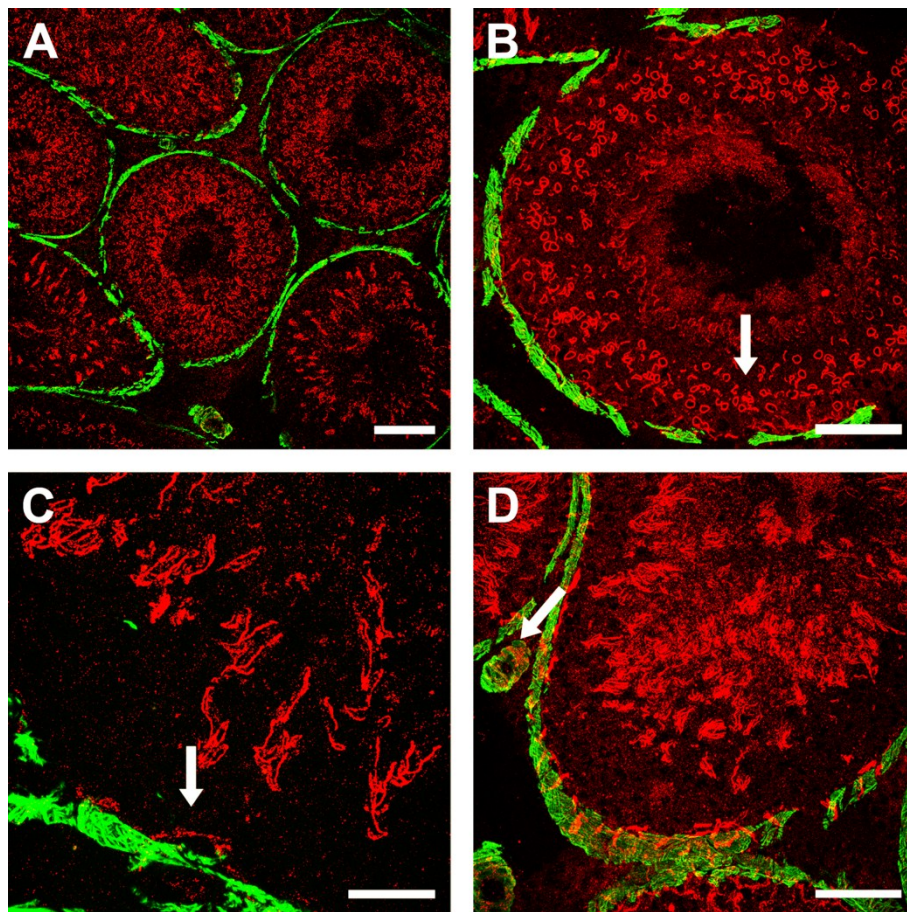


Fig. 18: Multiple labelling immunohistochemistry for ChAT.

Cryo-sections of fresh frozen testis were fixed with methanol and labelled with sheep-anti-ChAT antiserum (red) and FITC-conjugated α -SMA antibody (green). Scale bars: A = 100 μ m, B & D = 75 μ m, C = 20 μ m. Arrows indicate spermatocytes (B), cells in the basal layer (C) and a blood vessel (D).

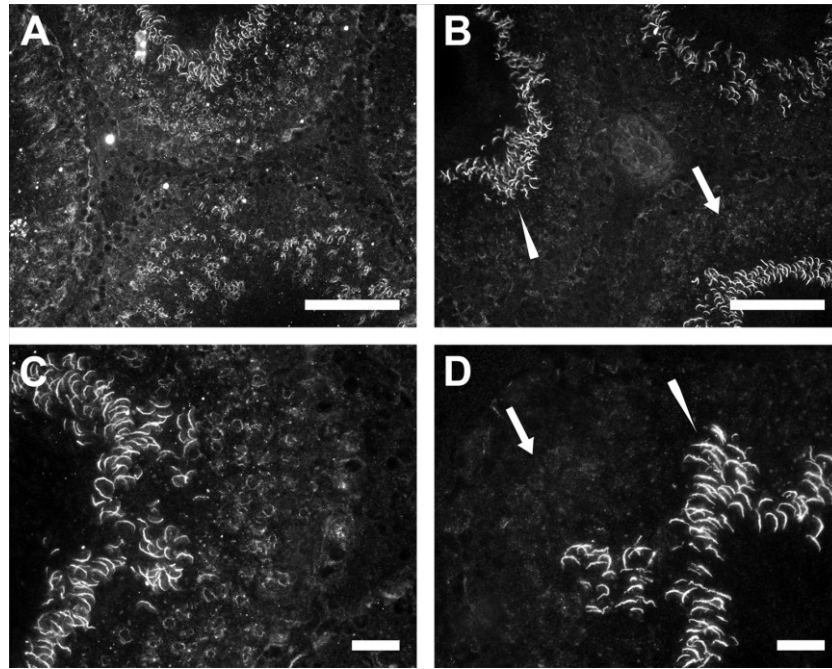


Fig. 19: Validation of ChAT antiserum.

Cryo-sections of fresh frozen testis were fixed with methanol and incubated with sheep-anti-ChAT antibody (A & C) or with a pre-incubated ChAT-peptide (40 $\mu\text{g}/\mu\text{l}$) – ChAT-antiserum-mix (B & D). Arrows = spermatocytes, arrowheads = spermatids. Scale bars: A & B = 100 μm , C & D = 25 μm .

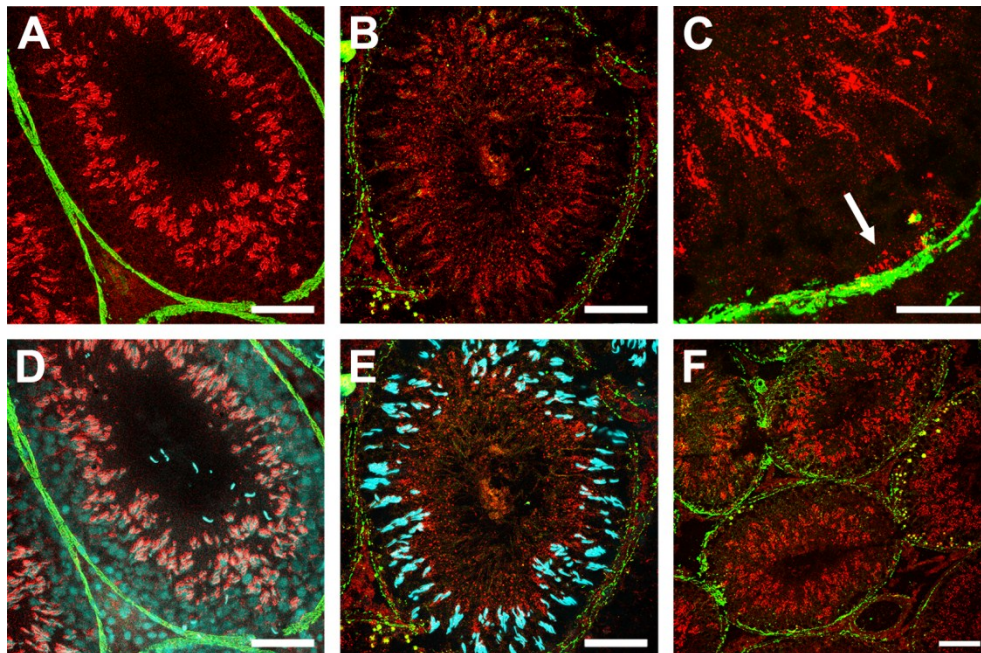


Fig. 20: Multiple labelling immunohistochemistry for ChT1.

Cryo-sections of fresh frozen testis were fixed with methanol and labelled with rabbit-anti-ChT1 antiserum (red), FITC-conjugated α -SMA antibody (green) and Hoechst (cyan). Arrow (C) indicating a ChT1 positive cell in the basal layer. Scale bars A, B, D & E = 75 μm , F = 100 μm , C = 20 μm .

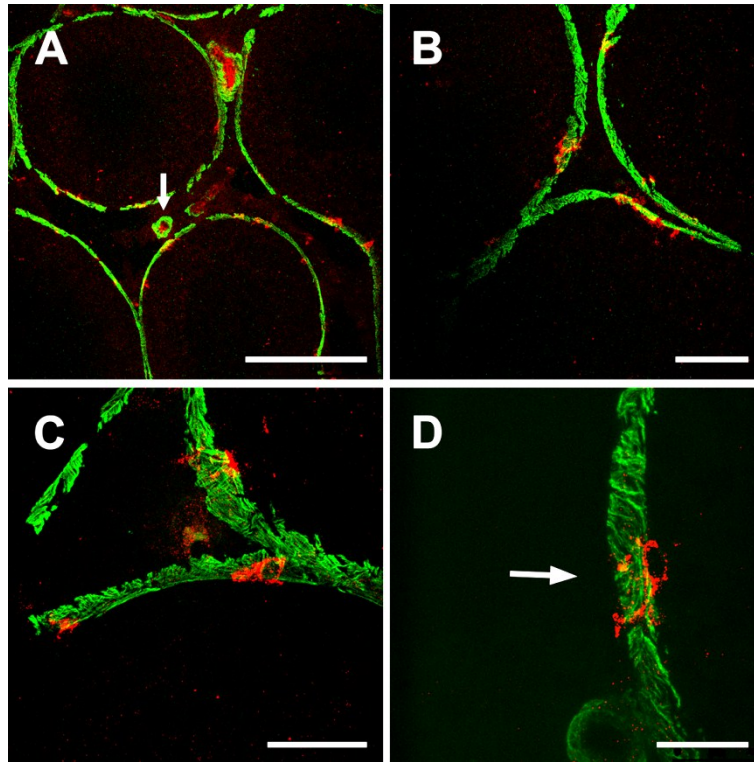


Fig. 21: VACHT multiple labelling immunohistochemistry.

Cryo-sections of fresh frozen testis were fixed with methanol and labelled with goat-anti-VACHT antiserum (red) and FITC-conjugated α -SMA antibody (green). Scale bars: A = 250 μ m, B = 75 μ m, C = 50 μ m, E = 25 μ m.

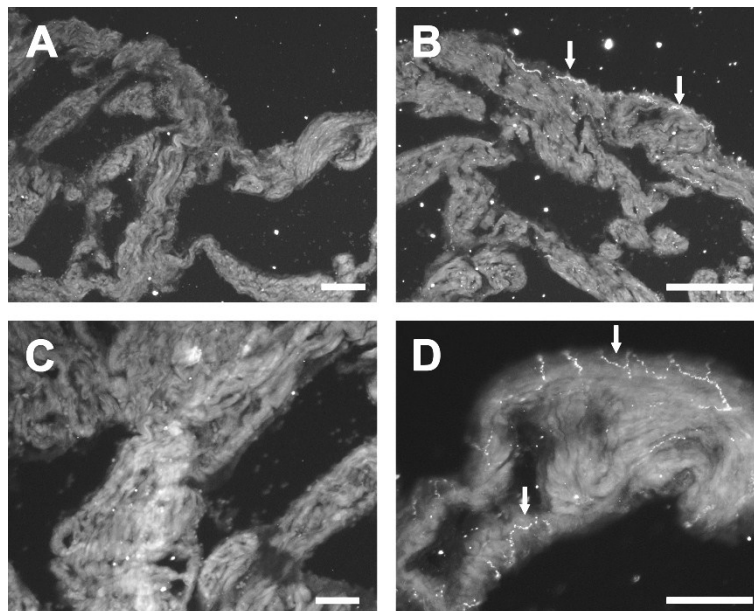


Fig. 22: Validation of the VACHT antiserum.

Cryo-sections of fresh frozen testis were fixed with methanol and incubated with goat-anti-VACHT antiserum (B & D) or with a pre-incubated VACHT-peptide (80 μ g/ μ l) – VACHT-antiserum-mix (A & C). Scale bars: A-D = 100 μ m.

9.6. *In situ* hybridisation for the $\alpha 7$ nAChR-subunit and ChAT in rat testis

Since subunit-specific nAChR and subtype-specific MR antisera were not available [246, 247], it was not possible to further analyse the expression at the level of receptor proteins. Therefore, the localisation of the $\alpha 7$ -nAChR subunit and in addition the ACh synthesising enzyme ChAT were analysed by ISH.

9.6.1. Optimisation of *in situ* hybridisation probes using spinal cord as control tissue

In situ hybridisation probes were generated via DIG RNA-Labeling Kit and PCR. ChAT and $\alpha 7$ specific ISH primers were used for standard PCR to prove their tissue specificity (Fig. 23). ChAT and $\alpha 7$ standard PCR primers were used as primer specific controls. RPL-19 served as a reference gene and positive control for the analysed tissue: testicular parenchyma. Both primer worked nicely in standard PCR and could be used for further experiments. The higher bp values of the ISH primers are related to the additional sequence for T7 and SP6 binding sites.

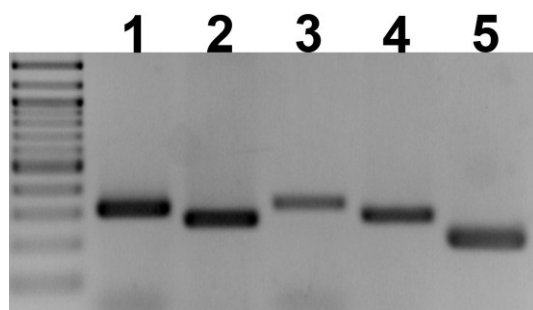


Fig. 23: Control PCR with ISH primer pairs.

Primers for ISH were used in standard PCR to check the specificity (lane 1: ChAT; lane 3: $\alpha 7$). Standard primer for ChAT, $\alpha 7$ (lane 2 and 4) and RPL-19 (lane 5) served as controls.

Because of the unknown localisation of $\alpha 7$ - and ChAT-mRNA within the testis, sequence specific probes were checked for their localisation on rat spinal cord sections. The protocol was used as described in 6.5.2 with the recommended hybridisation temperature of 72°C. The results using this temperature were not satisfying (Fig. 24A-C). The hybridisation temperature for the $\alpha 7$ - and ChAT-probes had to be optimised and was finally set to 65°C, which lead to the detection of $\alpha 7$ and ChAT in cells of the control tissue spinal cord using antisense but not sense probes (Fig. 24D-F). After successful ISH in the positive control spinal cord, the probes could be used for mRNA detection in rat testis.

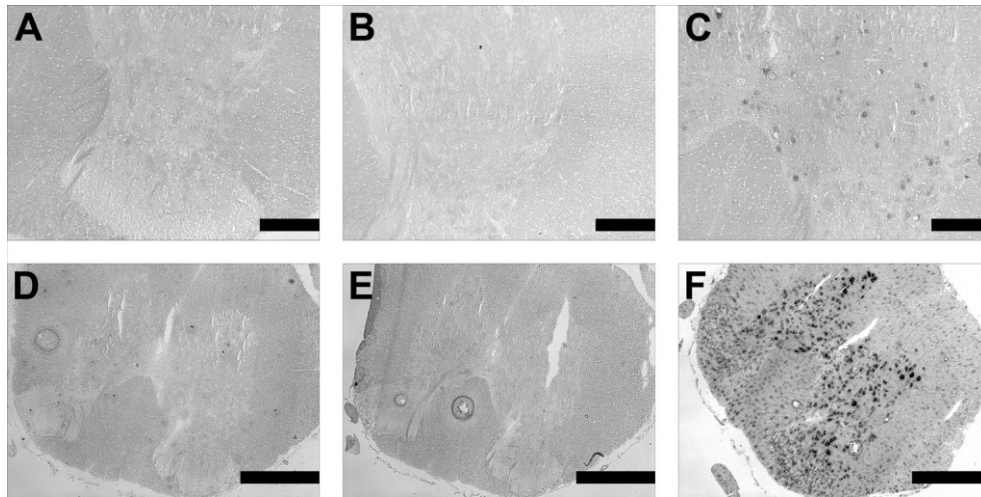


Fig. 24: ChAT mRNA detection in rat spinal cord via ISH.

ISH was performed with ChAT sense (B & E) and antisense (C & F) or in absence of DIG labelled probes (control, A & D) at 72°C (A-C) or 65°C (D-F). Scale bars: A-C = 75 μ m and D-F = 100 μ m.

9.6.2. Localisation of mRNA expression for the $\alpha 7$ nAChR-subunit and ChAT in rat testis

ChAT mRNA could be detected mainly in primary spermatocytes and weaker in round spermatids (Fig. 25B-D, G & H). The expression was similar in different populations of seminiferous tubules of the same sample (Fig. 25 B).

In addition, the mRNA for $\alpha 7$ -subunit was identified in seminiferous tubules (Fig. 15). In contrast to ChAT, the mRNA for $\alpha 7$ was not equally present in all tubules of one analysed section indicating stage specificity (Fig. 26C & D). Mostly round spermatids were strongly positive for $\alpha 7$ mRNA, with weaker labelling in primary spermatocytes and no visible staining in spermatogonia. Nevertheless in some tubules $\alpha 7$ mRNA seems to be present in primary spermatocytes and spermatogonia (Fig. 26).

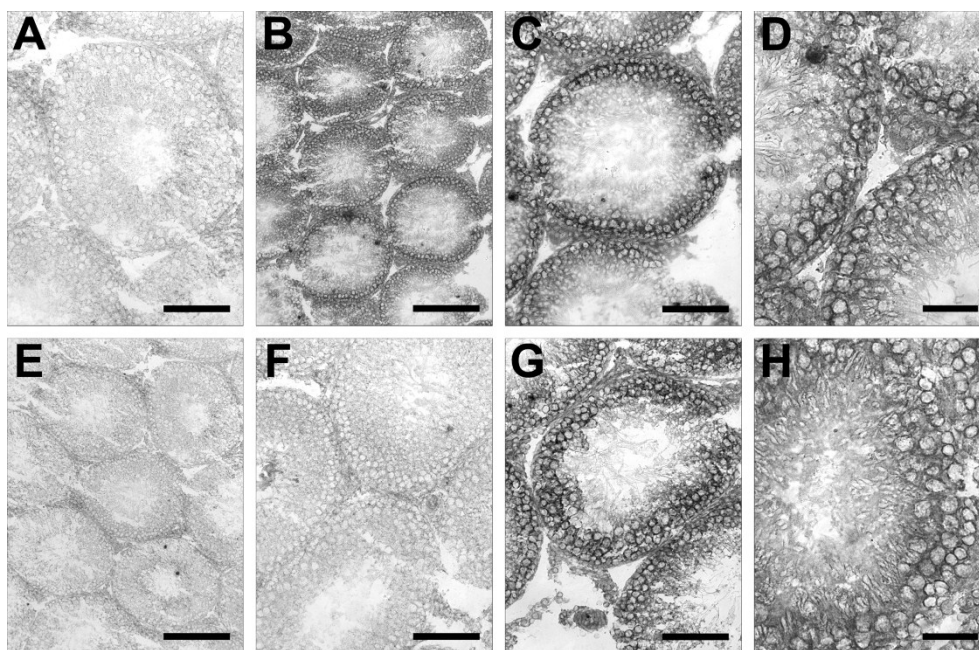


Fig. 25: ChAT mRNA detection at rat testis via ISH.

Testis cryo-sections were incubated with anti-sense probe (B-D, G & H), sense probe (E & F) or with no DIG labelled probes (control, A). Scale bars: A, C, F & G = 50 μ m; D & H = 20 μ m and B & E = 200 μ m.

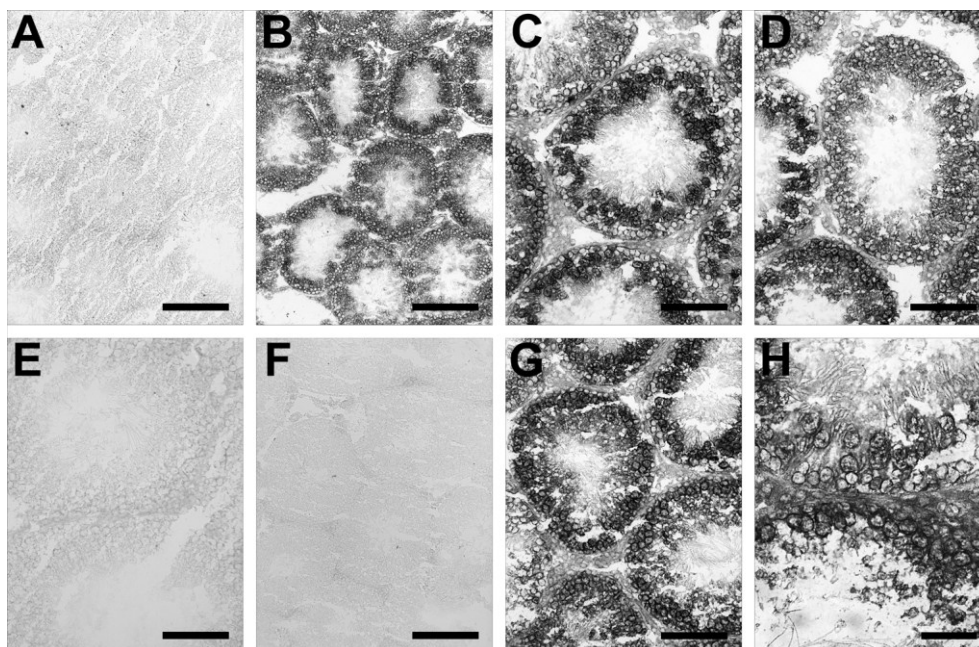


Fig. 26: α 7 mRNA detection at rat testis via ISH.

Testis cryo-sections were incubated with anti-sense probe (B-D, G & H), sense probe (E & F) or with no DIG labelled probes (control, A). Scale bars: A, C, F & G = 50 μ m; D & H = 20 μ m and B & E = 200 μ m.

10. Testicular somatic cells: peritubular cells, Sertoli cells and testicular macrophages

10.1. Immunohistochemical characterisation of isolated and cultured testicular somatic cells

To test the purity of isolated primary testicular somatic cells, they were cultured on coverslips and the presence of characteristic marker proteins was determined using immunohistochemistry (Fig. 27).

Testicular macrophages were characterised by immunolabelling with ED1 (CD68) and ED2 (CD163) antibodies, which recognise migrated monocytes and resident macrophages. Nuclei were stained with DAPI. The ratio of ED1/ED2 positive cells and DAPI positive cells showed an 80% enrichment ($80.4\% \pm 3.57\%$, $n = 5$) of isolated primary TM cultures.

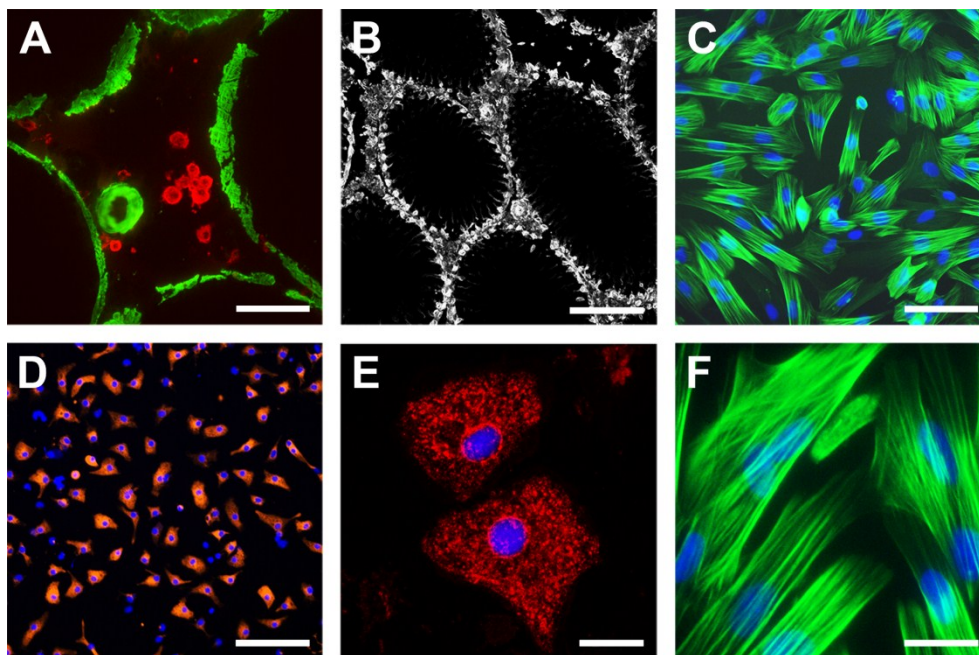


Fig. 27: Cell-type specific labelling of PTC, SC and TM.

Isolated testicular cells can be stained specifically. PTC are labelled with FITC-conjugated α -SMA (A, C & F), SC are visualised with mouse-anti-rat-vimentin (B) and mouse-anti-rat-ED1/ED2 (red) was used for detection of TM (A, D & E). DAPI is shown in blue. Scale bars: B & D = 100 μ m, A & C = 50 μ m, F = 25 μ m, E = 14.4 μ m.

Isolated PTC were allowed to passage three times, a process which destroys virtually all contaminants in parallel to expansion of PTC by proliferation. PTC were defined by the positive staining for α -SMA and DAPI. The purity of PTCs was around 98% ($97.6\% \pm 0.99\%$, $n = 4$). Sertoli cells were isolated and incubated for 6 days. The SCs were labelled with vimentin and DAPI and the purity was determined to be 90% ($89.5\% \pm 1.86\%$, $n = 4$).

10.2. The cholinergic system in testicular somatic cells

Beside various germ cell types, expression of ChAT-, ChT1-, VAChT-, OCT2-, nAChR α 4- and α 7-mRNAs has been analysed for PTC and SC as part of the thesis of Iris Eckhardt. In this study relative mRNA expression levels for the same molecules were analysed in TM, whilst SC and PTC were used as intraassay controls.

PTC, SC and TM were isolated as described previously, total RNA was isolated and reverse transcribed into cDNA (6.1.- 6.3.). The relative expression of mRNAs was analysed for the remaining nAChR-subunits and MR-subtypes via standard RT-PCR.

nAChR β -subunits. All analysed PTC samples contained mRNA for β 1, β 2 and β 3. Four out of five preparations also contained β 4 mRNA (Tab. 14A). In SC one out of four samples showed no PCR product that corresponded to β 3. All other SC samples showed positive results for β 1 to β 4 (Tab. 14A). The mRNA expression pattern for TM showed a variable detection of β -subunits. Only subunit β 3 was expressed in all analysed primary cultured TM (Tab. 14A). One, two or three out of six samples showed a positive result for β 4, β 1 and β 2 (Tab. 14A).

nAChR α -subunits. Overall, the expression for nAChR α -subunits analysed in PTC, SC and TM samples was heterogeneous in comparison to the β -subunits. In PTC samples mRNA was detected in 4/5 cases for α 5 and α 6. Even less mRNA was observed for α 2, α 9 and α 10 with two, three and two out of five samples. α 3 mRNA was not detectable in PTC (Tab. 14B). As seen for PTC, SCs do not express nAChR-subunit α 3 and additionally no α 6. Several samples showed a PCR product for the subunit α 2 (2/4), α 9 (3/4) and α 10 (4/5). Only mRNA for subunit α 5 was expressed in all analysed samples (Tab. 14B). In TMs α 5, α 6, α 9 and α 10 were observed in 4/6 and 5/7 samples. A lower number of samples did show mRNA expression for subunits

$\alpha 2$ (4/7) and $\alpha 3$ (2/6). PCR products corresponding to the mRNA for the nAChR-subunits $\alpha 4$ and $\alpha 7$ could be detected in all analysed samples (Tab. 14B).

Tab. 14: Standard PCR for nAChR-subunits in PTC, SC and TM

		positive detected samples in cell populations		
A	nAChR	PTC	SC	TM
	$\beta 1$	5/5	4/4	2/6
	$\beta 2$	5/5	4/4	3/6
	$\beta 3$	5/5	3/4	6/6
	$\beta 4$	4/5	4/4	1/6
B				
	$\alpha 2$	2/5	2/4	4/7
	$\alpha 3$	0/5	0/4	2/6
	$\alpha 4$	pos.	neg.	4/4
	$\alpha 5$	4/5	4/4	4/6
	$\alpha 6$	4/5	0/4	4/6
	$\alpha 7$	pos.	pos.	4/4
	$\alpha 9$	3/5	3/5	5/7
	$\alpha 10$	2/5	4/5	5/7

Three to seven independent samples of PTC, SC and TM were analysed for mRNA expression of nAChR-subunits α (B) and β (A) by standard PCR. For primer with more than one primer-set the following variants were used: $\alpha 2_{114}$, $\alpha 6_{139}$, $\alpha 9_{242}$, $\alpha 10_{168}$ (Tab. 5). Results are shown as positive detected samples out of all samples. Positive and negative results for $\alpha 4$ and $\alpha 7$ for PTC and SC are taken from a previous doctoral thesis (Tab. 14B).

mAChR subtypes. In PTC, mRNAs for M_2R , M_3R and M_4R were detected in all analysed preparations ($n = 4$), whereas M_1R and M_5R were present in 3/4 samples (Tab. 15). A similar result was observed for SC. mRNAs for MR subtypes 1, 2, 4 and 5 were detected in all preparations, whereas M_3R was present in 2/4 cultures (Tab. 15). In TM the mRNA expression for MR was again more heterogeneous. Only M_1R was present in all analysed samples, whereas M_2R was detectable in 3/6 and M_4R in 4/6 samples. mRNA for M_3R and M_5R could be amplified in 2 of 6 samples (Tab. 15).

ChAT, VAChT, OCT2 and ChT1. In a previous doctoral thesis, the presences of the ACh-synthesising enzyme and several related transporters was analysed for PTC and SC using standard PCR (thesis Iris Eckardt in Schirmer et al., 414). In this study TM were analysed for the same molecules. ChT1 and ChAT mRNA was detected in all

analysed samples. mRNA for OCT2 was present in only 1/4 samples, whereas no PCR product corresponding to VACHT was observed (Tab. 16).

Tab. 15: Standard PCR for MR subtypes in PTC, SC and TM.

	positive detected samples in cell populations		
mAChR	PTC	SC	TM
M ₁ R	3/4	4/4	6/6
M ₂ R	4/4	4/4	3/6
M ₃ R	4/4	2/4	2/6
M ₄ R	4/4	4/4	4/6
M ₅ R	3/4	4/4	3/6

mRNA expression profiles for MR subtypes were analysed for PTC, SC and TM in four to six independent samples for by standard PCR. For primer with more than one primer-set the following variants were used: M1_110, M2_192, M3_287, M4_166, M5_180 (Tab. 3). Results are shown as positive detected samples out of all samples.

Tab. 16: Standard PCR for ChAT, ChT1, VACHT and OCT2 in TM.

	positive detected samples in cell populations		
	PTC	SC	TM
ChAT	pos.	pos.	4/4
VACHT	neg.	neg.	0/4
ChT1	pos.	pos.	4/4
OCT2	neg.	neg.	1/4

Four independent samples of TM were analysed for mRNA expression for ChAT, ChT1, VACHT and OCT2 by standard PCR. For primer with more than one primer-set the following variants were used: OCT2_162 and ChT1_150 (Tab. 6). Results are shown as positive detected samples out of all samples. Positive and negative results for PTC and SC are taken from a previous doctoral thesis.

10.3. Cell specific functional analysis of ACh receptors using calcium-imaging experiments

PTC, SC and TM express mRNAs for several nAChR-subunits and MR-subtypes. Due to the fact that currently no antibodies are available for nAChR-subunits or MR-subtypes, it was impossible to detect AChR-proteins within cells or tissues. Besides analysis of the mRNA expression pattern, the presence of the AChRs was confirmed by functional assays such as calcium-imaging.

10.3.1. Peritubular cells showed muscarine-induced increase in $[Ca^{2+}]_i$

PTCs were treated in individual experiments with ACh, nicotine and muscarine. It has to be mentioned that unstimulated PTC often showed oscillatory effects (Fig. 28). If this was the case almost all cells on one coverslip showed this oscillation synchronically and with the same amplitude. This oscillation was up to $\pm 5\%$ of the baseline. Therefore the positive response of cells, which was set to an at least 5% increase in $[Ca^{2+}]_i$, had to be quantified for every cover-slip individually. To avoid false positive results a 'positive reaction' of a cell was committed to 5-10% over baseline depending on the oscillation amplitude.

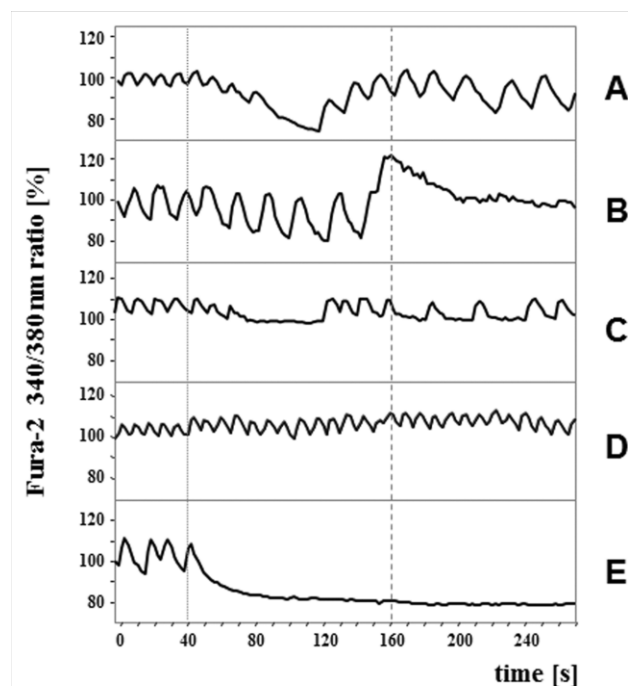


Fig. 28: PTCs show an oscillatory effect.

Each image (A-E) illustrates the mean of 60-80 analysed cells from one cover-slip. The oscillatory effect was not uniform for every cover-slip. Sometime the application of fluid ($t = 40$ s, dotted) induced changes in the amplitude (C & E) but not in all cases (B & D). The amplitude could increase (A), decrease (C) or disappear (E). The observation for a positive reaction on a drug was sometimes difficult to distinguish (B, addition of ACh at $t = 160$ s, dashed) and had to be analysed carefully. The Fura-2 ratio 340/380 nm is presented as percentage (%) over time (s).

The endogenous MR and nAChR agonist **ACh**, was added to the PTC with a concentration of 10 μM at $t = 160$ s. Immediately after the application an increase in $[\text{Ca}^{2+}]_i$ response of 47% ($\pm 47\%$ SD, $n = 95$ cells in $n = 3$ exp) over baseline could be observed (Fig. 29 black line; P -value in Fig. 33). About 10 s after reaching the peak the $[\text{Ca}^{2+}]_i$ slowly decreased, but did not return to the baseline level ($+ 24\% \pm 22\%$ SD) before ATP was added. Most cells (156/168) responded to ATP with an increase of about 70% over pre-ATP-level. In total 168 cells were analysed. 56.55% showed a positive reaction for ACh. 12.68% of ACh-responsive cells did not respond to the following ATP application. The remaining 87.32% were responsive to both ACh and ATP (Fig. 31). No increase in $[\text{Ca}^{2+}]_i$ response was observed for the control group treated with HEPES instead of ACh (Fig. 29).

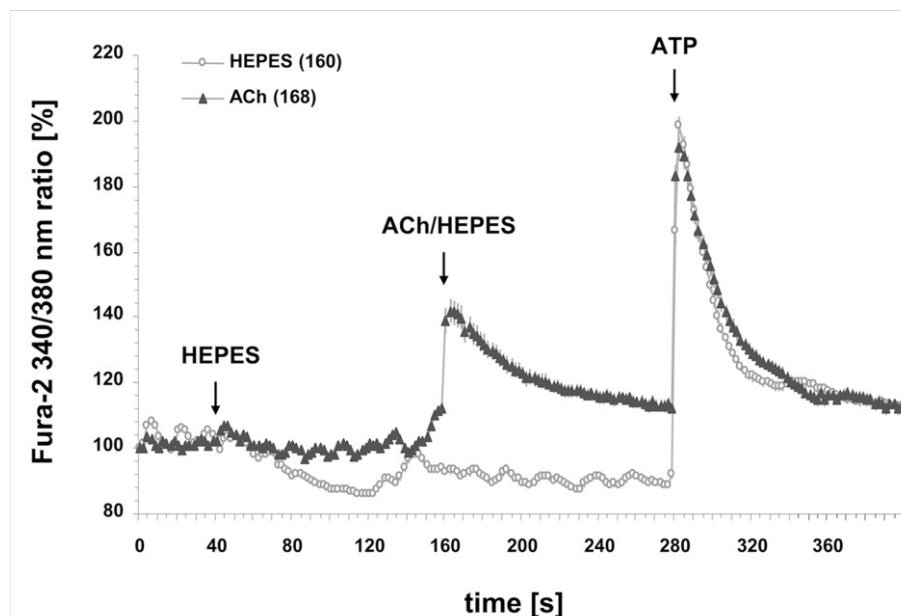


Fig. 29: ACh induces a $[\text{Ca}^{2+}]_i$ in PTC.

PTCs were treated three times during the experiment: at $t = 40$ s with HEPES, $t = 160$ s with ACh (10 μM) and $t = 280$ s with ATP (100 μM). The experimental group ($n = 3$) is shown in black. The control group ($n = 3$; grey) was treated at $t = 40$ s and $t = 160$ s with HEPES and at $t = 280$ s with ATP. The Fura-2 ratio 340/380 nm is presented as percentage (%) over time (s).

Muscarine, which activates all five MR subtypes, was applied to PTC with a concentration of 10 μM . Overall the cells were reacting similarly as previously seen during the ACh-treatment. After applying muscarine, the cells responded with an increase $[\text{Ca}^{2+}]_i$ of 61% ($\pm 48.7\%$ SD, $n = 112$ cells in $n = 3$ exp) over baseline (Fig. 30A black line; P -value in Fig. 33). The following decrease was slightly faster

compared to ACh-application without returning to baseline values ($+ 15\% \pm 18\%$ SD). 49.56% of the analysed 226 cells responded to muscarine. The vast majority of these cells (84.82%) responded to muscarine and ATP. Only 15.18% of the cells showed a reaction to muscarine, but did not respond to the following ATP application (Fig. 30B & 31).

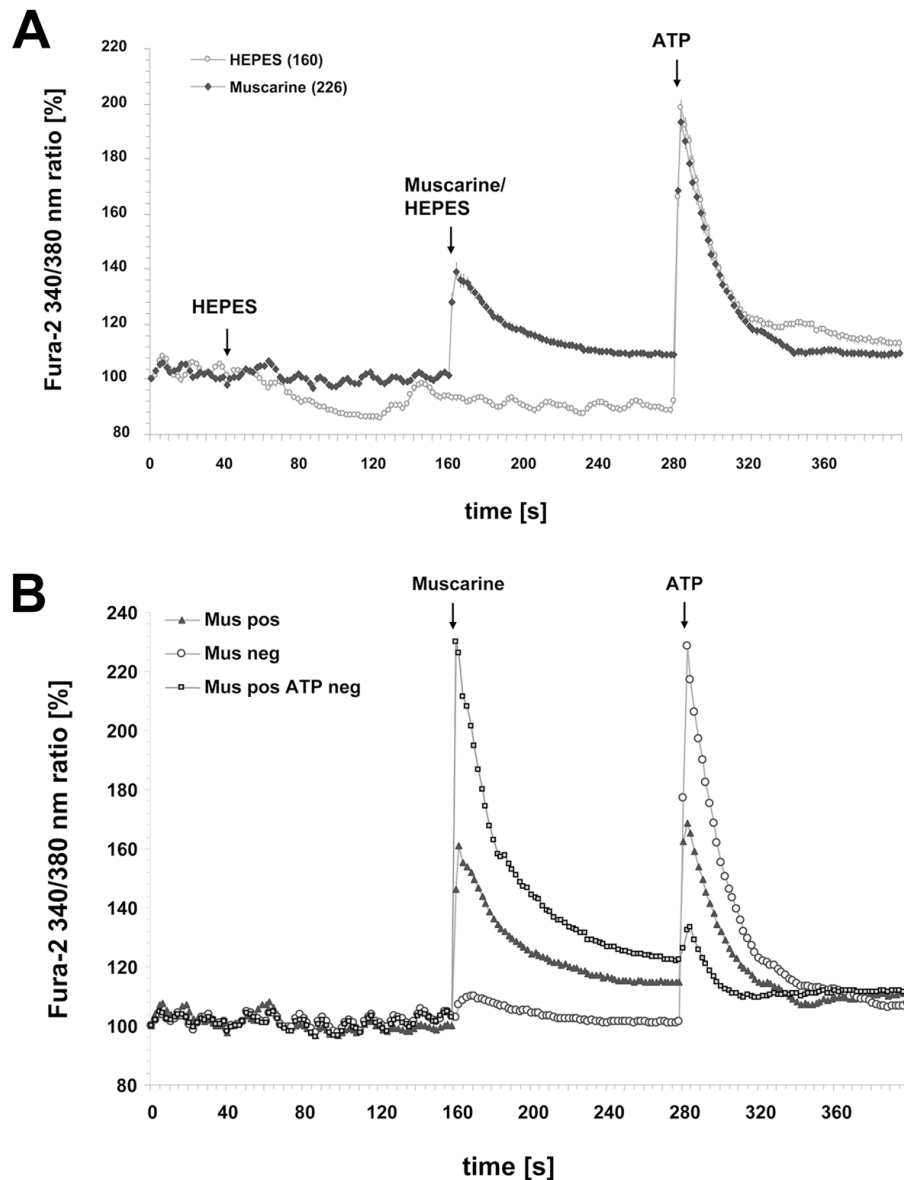


Fig. 30: Muscarine induces a $[Ca^{2+}]_i$ in PTC.

PTCs were treated three times during the experiment: at $t = 40$ s with HEPES, $t = 160$ s with muscarine ($10 \mu M$) and $t = 280$ s with ATP ($100 \mu M$). **(A)** The experimental group ($n = 3$) is shown in black. The control group ($n = 3$; grey) was treated at $t = 40$ s and $t = 160$ s with HEPES and at $t = 280$ s with ATP. **(B)** The different sub-populations of the PTC were separated dependent on the responsiveness to muscarine. Muscarine negative cells ($n = 114$, \circ), muscarine positive cells ($n = 112$, \blacktriangle) cells. Muscarine responsive and ATP non-responsive cells ($n = 17$, \blacksquare). The Fura-2 ratio 340/380 nm is presented as percentage (%) over time (s).

The shape of the curves after ATP-treatment to the cells was almost identical for both substances ACh and muscarine. The control cells ($n = 160$, $n = 3$ exp.), which were treated only with vehicle and ATP, did not show any reaction on the vehicle but all cells responded to ATP. The intensity of the response was similar to that for ACh and muscarine (Fig. 29 & 30A).

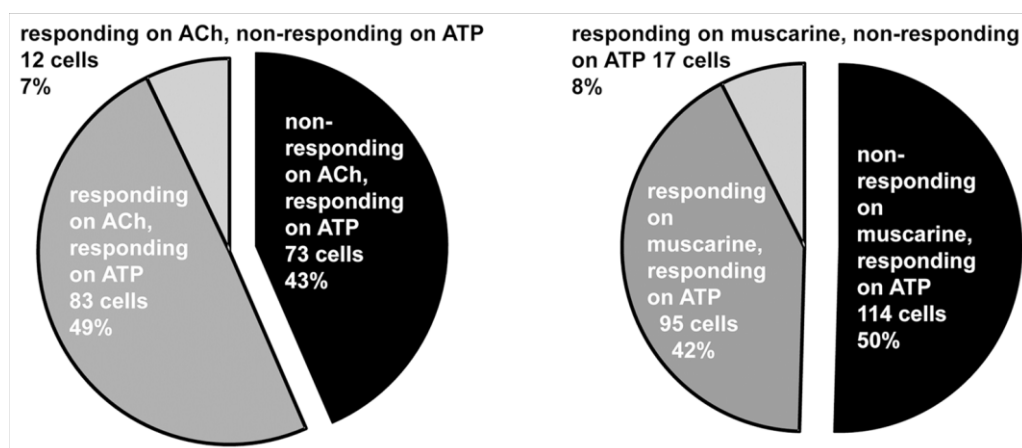


Fig. 31: Distribution of muscarine, ACh and ATP responsiveness of PTC.

Application of ACh (left panel) and muscarine (right panel) and subsequent treatment with ATP resulted in three PTC subpopulations: non-responding to ACh/muscarine but responding to ATP (black), responding to ACh/muscarine and ATP (dark grey) and responding to ACh/muscarine but non-responding to ATP (light grey). Amount of cells is indicated in numbers and percentage.

Nicotine, an ACh-agonist which binds specifically to nAChR, was added to the PTC with a concentration of 100 μ M. None of 197 cells responded to nicotine whereas all cells responded to ATP. The intensity of the ATP-response reached 120% over baseline (Fig. 32).

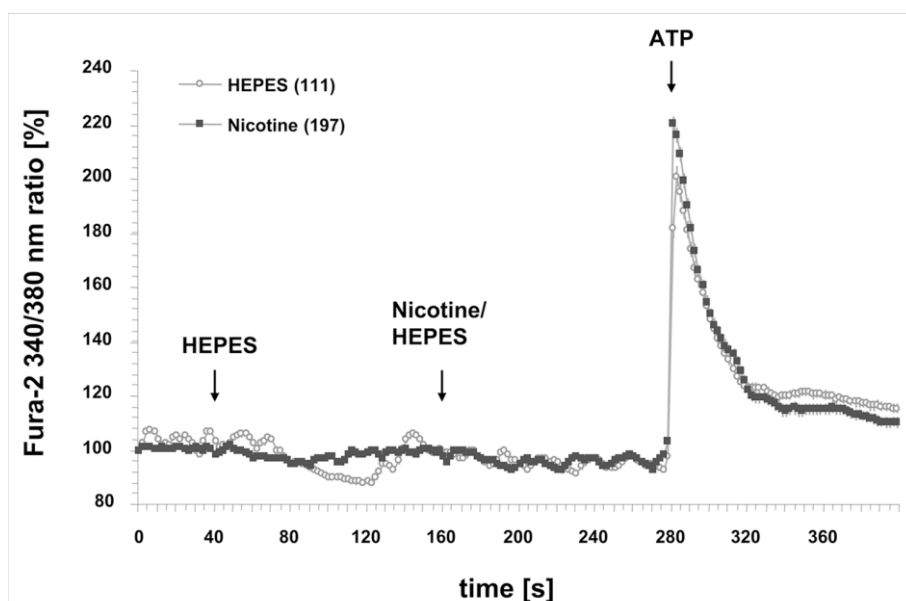


Fig. 32: Nicotine has no influence on the $[Ca^{2+}]_i$ in PTC.

PTCs were treated three times during the experiment: at $t = 40$ s with HEPES, $t = 160$ s with nicotine ($100 \mu M$) and $t = 280$ s with ATP ($100 \mu M$). The experimental group ($n = 3$) is shown in black. The control group ($n = 3$; grey) was treated with HEPES at $t = 40$ s and $t = 160$ s and once with ATP ($t = 280$ s). The Fura-2 ratio 340/380 nm is presented as percentage (%) over time (s).

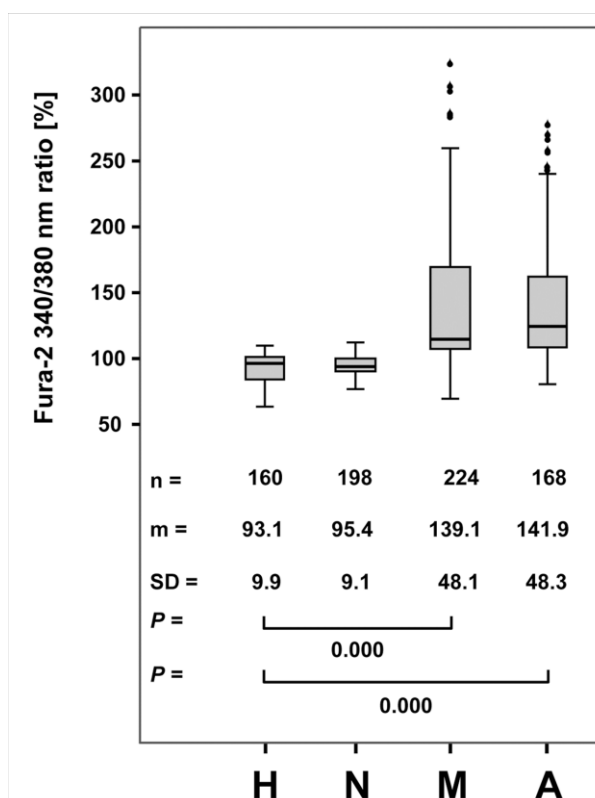


Fig. 33: *P*-values after agonist application in PTC-populations.

HEPES (H), nicotine (N), muscarine (M) or ACh (A) were applied to PTC at $t = 160$ s. Box plots show the distribution of the cells at time-point $t = 162$ s. Below the boxes are mentioned the amount of analysed cells (n), the mean (m), the standard deviation (SD) and the *P*-values. Significance was calculated using Kruskal-Wallis test followed by Mann-Whitney test. *P*-value for HEPES vs. nicotine was not significant.

10.3.2. Blockade of muscarine-induced receptor activation in PTC

To confirm the MR-dependent response of PTC to ACh and muscarine, the cells were pre-treated with 10 μ M atropine (Fig. 34-36). In both cases the calcium influx in response to muscarine and ACh was blocked. For both, muscarine and ACh, two experimental set-ups were used (Fig. 34).

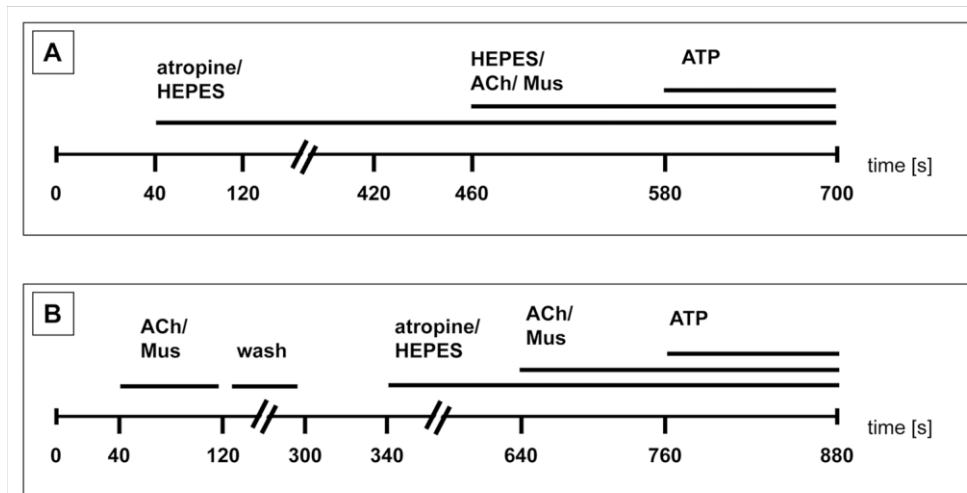


Fig. 34: Flow chart for inhibition experiment with PTC.

PTCs were incubated with atropine in two different experimental set-ups.

(A) Cells were treated with HEPES or atropine (10 μ M) at $t = 40$ s; with ACh (10 μ M), muscarine (10 μ M) or HEPES (control) at $t = 460$ s and with ATP (100 μ M) at $t = 580$ s. Atropine was incubated 5 min (//).

(B) Muscarine or ACh were applied to PTCs at $t = 40$ s and additionally removed by a 3 min wash step (//). Cells were treated with HEPES or atropine (10 μ M) at $t = 340$ s and incubated 5 min (//). At $t = 640$ s ACh (10 μ M) or muscarine (10 μ M) were added. The application of ATP (100 μ M) was at time point $t = 760$ s.

In the first set of experiments it was shown that atropine blocked the ACh- and muscarine-induced calcium-influx in all analysed cells ($n_{\text{ACh}} = 66$, $n_{\text{Mus}} = 75$) (Fig. 34A). Control cells, treated with HEPES and ACh or muscarine showed an increase in calcium-influx ($n = 1$, Fig. 35 A/B, grey line), whereas the cells pre-incubated with atropine did not respond to ACh or muscarine (Fig. 35 A/B, black line). The small peaks in both control curves (Fig. 35, grey line) are caused by oscillation and are no direct effect of ACh or muscarine.

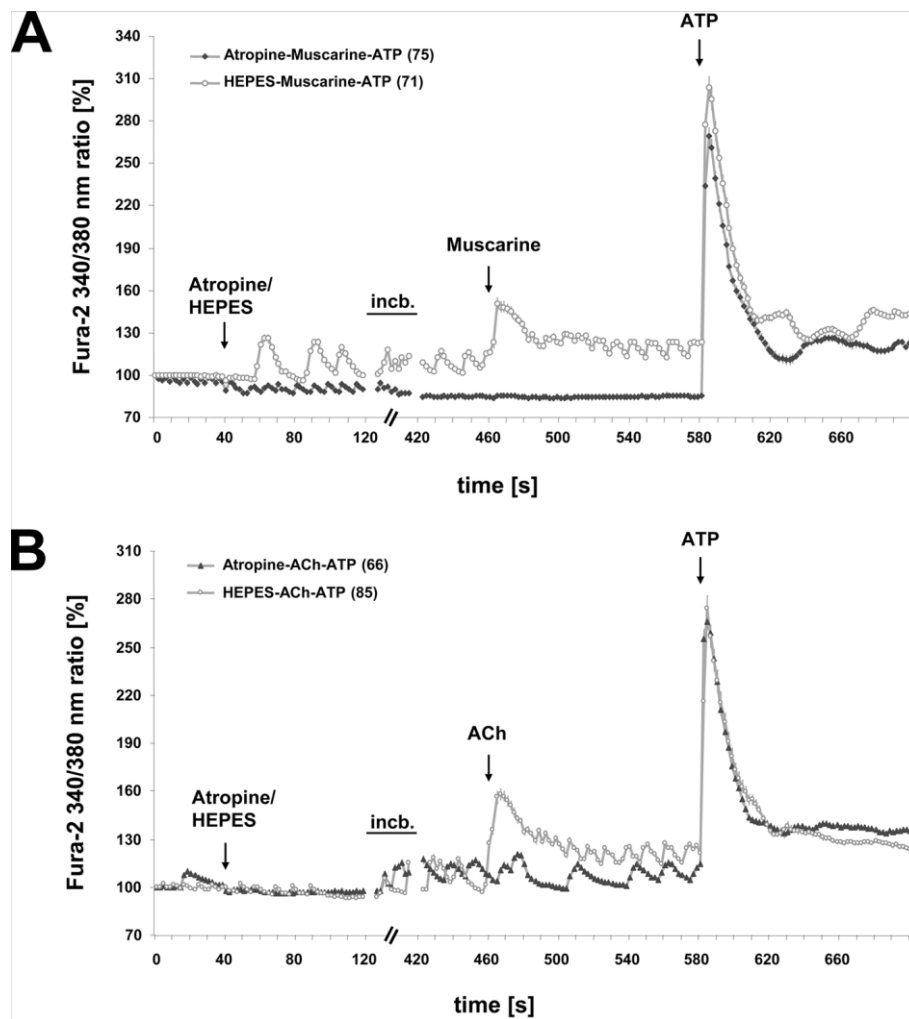


Fig. 35: ACh or muscarine induced calcium-influx can be blocked by atropine.

Experimental set-up was performed as described in Fig. 34A with $n = 1$ for each set-up. The grey lines represent the control groups, whereas the black lines show the atropine treated groups. PTC treated with muscarine are plotted in (A) and cells treated with ACh are shown in (B). The Fura-2 ratio 340/380 nm is presented as percentage (%) over time (s).

In the second experiment ($n = 1$), two cell populations were treated with ACh, which responded with an increase in Ca^{2+} ions as described previously (Fig. 29, 34B). ACh was removed by a 3 min wash step with HEPES buffer. Before an additional application of ACh, one population was pre-incubated with atropine and the other one with HEPES for 5 min each. In absence of the MR antagonist (Fig. 36A, grey line), the cells responded to ACh with an increase in $[\text{Ca}^{2+}]_i$, which was not present in the cell population pre-incubated with atropine (Fig. 36A, black line). With the same experimental set-up, cells were stimulated with muscarine instead of ACh (Fig. 36B).

The response of PTC to muscarine was similar as the response to ACh. A previously muscarine-induced calcium-influx was blocked with atropine (Fig. 36B).

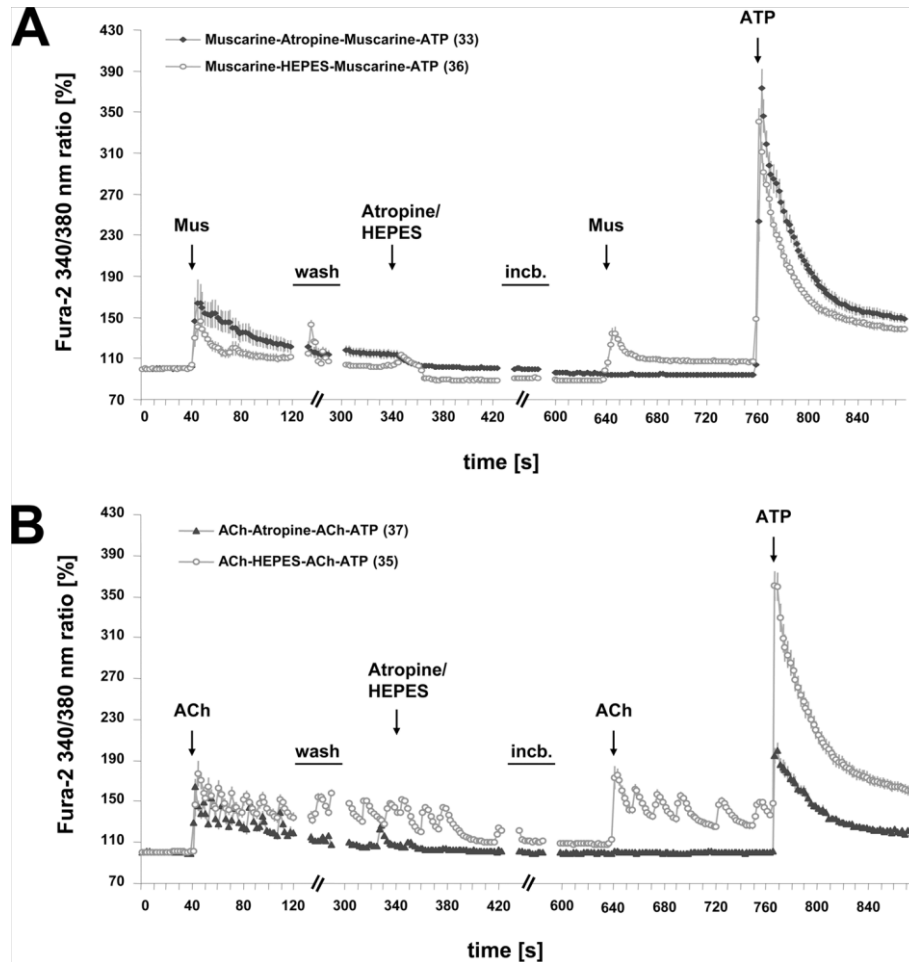


Fig. 36: Muscarine and ACh induced calcium-influx can be blocked by atropine.

Experimental set-up was performed as described in Fig. 34B with $n = 1$ for each set-up. The grey lines represent the control groups, whereas the black lines show the atropine treated groups. PTC treated with muscarine are plotted in (A) and cells treated with ACh are shown in (B). The Fura-2 ratio 340/380 nm is presented as percentage (%) over time (s).

10.3.3. Testicular macrophages showed no direct response to AChR stimulation

In five individual experiments TM were tested on their response for ACh, nicotine and muscarine. HEPES was used as control. TM showed no oscillations, therefore cells have been classified as positively responding if they showed at least 5% increase in $[Ca^{2+}]_i$ over baseline.

The treatment of TM with 100 μ M nicotine, 10 μ M muscarine or 10 μ M ACh resulted in the same response as seen for the non-stimulated control group (Fig. 37). Subsequent applications of ATP showed a response in all cells within all four groups. Overall the shape of the curves was similar. The steep increase was followed by a slower decrease. In detail, it could be observed that ATP-dependent Ca^{2+} -response differed dependent on the previous ACh-receptor stimulation.

A high Ca^{2+} increase in response on ATP was observed in the HEPES pre-treated control group. The fast increase up to about 80% over baseline was slowed down and followed by a “round peak” and a gradually decrease (Fig. 37). This “round peak” was almost like a plateau phase with increased Ca^{2+} levels for about 12 s and 96% ($\pm 61.8\%$ SD) over baseline.

Cells pre-incubated with nicotine and muscarine showed an almost identical shape of their curves after adding ATP (Fig. B & C, black line). A sharp peak with 99% ($\pm 62.1\%$ SD_{nic} & $\pm 75.5\%$ SD_{mus}) over baseline was reached 4 s after the application of ATP, but the following decrease was constant and faster compared to the control group. At the end of the experiment the cells, treated with nicotine or muscarine had a significant (20%) lower Fura-2 340/380 nm ratio compared to control cells.

Cells treated with ACh showed the lowest response to ATP within the 4 analysed groups. After the first increase at app. 81% ($\pm 54.9\%$ SD) over baseline there was a short transient decrease followed by a second increase and plateau phase 15 to 20 s later, which reached app. 85% ($\pm 49.7\%$ SD) over baseline. Subsequently, a slow and steady decrease of the curve was joining the nicotine and muscarine curves on the same level (Fig 37A, black line).

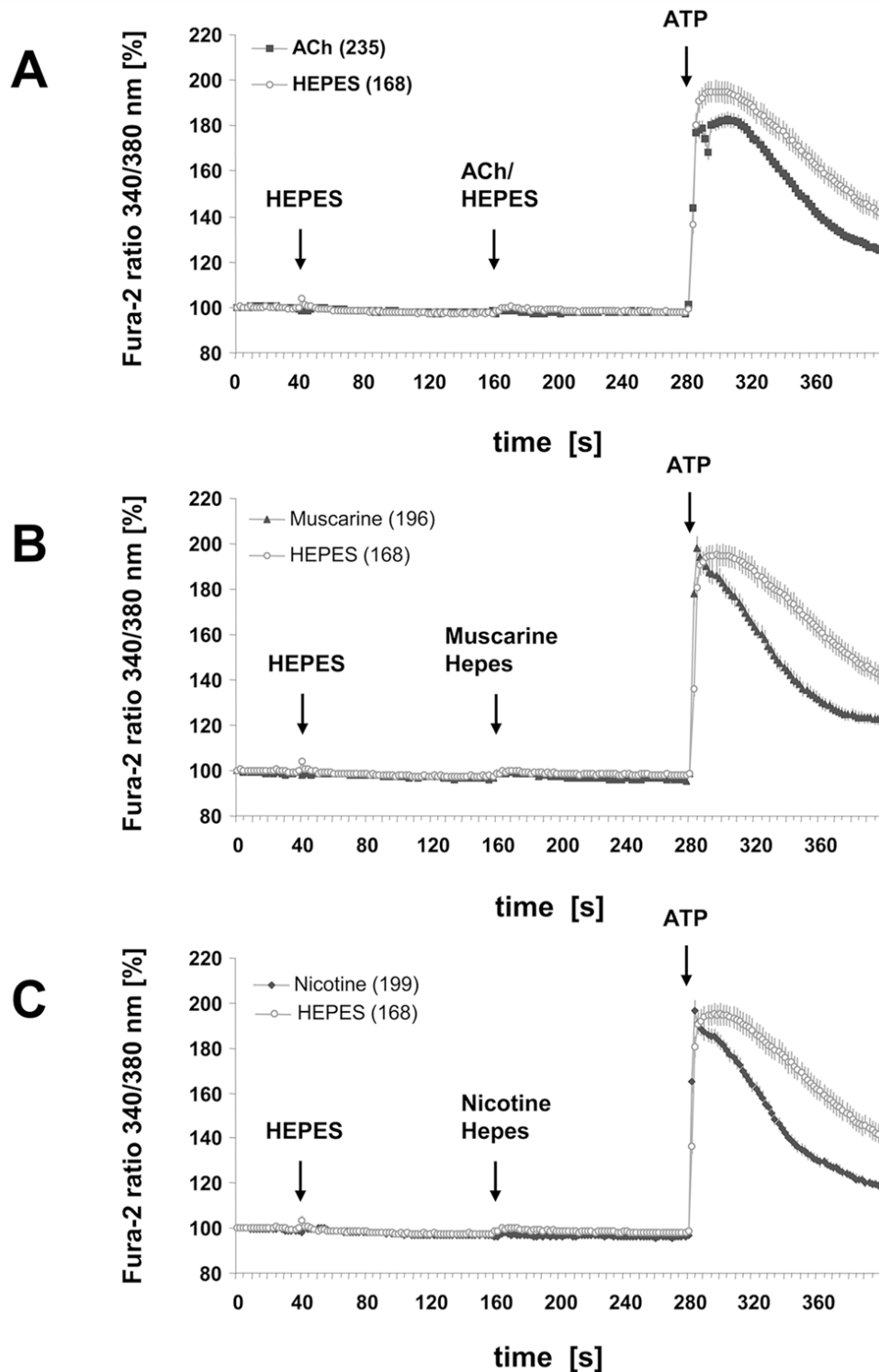


Fig. 37: ACh or -agonists have no direct effect on TM.

Control group (HEPES; $n = 5$) is shown in grey (A-C). The experimental groups ($n = 5$) are shown in black: ACh (A), muscarine (B) or nicotine (C). Cells were treated three times during the experiment: at $t = 40$ s with HEPES; $t = 160$ s with ACh ($10 \mu\text{M}$), muscarine ($10 \mu\text{M}$) nicotine ($100 \mu\text{M}$) or HEPES and $t = 280$ s with ATP ($100 \mu\text{M}$). The Fura-2 ratio 340/380 nm is presented as percentage (%) over time (s). Significance was tested for $t = 280$ s (Tab.17).

Tab. 17: Statistical analysis for calcium-imaging experiments on TM.

time-point [s]	<i>P</i> -values (Mann-Whitney-test)		
	Hep-Nic	Hep-Mus	Hep-ACh
278	n.s.	n.s.	n.s.
282	0.001	0.000	n.s.
286	n.s.	n.s.	0.000
296	n.s.	0.006	0.001
336	0.000	0.000	0.048
396	0.000	0.001	0.026

Significance was calculated using Kruskal-Wallis test followed by Mann-Whitney test for one time-point before ($t = 278$ s) and three time points after application of ATP ($t = 282$, 286 and 296 s). Two more samples were taken to investigate the course of the curves and their significant character at $t = 336$ s and 396 s. ATP was applied at $t = 280$ s. *P*-values are presented in numbers; n.s. = not significant.

10.3.4. Sertoli cells showed no direct response to AChR stimulation

SCs were tested on their response for ACh, nicotine and muscarine in three to five individual experiments. HEPES was working as control. Cells have been classified as positive if they did show an at least 5% increase in $[Ca^{2+}]_i$ over baseline after substance/drug application.

Similar to the results with TMs, the application of $100 \mu\text{M}$ nicotine, $10 \mu\text{M}$ muscarine or $10 \mu\text{M}$ ACh resulted in no direct response compared to the control group (Fig. 38, $t = 160$ s). Subsequent applications of ATP increased $[Ca^{2+}]_i$ levels within all four groups and consequently proved the cell viability. The trend of the curves after ATP was added differed group dependently in intensity and progress.

The cells pre-incubated with HEPES showed a fast Ca^{2+} influx with a maximum intensity of 136% ($\pm 44.3\%$ SD) over baseline. The subsequent fast decrease of the curve changed into a plateau phase with 87% ($\pm 44\%$ SD) over baseline (Fig. 38, grey line).

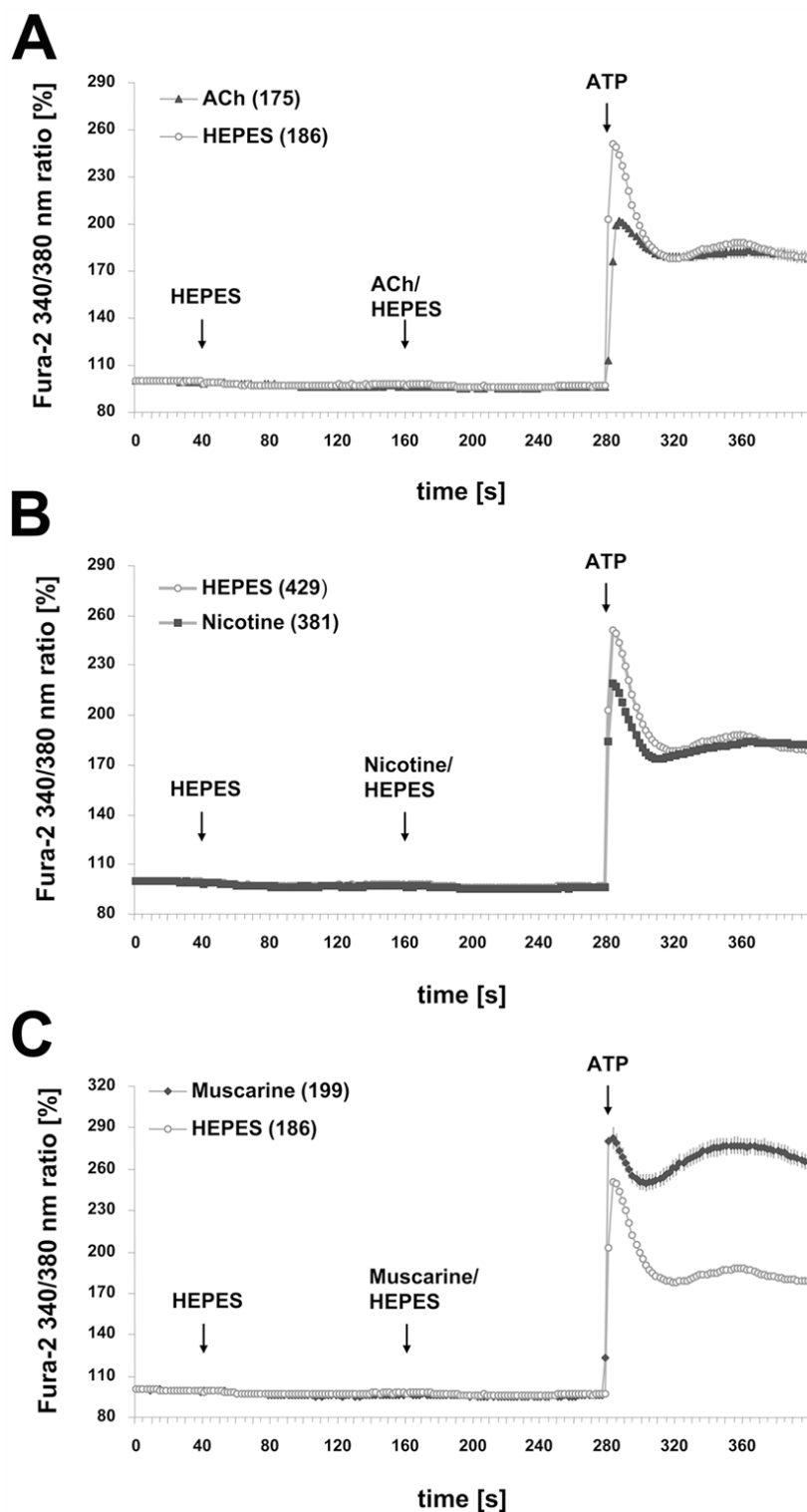


Fig. 38: SC treatment with nicotine, muscarine or ACh.

SCs were treated three times during the experiment: at $t = 40$ s with HEPES; at $t = 160$ s with ACh ($10 \mu\text{M}$), nicotine ($100 \mu\text{M}$), muscarine ($10 \mu\text{M}$) or HEPES and at $t = 280$ s with ATP ($100 \mu\text{M}$). Control group (HEPES, $n = 3$ or 5) is shown in grey and experimental groups treated with ACh (A) ($n = 3$), nicotine (B) ($n = 5$) or muscarine (C) ($n = 3$) are shown in black. The Fura-2 ratio 340/380 nm is presented as percentage (%) over time (s).

Cell populations pre-incubated with nicotine and ACh resulted in ATP induced fast Ca^{2+} influx and a following plateau. Although both curves joined the same plateau phase as seen for the control group, the initial shape of the curves straight after ATP application varied from each other in their intensity.

While pre-incubation with ACh resulted in a calcium-influx peak of 106% ($\pm 30.6\%$ SD) over baseline, cells pre-incubated with nicotine reached a peak, which had the tendency to be 16% higher (122%, $\pm 68.2\%$ SD) (Fig. 38A & B, Fig. 39 for *P*-values).

The observations for cell pre-incubated with muscarine deviated most from the others. A steep increase in the calcium-influx curve was observed after ATP application. The peak reached 186% ($\pm 102\%$ SD) over baseline followed by a fast transient decrease app. 25 s later with app. 150% over baseline. Another 35 s later a second increase followed by a plateau phase with 180% ($\pm 84.9\%$ SD) over baseline was observed (Fig. 38C).

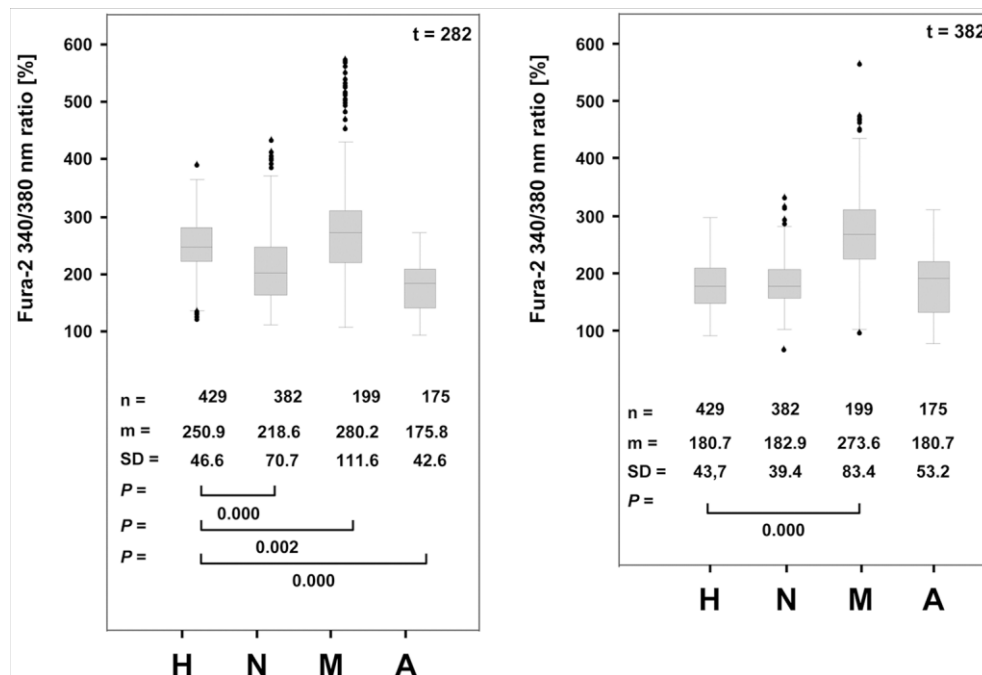


Fig. 39: *P*-values after ATP application between SC-populations.

Box plots ($t = 282$ and $t = 382$) showing the changed Ca^{2+} -influx after ATP application to SC pre-treated with nicotine, ACh, muscarine or HEPES. Significance was calculated using Mann-Whitney-test 2 s after ATP application and 100 s afterwards to determine long-time changes. *P*-values are presented in numbers. Black dots represent outliers.

10.3.5. AChR blockade modulates the ATP-induced calcium response in Sertoli cells

It has been reported that immune cells show alternated responsiveness to ATP after treatment with a nicotinic antagonist [248]. According to these data, three experiments have been designed with SC. Cells were treated either with a nicotine-inhibitor (methyllycaconitine (MLA), dihydro- β -erythroidine (DH β E) or mecamlamine (Meca)) or HEPES (t = 40 s) and with nicotine or HEPES (t = 480 s) prior ATP application (Fig. 40). $[Ca^{2+}]_i$ was recorded as Fura-2 fluorescence intensity ratio of 340/380 nm excitation.

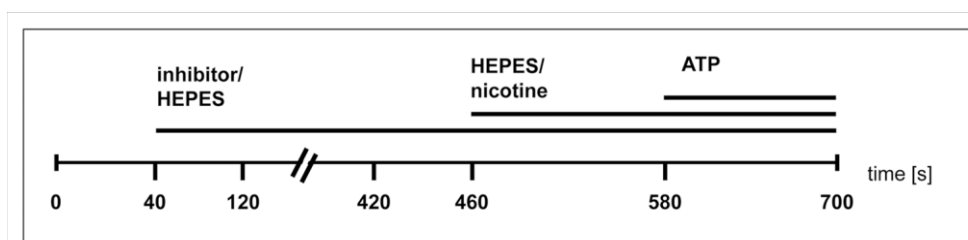


Fig. 40: Flow chart for inhibition experiment on SC.

SCs were incubated with nicotinic antagonist methyllycaconitine (MLA), mecamlamine (Meca) or dihydro- β -erythroidine (DH β E) and incubated for 5 min (//). Cells were treated with an inhibitor or HEPES at t = 40 s; with nicotine (100 μ M) or HEPES at t = 460 s and with ATP (100 μ M) at t = 580 s.

Responsiveness to ATP was significant reduced when SCs were pre-treated with nicotine compared to the control (Fig. 41, black and grey lines). Cell groups pre-incubated with mecamlamine or DH β E and either nicotine or HEPES before ATP application showed a significant increased response compared to the corresponding control group without application of Meca or DH β E (Fig. 41A & C).

SC incubated with MLA and HEPES show a significant decreased Ca^{2+} -response compared to the control group whereas there is no difference between the MLA/nicotine treated group compared to the HEPES/nicotine control group (Fig. 41B). *P*-values are shown in Tab. 18.

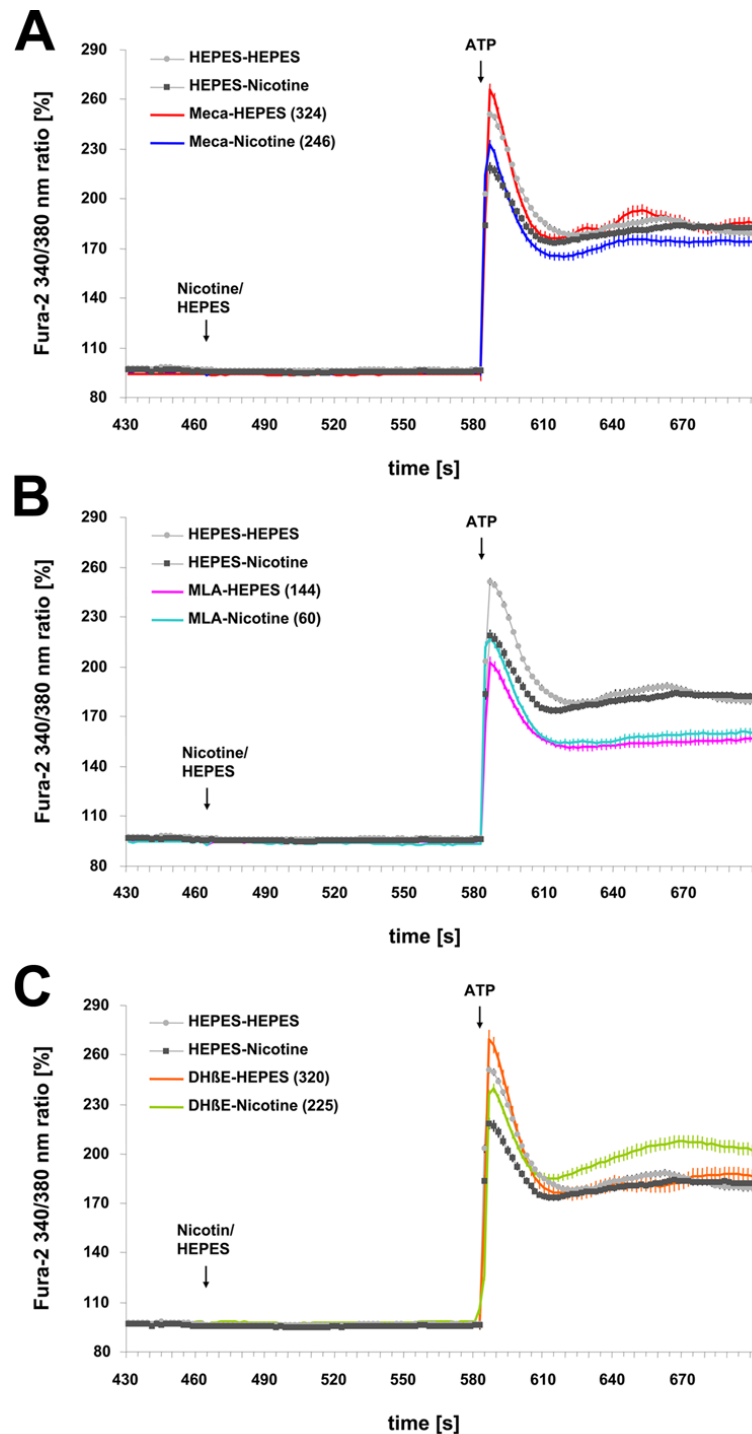


Fig. 41: nAChR-inhibitor influence ATP reaction in SCs.

SCs were treated three times during the experiment: at $t = 40$ s with HEPES or a nAChR-inhibitor (MLA, Meca, DHβE), at $t = 460$ s with nicotine ($100 \mu\text{M}$) and at $t = 580$ s with ATP ($100 \mu\text{M}$). The control groups are shown in grey (HEPES & HEPES) and black (HEPES & nicotine). Experimental groups ($n = 1-3$) are shown in (A) Meca & HEPES (red) and Meca & nicotine (blue); in (B) MLA & HEPES (purple) and MLA & nicotine (cyan) and in (C) DHβE & HEPES (orange) and DHβE & nicotine (green). Significances were tested for $t = 578$, 582 and 590 s and are described in Tab. 18. The Fura-2 ratio 340/380 nm is presented as percentage (%) over time (s).

Tab. 18: *P*-value for experiments with nicotinic inhibitors on SC.

<i>P</i>-values (Mann-Whitney-test)	n	time-point [s]		
		578	582	590
Hep vs. Nic	3	n.s.	0.000	n.s.
Meca-Hep vs. Hep	3	n.s.	0.014	0.013
Meca-Nic vs. Nic	3	n.s.	0.000	0.006
MLA-Hep vs. Hep	2	n.s.	0.000	0.000
MLA-Nic vs. Nic	1	n.s.	n.s.	n.s.
DH β E-Hep vs. Hep	3	n.s.	0.046	0.000
DH β E-Nic vs. Nic	3	n.s.	0.000	0.000

Significance was calculated using Mann-Whitney-test for one time-point before ($t = 578$ s) and two after application of ATP ($t = 582$ and 590 s). ATP was applied at $t = 580$ s. *P*-values are presented in numbers; n.s = not significant.

11. The cholinergic system in an inflammatory model (EAO)

As shown before, AChR and molecules needed for ACh synthesis could be detected in testicular parenchyma of non-inflamed testis. Several studies showed an influence of the ACh system in inflammatory processes [56, 125, 249, 250]. Here, the expression levels of AChR and related molecules were analysed under inflammatory conditions (experimental autoimmune orchitis). mRNA expression levels of animals treated with testis homogenate were compared to adjuvant and non-treated animals. The gene expression levels were analysed via real-time RT-PCR.

11.1. Relative mRNA expression analysis of inflammation markers MCP-1, IL-6 and TNF- α in orchitis

Pro-inflammatory cytokines are up-regulated in inflammatory processes and can be used as inflammation-markers. Here tumour necrosis factor- α (TNF- α), monocyte chemotactic protein-1 (MCP-1) and interleukin-6 (IL-6) were analysed in TP of each group of animals: untreated, Freund's adjuvant and orchitis. For all three markers a significant increase in mRNA expression levels was observed within the TP between orchitis-group and adjuvant-group, whereas there was no difference between the untreated- and adjuvant-group (Fig. 42). MCP-1 and IL-6 showed a great variation

between individual samples within the orchitis group, which was not the case for TNF- α . Nevertheless all values for mRNA expression of orchitis-group were higher compared to the adjuvant group (Tab. 19).

Tab. 19: Statistical analysis for MCP-1, TNF- α and IL-6.

target	untreated mean \pm SD	adjuvant mean \pm SD	orchitis mean \pm SD	<i>P</i> -value U vs. A	<i>P</i> -value A vs. O
MCP-1	1.00 \pm 0.50	0.67 \pm 0.19	99.22 \pm 82.81	n.s.	0.003
TNF- α	1.00 \pm 0.54	1.81 \pm 0.85	19.60 \pm 8.48	n.s.	0.003
IL-6	1.00 \pm 0.40	1.48 \pm 0.10	74.80 \pm 141.80	n.s.	0.003

Relative expression levels [$2^{-(\Delta CT)}/MW_{untr} \cdot 2^{-(\Delta CT)}$] and standard deviation for untreated (U), adjuvant (A) and orchitis (O) groups are shown in column two-four. The data were analysed by a Kruskal-Wallis-test followed by a Mann-Whitney-test and *P*-values are shown in numbers; n.s. = not significant (columns five and six).

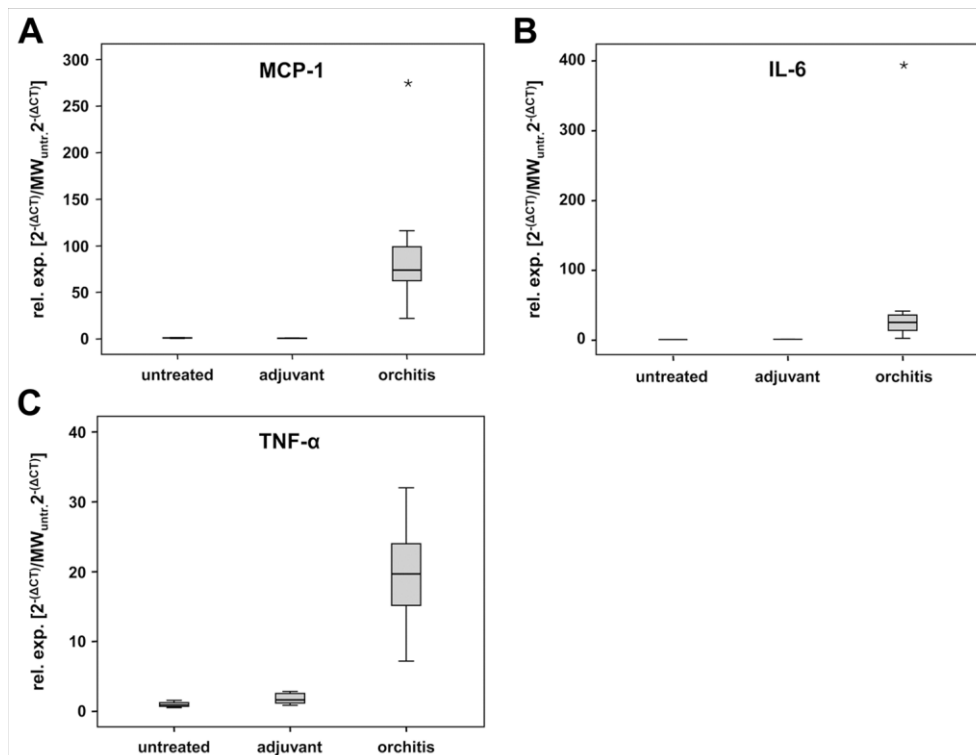


Fig. 42: The mRNA expression level of MCP-1, TNF- α and IL-6 in orchitis induced animals.

Data for monocyte chemotactic protein-1 (MCP-1), tumour necrosis factor- α (TNF- α) and interleukin-6 (IL-6) are plotted as Box plot. Samples of orchitis animals ($n = 7$) were compared to the adjuvant ($n = 5$) and untreated ($n = 3$) group. Used primers are described in Tab. 4. Relative expression was calculated by [$2^{-(\Delta CT)}/MW_{untr} \cdot 2^{-(\Delta CT)}$] and analysed by Kruskal-Wallis-test followed by Mann-Whitney-test (Tab. 19). Asterisk = outlier.

11.2. Relative mRNA expression analysis of nicotinic AChR-subunits in orchitis

Relative mRNA expression levels for nAChR-subunits $\alpha 3$ - $\alpha 7$ and $\alpha 10$ were analysed. A significantly lower expression was seen for the subunits $\alpha 3$, $\alpha 4$, $\alpha 5$, $\alpha 7$ and $\alpha 10$ in orchitis tissue compared to adjuvant tissue and for the subunits $\alpha 4$, $\alpha 5$ and $\alpha 7$ in orchitis samples compared to untreated samples. There were no significant differences between untreated, adjuvant and orchitis group for the $\alpha 6$ mRNA expression level. The mRNA for nAChR-subunit $\alpha 6$ could not be detected in all samples. Adjuvant and untreated groups showed similar mRNA expression levels for $\alpha 3$ - $\alpha 6$, but $\alpha 7$ and $\alpha 10$ subunit mRNA were significantly different expressed (Fig. 43A, Tab. 20).

The nAChR subunits $\beta 1$ and $\beta 4$ showed no differences in mRNA expression level between the three analysed groups. Significant down-regulation in the mRNA expression level was observed for $\beta 2$ and $\beta 3$ between adjuvant and orchitis groups. In the case of the $\beta 3$ subunit this significance could be seen as well between the untreated and orchitis group. For both targets $\beta 2$ and $\beta 3$, samples in the untreated and adjuvant group were expressed equally (Fig. 43B, Tab. 20).

Tab. 20: Statistical analysis for nAChR-subunits α and β .

target	untreated mean \pm SD	adjuvant mean \pm SD	orchitis mean \pm SD	<i>P</i> -value U vs. A	<i>P</i> -value U vs. O	<i>P</i> -value A vs. O
$\alpha 3$	1.00 \pm 1.04	1.63 \pm 0.98	0.40 \pm 0.64	n.s.	n.s.	0.033
$\alpha 4$	1.00 \pm 0.67	0.64 \pm 0.09	0.18 \pm 0.23	n.s.	0.014	0.009
$\alpha 5$	1.00 \pm 0.64	1.19 \pm 0.46	0.27 \pm 0.35	n.s.	0.028	0.004
$\alpha 6$	1.00 \pm 0.97	0.04 \pm 0.03	0.02 \pm 0.02	n.s.	n.s.	n.s.
$\alpha 7$	1.00 \pm 0.41	1.57 \pm 0.44	0.38 \pm 0.55	0.047	0.028	0.009
$\alpha 10$	1.00 \pm 0.49	3.28 \pm 0.45	1.55 \pm 1.33	0.009	n.s.	0.045
$\beta 1$	1.00 \pm 0.32	1.14 \pm 0.18	0.79 \pm 0.41	n.s.	n.s.	n.s.
$\beta 2$	1.00 \pm 0.33	2.03 \pm 1.09	0.79 \pm 0.53	n.s.	n.s.	0.019
$\beta 3$	1.00 \pm 0.31	1.23 \pm 0.34	0.32 \pm 0.32	n.s.	0.012	0.006
$\beta 4$	1.00 \pm 2.24	0.00 \pm 0.00	0.08 \pm 0.23	n.s.	n.s.	n.s.

Relative expression [$2^{-(\Delta CT)}/MW_{\text{untr.}}2^{-(\Delta CT)}$] and standard deviation (SD) for untreated (U), adjuvant (A) and orchitis (O) groups are shown in column two to four. The data were analysed by Kruskal-Wallis-test followed by Mann-Whitney-test (columns five to seven). *P*-values are shown in numbers; n.s. = not significant. Sample size: untreated and adjuvant $n = 5$; orchitis $n = 6-9$.

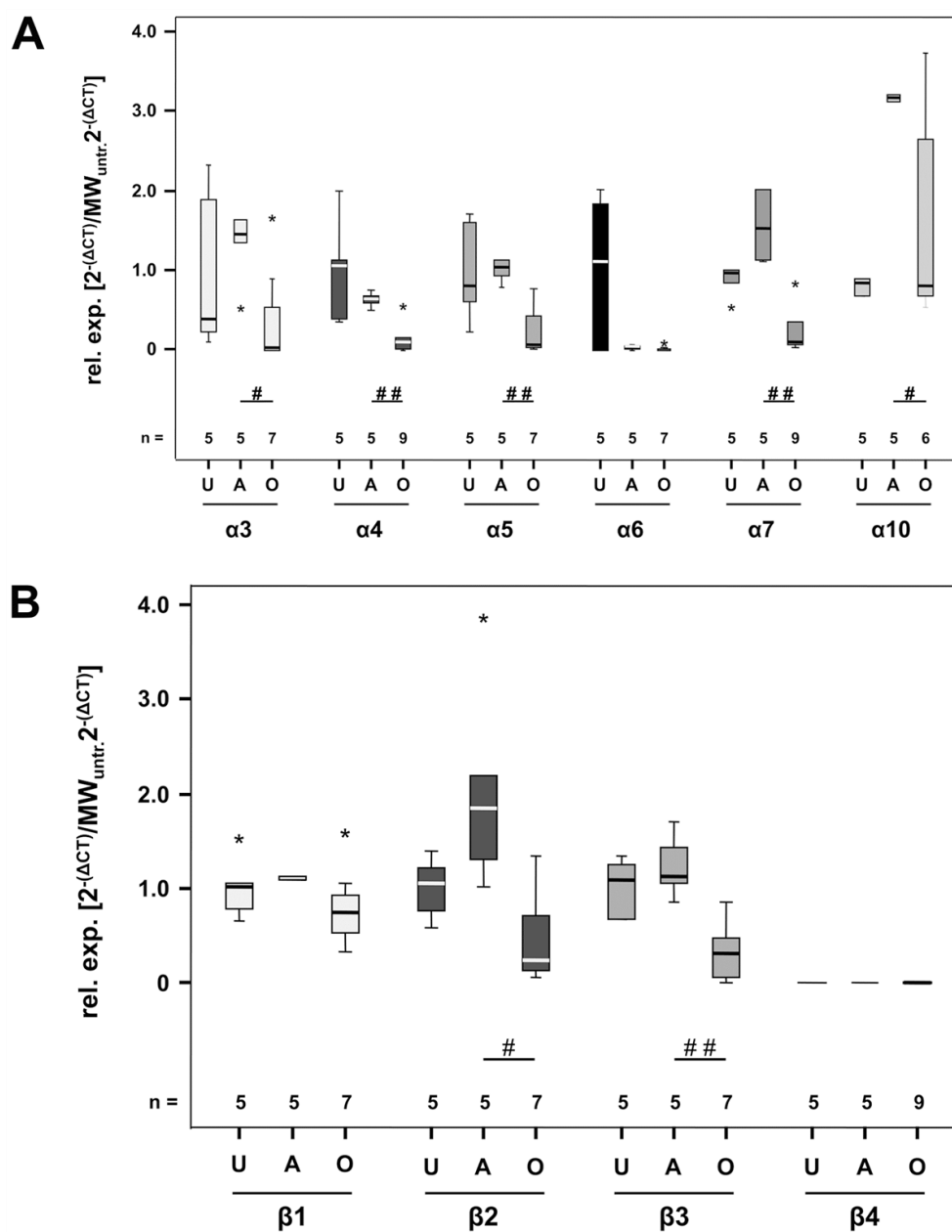


Fig. 43: mRNA expression level of nAChR α - and β -subunits in orchitis induced testis.

Data for nAChR-subunits α (A) and β (B) are plotted as Box plots. Samples for orchitis group (n = 6-9) were compared to adjuvant (n = 5) and untreated (n = 5) samples. Relative expression was calculated $[2^{-(\Delta CT)}/MW_{untr.} 2^{-(\Delta CT)}]$ and analysed by Kruskal-Wallis-test followed by Mann-Whitney-test (Tab. 7). For primer with more than one primer-set the following variants were used: $\alpha 6$ 139, $\alpha 10$ 107 (Tab. 5). U = untreated, A = adjuvant, O = orchitis, asterisk = outlier. # = P -value ≤ 0.05 , ## = P -value ≤ 0.01 .

11.3. Relative mRNA expression analysis of muscarinic AChR subtypes in orchitis

mRNAs for M₁R-M₅R subtypes were expressed in all three analysed groups: untreated, adjuvant and orchitis. The expression levels for M₁R-M₃R mRNAs were similar in the analysed groups, whereas the mRNA expression levels for M₄R and M₅R subtypes were significantly lower in the orchitis group compared to adjuvant and untreated groups (Tab. 21, Fig. 44). Adjuvant and untreated groups showed similar mRNA expression levels for M₅R but significant differences for M₄R mRNA expression (Tab. 21, Fig. 44).

Tab. 21: Statistical analysis of MR-subtype expression.

target	untreated mean ± SD	adjuvant mean ± SD	orchitis mean ± SD	<i>P</i> -value U vs. A	<i>P</i> -value U vs. O	<i>P</i> -value A vs. O
M ₁ R	1.00 ± 0.90	0.73 ± 0.41	0.73 ± 0.65	n.s.	n.s.	n.s.
M ₂ R	1.00 ± 1.66	0.14 ± 0.19	0.08 ± 0.10	n.s.	n.s.	n.s.
M ₃ R	1.00 ± 0.68	0.64 ± 0.62	0.54 ± 0.19	n.s.	n.s.	n.s.
M ₄ R	1.00 ± 0.33	1.63 ± 0.34	0.16 ± 0.32	0.028	0.028	0.004
M ₅ R	1.00 ± 0.30	0.75 ± 0.36	0.10 ± 0.05	n.s.	0.004	0.004

Relative expression [$2^{-(\Delta CT)}/MW_{\text{untr.}}2^{-(\Delta CT)}$] and standard deviation (SD) for untreated (U), adjuvant (A) and orchitis (O) groups are shown in column two to four. The data were analysed by Kruskal-Wallis-test followed by Mann-Whitney-test (columns five to seven) Significance is shown in numbers; n.s. = not significant. Sample size: untreated and adjuvant n = 5; orchitis n = 7-9.

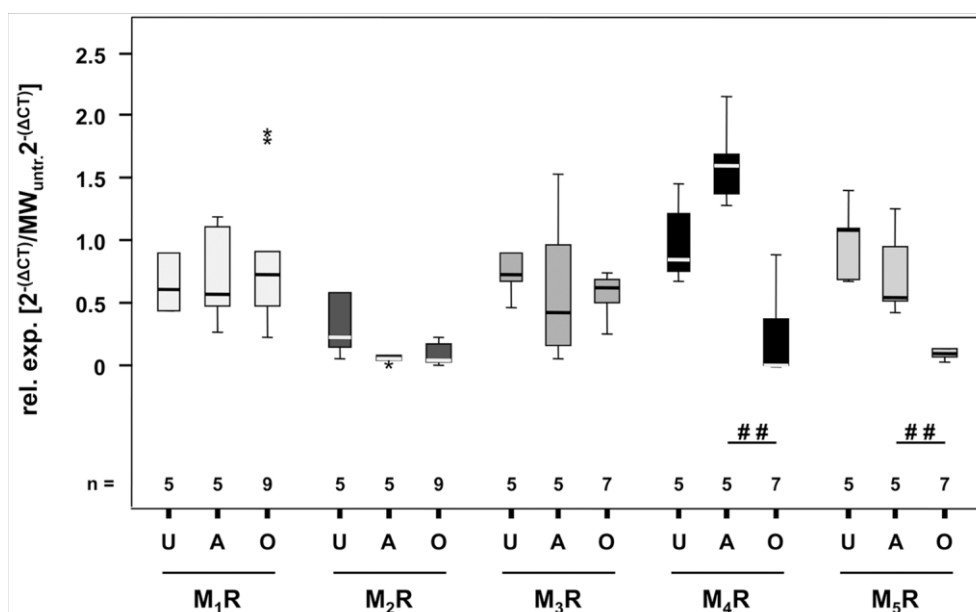


Fig. 44: mRNA expression level of MR subtypes in orchitis induced animals.

Data for MR-subtypes are plotted as Box plot. Samples of orchitis animals (n = 7-9) were compared to adjuvant (n = 5) and untreated (n = 5) groups. ΔC_T values are shown as relative expression $[2^{-(\Delta C_T)}/MW_{untr.} 2^{-(\Delta C_T)}]$. Significances were analysed by Kruskal Wallis test followed by Mann-Whitney-test (Tab. 21). For primer with more than one primer-set the following variants were used: M1_110, M2_192, M3_287, M4_166, M5_180 (Tab. 3). U = untreated, A = adjuvant, O = orchitis, asterisk = outlier. ## = P -value ≤ 0.01 .

11.4. Relative mRNA expression analysis of ChAT, ChT1, OCT2 and VACHT in orchitis

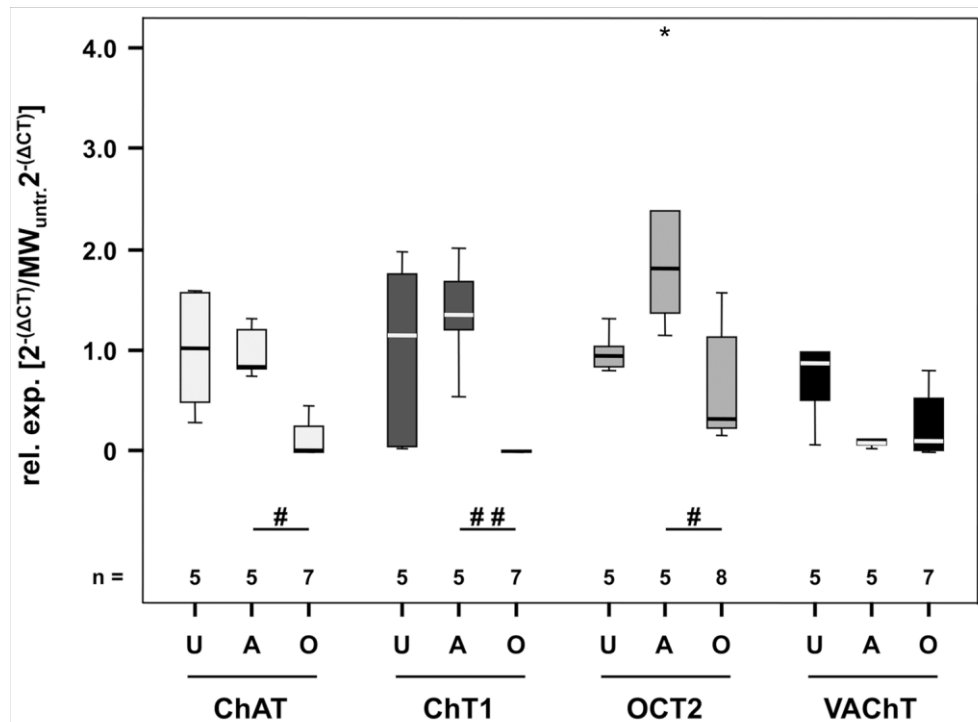
mRNA expression levels for VACHT were not significantly different between groups. Analysis for ChAT and ChT1 showed significant down-regulation for mRNA expression levels in both cases: orchitis group vs. adjuvant group and orchitis group vs. untreated group. Untreated and adjuvant groups showed an equal mRNA expression level (Tab. 22, Fig 45).

OCT2 mRNA expression was significant down-regulated in the orchitis group compared to adjuvant group whereas the mRNA expression level for the adjuvant group was significant up-regulated in comparison to the untreated group (Tab. 22, Fig 45).

Tab. 22: Statistical analysis for ChAT, ChT1, OCT2 and VACHT.

target	untreated mean \pm SD	adjuvant mean \pm SD	orchitis mean \pm SD	<i>P</i> -value U vs. A	<i>P</i> -value U vs. O	<i>P</i> -value A vs. O
ChAT	1.00 \pm 0.61	1.00 \pm 0.26	0.11 \pm 0.20	n.s.	0.023	0.019
ChT1	1.00 \pm 0.61	1.37 \pm 0.55	0.23 \pm 0.49	n.s.	0.012	0.005
OCT2	1.00 \pm 0.93	2.18 \pm 1.19	0.63 \pm 0.60	0.016	n.s.	0.019
VACHT	1.00 \pm 0.92	0.32 \pm 0.53	0.24 \pm 0.34	n.s.	n.s.	n.s.

Relative expression $[2^{-(\Delta C_T)}/MW_{untr.} 2^{-(\Delta C_T)}]$ and standard deviation (SD) for untreated (U), adjuvant (A) and orchitis (O) groups are shown in column two to four. The data were analysed by Kruskal-Wallis-test followed by Mann-Whitney-test (columns five to seven) *P*-values are shown in numbers; n.s. = not significant. Sample size: untreated and adjuvant $n = 5$; orchitis $n = 7-8$.

**Fig. 45: mRNA expression level of ChAT, ChT1, OCT2 and VACHT in orchitis induced animals.**

Data for ChAT, ChT1, OCT2 and VACHT are plotted as Box plot. Samples of orchitis animals ($n = 7-8$) were compared to adjuvant ($n = 5$) and untreated ($n = 5$) groups. ΔC_T values are shown as relative expression $[2^{-(\Delta C_T)}/MW_{untr.} 2^{-(\Delta C_T)}]$. Significances were analysed by Kruskal-Wallis-test followed by Mann-Whitney-test (Tab. 22). For primer with more than one primer-set the following variants were used: ChT1_150, OCT2_162 (Tab. 6). U = untreated, A = adjuvant, O = orchitis, asterisk = outlier. # = P -value ≤ 0.05 , ## = P -value ≤ 0.01 .

12. Sensory innervation of the rat testis

12.1. Morphological observations of the rat testis

The testis was examined and analysed for the presence of sensory nerve fibres. In brief, the scrotum was opened and the testis isolated. The fascia was cut and the testis was separated into the different tissue layers and adjacent organs (Fig. 46A).

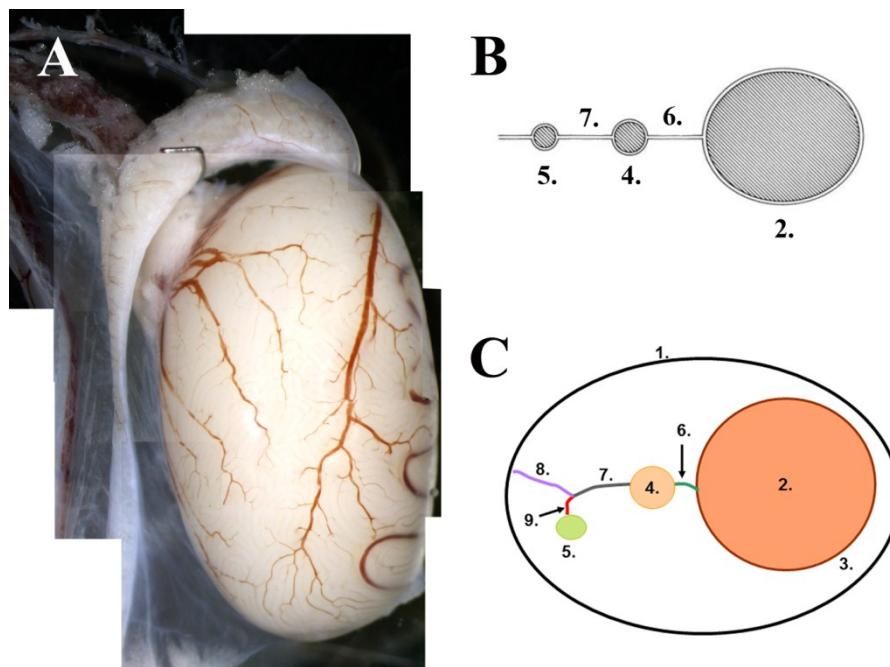


Fig. 46: Mesos of the rat testis.

Microscopic longitudinal image (A) and horizontal models (B & C) of the rat testis showing the fascia (1), testicular parenchyma (2), testicular capsule (3), epididymis (4), vas deferens (5), mesoepididymis (6), mesodeferens I (7), mesofascia (8) and mesodeferens II (9). Horizontal model (B) from Zhu et al. [12].

The majority of the investigated macroscopic structures were localised as previously described [12], except the morphology of the meso-structures. According to Zhu et al. there are three meso-structures which are the mesoepididymis (1) between testis and epididymis, the mesodeferens (2) between the epididymis and the vas deferens and an unnamed meso (3), which connects the vas deferens to the fascia [12]. Only one meso was found, which is located between the epididymis and the fascia with an additional substructure diverging to the vas deferens (Fig. 46B & C). This diverging substructure

had a clear visible separation-line. The names of the meso-structures were modified after Zhu et al. [12]. In this study the mesos are called mesoepididymis, mesodeferens I, which is the part from the epididymis to the separation line, mesodeferens II, which is the part from the separation line to the vas deferens and mesofascia, the meso that links the separation line to the fascia (Fig. 46C, no. 6-9).

12.2. Neurochemical characterisation of testicular nerve fibres

Compartments, which are described in Tab. 23, were subdivided or random samples were analysed according to the tissue-size. Markers for sensory nerve fibres (Nf200, peripherin) and subpopulations of nociceptive (peptidergic CGRP-containing) nerve fibres were used for the immunohistochemical analysis of neurochemical characteristics. PGP9.5 as a pan-neuronal marker was chosen for the visualisation of all existing nerve fibres.

Tab. 23: Tissue samples used for whole mount multiple labelling IHC.

tissue	samples
fascia (external spermatic fascia, internal spermatic fascia, cremaster muscle)	random samples, n = 10
vas deferens	random samples, n = 4
superior ligament (SL)	whole SL divided in 3 parts
inferior ligament (IL)	whole SL divided in 3 parts
testicular artery/vein	random samples, n = 3
mesodeferens I (md I)	whole md, divided in 2 parts
mesoepididymis (me)	whole md, divided in 2 parts
mesofascia (mf)	whole md, divided in 4 parts
mesodeferens II (md II)	whole md, divided in 2 parts
testicular capsule	random samples, n = 18
testicular parenchyma	cryo-sections, random samples

Analysed tissues were subdivided or random samples were taken from three different animals. Tissue samples were used for IHC and different neuronal markers were investigated as shown in Tab. 24.

Nerve fibres which were found within the tissue could be further subdivided into 3 groups according to their location: (1) being wrapped around blood vessels, (2) running alongside blood vessels and (3) nerve fibres in non-vascular areas (Fig. 47A). The presence and frequency as well as the neurochemical characteristics of nerve fibres for each group were determined.

Blood vessels could be found in all of the analysed structures although the density differed between distinct compartments. Unlike in other structures, blood vessels of the fascia and the TC were not always innervated and innervation was absent in TP. The nerve fibres, which innervated blood vessels, were positive for PGP9.5 only. In some cases nerve-fibre-endings could be found directly attached to blood vessels, as shown in Fig. 47B.

Nerve fibres, that were running alongside to blood vessels and in non-vascular areas, showed similar neurochemical characteristics. Both fibre populations were positive for PGP9.5 and sensory and nociceptive markers (Tab. 24).

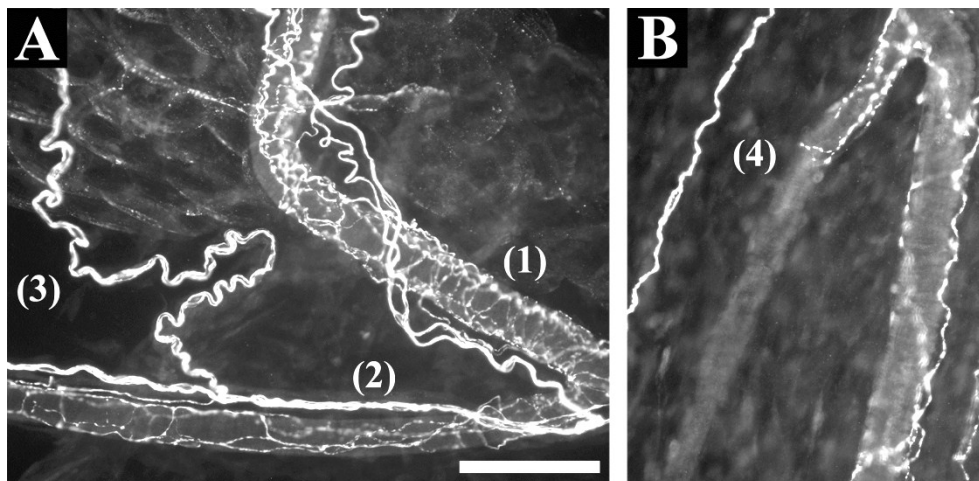


Fig. 47: Immunohistochemistry of nerve fibres in structures adjacent to the testicular parenchyma.

Nerve fibres were labelled with rabbit-anti PGP9.5. **(A)** Nerve fibres and fibre bundles were found wrapped around blood vessels (1), running alongside with blood vessels (2) and in non-vascular areas (3). **(B)** A nerve fibre which innervates a blood vessel and ends in a branch-like structure is shown (4). Scale bar in A (100 μ m) applies to both A & B.

12.2.1. Sensory nerve fibres (Nf200 & peripherin)

First experiments finding sensory nerve fibres in the testis and adjacent structures were performed using the following combination of antisera PGP9.5 & Nf200 or PGP9.5 & peripherin. Tissue samples of vas deferens, fascia and testicular parenchyma were tested and results were obtained for labelling with PGP9.5 and Nf200 in vas deferens and fascia. Unfortunately, using the antiserum for peripherin resulted in labelling, which was weak and instable in appearance, therefore a clear positive or negative identification of nerve fibres was not possible (data not shown). For further examinations only Nf200 was used to identify myelinated sensory nerve fibres.

The **testicular parenchyma** was not innervated (Fig. 48). Cryo-sections of TP labelled with PGP9.5 did not show any nerve fibre structures in non-vascular areas. Blood vessels which were accompanied by nerve fibres outside the TP did not show any innervation after entering the parenchyma.

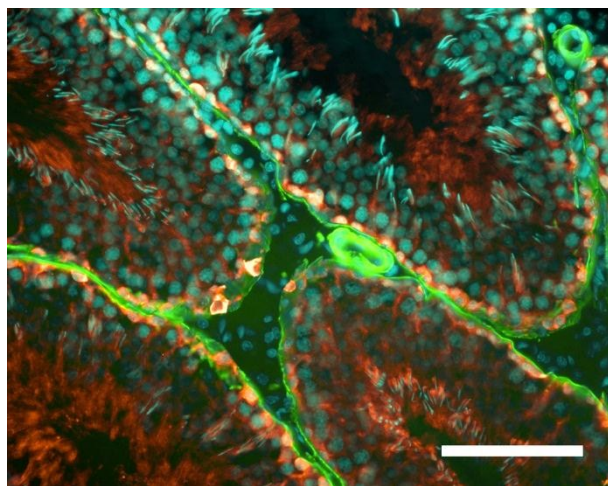


Fig. 48: PGP9.5 IHC on testicular parenchyma.

A 14 µm cryo-section of testicular parenchyma was fixed in methanol and labelled with rabbit-anti PGP9.5 (red), FITC-conjugated α -SMA (green) and the nuclear stain Hoechst (blue). Scale bar = 100 µm.

12.2.2. Sensory nociceptive nerve fibres (Nf200 & CGRP)

Nociceptive nerve fibres were analysed using the following combination of antisera PGP9.5 & Nf200 & CGRP. Table 24 gives an overview about the examined tissues, the amount of nerve fibres and their neurochemical characteristics. As mentioned before nerve fibres innervating blood vessel were PGP9.5-positive, Nf200-negative and CGRP-negative and are not listed in Tab. 24.

In the **fascia** a high density of blood vessels, nerve fibre bundles and nerve fibres was observed. Nerve fibres could be found which were positive for Nf200 alone, CGRP alone and Nf200 & CGRP respectively (Tab. 24, Fig. 50A-D). In the cremaster muscle, situated between the external and internal fascia, motoric end plates were detected which were negative for CGRP, but positive for PGP9.5 and Nf200 (Fig. 49D).

Tab. 24: Neurochemical characteristics of nerve fibres running alongside with blood vessels or in non-vascular tissue.

tissue	nerve fibres			
	alongside to nerve fibres		non-vascular tissue	
	number of nerve fibres	marker	number of nerve fibres	marker
internal & external fascia and cremaster muscle	+	Nf200+/CGRP- Nf200-/CGRP+ CGRP+/Nf200+	++	Nf200+/CGRP- Nf200-/CGRP+ CGRP+/Nf200+
vas deferens	+	Nf200+/CGRP- Nf200-/CGRP+ CGRP+/Nf200+	++	Nf200+/CGRP- Nf200-/CGRP+ CGRP+/Nf200+
testicular artery	+++	PGP9.5		
superior ligament	++	Nf200+/CGRP- Nf200-/CGRP+ CGRP+/Nf200+	+++	Nf200-/CGRP- Nf200+/CGRP- Nf200-/CGRP+ CGRP+/Nf200+
anterior ligament	++	Nf200+/CGRP- Nf200-/CGRP+ CGRP+/Nf200+	++	
testicular capsule	+	PGP9.5	++	PGP9.5
mesoepididymis	++	Nf200+/CGRP- Nf200-/CGRP+ CGRP+/Nf200+	+++	Nf200+/CGRP- Nf200-/CGRP+ CGRP+/Nf200+
mesodeferens I	++		+++	
mesodeferens II	++		+++	
mesofascia	+		+	

Frequency of nerve fibres were estimated and divided in four groups (absent = 0, rarely = +, often = ++, frequent = +++). Samples were incubated with an anti-sera mix of PGP9.5, Nf200 and CGRP. All nerve fibres were positive for PGP9.5 and therefore it is not mentioned.

The **vas deferens** contains a thick smooth muscle layer which is surrounded by an adventitia of connective tissue. Within the adventitia, blood vessels, nerve fibre bundles and nerve fibres were frequently found, but only thin nerve fibres were observed travelling into the muscle layer. The nerve fibres were either positive for Nf200 alone, CGRP alone or Nf200 & CGRP (Tab. 24).

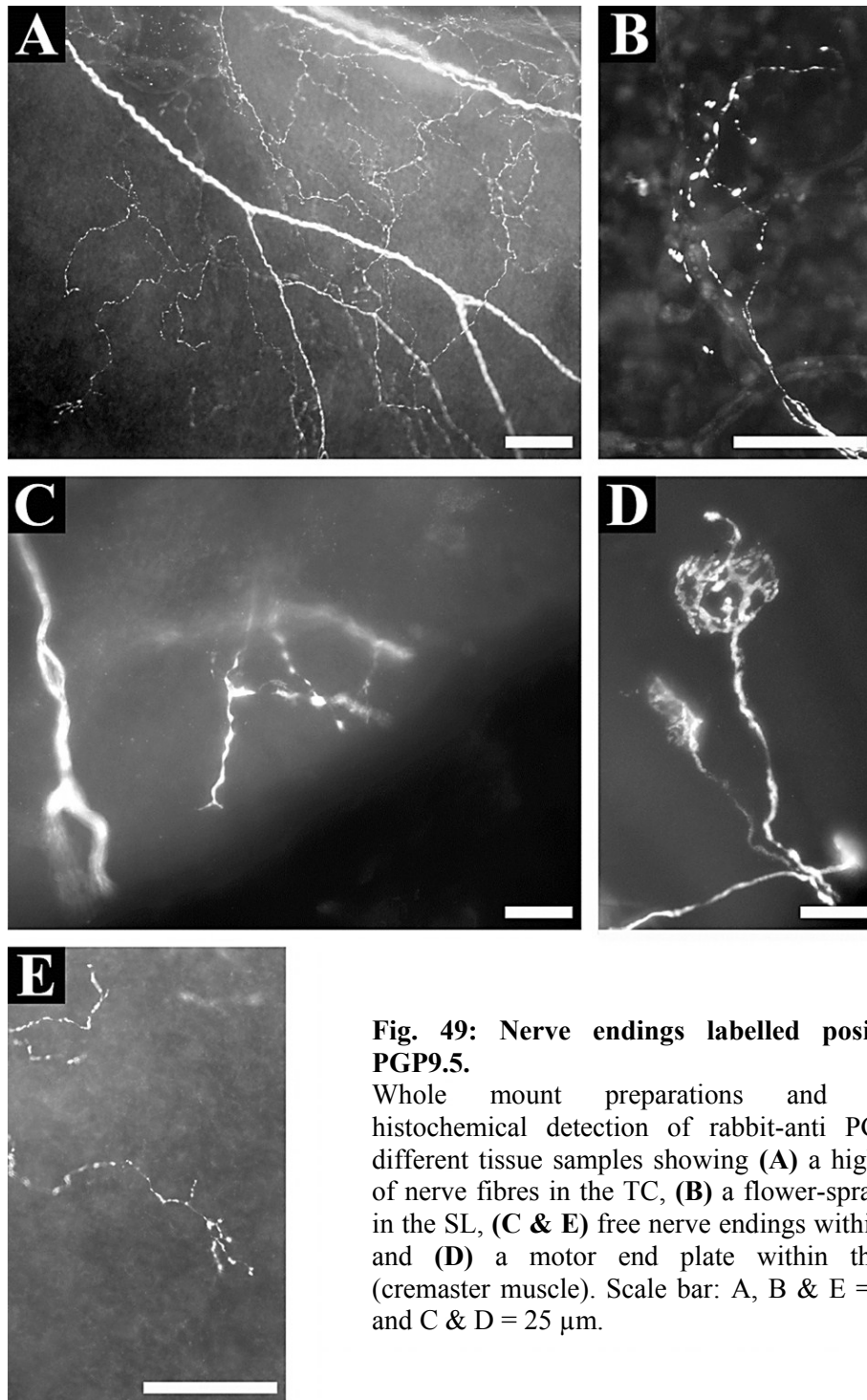


Fig. 49: Nerve endings labelled positive for PGP9.5.

Whole mount preparations and immunohistochemical detection of rabbit-anti PGP9.5 in different tissue samples showing (A) a high density of nerve fibres in the TC, (B) a flower-spray ending in the SL, (C & E) free nerve endings within the TC and (D) a motor end plate within the fascia (cremaster muscle). Scale bar: A, B & E = 100 μ m and C & D = 25 μ m.

The **testicular artery**, a described access route for nerve fibres to the testis [78, 390, 391], is surrounded by several layers of adipose tissue, which made it difficult to prepare whole mount tissue samples or cryo-sections for IHC. The presence of nerve fibres and nerve fibre bundles was confirmed using PGP9.5 antiserum, but no further investigations were made with respect to characterisation.

Mesodeferens I, mesodeferens II and mesoepididymis displayed a high density of nerve fibres, nerve fibre bundles and blood vessels. A low number of nerve fibres were found in the **mesofascia**. Nerve fibres located in meso-structures were positive for Nf200 alone, CGRP alone and Nf200 & CGRP (Tab. 24).

The **superior and inferior ligaments** (SL, IL) are the connections between the testicular capsule and the epididymis. There are also supposed to be the entrance for nerve fibres into the parenchyma and the capsule [12]. Nerve fibres in both structures were positive for Nf200 alone or CGRP alone and Nf200 & CGRP. In contrast to other tissue-compartments there were a higher number of PGP9.5-positive, Nf200- and CGRP-negative nerve fibres in non-vascular areas (Tab. 24, Fig. 49B & 50E-H).

Innervation of the **capsule** was found only in regions surrounding the connections of the SL and IL and close to the rete testis, whereas nerve fibres were absent in other capsule areas (in particular the region opposite the rete testis). All nerve fibres in these innervated regions displayed the same characteristics as described for IL and SL: Nf200 alone or CGRP alone and Nf200 & CGRP (Tab. 24). Additionally, free nerve endings were observed (Fig. 49A, C & E).

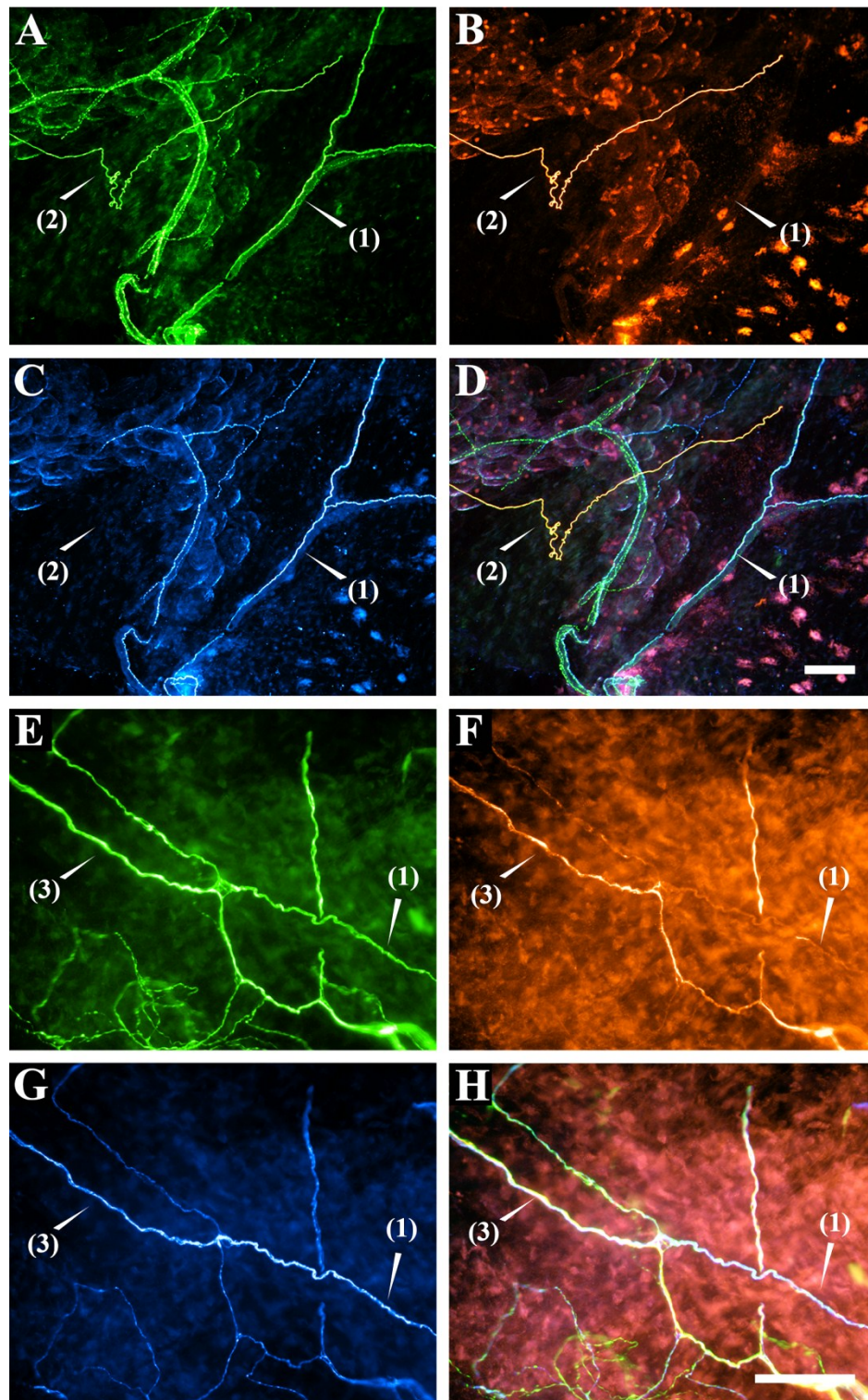


Fig. 50: Myelinated and unmyelinated nociceptive nerve fibres.

Samples of tissue prepared as whole mount were incubated with an antisera mix to detect rabbit-anti PGP9.5 (green, A, E), mouse-anti Nf200 (red, B, F) and goat-anti CGRP (blue, C, G). Images D & H show the merge of the three markers. A-D = fascia, E-H = IL. Nerve fibres with different neurochemical characteristics are numbered as follows: **(1)** Nf200-/CGRP+, **(2)** Nf200+/CGRP- and **(3)** Nf200+/CGRP+. Scale bar in D applies to A-D and in H applies to E-H. Scale bars = 100 μ m

12.2.3. Nerve fibres in meso-structures are positive for IB4, TRPV1 and VGluT1

Less information is provided about the neuronal characteristics of meso-structures, although they demonstrate a dense innervation. Therefore investigations were focused on these tissues to further differentiate sensory nerve fibres. IB4, VGluT1 and TRPV1 were used in combination with either Nf200 or CGRP, both of which served as controls for the experimental set-up. The tissue samples were incubated with the following antisera-mix: (1) IB4 & VGluT1 & Nf200, (2) TRPV1 & Nf200 and (3) IB4 & CGRP & VGluT1 (Fig. 51).

Tissue samples of one animal were analysed for the meso-structures, thus the data here have to be considered as preliminary. Table 25 presents the combinations of neurochemical markers which were found in nerve fibres within the meso-structures. VGluT1 and TRPV1 were detectable in the majority of nerve fibres in all analysed meso-structures. IB4-staining was occasionally very weak and showed higher background staining. Therefore, a clear statement about the presence of IB4 is not always possible. Unclear results are indicated as IB4±.

Tab. 25: IB4, TRPV1 and VGluT1 positive nerve fibres within meso-structures.

tissue	marker		
me	N/A	IB4+/CGRP+/VGluT1+ IB4± CGRP+/VGluT1-	N/A
md I	IB4+/VGluT1+/Nf200- IB4+/VGluT1+/Nf200+	IB4-/CGRP+/VGluT1- IB4+/CGRP-/VGluT1+ IB4+/CGRP+/VGluT1+	TRPV1+/Nf200+ TRPV1+/Nf200±
md II	IB4±/VGluT1+/Nf200- IB4+/VGluT1+/Nf200+	IB4-/CGRP+/VGluT1- IB4+/CGRP-/VGluT1+ IB4+/CGRP+/VGluT1+	TRPV1+/Nf200+
mf	IB4±//VGluT1+/Nf200- IB4±/VGluT1+/Nf200+	N/A	TRPV1+/Nf200+ TRPV1+/Nf200±

Meso-structures were prepared as whole mount and analysed for IR of rabbit-anti VGluT1, guinea pig-anti TRPV1 and IB4-Alexa₄₈₈. Goat-anti CGRP and mouse-anti Nf200 served as controls. N/A = not analysed. Abbreviations: mf = mesofascia, me = mesoepididymis, md = mesodeferens (I & II). n = 1.

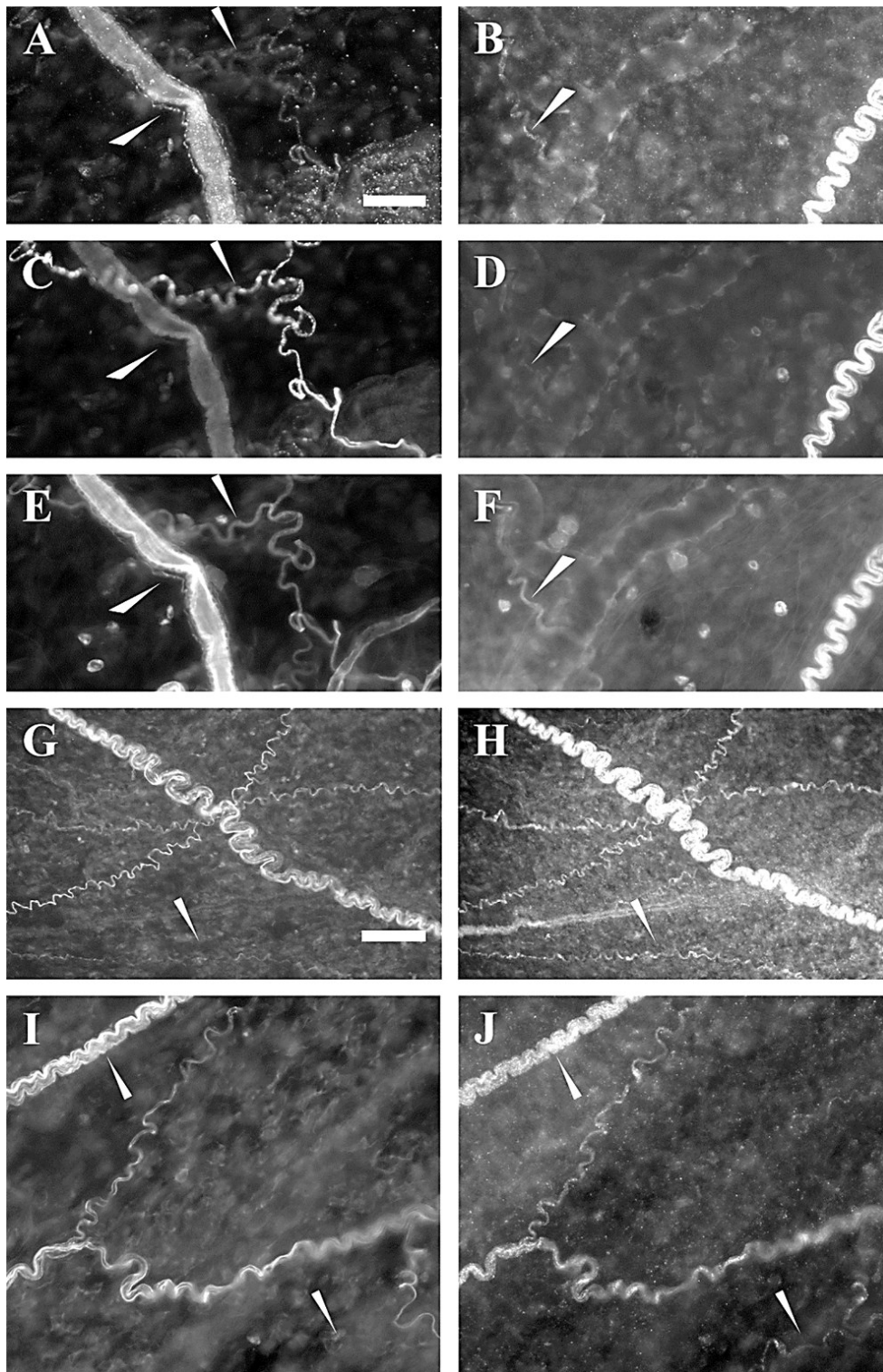


Fig. 51: IB4, VGluT1 and TRPV1 positive nerve fibres in meso-structures.

Multiple labelling IHC of whole mounts: **(1)** VGluT1 & CGRP & IB4 (A, C, E), **(2)** VGluT1 & Nf200 & IB4 (B, D, F) or **(3)** Nf200 & TRPV1 (G, H & I, J). Example shown here originate from mesodeferens I (A, C, E & I, J), mesoepididymis (G, H) and mesodeferens II (B, D, F). Nerve fibres with different neurochemical characteristics are marked with arrows. Scale bar in A (50 μ m) applies to A-F, I & J. Scale bar in G (100 μ m) applies to G & H.

12.3. Tracing from the mesodeferens I and II to the dorsal root ganglia

The neurons within the DRG lumbar 1 (DRG L1) are responsible for innervating the testis [97, 405, 412]. Therefore, the main focus was on ipsi- and contra-lateral DRGs L1 for all rats. To identify the origin of nociceptive neurons, two tracers were applied. Cholera toxin-Biotin (Ctx_{BT}) was injected into the testis parenchyma and Cholera toxin-Alexa₅₅₅ (Ctx₅₅₅) was applied to the mesodeferens I & II. A differentiation between mesodeferens I and II was not possible because they are connected to each other as seen in Fig. 46C.

In the first experimental part, every DRG section of L1 was checked for cells labelled positive for the tracer Ctx₅₅₅. These sections were used for subsequent IHC experiments. All sections without and several sections with Ctx₅₅₅ positive cells were incubated with FITC-conjugated Streptavidin to identify the Ctx_{BT} labelled cells.

No cell labelled positive for Ctx_{BT} was found. Sections with cells labelled positive for Ctx₅₅₅ were stained in addition with anti-sera for IB4, CGRP and Nf200. All analysed cells have been CGRP positive, Nf200 negative and IB4 negative. However fluorescence of Ctx₅₅₅ positive labelled cells was fading in some cases and these cells could not be used for further analysis (Tab. 26).

Tab. 26: Data of the first tracing experiment.

animal no.	location DRG	Ctx ₅₅₅ pos. cells	neurochemical characteristics	amount of cells	analysed cell-number
1		0			
2		0			
3	L1 ips	7	CGRP+/Nf200-/IB4-	4	4
	L1 con	0			

Amount of cells positive for Ctx₅₅₅ of n = 3 animals are shown in columns 1-3. Cells identified as CGRP-positive but IB4 and Nf200 negative are shown in columns 4-6.

In the second experiment Ctx₅₅₅ was applied to mesodeferens I & II in three rats. One out of three animals died during surgery. From the remaining two rats the DRGs were isolated, processed and analysed starting again with DRG L1. Cells were incubated with antisera of the neuronal markers Nf200, CGRP and IB4. Three Ctx₅₅₅ positive

cells were observed in the ipsi-lateral DRG L1 but none in the contra-lateral DRG L1 of animal number one. These cells were all CGRP positive, Nf200 negative and IB4 negative. The amount of Ctx₅₅₅ positive cells in the ipsi-lateral DRG L1 of the second analysed rat was with 413 much higher. Beside this, 8 cells were discovered in the contra-lateral DRG L1.

The filter equipment of available microscopes made it necessary to analyse specimens at two different fluorescence microscopes to cover the full spectrum of analysis. The tissue sections were evaluated in two blocks: (1) IB4 (AMCA), Ctx₅₅₅ (Cy3), CGRP (FITC) and (2) Nf200 (Cy5), Ctx₅₅₅ (Cy3), CGRP (FITC). The variation of analysed cells of the two groups compared to each other (1. n = 292 and 2. n = 351) and to the total amount of Ctx₅₅₅ labelled cells (n = 413) was a result of the fading of fluorescence of Ctx₅₅₅ (Tab. 27). In both analysed groups approximately 98% of the neurons were positive for CGRP. Around 80% were negative either for Nf200 or IB4. The remaining cells, 16-18%, were labelled positive for Nf200 or IB4 (Tab. 27). Less than 2% of the analysed DRG neurons were CGRP negative. Within this population cells were identified as NF200 positive, NF200 negative or IB4 negative (Tab. 27). Examples for Ctx₅₅₅ positive labelled neurons with additional multiple IHC for IB4, CGRP and Nf200 are shown in Figure 52.

Tab. 27: Data of the second tracing experiment.

animal no.	location DRG	Ctx ₅₅₅ pos. cells	neurochemical characteristics	amount of cells in %		analysed cell-number
1	L1 ips	3	CGRP+/Nf200-/IB4-	100		3
2	died during surgery					
3	L1 con	8	CGRP+/Nf200+/IB4+	16.66		
			CGRP+/Nf200-/IB4-	66.66		
			CGRP+/Nf200-/IB4+	16.66		6
	L1 ips	413	CGRP+	98.58	98.97	
				Nf200+	16.52	
				Nf200-	82.05	351
				IB4+	18.15	
				IB4-	80.82	292
			CGRP-	1.4	1.03	
				Nf200+	0.57	
				Nf200-	0.85	351
				IB4+	0	
				IB4-	1.03	292

Cholera toxin-Alexa₅₅₅ positive cells were found in two out of two analysed rats in ipsi-lateral DRG L1 (L1 ips). Additionally, Ctx₅₅₅ positive cells were detected in contra-lateral DRG L1 (L1 con) for one rat (columns 1 & 2). Amount of Ctx₅₅₅ positive cells and analysed cells are shown in numbers (no.) in columns 3 & 6. Amount of cells with specific neurochemical characteristics are shown in percentage (%) in columns 4 & 5.

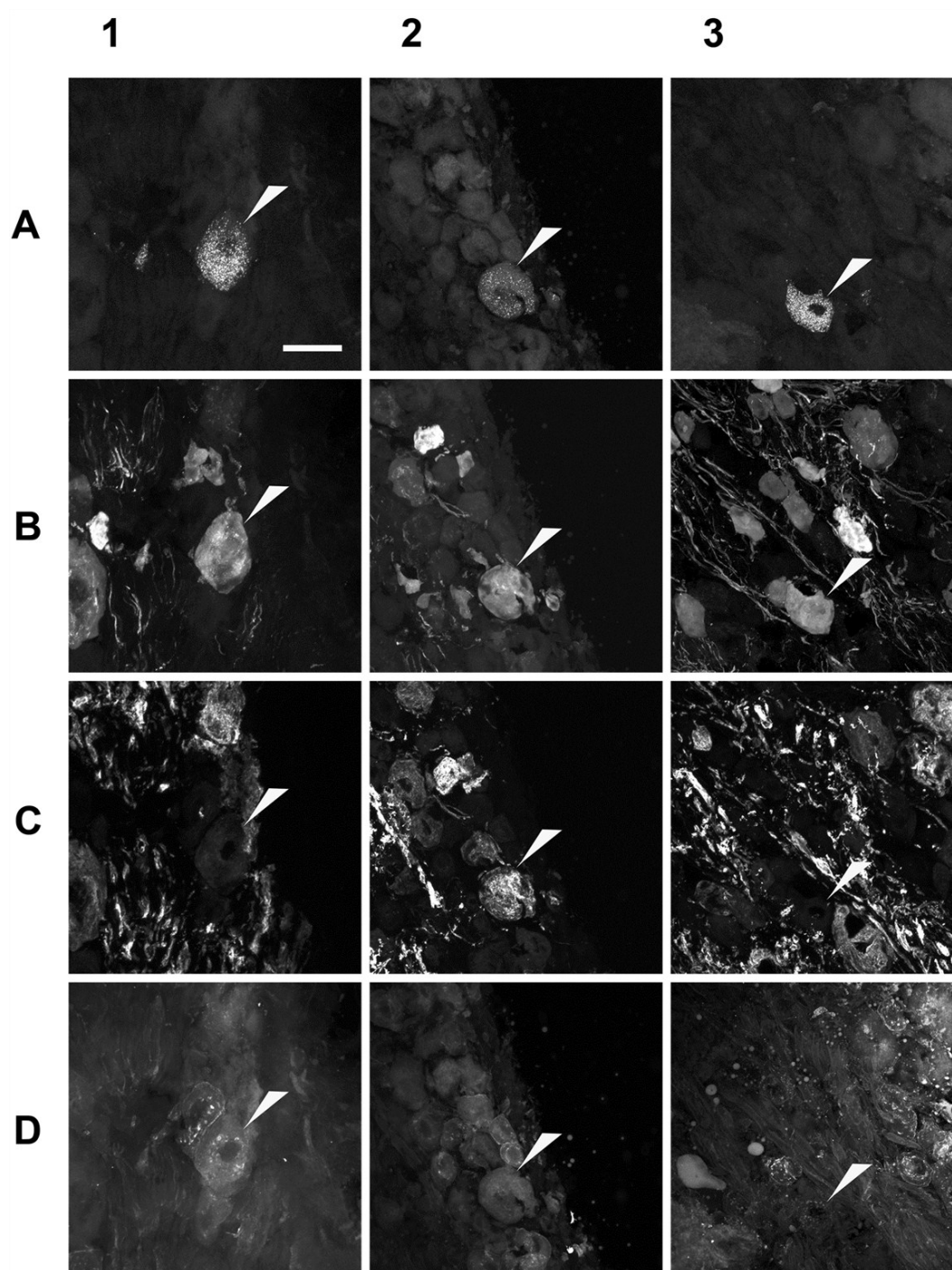


Fig. 52: Retrograde tracing of cells projecting to mesoepididymis I and II.

Dorsal root ganglion neurons of L1 labelled positive for Ctx₅₅₅ (arrowheads in A 1-3) were multiple labelled with rabbit-anti CGRP (B), mouse-anti Nf200 (C) and IB4-Biotin (D). Images marked with the same number belong to the same cell. Neurochemical characteristics of the cells are in column (1) CGRP+/Nf200-/IB4+, (2) CGRP+/Nf200+/IB4- and (3) CGRP+/Nf200-/IB4-. Scale bar in A1 (25 µm) applies to all images.

Discussion

13. The non-neuronal cholinergic system in rat testis

The work reported here demonstrates that non-neuronal cells in the testicular parenchyma of rat testis have all the components necessary for cholinergic signalling. mRNAs were detected for the ACh synthesizing enzyme, transporters and ACh receptors in locations completely lacking any form of innervation as demonstrated by the absence of PGP9.5 labelling [12].

Acetylcholine is well-known chemical neurotransmitter in the nervous system, but not limited to it. ACh binds to two structurally diverse families of membrane-bound proteins: (1) ACh-gated ion-channels comprised of different nicotinic receptor subunits (nAChR) and (2) G-protein coupled single-subunit transmembrane proteins – muscarinic acetylcholine receptor (MR) [206, 208, 251]. Both receptor classes are expressed pre- and postsynaptically and are distributed throughout the central and peripheral nervous systems [206]. After the first presumptions about a non-neuronal cholinergic system in mammalian cells by Morris in 1966 and Sastry & Sadavongvivad in 1979 [105, 252], it is now well established that ACh is produced by many types of cells in addition to neurons [139, 253, 254]. Within non-neuronal cells ACh influences cell proliferation, migration or apoptosis [218, 255] by paracrine or autocrine binding to the target cells. Such communications between cells within a multi-cellular organism are necessary to maintain all body-functions and to survive in their environment.

13.1. ACh synthesizing enzyme and transporters are present in testicular parenchyma and capsule

Previous studies suggested a non-neuronal cholinergic system in testis. ChAT mRNA and activity was present in human and rat spermatozoa and spermatocytes [256, 257], whilst the ACh degrading enzyme AChE was found in rat spermatozoa [258]. The overexpression of AChE in spermatozoa lead to enhanced sperm motility but also to increased germ cell apoptosis [233].

In this study a comprehensive analysis of the expression of the cholinergic signalling system within the testis was performed. Although innervation of mammalian testis such as cat or human was described [259, 260], no nerve fibres could be found in rat testicular parenchyma corroborating experiments from Zhu et al. [12]. In contrast, it was shown in this study that the testicular capsule surrounding the parenchyma is densely innervated at both poles and the position of the incoming pampiniform plexus. To exclude any contamination with e.g. autonomic neurons both tissues, TP and TC, were separated for mRNA expression analysis.

Testicular parenchyma. **ChAT** is the main enzyme for synthesising ACh in neuronal and non-neuronal tissue. Both, mRNA and protein were found in TP of rat testis. Quantitative RT-PCR showed the high relative mRNA expression level for ChAT in comparison to ChT1, VAChT and OCT2. The localisation of ChAT-mRNA within the TP was investigated by ISH with sequence-specific probes, where it was detected mainly in primary spermatocytes. This finding was confirmed by ChAT-mRNA detection in isolated primary spermatocytes (thesis Iris Eckhardt, data in Schirmer et al., 414). At the post-transcriptional level, ChAT protein was found in primary and secondary spermatocytes, spermatids and endothelial cells of small interstitial arteries. A previous study revealed the presence of several splice variants of ChAT, which were found to lack enzymatic activity. Further investigations about their function were not done [261]. Thus, the presence of a truncated ChAT variant cannot be excluded for this study. Nevertheless, there is increasing evidence, that ACh is important in spermatogenesis and fertilisation events such as the acrosome reaction in human and mouse sperm [228, 229]. The high amount of ChAT mRNA and the detection of ChAT protein imply relevance within testicular function.

ACh-synthesis through ChAT is impossible without uptake of choline [262], (see Fig. 4). Immunoreactivity for the specific choline-uptake transporter, **ChT1**, was present in the same cell types that expressed ChAT. Following ChAT, ChT1 showed the second highest mRNA expression level compared to VAChT and OCT2. Protein detection of ChT1 for spermatocytes and spermatids corroborates findings that described mRNA expression in both isolated cell populations (thesis Iris Eckhardt, data in Schirmer et al., 414). This suggests that spermatozoa and spermatids are

capable of taking up choline and synthesizing ACh and might explain the dramatic effects of AChE overexpression in spermatids which results in increasing germ cell apoptosis [233].

Synthesis is followed by the release of ACh. This occurs via two different pathways (a) the classical storage in vesicles by **VACHT** and secretion via exocytosis [135-137] or (b) the constant release via the class of organic cation transporters [140-142]. The relative mRNA expression level of VACHT was significant lower compared to ChAT, ChT1 and OCT2. This was reflected by the restricted appearance of VACHT in cells of the TP. Overall only a slight VACHT-IR was detectable within the testis, except a population of basal cells in the seminiferous epithelium, presumably spermatogonia, which showed a strong IR for VACHT. Similar cells were also positive for ChAT and ChT1, but only for cells positive for VACHT-protein processes were could observed that reached into or through the layer of PTC. The localisation of these cells with immunoreactivity for three proteins, VACHT, ChT1 and ChAT, in the basal germ cell layer leads to the assumption that these cells could be spermatogonia. However, mRNA could only be found for ChT1, but not for ChAT or VACHT in isolated spermatogonia (thesis Iris Echhardt, data in Schirmer et al., 414). This is making a clear-cut localisation difficult. Zhou et al. [263] described the differentiation and regulation of spermatogonia from spermatogonial stem cells to the first mitotic differentiation, wherein the cells pass through different developmental stages with developmental specific markers. Thus spermatogonial subtypes may express only a selection of these molecules (ChAT, ChT1 or VACHT). This assumption is supported by the finding that VACHT-IR positive cells are not localised in every seminiferous tubule, and that cells within the same cross section of a tubule are in the same stage of maturation. In this study, similar observations were made for the $\alpha 7$ nAChR subunit, which was detected in primary spermatocytes and round spermatids by ISH (Fig. 25).

As an alternative to the visuclar transport mediated by VACHT, ACh can also be released by **OCT2** via an alternative non-vesicular route [262, 264]. The mRNA expression level for OCT2 was lower in comparison to ChAT and ChT1. In TP the rank order of the relative mRNA expression levels was ChAT > ChT1 > OCT2 > VACHT. The same rank order is reflected as well in the mRNA expression profile of

isolated testicular cell populations. While ChAT- and ChT1-mRNAs are expressed in germ cell (spermatogonia, spermatocytes and spermatids) and non-germ cell (PTC, SC and Leydig cell) populations, the mRNA-expression level for VACHT and OCT2 showed only low or undetectable levels in non-germ cell populations and spermatogonia (thesis Iris Echhardt, data in Schirmer et al., 414). Taken together, these observations strongly support the possibility that the germinal epithelium has the capability to synthesise and release ACh. Recently, ACh was detected within TP, which supports the data in this study (Prof. Klein, data in Schirmer et al., 414).

However, the question remains how non-germ cells release ACh. Testicular somatic cells (TM, SC and PTC) do express mRNA for ChAT and ChT1, but no mRNA was detectable for OCT2 or VACHT. Thus, other choline transporter may be involved in the ACh-release. In addition to OCTs, a proteolipid called “mediatophore” seems to be able to shuffle ACh across the cell membrane. The mammalian homologue of the mediatophore, is part of the vacuolar H^+ -ATPase (V-ATPase) found mostly in acidic organelles [265]. Originally the mediatophore was found in the plasma membrane of the electric organ of the electric ray *torpedo marmorata* [265]. Non-neuronal cells co-transfected with ChAT and the proteolipid gained the ability to release ACh [265, 266]. Furthermore the V-ATPase was localised in human lung microvascular endothelial cells [267] and rabbit AM [268]. The mediatophore could be another alternative ACh release mechanism for the VACHT and OCT2 negative cell populations TM, PTC and SC.

In summary, ChAT, ChT1, VACHT and OCT2 were detected on mRNA and protein level in the rat TP. Analysis of isolated cell populations showed cell specific differences in the mRNA expression with respect to germ cell stages vs. non-germ cell populations.

Testicular capsule. The similar rank order for the relative mRNA expression as seen in the parenchyma was also observed for the capsule: ChAT > ChT1 > OCT2 > VACHT. However, significant difference in the mRNA expression level was observed for ChT1. Individual cells within the capsule could not be separated.

Cholinergic nerve fibres are present within the TC, which are positive for molecules of the cholinergic system. However the expression of mRNA should be originated from cells within the capsule, because protein synthesis in neurons, and, hence mRNA, is for most mRNAs confined to the perikaryon. From there the proteins are transported to their destination by axonal transport [126].

13.2. Presence of nAChRs in testicular cells

As previously discussed, cells within the rat testicular parenchyma contain all molecules necessary for the synthesis of non-neuronal ACh. To further investigate the non-neuronal cholinergic system the targets for ACh were analysed. Previous studies demonstrated mRNA expression of nAChR-subunit $\alpha 3$, $\alpha 5$, $\alpha 7$, $\alpha 9$ and $\beta 4$ in human testis and demonstrated nAChR dependent influence on the acrosome reaction [231, 269]. The absence of nAChR-subunit $\alpha 7$ in mouse sperm resulted in impaired sperm motility [230].

13.2.1. Presence of nAChRs in testicular parenchyma and -capsule

In this study mRNAs for eight α - and three β -subunits of nAChR were detected in testicular cells. In addition mRNAs for all mammalian α - and β -subunits were amplified in TC, including mRNAs for the supposedly “muscle specific” $\alpha 1$ - and $\beta 1$ -subunits. Recent work showed that these subunits are present in non-skeletal muscle tissues, such as mouse lymphocytes and thymus; human macrophages; the inner root sheath of the hair follicle, airway fibroblasts and keratinocytes [56, 197, 270-272]. Their functions remain to be determined.

The mRNA expression levels for $\alpha 6$ and $\beta 4$ have been very low or even undetectable within the parenchyma. However, mRNA for both subunits was measured in isolated cell populations. mRNA for $\alpha 6$ was detected in PTC and SC, whereas $\beta 4$ is present in PTC and TM. Although two out of three analysed cell populations express either $\alpha 6$ or $\beta 4$, the low or undetectable mRNA expression of $\alpha 6$ and $\beta 4$ within the parenchyma-cell-mix leads to the suggestions that both subunits might be expressed in: (1) some populations of cells and the expression was masked by the huge amount

of germ cells in the preparation or (2) isolated cell populations increase expression of $\alpha 6$ and $\beta 4$. Both aspects mentioned here could explain the observations.

All remaining receptor subunits are expressed within the parenchyma, which makes it hard to predict the possible pentameric-receptor-structures of the mature nAChRs (for known pentamer-combinations see Tab. 1 & 2).

Whereas, there were almost no differences in mRNA expression levels between $\beta 1$, $\beta 2$ and $\beta 3$ subunits, the expression-profile between the α -subunits was variable. nAChR subunits $\alpha 4$ and $\alpha 7$ showed the highest expression of all α -subunits within TP, potentially as part of the heteropentameric $\alpha 4\beta 2$ nAChR, which constitutes the major nAChR subtypes in neuronal tissues like brain [273] and $\alpha 7$ homopentameric nAChR which has also been demonstrated in autonomic ganglia and brain [187, 274].

The relative mRNA expression levels for subunits $\alpha 1$, $\alpha 2$ and $\alpha 3$ were comparable to each other, while the amount of mRNA for $\alpha 5$ was nearly the same level than $\alpha 7$. Both subunit, $\alpha 5$ and $\beta 3$, need to be co-expressed with another α and β subunit to form functional channels [156, 162, 269]. Furthermore, nAChR-subunit $\alpha 5$ is usually co-assembled with $\alpha 3$, $\alpha 4$, $\beta 2$, or $\beta 4$ to form various nAChR subtypes such as $\alpha 4\alpha 5\beta 2$ or $\alpha 3\alpha 5\beta 4$ [174, 275]. The absence of $\alpha 5$ in the pentamers $\alpha 3\alpha 5\beta 2$ and $\alpha 3\alpha 5\beta 4$ decreased their Ca^{2+} permeability and the rate of desensitisation [162, 276] and in chick sympathetic neurons, the deletion of $\alpha 5$ altered the sensitivity of native receptors to both agonist and antagonists [168]. These data indicate that both the $\alpha 5$ and $\beta 3$ subunits (known as auxiliary subunits) may have a role in controlling ion-permeability and perhaps receptor-localisation [162].

Subunits $\alpha 9$ and $\alpha 10$ are expressed almost equally with a slightly higher expression level for $\alpha 9$. This finding is not surprising due to the facts that $\alpha 9$ is able to form functional homopentameric receptor and $\alpha 10$ only demonstrates activity when co-expressed with $\alpha 9$ [159, 170, 277].

Further analysis of the distribution of receptor-subunit-proteins was not possible due to the fact that available antisera are prone to unspecific binding [246, 278]. However, mRNA for the nAChR-subunit $\alpha 7$ was localised by ISH. The $\alpha 7$ -mRNA within the seminiferous tubules was expressed mainly in round spermatids and primary spermatocytes. Although the highest concentration was observed in these cells, moderate staining could be found in earlier cell stages such as spermatogonia.

Another possible source for $\alpha 7$ mRNA may be Sertoli cells, which are located between the germ cells. These findings are supported by the detection of mRNA in both spermatogonia and SCs in a previous study (thesis Iris Eckhardt, data in Schirmer et al., 414).

nAChRs belong to the gene superfamily of ligand-gated ion-channels, which are permeable for mono- and bivalent-ions such as calcium [279]. Subunits with a high permeability for Ca^{2+} are homopentamers consisting subunits $\alpha 7$, $\alpha 8$ or $\alpha 9$ [165, 280], while heteropentamers $\alpha 3\beta 4$ and $\alpha 4\beta 2$ have a lower Ca^{2+} permeability [281, 282]. Within the testis, calcium is an important molecule in different cell types and a variety of processes. (1) In mammalia sperm, a calcium increase from the extracellular space initiates the acrosome exocytosis [283, 284] followed by a second release from intracellular stores, which completes this process [285, 286]. (2) Spermatozoa are exclusively transported in the luminal compartment of the male and female reproductive tract separated by epithelial cells from nerve endings that could release ACh. In human and mouse sperm, ACh triggered the acrosome reaction, which was blocked by nAChR antagonists such as α -bungarotoxin or MLA [228, 229]. This clearly indicates a function for ACh and ACh-receptors and supports the non-neuronal origin of ACh. (3) Beside capacitation, sperm motility is regulated by $[\text{Ca}^{2+}]_i$ [287, 288] and mouse sperm deficient for the $\alpha 7$ nAChR show impaired motility [230]. Similar functions for $\alpha 7$ can be suggested for rats. In contrast, in this study $\alpha 7$ mRNA was not detected in spermatozoa by ISH, likely to be based on the fact that spermatozoa contain little mRNA which in addition is compacted and not readily accessible by probes. (4) Spermatozoa maintain their calcium homeostasis through the regulation of several types of calcium channels [284, 289]. (5) Mammalian spermatogenesis is temperature sensitive. In rats the exposure of the testis to temperatures $>37^\circ\text{C}$ results in increased death of germ cells [290]. Herrera and colleges [291] showed a connections between temperatures and intracellular Ca^{2+} homeostasis in rat pachytene spermatocytes and round spermatids. In neurons, nAChRs activation can play a relevant role in Ca^{2+} homeostasis [162].

Within the testis parenchyma the nAChR-subunits $\alpha 7$ and $\alpha 4$ show the highest mRNA expression level and therefore their influence in calcium dependent processes is possible. Beside the known influence on sperm motility subunits $\alpha 7$ and $\alpha 4$ and their

corresponding receptors may be involved in acrosome reaction or the response to temperature. The participation of receptors containing other subunits with similar characteristics such as $\alpha 9$ or $\alpha 5$ can not be excluded. Both receptor subunits are able to increase the calcium permeability, if they are co-expression with other subunits.

13.2.2. Presence of nAChRs in PTC, SC and TM

The mRNA expression profiles for the analysed cell populations namely TM, PTC and SC are more inhomogeneous compared to the mRNA expression profile for the TP.

Testicular macrophages demonstrated the highest variability in the relative mRNA expression of nAChR α -subunits. All or most samples expressed mRNA for $\alpha 2$, $\alpha 4$, $\alpha 5$, $\alpha 6$, $\alpha 7$, $\alpha 9$ and $\alpha 10$. The $\alpha 3$ -subunit was absent in 4 of 6 samples. In contrast to PTC and SC only the mRNA for $\beta 3$ was expressed in all TM-samples. mRNAs for $\beta 1$, $\beta 2$ and $\beta 4$ were detectable only in 1 to 3 out of 6 samples. $\beta 3$ is reported to be co-expressed with $\alpha 6$ in the CNS [275], which form functional nAChR in the brain [185]. In fact, the genes for $\alpha 6$ and $\beta 3$, CHRNA6 and CHRNB3, are located closely on chromosome 8 (8p11.21 and 8p11.2, respectively), and it is possible that they share a common regulatory mechanism. Considering these findings, disregarding $\beta 4$ from the calculations and putting less emphasis on the low expressed $\alpha 3$ the nAChR-compositions mainly contain subunits $\alpha 2$, $\alpha 4$, $\alpha 5$, $\alpha 6$, $\alpha 7$, $\alpha 9$, $\alpha 10$ and $\beta 3$. Subunits $\alpha 2$, $\alpha 4$, $\alpha 5$, $\alpha 6$, $\beta 2$ and $\beta 4$ usually form hetero-pentamers with each other. Excluding $\alpha 3$, $\beta 2$ and $\beta 4$ from the calculation, as their expression was not found to be consistent, reduces the nAChR combinations to: $\alpha 7$, $\alpha 5\alpha 7\beta$, $\alpha 9$ and $\alpha 9\alpha 10$. Considering $\beta 2$ and $\alpha 3$ the following AChR combinations can be included: $\alpha 4\beta 2$, $\alpha 3\beta 2 \pm \alpha 5$, $\alpha 4\alpha 5\beta 2$, $\alpha 5\alpha 6\beta 2$, $\alpha 6\beta 2\beta 3$, $\alpha 4\alpha 5\alpha 6\beta 2$ and $\alpha 4\alpha 6\beta 2\beta 3$. It was reported that $\alpha 6$ and $\beta 3$ are co-expressed [275], and that they are able to form functional $\alpha 6\beta 3$ nAChR [115]. On the other hand it was described that $\beta 3$ can only form functional channels, when it is co-expressed with both α and β subunits [156, 162]. Thus the nAChR combinations $\alpha 6\beta 3$, $\alpha 3\beta 3$ and $\alpha 7\beta 3$ seem to be controversial.

An interesting observation is the presence of both, subunits $\alpha 4$ and $\alpha 7$, in TM. Until now, most studies reported the presence of $\alpha 4$ and the absence of $\alpha 7$ in macrophage subpopulations such as mouse alveolar macrophage (AM) cell line MH-S, AM of FVB mice, rat AM, macrophages from the gut and peritoneal macrophages [122, 308-310]. However, Wang et al. [56] demonstrated the mRNA expression of $\alpha 7$ in human monocyte-derived macrophages. These previous data and the finding in this study might lead to the proposal of species-specific differences and even tissue specific differences within the same species for the nAChR-mRNA expression profile in macrophages [308]. Variations in the expression-level of other molecules such as cytokines (IL-1 and TNF α) or cell surface proteins (receptors, CD) have been described for macrophages in liver, lung and peritoneum [305, 306, 311]. TM and peritoneal macrophages (PM) feature differences in the mRNA expression level of TLRs [304]. Similar results could be observed for AM, PM and intestinal macrophages (IM). CD14, TLR4, MD2, iNOS, TNF α and iNOS displayed cell-specific mRNA expression profiles in absence or presence of LPS [302, 303]. Differentiation of adipose tissue macrophages (ATM) in adipose (F4/80⁺CD11c⁺) and normal mice (F4/80⁺CD11c⁻) results in modified subsequent gene expression of IL-6, iNOS and ApoE [307].

Additionally, subunits $\alpha 9$ and $\alpha 10$ were found in rat AM, human lymphocytes and AM of FVB mice [277, 308, 310, 312], where they may compensate the function of the missing $\alpha 7$ subunit resulting from general pharmacological properties shared between $\alpha 7$, $\alpha 9$ and $\alpha 10$ nAChR subunits [308, 313].

Analysed **peritubular cell** samples did not show any expression of $\alpha 3$ and $\alpha 2$, $\alpha 9$ and $\alpha 10$ could only be detected in 50% or less of the samples. Resulting from these findings, the main subunits in PTC, which could assemble to nAChR pentamers are $\alpha 4$, $\alpha 5$, $\alpha 6$ and $\alpha 7$ in combination with $\beta 2$, $\beta 3$ and $\beta 4$. Possible combinations of nAChR are therefore: $\alpha 4\beta 2$, $\alpha 4\beta 4$, $\alpha 6\beta 2$, $\alpha 6\beta 4$, $\alpha 4\alpha 5\beta 2$, $\alpha 5\alpha 6\beta 2$, $\alpha 6\beta 2\beta 3$, $\alpha 6\beta 3\beta 4$, $\alpha 4\alpha 5\alpha 6\beta 2$, $\alpha 4\beta 2\beta 3\beta 4$, $\alpha 4\alpha 6\beta 2\beta 3$, $\alpha 7\beta 2\beta 3$, $\alpha 7$ and $\alpha 5\alpha 7\beta$. Several laboratories have described the presence of nAChR subunits mainly without reporting specific nAChR-combinations [292]. The following combinations have been shown before: $\alpha 4\beta 2$ and $\alpha 4\beta 4$ in airway and bronchial epithelial cells [293] and $\alpha 7$ in human epithelial cells, vascular endothelial cells or HUVECS [54, 118]. As mentioned before nAChR-

subunit $\alpha 5$ is usually co-assembled with $\alpha 3$, $\alpha 4$, $\beta 2$, or $\beta 4$ to form various nAChR subtypes [174, 275]. In PTC $\alpha 3$ is not detectable. Therefore, $\alpha 5$ most likely assembles to $\alpha 4\alpha 5\beta 2 \pm \alpha 6$. However, other combinations are also possible.

In comparison to PTC and TM the lowest number of nAChR α -subunits was found in **Sertoli cells**. mRNA was not detectable for $\alpha 3$, $\alpha 4$, $\alpha 6$. For subunits $\alpha 2$ and $\alpha 9$ mRNA were found in 2/4 and 3/5 analysed samples. Subtracting the missing subunits from known receptor-compositions only a few nAChR are possible, which mainly contain the subunits $\alpha 7$, $\alpha 9$ and $\alpha 10$ in combination with $\alpha 5$ and $\beta 2$ - $\beta 4$. Possible combinations of nAChR are therefore: $\alpha 7$, $\alpha 7\beta 2$, $\alpha 5\alpha 7\beta$, $\alpha 9$ and $\alpha 9\alpha 10$. nAChR combinations described before are: $\alpha 7$ in airway- and bronchial epithelial cells or keratinocytes [294, 295], $\alpha 7\beta 2$ in an *in vitro* experiment with *Xenopus* oocytes [166] and $\alpha 9\alpha 10$ in human lymphocytes [170, 296].

The function of SC is the physical support of germ cells and the provision of essential nutrients and growth factors [297, 298]. Additionally, they form tight junctions (ZO-1, connexin) between each other, which restrict the passage of molecules (blood-testis-barrier) [22, 23]. nAChR may be involved in function of the blood-testis barrier. Bovine brain microvascular endothelial cells demonstrate a characteristic expression pattern for the nAChR subunits $\alpha 3$, $\alpha 5$, $\alpha 7$, $\beta 2$, $\beta 3$ and the absence of $\alpha 4$ [299]. In addition they showed nicotine-dependent changes in the expression profile for the subunits $\alpha 7$ and $\beta 2$. Stimulation of nAChR using nicotine altered the blood-brain barrier permeability and tight-junctional protein expression of the zona occludens protein, ZO-1 [300, 301]. Concluding these findings and the presence of nAChR-subunits in SC might indicate an involvement of the ACh-system in the regulation of the blood-testis-barrier and Sertoli cell-germ cell contacts.

13.3. MRs are present within the testis

13.3.1. Presence of MRs in testicular parenchyma and -capsule

In this study the relative mRNA expression level was analysed in both: (1) the testicular parenchyma (TP), which mainly consists of germ cells, SC, PTC, Leydig cells and immune cells; and (2) the testicular capsule (TC), which contains mainly

fibroblasts, collagen fibres and contractile cells such as smooth muscle cells. The presence of all five MR-subtypes could be demonstrated in both tissues. The relative mRNA expression profiles in TP had a rank order of $M_4R > M_3R > M_5R > M_1R > M_2R$ and in TC the rank order was $M_2R > M_4R > M_3R > M_1R > M_5R$. All MR subtypes except M_5R were significantly different expressed between the two analysed tissues TP and TC. All five MR subtypes are G-protein-coupled transmembrane receptor proteins. Sequence homologies between the family members are reflected in similar functions [208]. The “odd-numbered” muscarinic receptors (M_1R , M_3R and M_5R) typically couple via α -subunits to the Gq/11 family, whereas the “even-numbered” members (M_2R & M_4R) couple via G_i and G_o α -subunits.

Within the **capsule** mRNA for the even numbered MR subtypes are expressed at higher levels while the odd-numbered MR subtypes are expressed at lower levels. Overall M_2R was the main receptor subtype mRNA within TC. As mentioned before fibroblasts and smooth muscle cells are an essential part in the capsule. Both, fibroblasts and smooth muscle cells have been shown to express several MR subtypes with high mRNA levels rates for M_2R [314-316]. Human lung fibroblasts express most MRs with dominance on M_2R . The stimulation of MRs leads to increased proliferation of these cells [317]. Airway smooth muscles cells express mainly M_2R and M_3R subunits, the former being the predominant population [318, 319]. ACh-binding to M_2R and M_3R modifies the expression of contractile proteins and induces an increased mitogenic effect as response to growth factors in airway smooth muscle cells [319]. Within the group of odd-numbered MR, M_3R shows the highest mRNA expression level in TC. This might indicate similar functions for MR subtypes within TC.

In **parenchyma** the separation of the two groups, odd and even numbered MR, does not exist. Here, M_4R shows the highest and M_2R the lowest mRNA expression level. Comparable with TC, M_3R had the highest mRNA expression level within the odd-numbered MR. Based on the heterogeneity of the subtype expression within the tissue it is not possible to conclude a function. Except for the MR-subtype expression-profile of Sertoli cells and sperm no other data have been presented for single cell populations within the TP. In 2001 Borges et al. described the presence of all five MR

subtypes in Sertoli cells of 30 days old rats and suggested a role in cell proliferation [236]. Muscarinic receptors were found mainly in the sperm head regions of several species including human sperm [227] or rabbit spermatozoa by binding-experiments using the muscarinic antagonist quinuclidinyl benzilate [320]. The localisation of MR in sperm heads may be correlated to a role in sperm-egg interaction [227].

13.3.2. Presence of MRs in PTC, SC and TM

Additionally to the real-time RT-PCR for TP, standard RT-PCR was performed with isolated PTC, SC and TM. The mRNA expression level for MR-subtypes in SC showed corresponding result to these presented from Borger et al. [235]. All five MR subtypes were found in Sertoli cells. MRs are supposed to mediate proliferation and differentiation in embryonic cells, dorsal root ganglia and Schwann cells [221, 321]. Sertoli cells proliferate during prepubertal development, but stoped dividing when the the first meiotic germ cells appears. This process could be mediated by MRs.

In contrast to SC and PTC, **testicular macrophages** showed variations in the mRNA expression level of MR-subtypes. Except M₁R, which was always present, the presence of M₂R-M₅R varied. Variability of MR mRNAs was described between mesenteric-lymph-nodes containing monocytes, B- and T-cells of different individuals by Kawashima & Fujii [218]. They showed the constant expression for M₄R and M₅R mRNAs and variations for M₁R to M₃R. Macrophage populations in other species express mRNA for MR-subtypes too, such as mouse peritoneal macrophages (M₁R-M₅R) or human airways macrophages (M₂R & M₃R) [253, 341]. Therefore it may be suggested that the expression of MR-subtypes in macrophage subpopulations is dependend on the environment. Furthermore, Kawashima et al. [218] described variations in the mRNA expression of M₁R, M₂R and M₃R in lymphocytes between human test subjects.

Peritubular cellss are contractile cells, which can be characterized using smooth muscle-specific antibodies. PTCs isolated in this study expressed mRNA for all five MR. Siu and colleges described the presence of M₃R in PTC [322].

Several organs and tissues contain smooth muscle cells, which have been analysed on the presence of MR-subtypes such as airway- or bronchial cells, detrusor cells in the bladder or vascular cells within blood vessels [318, 323-327]. Nevertheless functional studies are problematic due to the paucity of pharmacologically subtype-specific antagonists [206]. In canine saphenous veins the M₁R-subtype is supposed to mediate cell contractions [328-330]. The contraction of the guinea-pig ileum and indeed of many other smooth muscle cell types is mediated by MR-subtypes. Contractions are supposed to be mediated by M₃R [212], whereas M₂R is most likely its antagonist [316, 331, 332]. Other studies indicated, that the M₃-receptor mediates relaxation of vascular smooth muscle cells [225, 333, 334].

Within the testis the presence of MR-subtypes was also found in correlation with contractile elements. mRNAs for MR-subtypes were detected in the vas deferens of dog, human, guinea pig and rat [335-339]. Known functions of the MR-subtypes depend on the species and tissue. In guinea-pig, the M₃R potentiates P₂X receptor-mediated contractions [338], whereas the rabbit M₁R inhibited the contractile response of the vas deferens [339]. Rat epididymis and efferent ductules contained mRNA for M₁R, M₂R and M₃R with PTC positive just for M₃R [237, 322].

Overall, former data showed a co-expression of M₂R and M₃R in many types of smooth muscle cells such as in urinary bladder, vascular and airway tissue with the main focus on M₂R [316, 340]. M₂R and M₃R are the main players for cell contraction. Similar functions can be suggested for PTC.

13.4. Similarities of the cholinergic system in mouse and rat testes

Molecules necessary to synthesize and release ACh and MR-subtypes were analysed for mouse testicular parenchyma and -capsule. Overall, mRNA expression for MR-subtypes in mouse showed a similar pattern as seen in rats, with the exceptions that subtypes showing the highest significant differences between TP and TC are M₂R in rats and M₃R in mice. A high amount of M₄R-mRNA was found in both tissues in rat and mouse, implying a relevance of this subtype. Unfortunately, the function of the M₄R in non-neuronal cells is largely unknown with one exception in keratinocytes, where M₄R facilitated migration and wound reepithelialisation [342].

A different picture was observed for the mRNA expression profile of ChAT, VACHT, OCT2 and ChT1 in mice. While in rats ChAT and ChT1 were the predominant molecules, the relative expression values for VACHT and OCT2 were higher in mice. Currently, it is not possible to determine the location of these molecules in mice in detail. This question might be answered performing immunohistochemical experiments, analysis of isolated cell populations or the usage of knockout mice. Species specific differences (mouse vs. rat) were demonstrated by Lips et al. for the lung previously [126]. Both species were challenged with ovalbumin (OVA) and mRNA expression for ChT1, VACHT, OCT2 and ChAT was compared to control animals. In rats a time dependent down-regulation was observed after 24 h (ChAT & OCT2) and 48 h (ChT1, VACHT and OCT2), whereas ChAT, ChT1, VACHT and OCT2 were not detectable in the mouse lung after 24 h. These data indicate a similar tendency (mRNA down-regulation after OVA) in mice and rats, but there are slight differences between the targets and the intensity of the down-regulation [126].

13.5. The function of the cholinergic system in EAO

Within recent years the close relationship between CNS and the immune system was more and more established. The CNS is able to induce the rise of the serum corticosteroid concentration to prevent the development of lethal systemic inflammation [49, 50]. The excessive production of pro-inflammatory cytokines such as HMGB1, TNF- α or IL-1 β and their release into the circulation can be more harmful than the initial inflammation itself and might result in tissue injury, systemic inflammation, shock or death [51-54]. The neural inhibition of inflammation is supposed to be mediated by the vagus nerve, whose stimulation can control the production of pro-inflammatory cytokines in experimental models of systemic inflammation such as lethal endotoxemia [55-57], allergic lung inflammation [126, 343] or sepsis [57, 344, 345]. The principle neurotransmitter of the vagus nerve is ACh, therefore this system was termed the “cholinergic anti-inflammatory pathway” [55]. In this study, the rodent in-vivo model of experimental autoimmune orchitis (EAO) was used to examine the response of the cholinergic system in testicular inflammation.

Local testicular inflammation induced massive changes in the mRNA expression profile for a number of nAChR subunits, ACh synthesis, storage molecules and MR. All mRNAs were down-regulated under inflammatory conditions. In comparison between adjuvant group and orchitis groups the following molecules showed significant reduced relative mRNA expression levels: nAChR subunits $\alpha 3$, $\alpha 4$, $\alpha 5$, $\alpha 7$, $\alpha 10$, $\beta 2$ and $\beta 3$; MR subtypes 4 and 5; ChAT, ChT1 and OCT2.

In addition, there were significant difference between mRNAs of untreated and adjuvant groups for $\alpha 10$, M_4R and OCT2. In these three cases treatment with complete Freund's adjuvant (CFA) lead to significant higher mRNA expression levels. The stimulation of the immune system by CFA is a known effect. Animals treated with CFA and testis homogenate demonstrated mRNA down-regulation compared to animals treated only with CFA. OCT2 and the $\alpha 10$ nAChR subunit did not show any mRNA down-regulation between untreated and orchitis group, an observation which could be made for M_4R .

Molecules involved in ACh synthesis, release, binding and up-take were up- and down-regulated under different inflammatory conditions. In a rat model of acute allergic-airway-disease, mRNA levels for ChAT, ChT1, VACHT and OCT2 were decreased in the group of allergen challenged animals. Interestingly changes in ChAT and OCT2 mRNA expression occurred within 24 h, whereas VACHT and ChT1 were significantly down-regulated after 48 h. At the second time-point ChAT started already to return to its normal level [126]. In superficial skin of patients with atopic dermatitis ACh levels were increased 14-fold in comparison to healthy skin [346], a later study described the parallel down-regulation of nAChR subunits $\alpha 3$, $\alpha 7$, $\alpha 9$ and $\alpha 10$ in the skin of patients suffering of atopic dermatitis and the up-regulation of subunits $\alpha 3$ and $\alpha 5$ in mast cells in these patients [347]. In this study the analysed targets, if changed at all, were down-regulated on mRNA level. Short term experiments exposing the transcriptional level in the acute phase have not yet performed. A transient up-regulation of the ACh-related molecules in the acute phase of EAO, which would be 24 to 48 h after the immunisation, cannot be excluded but at the final stage of orchitis "cholinergic" mRNAs seem to be down regulated.

Previous studies analysing the role of the “cholinergic anti-inflammatory pathway” mainly focused on the $\alpha 7$ nAChR subunit, which abrogates the endotoxin-mediated rise of pro-inflammatory cytokines by stimulating cells directly (ACh or nicotine) or indirectly (electric impulses) via the vagus nerve [55, 56, 344, 348, 349]. Experiments on single cell-populations were performed on macrophages of different tissues and species, but without analysing the entire mRNA expression profile for nAChR subunits [55, 56, 348]. As mentioned above, macrophage subpopulations express different expression profiles for nAChR subunits (13.2.) with characteristic variability for the subunits $\alpha 4$ and $\alpha 7$. Recently, one former statement, the $\alpha 7$ -mediated TNF- α inhibition after ACh stimulation in peritoneal macrophages (PM), was challenged by the presence of $\alpha 4$ and the absence of $\alpha 7$ in PM [122]. Furthermore, Kelso et al. described an unexpected α -Btx-binding in $\alpha 7^{-/-}$ knockout mice [350]. Resulting from these findings it is possible that receptor subunits that would include $\alpha 7$, $\alpha 1$ or $\alpha 9$ compensate each other because they can all be a target for α -Btx [157, 351].

In this study, several nAChR receptor subunits and MR subtypes are present in the healthy and inflamed rat testis, which makes an exact implementation of the main receptor subunit or subtype impossible. The main outcome of the “cholinergic anti-inflammatory pathway” is, that the expression and release of pro-inflammatory molecules such as TNF- α are inhibited by the activation of nAChR such as $\alpha 7$ [56, 57]. In this study, the ACh related molecules were mostly down regulated. Cells within the inflamed testis do not transcribe the same amount of mRNAs suggesting that ACh-synthesis is impaired compared to the healthy testis.

This implies that ACh cannot function with the same intensity as usually and the expression of cytokines such as TNF- α or HMGB1 might not be suppressed as necessary. Unfortunately, previous studies, which analysed the function of $\alpha 7$ in the presence or absence of endotoxin, missed to determine the mRNA expression levels. This would lighten the question about the $\alpha 7$ mRNA level under normal and inflamed conditions.

However, it has to be considered that the reduction in relative mRNA expression levels of molecules related to ACh-synthesis, -release and -binding may be related to the loss of germ cells. As the disease progresses a characteristic of EAO is the detachment and loss of developing germ cells, which finally results in the total impairment of spermatogenesis [60, 64]. Whilst germ cells are lost, mononuclear cells

infiltrate into the interstitial space largely increasing the percentage of inflammatory cells within the testis [64]. Therefore estimation about the regulation of the genes in individual cell populations is difficult. Nevertheless, the nAChR subunits $\alpha 4$ and $\alpha 7$ are expressed predominantly in SC, TM, PTC, spermatogonia and Leydig cells, whereas ChAT, ChT1, VACHT and OCT2 are more present in pachytene spermatocytes and round spermatids (thesis Iris Eckhardt, data in Schirmer et al., 414). Therefore, the absence of spermatids, which express ChT1, VACHT, OCT2 and ChAT, might be related to the lower expression of subunits in orchitis. The presence $\alpha 4$ and $\alpha 7$ in non-germ cells and early germ cell stages leads to the suggestion that the low expression of $\alpha 4$ and $\alpha 7$ subunits is related rather to a down-regulation than to the loss of cells.

13.6. Functional evidence for ACh receptors in testicular cells

Calcium, an important messenger molecule within cells, has a concentration of app. 100 nM in resting cells. Increasing calcium concentrations (500-1000 nM derived either from the external medium or from internal stores) lead to cell activation [352]. Calcium influx from external space is mediated by different types of receptors such as ligand-specific-nicotinic and muscarinic AChR.

nAChRs are permeable for cations (Ca^{2+} , Na^{+} , K^{+} and Mg^{2+}). The composition of the subunits determines the preference for the type of cation [198, 199]. nAChR containing subunit $\alpha 7$ (as homo- or heteropentamere), or $\alpha 9$ and $\alpha 10$ show high permeability for Ca^{2+} [156, 165, 200]. MRs are G-protein coupled-proteins, which can be divided into two groups: (1) M_1R , M_3R and M_5R are coupled to subunit $\text{G}\alpha_q$, which activates PLC- β . The down-stream product of PLC- β , IP₃, binds to intracellular calcium-stores and releases Ca^{2+} into the cytosol; (2) M_2R and M_4R activate $\text{G}\alpha_i$, which results in a decreasing cAMP formation and a decreasing concentration of protein kinases A (PKA) [223, 224, 226]. PKs mediate gene transcription via the modulation of transcription factors such as cAMP response element-binding protein (CREB).

As mentioned before, TP and isolated testicular cell populations (PTC, SC and TM) do express mRNA for several nAChR subunits and MR-subtypes, but the detection of

related receptor proteins was not possible due to the absence of commercially available subunit- or subtype-specific antisera [246, 247]. However, receptor functionality can be analysed by live-cell essays such as calcium-imaging, where changes in intracellular Ca^{2+} -concentrations are measured. To investigate the presence of functional nAChR receptors and MR-subtypes in individual testicular cells, calcium-imaging experiments were performed using PTC, SC and TM.

All three cell types were used previously to measure intracellular calcium concentrations, but not with respect to ACh receptor activation. PTC treated with the proteinase-activated receptor-2 activating peptide (PAR2) showed an increase of intracellular Ca^{2+} , which was blocked by the PAR2-reverse peptide [353]. SCs do express TRPV1 and the intracellular Ca^{2+} concentration rose after stimulation with capsaicin. This could be blocked by the capsaicin-antagonist ruthenium red [354]. Furthermore, extracellular ATP triggers both Ca^{2+} release from intracellular stores and Ca^{2+} influx from extracellular space [355]. In testicular macrophages melatonin elicits a rapid and sustained increase in $[\text{Ca}^{2+}]_i$ in the presence of extracellular Ca^{2+} [356].

13.6.1. PTCs express neuronal-like muscarinic receptors

Stimulation with ACh, the endogenous agonist for both, nAChR and MR, resulted in a Ca^{2+} -influx in PTC. Further investigations showed that MR, but not nAChR are responsible for the response to ACh and muscarine in PTC. Treatment of PTC with either muscarine or ACh resulted in a similar Ca^{2+} -response in about 50% of the analysed cells (ACh: 56.6%; muscarine: 49.6%). A subpopulations of these cells (ACh: 12.7%; muscarine: 15.2%) could be characterised by a significantly higher response (30%) than the cell-average, but almost no response to the following ATP-treatment. These ACh or muscarine- responses were absent in presence of the muscarinic receptor-antagonist atropine. The experiments demonstrate the presence of functional neuronal-like MRs in PTCs.

The preference of the MR-subtypes to bind a specific GPCR α -subunit might lead to the constriction to M_1R , M_3R and M_5R , which are able to initiate the release of Ca^{2+}

from internal stores via PLC β and IP3 [223, 224, 226]. To confirm this hypothesis PTC could be treated with muscarine in the absence of extracellular calcium, which should result in the same rapid spike as seen in this study for the muscarine-treatment in a calcium-containing environment. Nevertheless, the involvement of M₂R or M₄R cannot be excluded because of their indirect connection to calcium-channels. M₂R can influence K⁺-channels which subsequently result in an increased intracellular Ca²⁺-concentration (calcium-activated potassium channel). In contrast to PTC, acute activation of ACh receptors via acetylcholine, nicotine and muscarine did not result in changes in [Ca²⁺]_i in SC or TM.

Although mRNAs for all MR-subtypes were detected in PTC, the observation of muscarine-responding and non-responding cells leads to the suggestion of PTC subpopulations within the rat testis. Previous data support the existence of subpopulations within PTC. The layer of so-called "peritubular cells" is a heterogeneous cell-population surrounding the seminiferous tubules and consists of myoid cells covered by non-myoid cells such as fibroblasts or endothelial cells [25, 357-360]. The ratio of the different cell populations *in vitro* is dependent on the preparation [359, 360] mostly done by enzymatic treatment including collagenase [25, 359-361]. Beside a non-clear use of the terminology PTC or myoid PTC (mPTC), the ratio of PTC vs. mPTC *in vivo* is unknown.

Isoactin is supposed to be a trustable differentiation marker between mPTC, PTC and cells within the tubules [362-364]. The staining intensity of reactive mPTCs in the same preparation varied considerably, which indicates a heterogeneity in degrees of spreading, in cell maturity or in subpopulations [362]. Further investigations showed that mPTC are partly positive for desmin [28, 362, 363], while another population reveals desmin negative [25, 359, 362]. Desmin positive mPTC are alkaline phosphatase (AP) positive [25, 359, 365, 366]. Unfortunately, there is no data available unifying a multiple-immunohistochemical-staining for desmin, isolectin and AP. In this study, the purity of mPTC-enriched cultures was determined to app. 98% by IHC with anti- α -SMA, achieved most probable by long time culture (9 days) and splitting of the cells. Tung & Fritz already mentioned an increased purity of mPTC if cultured 10 days in the presence of 10% FCS [362]. Detection of desmin-protein and AP were not performed in this study, but could help to determine PTC subpopulations

in addition to functional differentiation (responding and non-responding to muscarine). The presence of different populations of smooth muscle cells have been described in the pig and rat artery. The stimulation with substances such as PDGF or TGF β 2 influenced the differentiation into smooth muscle cell subpopulations in both species [367, 368].

13.6.2. ATP-induced Ca^{2+} -influx is influenced by ACh or -agonists

Cells respond on ATP or KCl with an increase in intracellular Ca^{2+} -concentration. This can be used to confirm the viability of cells. In this study ATP was utilized, which resulted in a Ca^{2+} -influx in all cells of the three cell populations.

This ATP-dependent increase of the Ca^{2+} -concentration was reported previously for neuronal [369, 370] and non-neuronal cells such as alveolar macrophages [371], cochlear outer hair cells [372], *Xenopus* oocytes [370] or HEK-293 cells [369]. ATP is able to induce Ca^{2+} -transients by binding to members of the receptor families P2X or P2Y [373]. ATP binds specifically to the transmitter-gated cation P2X channel-subtypes and GPCR-P2Y-subtypes 1, 11, 12 and 13 [374-380]. The ATP-mediated Ca^{2+} -response between PTC, SC and TM was different with respect to the response time. While there is a short rapid spike in PTC, the initial fast peak is followed by a long lasting plateau in SC. In TM the fast increase is followed by a slower decreasing Ca^{2+} -concentration.

In rat SC it was previously reported that ATP is able to trigger the synthesis of PI3 and the Ca^{2+} -release from intracellular stores, but also a Ca^{2+} -influx across the plasma membrane [355]. Foresta et al., focusing on the ATP-induced intracellular changes, demonstrated a sustained $[\text{Ca}^{2+}]_i$ plateau following the initial fast $[\text{Ca}^{2+}]_i$ transient [381]. This Ca^{2+} -influx from the extracellular space was triggered by voltage-gated Ca^{2+} -channels (VOCCs), which were activated by Na^+ -mediated membrane-depolarisation. Both inhibition of VOCCs and reduction of extracellular Na^+ reduced the plateau after the initial peak. These observations suggest more than one ATP-mediated signalling pathway in SC.

Both release mechanism, via P2X or P2Y seem to be possible for the observed slowly decreasing $[\text{Ca}^{2+}]_i$ in TM, which could be the result of continuous influx of Ca^{2+} into

the cytoplasm. The sharper peak in PTC implies a Ca^{2+} -influx from either internal stores or extracellular space. Cytoplasmic increase in Ca^{2+} can activate multiple downstream pathways. During this on-phase, Ca^{2+} -binding proteins such as buffer (calbindin D-28, calnexin) or effectors (calmodulin) attach to Ca^{2+} and therefore influence the free Ca^{2+} -concentration [382]. Various pumps and exchangers [383] remove Ca^{2+} from the cytoplasm, which starts the off-mechanism, until reaching the homeostatic level. Differences in the activity of pumps and exchangers might be another possible reason for the fast decreasing $[\text{Ca}^{2+}]_i$ in PTC or the slowly decreasing $[\text{Ca}^{2+}]_i$ in TM. Here further investigations are necessary to analyse the underlying signalling pathways.

Although, SC and TM did not show any direct response on nicotine, muscarine or ACh an indirect receptor-dependent modulation could be observed for the following ATP treatment. The stimulation of SC or TM with both, nicotine and ACh, reduced the ATP-induced Ca^{2+} -response. The time-course of the response to ATP was different in SC and TM. In TM the initial peaks in the ATP-induced Ca^{2+} -response between the HEPES, ACh and nicotine treated groups were similar. Significant differences occurred over time in TM, whereas in SC the divergence between the ACh-, nicotine- and control-treated groups is significant during the initial spike and all three groups converged into the same long lasting plateau. Interestingly, muscarine did not reduce the ATP-induced Ca^{2+} -response in SC as seen for TM, where the course of the curve was almost identical to the nicotine-treated group. In SC muscarine resulted in a significant increased ATP-induced Ca^{2+} -response compared to the control group, with an additional second plateau-like peak over time (Fig. 38). This suggests the successive release of internal Ca^{2+} followed by entry of Ca^{2+} from extracellular space. It seems that the activation of MRs and nAChRs in SC has an opposite effect on the ATP-induced Ca^{2+} -response (Fig. 38). In PTC ATP-triggered changes in $[\text{Ca}^{2+}]_i$ dependent on ACh, nicotine or muscarine were not observed.

Taking together, the ATP-induced Ca^{2+} -responses initiated by ACh, nicotine or muscarine stimulation seems to be mediated by different signalling pathways in SC, whereas there seems only one ACh-dependent response in TM. The ACh-dependent modulation of the ATP signalling was cell-type dependent since stimulation of MR

and nAChR did not influence the ATP-induced Ca^{2+} -responses in PTC.

The findings observed in the experiments with PTC, SC and TM can be summarised in the following way: (1) PTC expressed functional MR subtypes, that mediated the rise in intracellular Ca^{2+} in response to ACh and muscarine; (2) SC and TM did not respond directly to muscarine; (3) nAChR expressed in PTC, SC and TM did not induce a depolarisation-dependent increase in Ca^{2+} and thus not act in a neuronal-like way. Similar results were reported for human lymphocytes, rat leukocytes and rat alveolar macrophages [248, 296, 384]. Patch clamp recordings and calcium-imaging experiments with cells stimulated with nicotine did not result in any change of the intracellular Ca^{2+} -concentration, whereas the pre-treatment with nicotine reduced the Ca^{2+} -concentration in the analysed cells [248, 296, 308]. However, (4) the influence of muscarine/nicotine/ACh on the ATP-induced Ca^{2+} -response in SC and TM implies a connection or crosstalk between nAChRs and members of the ATP-receptor families P2X and/or P2Y.

Evidence for close relationships between nAChRs and other molecules have been described already, such as: (a) the association of nAChR-subunits $\alpha 3$, $\alpha 4$ and $\alpha 5$ with PI_3K [385]; (b) the assembly of nAChR-subunit $\alpha 7$ with β -arrestin [294] or (c) the connection of nAChR-subunit $\alpha 7$ with the T-cell receptor ($\text{CD}3\zeta$) to modulate the TCR/CD3 function [386].

A connection or relationship between MR-subtypes and other receptors or molecules were not yet reported. Therefore this study indicates for the first time a crosstalk between MR and ATP-receptors but cannot be excluded as the present data demonstrate.

13.6.3. Nicotinic antagonists modulate the ATP-induced Ca^{2+} -influx in SC

Nicotine or muscarine specific-antagonists usually abolish nicotine- or muscarine-induced responses, but there are known unexpected or opposite examples such as (1) the inhibition of $\alpha 9\alpha 10$ nAChR by the muscarinic receptor-antagonist atropine in lymphocytes [296]; (2) the stimulation of nAChRs by nAChR-antagonists MLA and α -BTX in T-cells or AM [308, 386] or (3) the ATP-triggered rise in $[\text{Ca}^{2+}]_i$ by MLA

in leucocytes [248]. Here, the influence of nicotinic-antagonists MLA, DH β E and mecamylamine (Meca) on the ATP-induced rise of $[Ca^{2+}]_i$ was analysed in SC.

The interpretation of the data achieved from this experiment is difficult, because of significant differences within all analysed groups. At neuronal-like nAChRs the non-selective-nAChR-antagonist Meca blocks nicotine effectively. Conveying this information to this study and implying a connection between the nAChR and the P2X/Y receptor, the ATP-induced Ca^{2+} -response should rise back to the same level for the Meca & nicotine treated group as seen for the HEPES group. But this is not the case in this study, caused probably by the missing neuronal-like behaviour of the nAChRs found in non-neuronal cells such as leukocytes, lymphocytes or macrophages [248, 296, 308]. A tendency which fits this theory was observed, although there was still a significant difference between the Meca & nicotine and HEPES group. The antagonist DH β E, which blocks $\alpha 4\beta 2$, but also other nAChR α -subunits smaller than $\alpha 7$ shows a similar profile as seen for Meca. The treatment with Meca or DH β E alone or in combination with nicotine increased the ATP-induced Ca^{2+} -response compared to the control group. nAChR-subunits $\alpha 3$, $\alpha 4$ and $\alpha 6$ could not be detected with standard RT-PCR, which makes $\alpha 5$ and $\alpha 2$ to the most promising candidate for the binding of DH β E.

Only for the treatment with MLA, an inhibitor for subunits $\alpha 7$, $\alpha 9$ and $\alpha 10$ [387], divergent results were observed. Here, the pre-treatment with MLA and additional treatment with nicotine showed the same ($P = 0.854$) ATP-induced Ca^{2+} -response as seen for the group treated with nicotine alone. Interestingly, cells incubated only with MLA diminished the ATP-induced Ca^{2+} -response as seen for the cell group treated with nicotine alone. These findings indicate that both, nicotine and MLA are able to reduce the ATP-induced Ca^{2+} -response and that the combination of both does not potentiate their actions.

Previous studies reported the direct or indirect stimulation of MLA on different immune cells [248, 386]. Here, an opposite response could be demonstrated, where MLA dampened the ATP-induced Ca^{2+} -response. The presence of extracellular ATP is well recognised as “danger” or “host tissue damage” signal, which is mostly considered to be pro-inflammatory [388, 389]. The binding of nicotine or MLA to $\alpha 7$,

$\alpha 9$ and $\alpha 10$ reduces the ATP-induced Ca^{2+} -response, which indicates an anti-inflammatory reaction. These findings would support the anti-inflammatory influence of $\alpha 7$, which in case of stimulation by nicotine or ACh, inhibited the TNF- α production [249].

14. Sensory innervation of testicular adjacent structures

In mammals, efferent fibres innervate the testis using two main routes (1) via the superior spermatic nerve and testicular artery and (2) via the inferior spermatic nerve and vas deferens to the epididymis [12, 78, 390, 391]. Nerve fibres in mammalian testis are usually non-myelinated [392]. Nevertheless myelinated afferent fibres were found in the superior spermatic nerve of cats [393] and camels [101, 392]. Furthermore, myelinated and unmyelinated nerve fibres were found in dogs [394-397]. The detection of nociceptive nerve fibres within the testis and adjacent structures in rats was the main target of the experiments with special focus on CGRP containing fibres. Neuropeptides such as CGRP, substance P (SP) or somatostatin are released from central and peripheral terminals of nociceptive neurons [398-403]. In the spinal cord CGRP is believed to be associated with transmission and processing of noxious information, whereas in the periphery it seems to be responsible for neurogenic inflammation [404, 405]. Both known entering routes were analysed and nerve fibres were found in the fascia (internal & external fascia and cremaster muscle), vas deferens, superior- and inferior ligament (SL, IL) and the meso-structures. Myelinated (Nf200+) and unmyelinated (Nf200-) CGRP containing fibres as well as myelinated CGRP negative fibres could be observed. Analysis of the testicular artery and pampiniform plexus was less successful resulting from preparation problems due to the enormous amount of adipose tissue around the blood vessel/plexus. However, the existence of nerve fibres travelling alongside the testicular artery was confirmed by PGP9.5 staining. Beside the testicular artery, the testicular capsule was examined with the pan-neuronal marker PGP9.5. Nevertheless, myelinated and unmyelinated nociceptive nerve fibres can be predicted as well in the capsule. SL and IL are supposed to be the entrance for nerve fibres into the capsule and therefore having the same neurochemical characteristics [12]. The density of nerve fibres within the capsule was not equally distributed. A dense innervation was

found at both poles of the testis with decreasing levels towards the equatorial region. A third “hot spot” was observed at the entrance of the pampiniform plexus with decreasing density in all directions (Fig. 53). “Free nerve endings”, how the terminals of nociceptive nerve fibres were named [406], were observed in samples of SL and capsule (Fig. 49). Within the parenchyma no nerve fibres were detected, which confirmed the previously findings of Lundberg and Zhu [12, 67]. However, absence of nerve fibres in rat parenchyma might be an age dependent event as seen in pigs. Here, the density of testicular nerves changes from rich innervation in 3-5 weeks old piglets to absence of any intrinsic innervation in 2-3 years old adult boar [407]. Similar results were found for bulls & 25 weeks old calves and young & adult donkey [99, 100]. Rats used in this study have not been that old, but they already passed puberty.

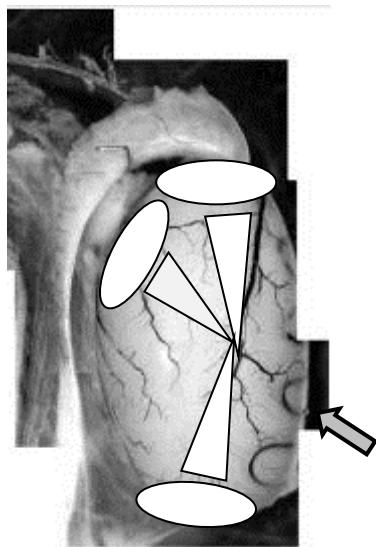


Fig. 53: Distribution of nerve fibres within the testicular capsule.

A high nerve fibre density was observed at the entry sites of the testicular artery and the superior and inferior ligaments (ellipses). Nerve fibre density decreases from these places towards the “equatorial” region of the testis and the opposite site of the rete testis (triangle, arrow).

14.1. Meso-structures show dense innervation of nociceptive nerve fibres

Since no innervation is present in the testis of adult rats the reception and transmission of information to the CNS happens by the surrounding structures such as the TC.

Besides, the meso-structures are dense innervated. In contrast to former studies difference within the morphology of the meso-structures were observed.

Zhu et al. described the bead-like arrangement of testis, epididymis and vas deferens, which are connected by meso-structures [12]. This could not be fully confirmed (Fig. 46B & C). The morphological differences might be caused by the usage of different rat strains. Zhu et al. used Sprague-Dawley rats for their studies, whereas Wistar rats were used in this study.

Myelinated (Nf200+) and unmyelinated (Nf200-) CGRP containing fibres as well as myelinated CGRP negative fibres could be observed within the meso-structures. Other markers describing nociceptive neurons are molecules of the TRP-family, VGLuT1-3 or substance P. In this study, nerve fibres labelled positive for VGLuT1 and TRPV1 were detected in meso-structures. Glutamate is an important transmitter of nociceptive neurons stored in small synaptic vesicles [401-403]. Its uptake in these vesicles occurs actively by vesicular glutamate transporters. Furthermore, TRPV1 is found in sensory neurons with small diameter, which give rise to unmyelinated C-fibres [408, 409]. TRPV1 receptors are sensitive to heat, capsaicin and protons [73, 408, 409]. mRNA was detected for TRPV1 (VR1) and TRPM8 (CMR1: cold and menthol sensitive receptor-1) in rat testis and prostate [89].

14.2. Neurons of DRG L1 projecting to mesodeferens

Data which were presented so far in mammals located DRG neurons in the lumbar (L) and sacral (S) region projecting to testicular structures. The rat scrotum is innervated by neurons of DRGs L5, L6 and S1 [410], whereas nerve fibres innervating the cremaster muscle in pigs originated from neurons in ipsi-lateral DRGs L2-L6 and S1-2 [411]. Innervation of rat vas deferens originates mainly from ipsi-lateral DRGs L1, L2, L6 & S1 and contra-lateral DRG L1 [97]. Similar findings were presented in dogs. Here CGRP positive nerve fibres within the SSN originate from DRGs L1 and L2 [405, 412].

In this study the meso-structures were brought into focus. These structures, which connect testis, epididymis, vas deferens and fascia to each other, show a dense innervation. For the tracing experiments the tissue between epididymis and vas deferens was chosen, which consists of two parts: mesodeferens I and II (Fig. 46C).

In two separate experiments, nerve fibres were identified, which projecting from ipsilateral DRG L1 to the mesodeferens. The Ctx-labelled neurons within DRG L1 and the nerve fibres within the mesodeferens showed the same neurochemical characteristics. Although the examination of the multiple labelled DRG-neurons was done in two groups, cells with the combination CGRP+/Nf200-/IB4- seem to be the main subpopulation (app. 80%). Therefore, neurons should be peptidergic (CGRP) and their releasing nerve fibres should be thinly or unmyelinated (A δ or C-fibres). Other subpopulations of neurons (both app. 17%) were peptidergic and myelinated (CGRP+/Nf200+) or unmyelinated (CGRP+/IB4+). Beside peptidergic nociceptive neurons (CGRP, substance P), there is another population of nociceptive neurons that lack any known peptides. These cells can be identified by binding to the lectin IB4. Although in mice IB4-containing neurons are completely distinct from those expressing CGRP or SP, some peptide-containing neurons are labelled by IB4 in rats [413]. This might explain the findings of cells positive for the peptide CGRP and additionally positive for IB4. Nerve fibre populations for both marker-combinations (CGRP+/IB4- and CGRP+/IB4+) were found in mesodeferens I & II, which supports these observations.

15. Summary

The task of the mammalian testis is the production and controlled release of androgens and the development of germ cells. Impairment of these processes e.g. by trauma, inflammation or idiopathic reasons can result in sub- or infertility. Some of these insults can cause intense pain. Surprisingly, the innervation of the testis is not well characterised in spite of the presence of archetypical neurotransmitter such as acetylcholine (ACh). Of note, ACh has been shown to play an important role in many cellular processes including the male reproductive tract.

Therefore, the aim of this project was to investigate if the presence of ACh is based on neuronal or non-neuronal origin and in case of the latter which cells would have the molecular components to synthesise and respond to ACh.

Adjacent mesenteric tissue (meso) connecting testis, epididymis and vas deferens were isolated from Wistar Furth rats. Nerve fibres were detected using multiple labelling immunohistochemistry (IHC). Nf200-positive-labelled sensory nerve fibres within the meso-structures were identified positive for the known nociceptive markers CGRP, TRPV1, IB4 and VGluT1. Primary afferent innervation of the mesodeferens was examined using retrograde transport of Cholera toxin-B. Positive dorsal root ganglia neurons (DRG) were further analysed using IHC. Our data confirm the DRG lumbar 1 as major origin of nociceptive nerve fibres, which reach the testis via testicular artery or vas deferens.

Due to the absence of nerve fibres within the rat testicular parenchyma (TP), a neuronal origin of ACh can be excluded. Thus, the presence of molecules related to the ACh-system were investigated within the TP and testicular capsule (TC) using qRT-PCR and subsequently for isolated testicular macrophages (TM), peritubular cells (PTC) and Sertoli cells (SC) using standard RT-PCR.

The mRNA expression of ACh-receptors and molecules necessary for ACh synthesis (choline acetyltransferase, ChAT; high-affinity choline transporter-1, ChT1) and release (vesicular ACh transporter, VACHT; organic cation transporter, OCT2) were investigated in rat TP, TC and subsequently in TM, SC and PTC. Except for the absence of $\alpha 6$ and $\beta 4$ in TP all analysed molecules of the ACh-system are present in

TC and TP. The presence of ChAT-, ChT1- and VACHT- mRNAs was supported by IHC. ChAT and $\alpha 7$ mRNAs were determined by *in situ* hybridisation.

Most components of the cholinergic system were present in isolated testicular cells (TM, SC, PTC), but showed cell specific differences mainly in nAChR subunits. TM and SC were stimulated with nicotine and muscarine, which both did not reveal any change of the intracellular calcium concentration ($[Ca^{2+}]_i$). The MR-stimulation of PTC induced a rise in $[Ca^{2+}]_i$, whereas there was no response to nicotine. This metabotropic response in PTC as seen in neurons was blocked by the muscarinic-antagonist atropine. However, nicotine and muscarine given 2 min prior to ATP significantly changed the agonist-induced rise of $[Ca^{2+}]_i$ in SC and TM. These data demonstrate that TM and SC have nAChR and MR with functions distinct from the known neuronal-like ones.

Based on the established role of the cholinergic anti-inflammatory pathway, the influence of the ACh-system was analysed in a chronic inflammatory model i.e. autoimmune orchitis. Samples from TP of 3 groups stimulated with saline buffer, Freund's adjuvant or testicular homogenate were analysed using qRT-PCR. The orchitis group showed a reduced mRNA expression profile for: $\alpha 3$ - $\alpha 5$, $\alpha 7$, $\alpha 10$, $\beta 2$, $\beta 3$, M_4R , M_5R , ChAT, ChT1 and OCT2. No changes in the mRNA expression level were observed for $\alpha 6$, $\beta 1$, $\beta 4$, M_1R - M_3R and VACHT.

Taken together, molecules necessary for synthesis, release, binding and uptake of ACh are present in rat testicular parenchyma and isolated testicular cells (TM, SC and PTC). Peritubular cells show neuronal-like activation via MR, whereas indirect influences on purinergic-receptor-signalling via signalling pathways distinct from the nervous system are demonstrated in TM and SC.

16. Zusammenfassung

Die Hauptaufgaben des Säugerhodens sind Produktion und kontrollierte Abgabe von Hormonen sowie die Bildung von Keimzellen. Fehlfunktionen dieser Prozesse, wie z.B. Trauma, Entzündungen oder idiopathische Effekte, können zur teilweisen oder völligen Unfruchtbarkeit führen. Einige dieser Ursachen sind mit erheblichen Schmerzen verbunden. Überraschenderweise ist die Innervation des Hodens bezüglich der Anwesenheit von archetypischen Neurotransmittern wie Acetylcholin (ACh) nicht besonders gut charakterisiert. Die enorme Bedeutung von ACh für viele zelluläre Prozesse inkl. denen in den männlichen Reproduktionsorganen, wurde bereits gezeigt. Die vorliegende Studie hatte das Ziel festzustellen, inwieweit das vorhandene ACh im Hoden einen neuronalen oder nicht-neuronalen Ursprung hat. Im Falle eines nicht-neuronalen Ursprungs sollten die Zellen identifiziert werden, welche Moleküle des ACh-Systems besitzen und auf ACh in funktioneller Weise reagieren.

Das mesenteriale Gewebe (Meso-Strukturen), welches Hoden, Nebenhoden und Samenleiter miteinander verbindet, wurde aus Wistar Furth Ratten isoliert und die darin enthaltenen Nervenfasern immunohistochemisch nachgewiesen. Neben sensorischen Nervenfasern (Nf200 positiv) innerhalb der Meso-Strukturen konnten nozizeptive Nervenfasern mittels CGRP, TRPV1, IB4 und VGluT1 identifiziert werden. Primäre afferente Fasern wurden vom Mesodeferens zu den Spinalganglien mittels retrograden Transports von Cholera toxin-B verfolgt. Cholera toxin-positive Neuronen wurden immunohistochemisch weiter untersucht. Nozizeptive Nervenfasern, die den Hoden entweder über die testikuläre Arterie oder den Samenleiter innervieren, entspringen dem Spinalganglion lumbar 1.

Da Nervenfasern im Hodenparenchym der Ratte fehlen, kann der neuronale Ursprung von ACh ausgeschlossen werden. Testikuläres Parenchym, die testikuläre Kapsel sowie TM, SC und PTC wurden auf das Vorhandensein von AChR und Moleküle die für ACh-Synthese (ChAT, ChT1) und Freisetzung (VACHT, OCT2) erforderlich sind mittels qRT-PCR untersucht. Mit Ausnahme von $\alpha 6$ und $\beta 4$, die nicht in TP detektierbar waren, konnten alle weiteren molekularen Komponenten des ACh-System in TP und TC nachgewiesen werden. Die vorhandenen ChAT-, ChT1- und VACHT-mRNAs wurden durch immunohistochemische Nachweise bestätigt. ChAT

und $\alpha 7$ -mRNA wurden zusätzlich durch *in situ* Hybridisierung nachgewiesen. Die meisten molekularen Komponenten des ACh-System wurden von den isolierten testikulären Zellen (TM, SC, PTC) exprimiert. Besonders die nAChR-Untereinheiten zeigten zellspezifische Unterschiede.

Die Stimulation mit Nikotin und Muskarin verursachte keine Veränderung der intrazellulären Calcium-Konzentration ($[Ca^{2+}]_i$) in testikuläre Makrophagen oder Sertoli Zellen. In PTC konnte ein klarer Anstieg der $[Ca^{2+}]_i$ durch Muskarin induziert werden, während Nikotin in PTC keine Reaktion auslöste. Diese für Neuronen bekannte metabotrope Reaktion wurde durch den muskarinischen-Antagonisten Atropin blockiert. Trotz fehlender direkter Wirkung von Nikotin und Muskarin auf SC und TM konnte eine indirekte Beeinflussung der durch ATP induzierten intrazellulären Ca^{2+} -Konzentration beobachtet werden. Diese Daten zeigen, dass TM und SC nAChR-Untereinheiten und MR-Subtypen besitzen, die sich in ihren Funktionen von den bekannten typischen neuronalen Funktionen unterscheiden.

Basierend auf etablierten Aufgaben des cholinergen entzündungshemmenden Signalweges, wurde der Einfluss des ACh-Systems in einem *in vivo* - Entzündungsmodell, der experimentellen Autoimmun-Orchitis, analysiert. 3 Gruppen von Versuchstieren wurden mit Kochsalzlösung, Freund's Adjuvant oder hodenspezifischen Antigenen immunisiert. Proben vom TP wurden mittels qRT-PCR analysiert. Die Orchitis-Gruppe wies für folgende Moleküle eine reduzierte mRNA Expression auf: $\alpha 3$ -5, $\alpha 7$, $\alpha 10$, $\beta 2$, $\beta 3$, M_4R , M_5R , ChAT, ChT1 und OCT2. Die mRNA Expression von $\alpha 6$, $\beta 1$, $\beta 4$, M_1R - M_3R und VACHT war unverändert.

Zusammenfassend ist festzustellen, dass Moleküle, die für die Synthese, Freisetzung, Bindung und Aufnahme von ACh notwendig sind, in Zellen des Rattenhodens exprimiert werden und es Unterschiede im mRNA-Expression Profil zwischen gesundem und entzündetem Gewebe gibt. Isolierte Hodenzellen (TM, SC und PTC) zeigen sowohl neuronal-ähnliche Aktivierung (PTC) mittels MR, als auch einen indirekten Einfluss auf purinerge Rezeptoren (TM, SC) über unbekannte Signalwege, die sich von denen im Nervensystem unterscheiden.

17. References

1. de Kretser, D.M. and J.B. Kerr, *The cytology of the testis.*, in *Physiology of Reproduction.*, N.J. Knobil E, eds., Editor. 1994, New York: Raven Press. p. 1177–1300.
2. Fawcett, D.W., *The mammalian spermatozoon.* Dev Biol, 1975. **44**(2): p. 394-436.
3. Hedger, M.P., *Testicular leukocytes: what are they doing?* Rev Reprod, 1997. **2**(1): p. 38-47.
4. Leung, P.C. and G.L. Steele, *Intracellular signaling in the gonads.* Endocr Rev, 1992. **13**(3): p. 476-98.
5. Huhtaniemi, I., *Molecular aspects of the ontogeny of the pituitary-gonadal axis.* Reprod Fertil Dev, 1995. **7**(5): p. 1025-35.
6. Coquelin, A. and C. Desjardins, *Luteinizing hormone and testosterone secretion in young and old male mice.* Am J Physiol, 1982. **243**(3): p. E257-63.
7. Ellis, G.B. and C. Desjardins, *Male rats secrete luteinizing hormone and testosterone episodically.* Endocrinology, 1982. **110**(5): p. 1618-27.
8. Sisk, C.L. and C. Desjardins, *Pulsatile release of luteinizing hormone and testosterone in male ferrets.* Endocrinology, 1986. **119**(3): p. 1195-203.
9. Seitz, J. and A. Meinhardt, *Fortpflanzung*, in *Lehrbuch Vorklinik*, S.R. Hrsg, U. K Editor. 2002, Deutscher Ärzte-Verlag GmbH: Köln. p. 503-532.
10. Arslan, M., et al., *FSH and testosterone, alone or in combination, initiate testicular growth and increase the number of spermatogonia and Sertoli cells in a juvenile non-human primate (Macaca mulatta).* J Endocrinol, 1993. **136**(2): p. 235-43.
11. Schlatt, S., et al., *Appearance of alpha-smooth muscle actin in peritubular cells of monkey testes is induced by androgens, modulated by follicle-stimulating hormone, and maintained after hormonal withdrawal.* J Androl, 1993. **14**(5): p. 340-50.
12. Zhu, B.C., et al., *Monoaminergic and peptidergic contributions of the superior and the inferior spermatic nerves to the innervation of the testis in the rat.* J Androl, 1995. **16**(3): p. 248-58.
13. Huckins, C. and Y. Clermont, *Evolution of gonocytes in the rat testis during late embryonic and early post-natal life.* Arch Anat Histol Embryol, 1968. **51**(1): p. 341-54.
14. Fawcett, D.W., W.B. Neaves, and M.N. Flores, *Comparative observations on intertubular lymphatics and the organization of the interstitial tissue of the mammalian testis.* Biol Reprod, 1973. **9**(5): p. 500-32.
15. Weinbauer, G., et al., *Physiologie der Hodenfunktion*, in *Andrologie-Grundlagen und Klinik der reproduktiven Gesundheit des Mannes*, N. Eds, E. und Behre, H., Editor. 1996, Springer Verlag. p. 29-59.
16. Wang, C.Q.F. and C.Y. Cheng, *A seamless trespass: germ cell migration across the seminiferous epithelium during spermatogenesis.* The Journal of Cell Biology, 2007. **178**(4): p. 549-556.
17. Jegou, B., *Spermatids are regulators of Sertoli cell function.* Ann N Y Acad Sci, 1991. **637**: p. 340-53.

-
18. Schnorr, B., *Embryologie der Haustiere: ein Kurzlehrbuch*. 1996, Stuttgart: Ferdinand Enke Verlag.
 19. McGinley, D.M., et al., *Gap junctions between Sertoli and germ cells of rat seminiferous tubules*. *Tissue Cell*, 1979. **11**(4): p. 741-54.
 20. Russell, L.D., *Further observations on tubulobulbar complexes formed by late spermatids and Sertoli cells in the rat testis*. *Anat Rec*, 1979. **194**(2): p. 213-32.
 21. Grove, B.D., et al., *Immunofluorescence localization of vinculin in ectoplasmic ("junctional") specializations of rat Sertoli cells*. *Am J Anat*, 1990. **188**(1): p. 44-56.
 22. Whitehead, S.S.N.S.A., *Endocrinology, An Integrated Approach*, ed. BIOS. 1999: Scientific Publishers Ltd.
 23. Cheng, C.Y. and D.D. Mruk, *Cell junction dynamics in the testis: Sertoli-germ cell interactions and male contraceptive development*. *Physiol Rev*, 2002. **82**(4): p. 825-74.
 24. Pelletier, R.T., *The tight junctions of the testis, epididymis and vas deferens*. 2nd edn. ed. 2001: Boca Raton: CRC Press
 25. Anthony, C.T. and M.K. Skinner, *Cytochemical and biochemical characterization of testicular peritubular myoid cells*. *Biol Reprod*, 1989. **40**(4): p. 811-23.
 26. Maekawa, M., K. Kamimura, and T. Nagano, *Peritubular myoid cells in the testis: their structure and function*. *Arch Histol Cytol*, 1996. **59**(1): p. 1-13.
 27. Setchell, B.P., *Possible physiological bases for contraceptive techniques in the male*. *Hum Reprod*, 1994. **9**(6): p. 1081-7.
 28. Virtanen, I., et al., *Peritubular myoid cells of human and rat testis are smooth muscle cells that contain desmin-type intermediate filaments*. *Anat Rec*, 1986. **215**(1): p. 10-20.
 29. Rossi, F., et al., *Angiotensin II stimulates contraction and growth of testicular peritubular myoid cells in vitro*. *Endocrinology*, 2002. **143**(8): p. 3096-104.
 30. Chiarenza, C., et al., *Platelet-derived growth factor-BB stimulates hypertrophy of peritubular smooth muscle cells from rat testis in primary cultures*. *Endocrinology*, 2000. **141**(8): p. 2971-81.
 31. Hedger, M.P., *Macrophages and the immune responsiveness of the testis*. *J Reprod Immunol*, 2002. **57**(1-2): p. 19-34.
 32. Mahi-Brown, C.A., T.D. Yule, and K.S. Tung, *Adoptive transfer of murine autoimmune orchitis to naive recipients with immune lymphocytes*. *Cell Immunol*, 1987. **106**(2): p. 408-19.
 33. Wang, J., et al., *Leukocyte populations of the adult rat testis following removal of the Leydig cells by treatment with ethane dimethane sulfonate and subcutaneous testosterone implants*. *Biol Reprod*, 1994. **51**(3): p. 551-61.
 34. Gerdprasert, O., et al., *The response of testicular leukocytes to lipopolysaccharide-induced inflammation: further evidence for heterogeneity of the testicular macrophage population*. *Cell Tissue Res*, 2002. **308**(2): p. 277-85.
 35. Hales, D.B., *Testicular macrophage modulation of Leydig cell steroidogenesis*. *J Reprod Immunol*, 2002. **57**(1-2): p. 3-18.
 36. Janeway, C.A., et al., *Autoimmunity and Transplantation*, in *Immunobiology* 2007, Garland Science: New York.

-
37. Head, J.R., W.B. Neaves, and R.E. Billingham, *Immune privilege in the testis. I. Basic parameters of allograft survival*. Transplantation, 1983. **36**(4): p. 423-31.
 38. Hedger, M.P. and A. Meinhardt, *Cytokines and the immune-testicular axis*. J Reprod Immunol, 2003. **58**(1): p. 1-26.
 39. Mahmoud, A. and F.H. Comhaire, *Immunological causes*, in *Andrology for the Clinician*, C.F. Schill W-B, Hargreave and TB, Editors. 2006, Springer: Berlin. p. 47-52.
 40. Naz, R.K., *Modalities for treatment of antisperm antibody mediated infertility: novel perspectives*. Am J Reprod Immunol, 2004. **51**(5): p. 390-7.
 41. Nieschlag, E. and H.M. Behre, *Andrology*, in *Male Reproductive Health and Dysfunction*. 2000, Springer: Berlin. p. 91-97.
 42. WHO, *Towards more objectivity in diagnosis and management of male infertility*. Int J Androl 1987: p. Suppl. 7.
 43. Bohring, C., et al., *Isolation and identification of sperm membrane antigens recognized by antisperm antibodies, and their possible role in immunological infertility disease*. Mol Hum Reprod, 2001. **7**(2): p. 113-8.
 44. Bohring, C., J. Skrzypek, and W. Krause, *Influence of antisperm antibodies on the acrosome reaction as determined by flow cytometry*. Fertil Steril, 2001. **76**(2): p. 275-80.
 45. Fijak, M. and A. Meinhardt, *The testis in immune privilege*. Immunol Rev, 2006. **213**: p. 66-81.
 46. Tung, K.S. and C. Teuscher, *Mechanisms of autoimmune disease in the testis and ovary*. Hum Reprod Update, 1995. **1**(1): p. 35-50.
 47. Lysiak, J.J., *The role of tumor necrosis factor-alpha and interleukin-1 in the mammalian testis and their involvement in testicular torsion and autoimmune orchitis*. Reprod Biol Endocrinol, 2004. **2**: p. 9.
 48. Meinhardt, A., et al., *Activin maintains the condensed type of mitochondria in germ cells*. Mol. Cell. Endocrinol., 2000. **25**, 11 117.
 49. Watkins, L.R. and S.F. Maier, *Implications of immune-to-brain communication for sickness and pain*. Proc Natl Acad Sci U S A, 1999. **96**(14): p. 7710-3.
 50. Sternberg, E.M., *Neural-immune interactions in health and disease*. J Clin Invest, 1997. **100**(11): p. 2641-7.
 51. Pavlov, V.A., et al., *The cholinergic anti-inflammatory pathway: a missing link in neuroimmunomodulation*. Mol Med, 2003. **9**(5-8): p. 125-34.
 52. Baumann, H. and J. Gauldie, *The acute phase response*. Immunol Today, 1994. **15**(2): p. 74-80.
 53. Tracey, K.J., et al., *Shock and tissue injury induced by recombinant human cachectin*. Science, 1986. **234**(4775): p. 470-4.
 54. Wang, H., et al., *HMGB1 as a late mediator of lethal systemic inflammation*. Am J Respir Crit Care Med, 2001. **164**(10 Pt 1): p. 1768-73.
 55. Borovikova, L.V., et al., *Vagus nerve stimulation attenuates the systemic inflammatory response to endotoxin*. Nature, 2000. **405**(6785): p. 458-62.
 56. Wang, H., et al., *Nicotinic acetylcholine receptor alpha7 subunit is an essential regulator of inflammation*. Nature, 2003. **421**(6921): p. 384-8.
 57. Wang, H., et al., *Cholinergic agonists inhibit HMGB1 release and improve survival in experimental sepsis*. Nat Med, 2004. **10**(11): p. 1216-21.
 58. Kaneko, T., et al., *Proinflammatory effects of exogenously administered IL-10 in experimental autoimmune orchitis*. Cytokine, 2003. **22**(1-2): p. 50-3.

-
59. Watanabe, M., et al., *Adeno-associated virus-mediated human IL-10 gene transfer suppresses the development of experimental autoimmune orchitis*. Gene Ther, 2005. **12**(14): p. 1126-32.
 60. Doncel, G.F., J.A. Di Paola, and L. Lustig, *Sequential study of the histopathology and cellular and humoral immune response during the development of an autoimmune orchitis in Wistar rats*. Am J Reprod Immunol, 1989. **20**(2): p. 44-51.
 61. Lustig, L., et al., *Phenotypic characterization of lymphocytic cell infiltrates into the testes of rats undergoing autoimmune orchitis*. Int J Androl, 1993. **16**(4): p. 279-84.
 62. Guazzone, V.A., et al., *Monocyte chemoattractant protein-1 (MCP-1/CCL2) in experimental autoimmune orchitis*. J Reprod Immunol, 2003. **60**(2): p. 143-57.
 63. Fijak, M., et al., *Identification of immunodominant autoantigens in rat autoimmune orchitis*. J Pathol, 2005. **207**(2): p. 127-38.
 64. Zhou, Z.Z., et al., *Actively-induced experimental allergic orchitis (EAO) in Lewis/NCR rats: sequential histo- and immunopathologic analysis*. Autoimmunity, 1989. **3**(2): p. 125-34.
 65. Suescun, M.O., R.S. Calandra, and L. Lustig, *Alterations of testicular function after induced autoimmune orchitis in rats*. J Androl, 1994. **15**(5): p. 442-8.
 66. Suescun, M.O., et al., *Correlation between inhibin secretion and damage of seminiferous tubules in a model of experimental autoimmune orchitis*. J Endocrinol, 2001. **170**(1): p. 113-20.
 67. Lundberg, L.M., et al., *Protein gene product 9.5 (PGP 9.5). A new neuronal marker visualizing the whole uterine innervation and pregnancy-induced and developmental changes in the guinea pig*. Histochemistry, 1988. **90**(1): p. 9-17.
 68. Wilson, P.O., et al., *The immunolocalization of protein gene product 9.5 using rabbit polyclonal and mouse monoclonal antibodies*. Br J Exp Pathol, 1988. **69**(1): p. 91-104.
 69. Dalsgaard, C.J., M. Rydh, and A. Haegerstrand, *Cutaneous innervation in man visualized with protein gene product 9.5 (PGP 9.5) antibodies*. Histochemistry, 1989. **92**(5): p. 385-90.
 70. Wang, L., et al., *Protein gene product 9.5-immunoreactive nerve fibres and cells in human skin*. Cell Tissue Res, 1990. **261**(1): p. 25-33.
 71. Luo, J., et al., *Protein gene product 9.5 is a spermatogonia-specific marker in the pig testis: application to enrichment and culture of porcine spermatogonia*. Mol Reprod Dev, 2006. **73**(12): p. 1531-40.
 72. Hoffman, P.N. and R.J. Lasek, *The slow component of axonal transport. Identification of major structural polypeptides of the axon and their generality among mammalian neurons*. J Cell Biol, 1975. **66**(2): p. 351-66.
 73. Szallasi, A. and P.M. Blumberg, *Vanilloid (Capsaicin) receptors and mechanisms*. Pharmacol Rev, 1999. **51**(2): p. 159-212.
 74. Nagy, J.I. and E. Senba, *Neural relations of cremaster motoneurons, spinal cord systems and the genitofemoral nerve in the rat*. Brain Res Bull, 1985. **15**(6): p. 609-27.
 75. Wang, B.R., E. Senba, and M. Tohyama, *Ultrastructural investigation of substance P-, leucine-enkephalin- and 5-hydroxytryptamine-like immunoreactive terminals in the area of cremaster motoneurons of the male rat*. Neuroscience, 1989. **28**(3): p. 711-23.

-
76. Kar, S., S.J. Gibson, and J.M. Polak, *Origins and projections of peptide-immunoreactive nerves in the male rat genitofemoral nerve*. Brain Res, 1990. **512**(2): p. 229-37.
 77. Zempoalteca, R., et al., *An anatomical and electrophysiological study of the genitofemoral nerve and some of its targets in the male rat*. J Anat, 2002. **201**(6): p. 493-505.
 78. Hodson, N.P., *he nerves of the testis, epididymis and scrotum.*, in *The Testis.*, G.W. Johnson AD, Vandermark NL,, Editor. 1970, Academic Press: New York.
 79. Greene, E.C., *Anatomy of the Rat*. 1955, New York: Hafner Publishing Co.
 80. Clegg, M.T. and L.L. Doyle, *Role in reproductive physiology of afferent impulses from the genitalia and other regions.* , in *Neuroendocrinology* L. Martin and W.F. Ganong, Editors. 1966, Academic Press: New York. p. 1-17.
 81. Hebel, R. and M.W. Stromberg, *Anatomy and Embryology of the Laboratory Rat*. 1986, Germany: Biomedical Verlag.
 82. Durwood, A., *The peripheral nervous system*, in *Cunningham's Textbook of Anatomy*, J.E. Romanes, Editor. 1964, Oxford University Press: London. p. 600-685.
 83. Miller, M.E., G.L. Christensen, and H.E. Evans, *Anatomy of the Dog*. 1964, Philadelphia: Saunders.
 84. Kojima, M. and H. Ohe, *Experimental study on the regulation of testicular function by the cremaster reflex in rats*. Tohoku J Exp Med, 1986. **150**(2): p. 175-80.
 85. Talbot, H.S., *The sexual function in paraplegia*. J Urol, 1955. **73**(1): p. 91-100.
 86. Brindley, G.S., *The fertility of men with spinal injuries*. Paraplegia, 1984. **22**(6): p. 337-48.
 87. Brindley, G.S., *Deep scrotal temperature and the effect on it of clothing, air temperature, activity, posture and paraplegia*. Br J Urol, 1982. **54**(1): p. 49-55.
 88. Mallidis, C., et al., *Necrostermia and chronic spinal cord injury*. Fertil Steril, 2000. **74**(2): p. 221-7.
 89. Stein, R.J., et al., *Cool (TRPM8) and hot (TRPV1) receptors in the bladder and male genital tract*. J Urol, 2004. **172**(3): p. 1175-8.
 90. Bell, C. and J.R. McLean, *The autonomic innervation of the rat testicular capsule*. J Reprod Fertil, 1973. **32**(2): p. 253-8.
 91. Properzi, G., G. Cordeschi, and S. Francavilla, *Postnatal development and distribution of peptide-containing nerves in the genital system of the male rat. An immunohistochemical study*. Histochemistry, 1992. **97**(1): p. 61-8.
 92. Prince, F.P., *Ultrastructural evidence of indirect and direct autonomic innervation of human Leydig cells: comparison of neonatal, childhood and pubertal ages*. Cell Tissue Res, 1992. **269**(3): p. 383-90.
 93. Kruger, L., et al., *Observations on electrophysiologically characterized receptive fields of thin testicular afferent axons: a preliminary note on the analysis of fine structural specializations of polymodal receptors*. Somatosens Res, 1988. **5**(4): p. 373-80.
 94. Kruger, L., *The functional morphology of thin sensory axons: some principles and problems*. Prog Brain Res, 1996. **113**: p. 255-72.
 95. Alm, P., *On the autonomic innervation of the human vas deferens*. Brain Res Bull, 1982. **9**(1-6): p. 673-7.

-
96. Ellis, J.L. and G. Burnstock, *Modulation of neurotransmission in the guinea-pig vas deferens by capsaicin: involvement of calcitonin gene-related peptide and substance P*. Br J Pharmacol, 1989. **98**(2): p. 707-13.
 97. Kolbeck, S.C. and W.D. Steers, *Origin of neurons supplying the vas deferens of the rat*. J Urol, 1993. **149**(4): p. 918-21.
 98. Kujat, R., C. Rose, and K.H. Wrobel, *The innervation of the bovine ductus deferens: comparison of a modified acetylcholinesterase-reaction with immunoreactivities of cholinacetyltransferase and panneuronal markers*. Histochemistry, 1993. **99**(3): p. 231-9.
 99. Wrobel, K.H. and N. Abu-Ghali, *Autonomic innervation of the bovine testis*. Acta Anat (Basel), 1997. **160**(1): p. 1-14.
 100. Wrobel, K.H. and M.N. Moustafa, *On the innervation of the donkey testis*. Ann Anat, 2000. **182**(1): p. 13-22.
 101. Saleh, A.M., et al., *Immunohistochemical investigations of the autonomous nerve distribution in the testis of the camel (Camelus dromedarius)*. Ann Anat, 2002. **184**(3): p. 209-20.
 102. Loewi, O., *Über humorale Übertragbarkeit der Herznervenzirkulation*. Pflügers Arch, 1921. **189**: p. 239-242.
 103. Wessler, I., C.J. Kirkpatrick, and K. Racke, *The cholinergic 'pitfall': acetylcholine, a universal cell molecule in biological systems, including humans*. Clin Exp Pharmacol Physiol, 1999. **26**(3): p. 198-205.
 104. Horiuchi, Y., et al., *Evolutional study on acetylcholine expression*. Life Sci, 2003. **72**(15): p. 1745-56.
 105. Morris, D., *The choline acetyltransferase of human placenta*. Biochem J, 1966. **98**(3): p. 754-62.
 106. Kurzen, H., et al., *The non-neuronal cholinergic system of human skin*. Horm Metab Res, 2007. **39**(2): p. 125-35.
 107. Fujii, T. and K. Kawashima, *An independent non-neuronal cholinergic system in lymphocytes*. Jpn J Pharmacol, 2001. **85**(1): p. 11-5.
 108. Grando, S.A., *Biological functions of keratinocyte cholinergic receptors*. J Invest Dermatol Symp Proc, 1997. **2**(1): p. 41-8.
 109. Lee, S.C., et al., *Increased voltage-gated potassium conductance during interleukin 2-stimulated proliferation of a mouse helper T lymphocyte clone*. J Cell Biol, 1986. **102**(4): p. 1200-8.
 110. Decoursey, T.E., et al., *Mitogen induction of ion channels in murine T lymphocytes*. J Gen Physiol, 1987. **89**(3): p. 405-20.
 111. Strassheim, D., et al., *M3 muscarinic acetylcholine receptors regulate cytoplasmic myosin by a process involving RhoA and requiring conventional protein kinase C isoforms*. J Biol Chem, 1999. **274**(26): p. 18675-85.
 112. Tournier, J.M., et al., *alpha3alpha5beta2-Nicotinic acetylcholine receptor contributes to the wound repair of the respiratory epithelium by modulating intracellular calcium in migrating cells*. Am J Pathol, 2006. **168**(1): p. 55-68.
 113. Trombino, S., et al., *Alpha7-nicotinic acetylcholine receptors affect growth regulation of human mesothelioma cells: role of mitogen-activated protein kinase pathway*. Cancer Res, 2004. **64**(1): p. 135-45.
 114. Wong, H.P., et al., *Nicotine promotes cell proliferation via alpha7-nicotinic acetylcholine receptor and catecholamine-synthesizing enzymes-mediated pathway in human colon adenocarcinoma HT-29 cells*. Toxicol Appl Pharmacol, 2007. **221**(3): p. 261-7.

-
115. Lam, D.C., et al., *Expression of nicotinic acetylcholine receptor subunit genes in non-small-cell lung cancer reveals differences between smokers and nonsmokers*. Cancer Res, 2007. **67**(10): p. 4638-47.
 116. Song, P., et al., *Activated cholinergic signaling provides a target in squamous cell lung carcinoma*. Cancer Res, 2008. **68**(12): p. 4693-700.
 117. Fucile, S., M. Napolitano, and E. Mattei, *Cholinergic stimulation of human microcytoma cell line H69*. Biochem Biophys Res Commun, 1997. **230**(3): p. 501-4.
 118. Heeschen, C., et al., *A novel angiogenic pathway mediated by non-neuronal nicotinic acetylcholine receptors*. J Clin Invest, 2002. **110**(4): p. 527-36.
 119. Dasgupta, P., et al., *Nicotine inhibits apoptosis induced by chemotherapeutic drugs by up-regulating XIAP and survivin*. Proc Natl Acad Sci U S A, 2006. **103**(16): p. 6332-7.
 120. Jin, Z., et al., *Nicotine induces multi-site phosphorylation of Bad in association with suppression of apoptosis*. J Biol Chem, 2004. **279**(22): p. 23837-44.
 121. Takahashi, H.K., et al., *alpha7 Nicotinic acetylcholine receptor stimulation inhibits lipopolysaccharide-induced interleukin-18 and -12 production in monocytes*. J Pharmacol Sci, 2006. **102**(1): p. 143-6.
 122. van der Zanden, E.P., et al., *Vagus nerve activity augments intestinal macrophage phagocytosis via nicotinic acetylcholine receptor alpha4beta2*. Gastroenterology, 2009. **137**(3): p. 1029-39, 1039 e1-4.
 123. Ghia, J.E., et al., *The vagus nerve: a tonic inhibitory influence associated with inflammatory bowel disease in a murine model*. Gastroenterology, 2006. **131**(4): p. 1122-30.
 124. van Westerloo, D.J., et al., *The cholinergic anti-inflammatory pathway regulates the host response during septic peritonitis*. J Infect Dis, 2005. **191**(12): p. 2138-48.
 125. Giebelen, I.A., et al., *Stimulation of alpha 7 cholinergic receptors inhibits lipopolysaccharide-induced neutrophil recruitment by a tumor necrosis factor alpha-independent mechanism*. Shock, 2007. **27**(4): p. 443-7.
 126. Lips, K.S., et al., *Down-regulation of the non-neuronal acetylcholine synthesis and release machinery in acute allergic airway inflammation of rat and mouse*. Life Sci, 2007. **80**(24-25): p. 2263-9.
 127. Hanna-Mitchell, A.T., et al., *Non-neuronal acetylcholine and urinary bladder urothelium*. Life Sci, 2007. **80**(24-25): p. 2298-302.
 128. Grando, S.A., et al., *Human keratinocytes synthesize, secrete, and degrade acetylcholine*. J Invest Dermatol, 1993. **101**(1): p. 32-6.
 129. Klapproth, H., et al., *Non-neuronal acetylcholine, a signalling molecule synthesized by surface cells of rat and man*. Naunyn Schmiedebergs Arch Pharmacol, 1997. **355**(4): p. 515-23.
 130. Fujii, T., et al., *Induction of choline acetyltransferase mRNA in human mononuclear leukocytes stimulated by phytohemagglutinin, a T-cell activator*. J Neuroimmunol, 1998. **82**(1): p. 101-7.
 131. Kawashima, K. and T. Fujii, *Expression of non-neuronal acetylcholine in lymphocytes and its contribution to the regulation of immune function*. Front Biosci, 2004. **9**: p. 2063-85.
 132. Ogawa, H., et al., *Expression of multiple mRNA species for choline acetyltransferase in human T-lymphocytes*. Life Sci, 2003. **72**(18-19): p. 2127-30.

-
133. Olubadewo, J.O. and B.V. Rama Sastry, *Human placental cholinergic system: stimulation-secretion coupling for release of acetylcholine from isolated placental villus*. J Pharmacol Exp Ther, 1978. **204**(2): p. 433-45.
 134. Paraoanu, L.E., et al., *Expression and possible functions of the cholinergic system in a murine embryonic stem cell line*. Life Sci, 2007. **80**(24-25): p. 2375-9.
 135. Haberberger, R.V., M. Bodenbenner, and W. Kummer, *Expression of the cholinergic gene locus in pulmonary arterial endothelial cells*. Histochem Cell Biol, 2000. **113**(5): p. 379-87.
 136. Kirkpatrick, C.J., et al., *The non-neuronal cholinergic system in the endothelium: evidence and possible pathobiological significance*. Jpn J Pharmacol, 2001. **85**(1): p. 24-8.
 137. Pfeil, U., et al., *Expression of the cholinergic gene locus in the rat placenta*. Histochem Cell Biol, 2004. **122**(2): p. 121-30.
 138. Lips, K.S., *Molekulare Anatomie des non-neuronalen cholinergen Systems in Institut für Anatomie und Zellbiologie*. 2005, Justus-Liebig Universität Giessen.
 139. Kummer, W., K.S. Lips, and U. Pfeil, *The epithelial cholinergic system of the airways*. Histochem Cell Biol, 2008. **130**(2): p. 219-34.
 140. Lips, K.S., et al., *Polyspecific cation transporters mediate luminal release of acetylcholine from bronchial epithelium*. Am J Respir Cell Mol Biol, 2005. **33**(1): p. 79-88.
 141. Wessler, I., et al., *Release of non-neuronal acetylcholine from the isolated human placenta is mediated by organic cation transporters*. Br J Pharmacol, 2001. **134**(5): p. 951-6.
 142. Kekuda, R., et al., *Cloning and functional characterization of a potential-sensitive, polyspecific organic cation transporter (OCT3) most abundantly expressed in placenta*. J Biol Chem, 1998. **273**(26): p. 15971-9.
 143. Verhaagh, S., et al., *Cloning of the mouse and human solute carrier 22a3 (Slc22a3/SLC22A3) identifies a conserved cluster of three organic cation transporters on mouse chromosome 17 and human 6q26-q27*. Genomics, 1999. **55**(2): p. 209-18.
 144. Okuda, M., et al., *cDNA cloning and functional expression of a novel rat kidney organic cation transporter, OCT2*. Biochem Biophys Res Commun, 1996. **224**(2): p. 500-7.
 145. Santos, S.C., et al., *Expression and subcellular localization of a novel nuclear acetylcholinesterase protein*. J Biol Chem, 2007. **282**(35): p. 25597-603.
 146. Haberberger, R.V., et al., *Expression of the high-affinity choline transporter, CHT1, in the neuronal and non-neuronal cholinergic system of human and rat skin*. J Invest Dermatol, 2002. **119**(4): p. 943-8.
 147. Michel, V., et al., *Choline transport for phospholipid synthesis*. Exp Biol Med (Maywood), 2006. **231**(5): p. 490-504.
 148. Starke, K., *Grundlagen der Pharmakologie des Nervensystems*, in *Allgemeine und spezielle Pharmakologie und Toxikologie*. 1996, Spektrum: Heidelberg. p. 112-115.
 149. Kandel, E.R., J.H. Schwartz, and T. Jessell, *Principles of Neural Science* 4th ed. 2000: McGraw-Hill Publ.Comp.
 150. Numa, S., et al., *Molecular structure of the nicotinic acetylcholine receptor*. Cold Spring Harb Symp Quant Biol, 1983. **48 Pt 1**: p. 57-69.

-
151. Karlin, A., *Emerging structure of the nicotinic acetylcholine receptors*. Nat Rev Neurosci, 2002. **3**(2): p. 102-14.
 152. Mishina, M., et al., *Expression of functional acetylcholine receptor from cloned cDNAs*. Nature, 1984. **307**(5952): p. 604-8.
 153. McGehee, D.S. and L.W. Role, *Physiological diversity of nicotinic acetylcholine receptors expressed by vertebrate neurons*. Annu Rev Physiol, 1995. **57**: p. 521-46.
 154. Lindstrom, J., *Neuronal nicotinic acetylcholine receptors*. Ion Channels, 1996. **4**: p. 377-450.
 155. Hogg, R.C., M. Raggenbass, and D. Bertrand, *Nicotinic acetylcholine receptors: from structure to brain function*. Rev Physiol Biochem Pharmacol, 2003. **147**: p. 1-46.
 156. Lindstrom, J., *The structures of neuronal nicotinic receptors*. , in *Neuronal Nicotinic Receptors. Handbook of Experimental Pharmacology series*, F. Clementi, D. Fornasari, and C. Gotti, Editors. 2000, Springer Berlin Heidelberg New York. p. 101-162.
 157. Lindstrom, J., et al., *Neuronal nicotinic receptor subtypes*. Ann N Y Acad Sci, 1995. **757**: p. 100-16.
 158. Elgoyhen, A.B., et al., *Alpha 9: an acetylcholine receptor with novel pharmacological properties expressed in rat cochlear hair cells*. Cell, 1994. **79**(4): p. 705-15.
 159. Sgard, F., et al., *A novel human nicotinic receptor subunit, alpha10, that confers functionality to the alpha9-subunit*. Mol Pharmacol, 2002. **61**(1): p. 150-9.
 160. Lee, C.Y., C.C. Chang, and Y.M. Chen, *Reversibility of neuromuscular blockade by neurotoxins from elapid and sea snake venoms*. Taiwan Yi Xue Hui Za Zhi, 1972. **71**(6): p. 344-9.
 161. Dani, J.A., *Overview of nicotinic receptors and their roles in the central nervous system*. Biol Psychiatry, 2001. **49**(3): p. 166-74.
 162. Gotti, C. and F. Clementi, *Neuronal nicotinic receptors: from structure to pathology*. Prog Neurobiol, 2004. **74**(6): p. 363-96.
 163. Sargent, P.B., *The diversity of neuronal nicotinic acetylcholine receptors*. Annu Rev Neurosci, 1993. **16**: p. 403-43.
 164. Couturier, S., et al., *A neuronal nicotinic acetylcholine receptor subunit (alpha 7) is developmentally regulated and forms a homo-oligomeric channel blocked by alpha-BTX*. Neuron, 1990. **5**(6): p. 847-56.
 165. Seguela, P., et al., *Molecular cloning, functional properties, and distribution of rat brain alpha 7: a nicotinic cation channel highly permeable to calcium*. J Neurosci, 1993. **13**(2): p. 596-604.
 166. Khiroug, S.S., et al., *Rat nicotinic ACh receptor alpha7 and beta2 subunits co-assemble to form functional heteromeric nicotinic receptor channels*. J Physiol, 2002. **540**(Pt 2): p. 425-34.
 167. Palma, E., et al., *Nicotinic acetylcholine receptors assembled from the alpha7 and beta3 subunits*. J Biol Chem, 1999. **274**(26): p. 18335-40.
 168. Yu, C.R. and L.W. Role, *Functional contribution of the alpha5 subunit to neuronal nicotinic channels expressed by chick sympathetic ganglion neurones*. J Physiol, 1998. **509** (Pt 3): p. 667-81.
 169. Crabtree, G., J. Ramirez-Latorre, and L.W. Role, *Assembly and Ca²⁺ regulation of neuronal nicotinic receptors including the alpha7 and alpha5 subunits*. Soc Neurosci Abstr 23:391, 1997.

-
170. Elgoyhen, A.B., et al., *alpha10: a determinant of nicotinic cholinergic receptor function in mammalian vestibular and cochlear mechanosensory hair cells*. Proc Natl Acad Sci U S A, 2001. **98**(6): p. 3501-6.
171. Gotti, C., M. Zoli, and F. Clementi, *Brain nicotinic acetylcholine receptors: native subtypes and their relevance*. Trends Pharmacol Sci, 2006. **27**(9): p. 482-91.
172. Papke, R.L., *The kinetic properties of neuronal nicotinic receptors: genetic basis of functional diversity*. Prog Neurobiol, 1993. **41**(4): p. 509-31.
173. Zwart, R. and H.P. Vijverberg, *Potentiation and inhibition of neuronal nicotinic receptors by atropine: competitive and noncompetitive effects*. Mol Pharmacol, 1997. **52**(5): p. 886-95.
174. Wang, F., et al., *Assembly of human neuronal nicotinic receptor alpha5 subunits with alpha3, beta2, and beta4 subunits*. J Biol Chem, 1996. **271**(30): p. 17656-65.
175. Gotti, C., et al., *Expression of nigrostriatal alpha 6-containing nicotinic acetylcholine receptors is selectively reduced, but not eliminated, by beta 3 subunit gene deletion*. Mol Pharmacol, 2005. **67**(6): p. 2007-15.
176. Ramirez-Latorre, J., et al., *Functional contributions of alpha5 subunit to neuronal acetylcholine receptor channels*. Nature, 1996. **380**(6572): p. 347-51.
177. Fenster, C.P., et al., *Upregulation of surface alpha4beta2 nicotinic receptors is initiated by receptor desensitization after chronic exposure to nicotine*. J Neurosci, 1999. **19**(12): p. 4804-14.
178. Nelson, M.E., et al., *Alternate stoichiometries of alpha4beta2 nicotinic acetylcholine receptors*. Mol Pharmacol, 2003. **63**(2): p. 332-41.
179. Gerzanich, V., et al., *"Orphan" alpha6 nicotinic AChR subunit can form a functional heteromeric acetylcholine receptor*. Mol Pharmacol, 1997. **51**(2): p. 320-7.
180. Fucile, S., et al., *The neuronal alpha6 subunit forms functional heteromeric acetylcholine receptors in human transfected cells*. Eur J Neurosci, 1998. **10**(1): p. 172-8.
181. Quik, M., et al., *Subunit composition of nicotinic receptors in monkey striatum: effect of treatments with 1-methyl-4-phenyl-1,2,3,6-tetrahydropyridine or L-DOPA*. Mol Pharmacol, 2005. **67**(1): p. 32-41.
182. Balestra, B., et al., *Chick optic lobe contains a developmentally regulated alpha2alpha5beta2 nicotinic receptor subtype*. Mol Pharmacol, 2000. **58**(2): p. 300-11.
183. Gotti, C., et al., *Heterogeneity and selective targeting of neuronal nicotinic acetylcholine receptor (nAChR) subtypes expressed on retinal afferents of the superior colliculus and lateral geniculate nucleus: identification of a new native nAChR subtype alpha3beta2(alpha5 or beta3) enriched in retinocollicular afferents*. Mol Pharmacol, 2005. **68**(4): p. 1162-71.
184. Turner, J.R. and K.J. Kellar, *Nicotinic cholinergic receptors in the rat cerebellum: multiple heteromeric subtypes*. J Neurosci, 2005. **25**(40): p. 9258-65.
185. Kuryatov, A., et al., *Human alpha6 AChR subtypes: subunit composition, assembly, and pharmacological responses*. Neuropharmacology, 2000. **39**(13): p. 2570-90.

-
186. Forsayeth, J.R. and E. Kobrin, *Formation of oligomers containing the beta3 and beta4 subunits of the rat nicotinic receptor*. J Neurosci, 1997. **17**(5): p. 1531-8.
187. Lukas, R.J., et al., *International Union of Pharmacology. XX. Current status of the nomenclature for nicotinic acetylcholine receptors and their subunits*. Pharmacol Rev, 1999. **51**(2): p. 397-401.
188. Moretti, M., et al., *Nicotinic acetylcholine receptor subtypes expression during rat retina development and their regulation by visual experience*. Mol Pharmacol, 2004. **66**(1): p. 85-96.
189. Zoli, M., et al., *Identification of the nicotinic receptor subtypes expressed on dopaminergic terminals in the rat striatum*. J Neurosci, 2002. **22**(20): p. 8785-9.
190. Vailati, S., et al., *Functional alpha6-containing nicotinic receptors are present in chick retina*. Mol Pharmacol, 1999. **56**(1): p. 11-9.
191. Conroy, W.G. and D.K. Berg, *Neurons can maintain multiple classes of nicotinic acetylcholine receptors distinguished by different subunit compositions*. J Biol Chem, 1995. **270**(9): p. 4424-31.
192. Klink, R., et al., *Molecular and physiological diversity of nicotinic acetylcholine receptors in the midbrain dopaminergic nuclei*. J Neurosci, 2001. **21**(5): p. 1452-63.
193. Clarke, P.B., *Nicotinic receptors in mammalian brain: localization and relation to cholinergic innervation*. Prog Brain Res, 1993. **98**: p. 77-83.
194. Wonnacott, S., *Presynaptic nicotinic ACh receptors*. Trends Neurosci, 1997. **20**(2): p. 92-8.
195. Wonnacott, S., et al., *Presynaptic nicotinic autoreceptors and heteroreceptors in the CNS.*, in *Effects of Nicotine on Biological Systems II. Advances in Pharmacological Sciences*, Q.M. Clarke PB, Adlkofer F, Thureau K, Editor. 1995, Birkhaeuser Verlag Basel. p. 87-94.
196. Buisson, B., et al., *The unusual nature of epibatidine responses at the alpha4beta2 nicotinic acetylcholine receptor*. Neuropharmacology, 2000. **39**(13): p. 2561-9.
197. Kurzen, H., et al., *Phenotypical and molecular profiling of the extraneuronal cholinergic system of the skin*. J Invest Dermatol, 2004. **123**(5): p. 937-49.
198. Adams, D.J. and T.J. Nutter, *Calcium permeability and modulation of nicotinic acetylcholine receptor-channels in rat parasympathetic neurons*. J Physiol Paris, 1992. **86**(1-3): p. 67-76.
199. Castro, N.G. and E.X. Albuquerque, *alpha-Bungarotoxin-sensitive hippocampal nicotinic receptor channel has a high calcium permeability*. Biophys J, 1995. **68**(2): p. 516-24.
200. Dajas-Bailador, F.A., A.J. Mogg, and S. Wonnacott, *Intracellular Ca²⁺ signals evoked by stimulation of nicotinic acetylcholine receptors in SH-SY5Y cells: contribution of voltage-operated Ca²⁺ channels and Ca²⁺ stores*. J Neurochem, 2002. **81**(3): p. 606-14.
201. Gueorguiev, V.D., et al., *Differing temporal roles of Ca²⁺ and cAMP in nicotine-elicited elevation of tyrosine hydroxylase mRNA*. Am J Physiol, 1999. **276**(1 Pt 1): p. C54-65.
202. Rathouz, M.M. and D.K. Berg, *Synaptic-type acetylcholine receptors raise intracellular calcium levels in neurons by two mechanisms*. J Neurosci, 1994. **14**(11 Pt 2): p. 6935-45.

-
203. Beker, F., et al., *Muscarinic and nicotinic ACh receptor activation differentially mobilize Ca²⁺ in rat intracardiac ganglion neurons*. J Neurophysiol, 2003. **90**(3): p. 1956-64.
204. Brain, K.L., et al., *Nicotine induces calcium spikes in single nerve terminal varicosities: a role for intracellular calcium stores*. Neuroscience, 2001. **106**(2): p. 395-403.
205. Shoop, R.D., et al., *Synaptically driven calcium transients via nicotinic receptors on somatic spines*. J Neurosci, 2001. **21**(3): p. 771-81.
206. Caulfield, M.P. and N.J. Birdsall, *International Union of Pharmacology. XVII. Classification of muscarinic acetylcholine receptors*. Pharmacol Rev, 1998. **50**(2): p. 279-90.
207. Kubo, T., et al., *Cloning, sequencing and expression of complementary DNA encoding the muscarinic acetylcholine receptor*. Nature, 1986. **323**(6087): p. 411-6.
208. Hulme, E.C., N.J. Birdsall, and N.J. Buckley, *Muscarinic receptor subtypes*. Annu Rev Pharmacol Toxicol, 1990. **30**: p. 633-73.
209. Hamm, H.E., *The many faces of G protein signaling*. J Biol Chem, 1998. **273**(2): p. 669-72.
210. Strader, C.D., et al., *Structure and function of G protein-coupled receptors*. Annu Rev Biochem, 1994. **63**: p. 101-32.
211. Harvey, R.D. and A.E. Belevych, *Muscarinic regulation of cardiac ion channels*. Br J Pharmacol, 2003. **139**(6): p. 1074-84.
212. Eglen, R.M., S.S. Hegde, and N. Watson, *Muscarinic receptor subtypes and smooth muscle function*. Pharmacol Rev, 1996. **48**(4): p. 531-65.
213. Felder, C.C., et al., *Therapeutic opportunities for muscarinic receptors in the central nervous system*. J Med Chem, 2000. **43**(23): p. 4333-53.
214. Wess, J., *Muscarinic acetylcholine receptor knockout mice: novel phenotypes and clinical implications*. Annu Rev Pharmacol Toxicol, 2004. **44**: p. 423-50.
215. Wess, J., et al., *Muscarinic receptor subtypes mediating central and peripheral antinociception studied with muscarinic receptor knockout mice: a review*. Life Sci, 2003. **72**(18-19): p. 2047-54.
216. Eglen, R.M. and S.R. Nahorski, *The muscarinic M(5) receptor: a silent or emerging subtype?* Br J Pharmacol, 2000. **130**(1): p. 13-21.
217. Oki, T., et al., *Quantitative analysis of binding parameters of [3H]N-methylscopolamine in central nervous system of muscarinic acetylcholine receptor knockout mice*. Brain Res Mol Brain Res, 2005. **133**(1): p. 6-11.
218. Kawashima, K. and T. Fujii, *The lymphocytic cholinergic system and its biological function*. Life Sci, 2003. **72**(18-19): p. 2101-9.
219. Fryer, A.D. and E.E. el-Fakahany, *Identification of three muscarinic receptor subtypes in rat lung using binding studies with selective antagonists*. Life Sci, 1990. **47**(7): p. 611-8.
220. Barnes, P.J., *Muscarinic receptor subtypes in airways*. Life Sci, 1993. **52**(5-6): p. 521-7.
221. Lammerding-Koppel, M., A. Greiner-Schroder, and U. Drews, *Muscarinic receptors in the prenatal mouse embryo. Comparison of M35-immunohistochemistry with [3H]quinuclidinyl benzylate autoradiography*. Histochem Cell Biol, 1995. **103**(4): p. 301-10.
222. Neves, S.R., P.T. Ram, and R. Iyengar, *G protein pathways*. Science, 2002. **296**(5573): p. 1636-9.

-
223. Alberts, B., et al., *Molecular Biology of the Cell*. 4th ed. 2002: Garland Science.
224. Eglen, R.M., *Muscarinic receptor subtypes in neuronal and non-neuronal cholinergic function*. Auton Autacoid Pharmacol, 2006. **26**(3): p. 219-33.
225. Caulfield, M.P., *Muscarinic receptors--characterization, coupling and function*. Pharmacol Ther, 1993. **58**(3): p. 319-79.
226. Felder, C.C., *Muscarinic acetylcholine receptors: signal transduction through multiple effectors*. Faseb J, 1995. **9**(8): p. 619-25.
227. Baccetti, B., et al., *Localisation of two classes of acetylcholine receptor-like molecules in sperms of different animal species*. Zygote, 1995. **3**(3): p. 207-17.
228. Bray, C., J.H. Son, and S. Meizel, *A nicotinic acetylcholine receptor is involved in the arosome reaction of human sperm initiated by recombinant human ZP3*. Biol Reprod, 2002. **67**(3): p. 782-8.
229. Son, J.H. and S. Meizel, *Evidence suggesting that the mouse sperm acrosome reaction initiated by the zona pellucida involves an alpha7 nicotinic acetylcholine receptor*. Biol Reprod, 2003. **68**(4): p. 1348-53.
230. Bray, C., et al., *Mice deficient in CHRNA7, a subunit of the nicotinic acetylcholine receptor, produce sperm with impaired motility*. Biol Reprod, 2005. **73**(4): p. 807-14.
231. Kumar, P. and S. Meizel, *Nicotinic acetylcholine receptor subunits and associated proteins in human sperm*. J Biol Chem, 2005. **280**(27): p. 25928-35.
232. Bray, C., J.H. Son, and S. Meizel, *Acetylcholine causes an increase of intracellular calcium in human sperm*. Mol Hum Reprod, 2005. **11**(12): p. 881-9.
233. Mor, I., et al., *Acetylcholinesterase-R increases germ cell apoptosis but enhances sperm motility*. J Cell Mol Med, 2008. **12**(2): p. 479-95.
234. Favaretto, A.L., et al., *Inhibitory role of cholinergic agonists on testosterone secretion by purified rat Leydig cells*. Arch Int Physiol Biochim Biophys, 1993. **101**(6): p. 333-5.
235. Borges, M.O., et al., *Characterization of muscarinic acetylcholine receptor in rat Sertoli cells*. Endocrinology, 2001. **142**(11): p. 4701-10.
236. Lucas, T.F., M.C. Avellar, and C.S. Porto, *Effects of carbachol on rat Sertoli cell proliferation and muscarinic acetylcholine receptors regulation: an in vitro study*. Life Sci, 2004. **75**(14): p. 1761-73.
237. Marostica, E., et al., *Characterization of muscarinic acetylcholine receptors in the rat epididymis*. Biol Reprod, 2001. **65**(4): p. 1120-6.
238. Marostica, E., M.C. Avellar, and C.S. Porto, *Effects of testosterone on muscarinic acetylcholine receptors in the rat epididymis*. Life Sci, 2005. **77**(6): p. 656-69.
239. Sofikitis, N., et al., *Effects of smoking on testicular function, semen quality and sperm fertilizing capacity*. J Urol, 1995. **154**(3): p. 1030-4.
240. Agarwal, A., et al., *Lifestyle and testicular dysfunction: a brief update*. Biomed Pharmacother, 2008. **62**(8): p. 550-3.
241. Gocze, P.M. and D.A. Freeman, *Cytotoxic effects of cigarette smoke alkaloids inhibit the progesterone production and cell growth of cultured MA-10 Leydig tumor cells*. Eur J Obstet Gynecol Reprod Biol, 2000. **93**(1): p. 77-83.
242. Pardue, M.L. and J.G. Gall, *Molecular hybridization of radioactive DNA to the DNA of cytological preparations*. Proc Natl Acad Sci U S A, 1969. **64**(2): p. 600-4.

-
243. John, H.A., M.L. Birnstiel, and K.W. Jones, *RNA-DNA hybrids at the cytological level*. *Nature*, 1969. **223**(5206): p. 582-7.
244. Langer, P.R., A.A. Waldrop, and D.C. Ward, *Enzymatic synthesis of biotin-labeled polynucleotides: novel nucleic acid affinity probes*. *Proc Natl Acad Sci U S A*, 1981. **78**(11): p. 6633-7.
245. Stefanini, M., C. De Martino, and L. Zamboni, *Fixation of ejaculated spermatozoa for electron microscopy*. *Nature*, 1967. **216**(5111): p. 173-4.
246. Moser, N., et al., *Evaluating the suitability of nicotinic acetylcholine receptor antibodies for standard immunodetection procedures*. *J Neurochem*, 2007. **102**(2): p. 479-92.
247. Jositsch, G., et al., *Suitability of muscarinic acetylcholine receptor antibodies for immunohistochemistry evaluated on tissue sections of receptor gene-deficient mice*. *Naunyn Schmiedebergs Arch Pharmacol*, 2009. **379**(4): p. 389-95.
248. Hecker, A., et al., *Pivotal Advance: Up-regulation of acetylcholine synthesis and paracrine cholinergic signaling in intravascular transplant leukocytes during rejection of rat renal allografts*. *J Leukoc Biol*, 2009. **86**(1): p. 13-22.
249. Tracey, K.J., *Physiology and immunology of the cholinergic antiinflammatory pathway*. *J Clin Invest*, 2007. **117**(2): p. 289-96.
250. Giebelen, I.A., et al., *Local stimulation of alpha7 cholinergic receptors inhibits LPS-induced TNF-alpha release in the mouse lung*. *Shock*, 2007. **28**(6): p. 700-3.
251. Millar, N.S. and C. Gotti, *Diversity of vertebrate nicotinic acetylcholine receptors*. *Neuropharmacology*, 2009. **56**(1): p. 237-46.
252. Sastry, B.V. and C. Sadavongvivad, *Cholinergic systems in non-nervous tissues*. *Pharmacol Rev*, 1978. **30**(1): p. 65-132.
253. Wessler, I. and C.J. Kirkpatrick, *Acetylcholine beyond neurons: the non-neuronal cholinergic system in humans*. *Br J Pharmacol*, 2008. **154**(8): p. 1558-71.
254. Grando, S.A., et al., *Recent progress in understanding the non-neuronal cholinergic system in humans*. *Life Sci*, 2007. **80**(24-25): p. 2181-5.
255. Wessler, I., et al., *The non-neuronal cholinergic system in humans: expression, function and pathophysiology*. *Life Sci*, 2003. **72**(18-19): p. 2055-61.
256. Sastry, B.V., V.E. Janson, and A.K. Chaturvedi, *Inhibition of human sperm motility by inhibitors of choline acetyltransferase*. *J Pharmacol Exp Ther*, 1981. **216**(2): p. 378-84.
257. Ibanez, C.F., et al., *Expression of choline acetyltransferase mRNA in spermatogenic cells results in an accumulation of the enzyme in the postacrosomal region of mature spermatozoa*. *Proc Natl Acad Sci U S A*, 1991. **88**(9): p. 3676-80.
258. Egbunike, G.N., *Changes in acetylcholinesterase activity of mammalian spermatozoa during maturation*. *Int J Androl*, 1980. **3**(4): p. 459-68.
259. Suburo, A.M., et al., *Peptidergic innervation of blood vessels and interstitial cells in the testis of the cat*. *J Androl*, 2002. **23**(1): p. 121-34.
260. Gong, Y.G., et al., *Peptidergic not monoaminergic fibers profusely innervate the young adult human testis*. *J Anat*, 2009. **214**(3): p. 330-8.
261. Lonnerberg, P. and C.F. Ibanez, *Novel, testis-specific mRNA transcripts encoding N-terminally truncated choline acetyltransferase*. *Mol Reprod Dev*, 1999. **53**(3): p. 274-81.

-
262. Ribeiro, F.M., et al., *The "ins" and "outs" of the high-affinity choline transporter CHT1*. J Neurochem, 2006. **97**(1): p. 1-12.
263. Zhou, Q., et al., *Expression of stimulated by retinoic acid gene 8 (Stra8) and maturation of murine gonocytes and spermatogonia induced by retinoic acid in vitro*. Biol Reprod, 2008. **78**(3): p. 537-45.
264. Erickson, J.D., et al., *The VAcHT/ChAT "cholinergic gene locus": new aspects of genetic and vesicular regulation of cholinergic function*. Prog Brain Res, 1996. **109**: p. 69-82.
265. Morel, N., *Neurotransmitter release: the dark side of the vacuolar-H+ATPase*. Biol Cell, 2003. **95**(7): p. 453-7.
266. Bloc, A., et al., *Acetylcholine synthesis and quantal release reconstituted by transfection of mediatophore and choline acetyltransferase cDNAs*. Eur J Neurosci, 1999. **11**(5): p. 1523-34.
267. Rojas, J.D., et al., *Plasmalemmal V-H(+)-ATPases regulate intracellular pH in human lung microvascular endothelial cells*. Biochem Biophys Res Commun, 2004. **320**(4): p. 1123-32.
268. Heming, T.A. and A. Bidani, *Effects of plasmalemmal V-ATPase activity on plasma membrane potential of resident alveolar macrophages*. Lung, 2003. **181**(3): p. 121-35.
269. Flora, A., et al., *Neuronal and extraneuronal expression and regulation of the human alpha5 nicotinic receptor subunit gene*. J Neurochem, 2000. **75**(1): p. 18-27.
270. Toyabe, S., et al., *Identification of nicotinic acetylcholine receptors on lymphocytes in the periphery as well as thymus in mice*. Immunology, 1997. **92**(2): p. 201-5.
271. Wakkach, A., et al., *Expression of acetylcholine receptor genes in human thymic epithelial cells: implications for myasthenia gravis*. J Immunol, 1996. **157**(8): p. 3752-60.
272. Carlisle, D.L., et al., *Nicotine signals through muscle-type and neuronal nicotinic acetylcholine receptors in both human bronchial epithelial cells and airway fibroblasts*. Respir Res, 2004. **5**: p. 27.
273. Albuquerque, E.X., et al., *Mammalian nicotinic acetylcholine receptors: from structure to function*. Physiol Rev, 2009. **89**(1): p. 73-120.
274. Jones, I.W. and S. Wonnacott, *Precise localization of alpha7 nicotinic acetylcholine receptors on glutamatergic axon terminals in the rat ventral tegmental area*. J Neurosci, 2004. **24**(50): p. 11244-52.
275. Jensen, A.A., et al., *Neuronal nicotinic acetylcholine receptors: structural revelations, target identifications, and therapeutic inspirations*. J Med Chem, 2005. **48**(15): p. 4705-45.
276. Gerzanich, V., et al., *alpha 5 Subunit alters desensitization, pharmacology, Ca++ permeability and Ca++ modulation of human neuronal alpha 3 nicotinic receptors*. J Pharmacol Exp Ther, 1998. **286**(1): p. 311-20.
277. Lustig, L.R., et al., *Molecular cloning and mapping of the human nicotinic acetylcholine receptor alpha10 (CHRNA10)*. Genomics, 2001. **73**(3): p. 272-83.
278. Herber, D.L., et al., *Biochemical and histochemical evidence of nonspecific binding of alpha7nAChR antibodies to mouse brain tissue*. J Histochem Cytochem, 2004. **52**(10): p. 1367-76.
279. Burnashev, N., *Calcium permeability of ligand-gated channels*. Cell Calcium, 1998. **24**(5-6): p. 325-32.

280. Fucile, S., et al., *Human neuronal threonine-for-leucine-248 alpha 7 mutant nicotinic acetylcholine receptors are highly Ca²⁺ permeable*. Proc Natl Acad Sci U S A, 2000. **97**(7): p. 3643-8.
281. Ragozzino, D., et al., *Ca²⁺ permeability of mouse and chick nicotinic acetylcholine receptors expressed in transiently transfected human cells*. J Physiol, 1998. **507** (Pt 3): p. 749-57.
282. Lax, P., S. Fucile, and F. Eusebi, *Ca(2+) permeability of human heteromeric nAChRs expressed by transfection in human cells*. Cell Calcium, 2002. **32**(2): p. 53-8.
283. Mayorga, L.S., C.N. Tomes, and S.A. Belmonte, *Acrosomal exocytosis, a special type of regulated secretion*. IUBMB Life, 2007. **59**(4-5): p. 286-92.
284. Jimenez-Gonzalez, C., et al., *Calcium signalling in human spermatozoa: a specialized 'toolkit' of channels, transporters and stores*. Hum Reprod Update, 2006. **12**(3): p. 253-67.
285. De Blas, G., et al., *The intraacrosomal calcium pool plays a direct role in acrosomal exocytosis*. J Biol Chem, 2002. **277**(51): p. 49326-31.
286. De Blas, G.A., et al., *Dynamics of SNARE assembly and disassembly during sperm acrosomal exocytosis*. PLoS Biol, 2005. **3**(10): p. e323.
287. Darszon, A., et al., *Ion channels in sperm motility and capacitation*. Soc Reprod Fertil Suppl, 2007. **65**: p. 229-44.
288. Darszon, A., et al., *Sperm channel diversity and functional multiplicity*. Reproduction, 2006. **131**(6): p. 977-88.
289. Harper, C.V. and S.J. Publicover, *Reassessing the role of progesterone in fertilization--compartmentalized calcium signalling in human spermatozoa?* Hum Reprod, 2005. **20**(10): p. 2675-80.
290. Kandeel, F.R. and R.S. Swerdloff, *Role of temperature in regulation of spermatogenesis and the use of heating as a method for contraception*. Fertil Steril, 1988. **49**(1): p. 1-23.
291. Herrera, E., et al., *Temperature dependence of intracellular Ca²⁺ homeostasis in rat meiotic and postmeiotic spermatogenic cells*. Reproduction, 2001. **122**(4): p. 545-51.
292. Arias, H.R., et al., *Role of non-neuronal nicotinic acetylcholine receptors in angiogenesis*. Int J Biochem Cell Biol, 2009. **41**(7): p. 1441-51.
293. West, K.A., et al., *Rapid Akt activation by nicotine and a tobacco carcinogen modulates the phenotype of normal human airway epithelial cells*. J Clin Invest, 2003. **111**(1): p. 81-90.
294. Dasgupta, P., et al., *Nicotine induces cell proliferation by beta-arrestin-mediated activation of Src and Rb-Raf-1 pathways*. J Clin Invest, 2006. **116**(8): p. 2208-2217.
295. Chernyavsky, A.I., et al., *The Ras/Raf-1/MEK1/ERK signaling pathway coupled to integrin expression mediates cholinergic regulation of keratinocyte directional migration*. J Biol Chem, 2005. **280**(47): p. 39220-8.
296. Peng, H., et al., *Characterization of the human nicotinic acetylcholine receptor subunit alpha (alpha) 9 (CHRNA9) and alpha (alpha) 10 (CHRNA10) in lymphocytes*. Life Sci, 2004. **76**(3): p. 263-80.
297. Jegou, B., *The Sertoli cell in vivo and in vitro*. Cell Biol Toxicol, 1992. **8**(3): p. 49-54.
298. Mruk, D.D. and C.Y. Cheng, *Sertoli-Sertoli and Sertoli-germ cell interactions and their significance in germ cell movement in the seminiferous epithelium during spermatogenesis*. Endocr Rev, 2004. **25**(5): p. 747-806.

-
299. Abbruscato, T.J., et al., *Nicotine and cotinine modulate cerebral microvascular permeability and protein expression of ZO-1 through nicotinic acetylcholine receptors expressed on brain endothelial cells*. J Pharm Sci, 2002. **91**(12): p. 2525-38.
300. Hawkins, B.T., R.D. Egleton, and T.P. Davis, *Modulation of cerebral microvascular permeability by endothelial nicotinic acetylcholine receptors*. Am J Physiol Heart Circ Physiol, 2005. **289**(1): p. H212-9.
301. Tsai, C.H., et al., *Down-regulating effect of nicotine on connexin43 gap junctions in human umbilical vein endothelial cells is attenuated by statins*. Eur J Cell Biol, 2004. **82**(12): p. 589-95.
302. Wang, M.J., K.C. Jeng, and P.C. Shih, *Differential expression of inducible nitric oxide synthase gene by alveolar and peritoneal macrophages in lipopolysaccharide-hyporesponsive C3H/HeJ mice*. Immunology, 1999. **98**(4): p. 497-503.
303. Nakata, K., et al., *Specific messenger RNA expression for signal transduction molecules by lipopolysaccharide in intestinal macrophages*. Clin Exp Immunol, 2006. **143**(3): p. 484-93.
304. Bhushan, S., et al., *Uropathogenic Escherichia coli block MyD88-dependent and activate MyD88-independent signaling pathways in rat testicular cells*. J Immunol, 2008. **180**(8): p. 5537-47.
305. Kern, S., et al., *Cytokine secretion by macrophages in the rat testis*. Biol Reprod, 1995. **53**(6): p. 1407-16.
306. Hayes, R., et al., *Secretion of bioactive interleukin 1 by rat testicular macrophages in vitro*. J Androl, 1996. **17**(1): p. 41-9.
307. Lumeng, C.N., J.L. Bodzin, and A.R. Saltiel, *Obesity induces a phenotypic switch in adipose tissue macrophage polarization*. J Clin Invest, 2007. **117**(1): p. 175-84.
308. Mikulski, Z., et al., *Nicotinic receptors on rat alveolar macrophages dampen ATP-induced increase in cytosolic calcium concentration*. Respir Res, 2010. **11**: p. 133.
309. Matsunaga, K., et al., *Involvement of nicotinic acetylcholine receptors in suppression of antimicrobial activity and cytokine responses of alveolar macrophages to Legionella pneumophila infection by nicotine*. J Immunol, 2001. **167**(11): p. 6518-24.
310. Galvis, G., K.S. Lips, and W. Kummer, *Expression of nicotinic acetylcholine receptors on murine alveolar macrophages*. J Mol Neurosci, 2006. **30**(1-2): p. 107-8.
311. Laskin, D.L., B. Weinberger, and J.D. Laskin, *Functional heterogeneity in liver and lung macrophages*. J Leukoc Biol, 2001. **70**(2): p. 163-70.
312. Nguyen, V.T., A. Ndoye, and S.A. Grando, *Novel human alpha9 acetylcholine receptor regulating keratinocyte adhesion is targeted by Pemphigus vulgaris autoimmunity*. Am J Pathol, 2000. **157**(4): p. 1377-91.
313. Baker, E.R., et al., *Pharmacological properties of alpha 9 alpha 10 nicotinic acetylcholine receptors revealed by heterologous expression of subunit chimeras*. Mol Pharmacol, 2004. **65**(2): p. 453-60.
314. Haddad el, B. and J. Rousell, *Regulation of the expression and function of the M2 muscarinic receptor*. Trends Pharmacol Sci, 1998. **19**(8): p. 322-7.
315. Matsui, M., et al., *Mice lacking M2 and M3 muscarinic acetylcholine receptors are devoid of cholinergic smooth muscle contractions but still viable*. J Neurosci, 2002. **22**(24): p. 10627-32.

-
316. Eglen, R.M., et al., *Muscarinic acetylcholine receptor subtypes in smooth muscle*. Trends Pharmacol Sci, 1994. **15**(4): p. 114-9.
317. Matthiesen, S., et al., *Muscarinic receptors mediate stimulation of human lung fibroblast proliferation*. Am J Respir Cell Mol Biol, 2006. **35**(6): p. 621-7.
318. Roffel, A.F., et al., *Muscarinic M2 receptors in bovine tracheal smooth muscle: discrepancies between binding and function*. Eur J Pharmacol, 1988. **153**(1): p. 73-82.
319. Gosens, R., et al., *Acetylcholine: a novel regulator of airway smooth muscle remodelling?* Eur J Pharmacol, 2004. **500**(1-3): p. 193-201.
320. Young, R.J. and J.C. Laing, *The binding characteristics of cholinergic sites in rabbit spermatozoa*. Mol Reprod Dev, 1991. **28**(1): p. 55-61.
321. Bernardini, N., A.I. Levey, and G. Augusti-Tocco, *Rat dorsal root ganglia express m1-m4 muscarinic receptor proteins*. J Peripher Nerv Syst, 1999. **4**(3-4): p. 222-32.
322. Siu, E.R., et al., *Expression and localization of muscarinic acetylcholine receptor subtypes in rat efferent ductules and epididymis*. Cell Tissue Res, 2006. **323**(1): p. 157-66.
323. Mak, J.C., J.N. Baraniuk, and P.J. Barnes, *Localization of muscarinic receptor subtype mRNAs in human lung*. Am J Respir Cell Mol Biol, 1992. **7**(3): p. 344-8.
324. Mak, J.C. and P.J. Barnes, *Autoradiographic visualization of muscarinic receptor subtypes in human and guinea pig lung*. Am Rev Respir Dis, 1990. **141**(6): p. 1559-68.
325. Mak, J.C., et al., *Visualization of muscarinic m4 mRNA and M4 receptor subtype in rabbit lung*. Life Sci, 1993. **53**(19): p. 1501-8.
326. Nilvebrant, L., K.E. Andersson, and A. Mattiasson, *Characterization of the muscarinic cholinceptors in the human detrusor*. J Urol, 1985. **134**(2): p. 418-23.
327. Walch, L., C. Brink, and X. Norel, *The muscarinic receptor subtypes in human blood vessels*. Therapie, 2001. **56**(3): p. 223-6.
328. O'Rourke, S.T. and P.M. Vanhoutte, *Subtypes of muscarinic receptors on adrenergic nerves and vascular smooth muscle of the canine saphenous vein*. J Pharmacol Exp Ther, 1987. **241**(1): p. 64-7.
329. Sagrada, A., et al., *Himbacine discriminates between putative muscarinic M1 receptor-mediated responses*. Life Sci, 1994. **54**(17): p. PL305-10.
330. Watson, N., H. Reddy, and R.M. Eglen, *Pharmacological characterization of the muscarinic receptors mediating contraction of canine saphenous vein*. J Auton Pharmacol, 1995. **15**(6): p. 437-41.
331. Thomas, E.A., S.A. Baker, and F.J. Ehlert, *Functional role for the M2 muscarinic receptor in smooth muscle of guinea pig ileum*. Mol Pharmacol, 1993. **44**(1): p. 102-10.
332. Struckmann, N., et al., *Role of muscarinic receptor subtypes in the constriction of peripheral airways: studies on receptor-deficient mice*. Mol Pharmacol, 2003. **64**(6): p. 1444-51.
333. Eglen, R.M. and R.L. Whiting, *Heterogeneity of vascular muscarinic receptors*. J Auton Pharmacol, 1990. **10**(4): p. 233-45.
334. van Zwieten, P.A. and H.N. Doods, *Muscarinic receptors and drugs in cardiovascular medicine*. Cardiovasc Drugs Ther, 1995. **9**(1): p. 159-67.
335. Miranda, H.F., et al., *Cholinergic receptors in the human vas deferens*. J Recept Res, 1992. **12**(1): p. 101-15.

336. Miranda, H.F., et al., *Pre- and postjunctional muscarinic receptor subtypes in the vas deferens of rat*. Gen Pharmacol, 1994. **25**(8): p. 1643-7.
337. Miranda, H.F., et al., *Muscarinic receptor subtypes in the bisected vas deferens of the rat*. Gen Pharmacol, 1995. **26**(2): p. 387-91.
338. Iram, S. and C.H. Hoyle, *Potentiation of sympathetic neuromuscular transmission mediated by muscarinic receptors in guinea pig isolated vas deferens*. Naunyn Schmiedebergs Arch Pharmacol, 2005. **371**(3): p. 212-20.
339. Shannon, H.E., et al., *Muscarinic M1 receptor agonist actions of muscarinic receptor agonists in rabbit vas deferens*. Eur J Pharmacol, 1993. **232**(1): p. 47-57.
340. Gosens, R., et al., *Muscarinic receptor signaling in the pathophysiology of asthma and COPD*. Respir Res, 2006. **7**: p. 73.
341. Kawashima, K., et al., *Expression and function of genes encoding cholinergic components in murine immune cells*. Life Sci, 2007. **80**(24-25): p. 2314-9.
342. Chernyavsky, A.I., et al., *Novel signaling pathways mediating reciprocal control of keratinocyte migration and wound epithelialization through M3 and M4 muscarinic receptors*. J Cell Biol, 2004. **166**(2): p. 261-72.
343. Blanchet, M.R., E. Israel-Assayag, and Y. Cormier, *Inhibitory effect of nicotine on experimental hypersensitivity pneumonitis in vivo and in vitro*. Am J Respir Crit Care Med, 2004. **169**(8): p. 903-9.
344. Huston, J.M., et al., *Splenectomy inactivates the cholinergic antiinflammatory pathway during lethal endotoxemia and polymicrobial sepsis*. J Exp Med, 2006. **203**(7): p. 1623-8.
345. Hofer, S., et al., *Pharmacologic cholinesterase inhibition improves survival in experimental sepsis*. Crit Care Med, 2008. **36**(2): p. 404-8.
346. Wessler, I., et al., *Increased acetylcholine levels in skin biopsies of patients with atopic dermatitis*. Life Sci, 2003. **72**(18-19): p. 2169-72.
347. Kindt, F., et al., *Reduced expression of nicotinic alpha subunits 3, 7, 9 and 10 in lesional and nonlesional atopic dermatitis skin but enhanced expression of alpha subunits 3 and 5 in mast cells*. Br J Dermatol, 2008. **159**(4): p. 847-57.
348. de Jonge, W.J., et al., *Stimulation of the vagus nerve attenuates macrophage activation by activating the Jak2-STAT3 signaling pathway*. Nat Immunol, 2005. **6**(8): p. 844-51.
349. Su, X., et al., *Activation of the alpha7 nAChR reduces acid-induced acute lung injury in mice and rats*. Am J Respir Cell Mol Biol, 2007. **37**(2): p. 186-92.
350. Kelso, M.L., et al., *The pathophysiology of traumatic brain injury in alpha7 nicotinic cholinergic receptor knockout mice*. Brain Res, 2006. **1083**(1): p. 204-10.
351. Leonard, S. and D. Bertrand, *Neuronal nicotinic receptors: from structure to function*. Nicotine Tob Res, 2001. **3**(3): p. 203-23.
352. Berridge, M.J., P. Lipp, and M.D. Bootman, *The versatility and universality of calcium signalling*. Nat Rev Mol Cell Biol, 2000. **1**(1): p. 11-21.
353. Iosub, R., et al., *Development of testicular inflammation in the rat involves activation of proteinase-activated receptor-2*. J Pathol, 2006. **208**(5): p. 686-98.
354. Auzanneau, C., et al., *Transient receptor potential vanilloid 1 (TRPV1) channels in cultured rat Sertoli cells regulate an acid sensing chloride channel*. Biochem Pharmacol, 2008. **75**(2): p. 476-83.
355. Filippini, A., et al., *Activation of inositol phospholipid turnover and calcium signaling in rat Sertoli cells by P2-purineric receptors: modulation of*

-
- follicle-stimulating hormone responses*. Endocrinology, 1994. **134**(3): p. 1537-45.
356. Pawlak, J., et al., *Effect of melatonin on phagocytic activity and intracellular free calcium concentration in testicular macrophages from normal and streptozotocin-induced diabetic rats*. Mol Cell Biochem, 2005. **275**(1-2): p. 207-13.
357. Leeson, C.R. and T.S. Leeson, *The Postnatal Development and Differentiation of the Boundary Tissue of the Seminiferous Tubule of the Rat*. Anat Rec, 1963. **147**: p. 243-59.
358. Dym, M. and D.W. Fawcett, *The blood-testis barrier in the rat and the physiological compartmentation of the seminiferous epithelium*. Biol Reprod, 1970. **3**(3): p. 308-26.
359. Palombi, F. and C. Di Carlo, *Alkaline phosphatase is a marker for myoid cells in cultures of rat peritubular and tubular tissue*. Biol Reprod, 1988. **39**(5): p. 1101-9.
360. Galdieri, M. and G. Ricci, *Characterization of different cell populations isolated from rat testis peritubular cells*. Differentiation, 1998. **63**(1): p. 13-9.
361. Romano, F., et al., *The contractile phenotype of peritubular smooth muscle cells is locally controlled: possible implications in male fertility*. Contraception, 2005. **72**(4): p. 294-7.
362. Tung, P.S. and I.B. Fritz, *Characterization of rat testicular peritubular myoid cells in culture: alpha-smooth muscle isoactin is a specific differentiation marker*. Biol Reprod, 1990. **42**(2): p. 351-65.
363. Palombi, F., et al., *Development and cytodifferentiation of peritubular myoid cells in the rat testis*. Anat Rec, 1992. **233**(1): p. 32-40.
364. Paranko, J. and L.J. Pelliniemi, *Differentiation of smooth muscle cells in the fetal rat testis and ovary: localization of alkaline phosphatase, smooth muscle myosin, F-actin, and desmin*. Cell Tissue Res, 1992. **268**(3): p. 521-30.
365. Santiemma, V., et al., *Development and hormone dependence of peritubular smooth muscle cells of the rat testis*, in *Recent Progress in Andrology*, S.E. Fabbrini A, Editor. 1978, London: Academic Press. p. 185-99.
366. Chapin, R.E., et al., *Alkaline phosphatase histochemistry discriminates peritubular cells in primary rat testicular cell culture*. J Androl, 1987. **8**(3): p. 155-61.
367. Hao, H., et al., *Heterogeneity of smooth muscle cell populations cultured from pig coronary artery*. Arterioscler Thromb Vasc Biol, 2002. **22**(7): p. 1093-9.
368. Walker, L.N., et al., *Production of platelet-derived growth factor-like molecules by cultured arterial smooth muscle cells accompanies proliferation after arterial injury*. Proc Natl Acad Sci U S A, 1986. **83**(19): p. 7311-5.
369. Khakh, B.S. and T.M. Egan, *Contribution of transmembrane regions to ATP-gated P2X2 channel permeability dynamics*. J Biol Chem, 2005. **280**(7): p. 6118-29.
370. Khakh, B.S. and G. Henderson, *Modulation of fast synaptic transmission by presynaptic ligand-gated cation channels*. J Auton Nerv Syst, 2000. **81**(1-3): p. 110-21.
371. Zhang, G.H., et al., *Regulation of cytosolic free Ca²⁺ in cultured rat alveolar macrophages (NR8383)*. J Leukoc Biol, 1997. **62**(3): p. 341-8.
372. Wikstrom, M.A., G. Lawoko, and E. Heilbronn, *Cholinergic modulation of extracellular ATP-induced cytoplasmic calcium concentrations in cochlear outer hair cells*. J Physiol Paris, 1998. **92**(5-6): p. 345-9.

-
373. Myrtek, D., et al., *Activation of human alveolar macrophages via P2 receptors: coupling to intracellular Ca²⁺ increases and cytokine secretion*. J Immunol, 2008. **181**(3): p. 2181-8.
374. Di Virgilio, F., et al., *Nucleotide receptors: an emerging family of regulatory molecules in blood cells*. Blood, 2001. **97**(3): p. 587-600.
375. Lemaire, I., et al., *Involvement of the purinergic P2X7 receptor in the formation of multinucleated giant cells*. J Immunol, 2006. **177**(10): p. 7257-65.
376. Ferrari, D., et al., *The P2X7 receptor: a key player in IL-1 processing and release*. J Immunol, 2006. **176**(7): p. 3877-83.
377. Ralevic, V. and G. Burnstock, *Receptors for purines and pyrimidines*. Pharmacol Rev, 1998. **50**(3): p. 413-92.
378. Schachter, J.B., et al., *Second messenger cascade specificity and pharmacological selectivity of the human P2Y1-purinoceptor*. Br J Pharmacol, 1996. **118**(1): p. 167-73.
379. van der Weyden, L., et al., *Pharmacological characterisation of the P2Y11 receptor in stably transfected haematological cell lines*. Mol Cell Biochem, 2000. **213**(1-2): p. 75-81.
380. Foster, C.J., et al., *Molecular identification and characterization of the platelet ADP receptor targeted by thienopyridine antithrombotic drugs*. J Clin Invest, 2001. **107**(12): p. 1591-8.
381. Foresta, C., et al., *Extracellular ATP activates different signalling pathways in rat Sertoli cells*. Biochem J, 1995. **311** (Pt 1): p. 269-74.
382. Berridge, M.J., M.D. Bootman, and H.L. Roderick, *Calcium signalling: dynamics, homeostasis and remodelling*. Nat Rev Mol Cell Biol, 2003. **4**(7): p. 517-29.
383. Blaustein, M.P. and W.J. Lederer, *Sodium/calcium exchange: its physiological implications*. Physiol Rev, 1999. **79**(3): p. 763-854.
384. Mikulski, Z., et al., *Serotonin activates murine alveolar macrophages through 5-HT_{2C} receptors*. Am J Physiol Lung Cell Mol Physiol, 2010. **299**(2): p. L272-80.
385. Blanchet, M.R., et al., *Dimethyphenylpiperazinium, a nicotinic receptor agonist, downregulates inflammation in monocytes/macrophages through PI3K and PLC chronic activation*. Am J Physiol Lung Cell Mol Physiol, 2006. **291**(4): p. L757-63.
386. Razani-Boroujerdi, S., et al., *T cells express alpha7-nicotinic acetylcholine receptor subunits that require a functional TCR and leukocyte-specific protein tyrosine kinase for nicotine-induced Ca²⁺ response*. J Immunol, 2007. **179**(5): p. 2889-98.
387. Drasdo, A., et al., *Methyl lycaconitine: A novel nicotinic antagonist*. Mol Cell Neurosci, 1992. **3**(3): p. 237-43.
388. Stockinger, W., et al., *Differential requirements for actin polymerization, calmodulin, and Ca²⁺ define distinct stages of lysosome/phagosome targeting*. Mol Biol Cell, 2006. **17**(4): p. 1697-710.
389. Iles, K.E. and H.J. Forman, *Macrophage signaling and respiratory burst*. Immunol Res, 2002. **26**(1-3): p. 95-105.
390. Kuntz, A. and R.E. Morris, Jr., *Components and distribution of the spermatic nerves and the nerves of the vas deferens*. J Comp Neurol, 1946. **85**: p. 33-44.

-
391. Santamaria, L., et al., *Histochemistry and ultrastructure of nerve fibres and contractile cells in the tunica albuginea of the rat testis*. Acta Anat (Basel), 1990. **139**(2): p. 126-33.
392. Wrobel, K.H. and E. Schenk, *Immunohistochemical investigations of the autonomous innervation of the cervine testis*. Ann Anat, 2003. **185**(6): p. 493-506.
393. Peterson, D.F. and A.M. Brown, *Functional afferent innervation of testis*. J Neurophysiol, 1973. **36**(3): p. 425-33.
394. Kumazawa, T. and K. Mizumura, *The polymodal receptors in the testis of dog*. Brain Res, 1977. **136**(3): p. 553-8.
395. Kumazawa, T. and K. Mizumura, *Effects of synthetic substance P on unit-discharges of testicular nociceptors of dogs*. Brain Res, 1979. **170**(3): p. 553-7.
396. Kumazawa, T. and K. Mizumura, *Mechanical and thermal responses of polymodal receptors recorded from the superior spermatic nerve of dogs*. J Physiol, 1980. **299**: p. 233-45.
397. Kumazawa, T., K. Mizumura, and J. Sato, *Response properties of polymodal receptors studied using in vitro testis superior spermatic nerve preparations of dogs*. J Neurophysiol, 1987. **57**(3): p. 702-11.
398. Jessell, T.M., K. Yoshioka, and C.E. Jahr, *Amino acid receptor-mediated transmission at primary afferent synapses in rat spinal cord*. J Exp Biol, 1986. **124**: p. 239-58.
399. Hope, P.J., et al., *Release and spread of immunoreactive neurokinin A in the cat spinal cord in a model of acute arthritis*. Brain Res, 1990. **533**(2): p. 292-9.
400. Sluka, K.A. and K.N. Westlund, *Spinal cord amino acid release and content in an arthritis model: the effects of pretreatment with non-NMDA, NMDA, and NK1 receptor antagonists*. Brain Res, 1993. **627**(1): p. 89-103.
401. Ueda, M., et al., *Evidence that glutamate is released from capsaicin-sensitive primary afferent fibers in rats: study with on-line continuous monitoring of glutamate*. Neurosci Res, 1994. **20**(3): p. 231-7.
402. Carlton, S.M., G.L. Hargett, and R.E. Coggeshall, *Localization and activation of glutamate receptors in unmyelinated axons of rat glabrous skin*. Neurosci Lett, 1995. **197**(1): p. 25-8.
403. Davidson, E.M., R.E. Coggeshall, and S.M. Carlton, *Peripheral NMDA and non-NMDA glutamate receptors contribute to nociceptive behaviors in the rat formalin test*. Neuroreport, 1997. **8**(4): p. 941-6.
404. Skofitsch, G. and D.M. Jacobowitz, *Calcitonin gene-related peptide coexists with substance P in capsaicin sensitive neurons and sensory ganglia of the rat*. Peptides, 1985. **6**(4): p. 747-54.
405. Tamura, R., K. Mizumura, and T. Kumazawa, *Coexistence of calcitonin gene-related peptide- and substance P-like immunoreactivity in retrogradely labeled superior spermatic neurons in the dog*. Neurosci Res, 1996. **25**(3): p. 293-9.
406. Kruger, L., et al., *Nociceptor structural specialization in canine and rodent testicular "free" nerve endings*. J Comp Neurol, 2003. **463**(2): p. 197-211.
407. Wrobel, K.H. and B. Brandl, *The autonomous innervation of the porcine testis in the period from birth to adulthood*. Ann Anat, 1998. **180**(2): p. 145-56.
408. Tominaga, M., et al., *The cloned capsaicin receptor integrates multiple pain-producing stimuli*. Neuron, 1998. **21**(3): p. 531-43.

-
409. Caterina, M.J., et al., *The capsaicin receptor: a heat-activated ion channel in the pain pathway*. Nature, 1997. **389**(6653): p. 816-24.
 410. Manzo, J., et al., *Influence of testosterone on the electrical properties of scrotal nerves at the cutaneous and spinal levels in the male rat*. J Peripher Nerv Syst, 2003. **8**(2): p. 75-81.
 411. Botti, M., et al., *Sensory, motor somatic, and autonomic neurons projecting to the porcine cremaster muscle*. Anat Rec A Discov Mol Cell Evol Biol, 2006. **288**(10): p. 1050-8.
 412. Tamura, R., et al., *Segmental distribution of afferent neurons innervating the canine testis*. J Auton Nerv Syst, 1996. **58**(1-2): p. 101-7.
 413. Kashiba, H., Y. Uchida, and E. Senba, *Difference in binding by isolectin B4 to trkA and c-ret mRNA-expressing neurons in rat sensory ganglia*. Brain Res Mol Brain Res, 2001. **95**(1-2): p. 18-26.
 414. Schirmer, S., et al., *The cholinergic system in rat testis is of non-neuronal origin*. Reproduction. 2011 Apr 11. [Epub ahead of print]

18. Appendix

18.1. Curriculum vitae

Publication:

Schirmer SU, Eckhardt I, DeGraaf Y, Lips KS, Pineau C, Gibbins IL, Kummer W, Meinhardt A & Haberberger RV

The cholinergic system in rat testis is of non-neuronal origin. Reproduction. 2011 Apr 11. [Epub ahead of print]

Poster:

Schirmer SU, DeGraaf Y, Gibbins I, Meinhardt A & Haberberger RV

The expression of the cholinergic system in rat testis is predominantly of non-neuronal origin.

104th International Meeting of the Anatomical Society, Antwerp, Belgium. 27.-30. March 2009

Schirmer SU, DeGraaf Y, Gibbins I, Meinhardt A & Haberberger RV

The expression of the cholinergic system in rat testis is predominantly of non-neuronal origin.

International Workshop, First Symposium of the Clinical Research Unit 181 "Molecular Andrology". Giessen, Germany. 08.-10. May 2009

Schirmer SU, DeGraaf Y, Gibbins IL, Meinhardt A & Haberberger RV

The cholinergic system in rat testis is of non-neuronal origin.

ISAN 2009, 6th Congress of the International Society for Autonomic Neuroscience. Sydney, Australia. 01.-04. September 2009

Oral presentation:

Schirmer SU, Vilimas P, Gibbins IL, Meinhardt A & Haberberger RV

Sensory innervation of the rat testis and adjacent mesenteric tissue.

Third GGLConference on Life Sciences. Giessen, Germany. 30. Sept - 01. Oct 2009

18.2 Acknowledgements

First I wish to thank Prof. Dr. Andreas Meinhardt and Prof. Dr. Reinhard Lakes-Harlan for the supervision of my work. Furthermore I would like to thank Prof. Dr. Andreas Meinhardt and A/Prof. Dr. Rainer Haberberger for giving me the chance to work and being part in this project.

I would like to express my sincere gratitude to Rainer Haberberger for his supervision in the lab, teaching of new techniques and constructive critique during my stay in Adelaide. I was always welcome in his family to make an excursion around Adelaide. I am grateful for all the hints and discussions about my data and the effort he invested into the revision of my thesis.

I would like to thank Prof. Ian Gibbins for the discussions, helpful suggestions and the possibility to be part of his lab for a while. In this regard it was a particular pleasure to work together with Patricia Vilimas, Yvette DeGraaf, Jennifer Clarke, Dimi Beroukas and Rebecca Anderson. Thanks for all the good hints and suggestions for IHC, ISH, qRT-PCR, cLSM etc. Most thankful I am to Dimi and Yvette for the time we spend together outside the lab.

I would like to thank Prof. Dr. Wolfgang Kummer for taking his time to answering my questions, giving me support for my experiments and being welcome in his lab. I am grateful to the people in the Cardiopulmonary Neurobiology Laboratory for sharing their knowledge, the provision with reagents and the supervision and usage of their equipment. I am thankful to Petra Hartmann, Tamara Papadakis, Silke Wiegand, Martin Bodenbenner, Zbigniew Mikulski and Karola Michael, for their contribution to successfully complete my PCR, IHC or Calcium-Imaging experiments from the living animal to the last picture or plot.

Thanks to my colleagues in the Reproductive Biology and the time and effort they invested to introduce lab-techniques to me: Monika Fijak and Eva Schneider for the help they gave with animal experiments, Sudhanshu Bushan and Yongning Lu for their support of PTC and SC and Suada Fröhlich and Jörg Klug for general support.

I gratefully acknowledge the financial support provided by the Else-Kröner-Fresenius foundation for this project and the German Academic Exchange Service (DAAD) for my temporary residence in Australia.

I am especially grateful to Miriam Wolff, Stefan Binder, Ferial Aslani, Philipp Lacher and Gitte Jositsch for the time we spend together in- and outside the lab. Thanks for the support in the lab and for my work, for all the scientific and non-scientific discussions and the fun we had together. Thanks for being like you are.

Finally, I would like to thank my friends and family for their great support.

18.3. Declaration

Ich erkläre: Ich habe die vorgelegte Dissertation selbständig und ohne unerlaubte fremde Hilfe und nur mit den Hilfen angefertigt, die ich in der Dissertation angegeben habe. Alle Textstellen, die wörtlich oder sinngemäß aus veröffentlichten Schriften entnommen sind, und alle Angaben, die auf mündlichen Auskünften beruhen, sind als solche kenntlich gemacht. Bei den von mir durchgeführten und in der Dissertation erwähnten Untersuchungen habe ich die Grundsätze guter wissenschaftlicher Praxis, wie sie in der „Satzung der Justus-Liebig-Universität Gießen zur Sicherung guter wissenschaftlicher Praxis“ niedergelegt sind, eingehalten.

Gießen, 09.02.2011

Sylvia Schirmer